# Porous Silicon – Polycaprolactone Composites for Orthopaedic Tissue Engineering

Dr. James R. Henstock BSc MPhil PhD


School of Biomedical Sciences
Medical School
University of Nottingham
Nottingham
UK

Thesis submitted to the University of Nottingham for the Degree of Doctor of Philosophy

June 2009

**CONTENTS**


**Contents.** **i - vi**

**Acknowledgements.** **vii**

**Abstract.** **viii**

**List of abbreviations.** **ix**

## Chapter 1 General Introduction. 1

**1.1. Bone biology.** **2**
1.1.1. Bone structure – growth and repair. 2
1.1.1.1. Structure and biology. 3
1.1.1.2. Cell types in bone metabolism. 6
1.1.1.3. Bone formation and metabolism. 7
1.1.1.4. Bone resorbtion. 9
1.1.2. Molecular biology of the osteoblast. 11
1.1.2.1. Collagen. 11
1.1.2.2. Bone sialoprotein II. 13
1.1.2.3. Osteopontin. 13
1.1.2.4. Osteonectin. 14
1.1.2.5. Osteoadherin. 14
1.1.2.6. Osteocalcin. 14
1.1.2.7. Alkaline phosphatase. 15
1.1.3. Mineralisation of bone matrix. 16
1.1.4. Mechanism of fracture repair. 19

**1.2. Biomaterials and tissue engineering.** **21**
1.2.1. Bioglass® and the response of osteoblasts to silicate biomaterials. 23
1.2.2. Silicon in biomaterials. 25
1.2.3. Silicon substitution in hydroxyapatite. 26
1.2.4. Silicon function in the osteoid. 27

**1.3. Silicon.** **29**
1.3.1. The biogeochemical cycle of silicon. 30
1.3.2. Polymerisation of orthosilicic acid. 31
1.3.3. Technological applications of silicon. 33

**1.4. Porous silicon.** **35**
1.4.1. Fabrication. 36
1.4.2. Degradation in water. 37
1.4.3. Biological activity. 37

**1.5. Aims of the investigation.** **39**

**Chapter 2 Characterisation of Porous Silicon – Polycaprolactone Composites. 40**

**2.1. Introduction. 41**
2.1.1. Choice of biodegradable polymer. 42
2.1.1.1. Polylactic acid. 43
2.1.1.2. Polyglycolide. 44
2.1.1.3. Polycaprolactone. 45
2.1.1.4. Poly-3-hydroxybutyrate. 46
2.1.1.5. Choice of polymer. 47
2.1.2. Degradation of the composite in acellular fluids. 48
2.1.3. Comparison to other bioactive composites. 49

**2.2. Materials and methods. 50**
2.2.1. Forming the composite. 50
2.2.2. Determining bioactivity. 51
2.2.2.1. Simulated body fluid. 51
2.2.2.2. Quantifying silicic acid. 52
2.2.2.3. pH. 52
2.2.2.4. Assessing silica gel formation. 53
2.2.2.5. Quantifying calcium. 53
2.2.2.6. SEM, ESEM and EDX. 53
2.2.3. Experimental. 54
2.2.3.1. Composite formation. 54
2.2.3.2. Porous silicon – porosity and particle size. 54
2.2.3.3. Polymer type – PCL, PHBV and PLGA. 55
2.2.3.4. Relationship of composite mass to silicic acid release. 56
2.2.3.5. Dissolution buffers and solution volume. 56
2.2.3.6. Comparison of pSi-PCL to 45S5 Bioglass®-PCL. 56
2.2.3.7. Long-term incubation. 57
2.2.3.8. Morphology and composition of apatite formation. 57

**2.3. Results. 58**
2.3.1. Forming the composite. 58
2.3.2. pSi particle size. 59
2.3.3. PLGA, PHBV and PCL. 62
2.3.4. Composite mass. 65
2.3.5. Solution and volume. 66
2.3.6. Comparison of pSi to Bioglass® in PCL composites. 67
2.3.7. Long-term study. 68
2.3.8. Morphology and composition of silica and apatite formation. 73

**2.4. Discussion. 78**

**Chapter 3 Osteoblast Response to Porous Silicon – Polycaprolactone Composites *in vitro.* 86**

**3.1. Introduction. 87**
3.1.1. Osteoblasts *in vitro.* 87
3.1.2. Practical *in vitro* culture of osteoblasts. 91
3.1.3. The effect of silicon on osteoblasts. 92
3.1.4. The effect of silicic acid-eluting biomaterials on osteoblasts *in vitro.* 93
3.1.5. Aims. 94

**3.2. Materials and methods. 95**
3.2.1. Osteoblast *in vitro* culture. 95
3.2.2. Analysis. 95
3.2.2.1. Silicic acid content of media. 96
3.2.2.2. DNA. 96
3.2.2.3. Collagen. 97
3.2.2.4. Alkaline phosphatase activity. 97
3.2.2.5. Glycosaminoglycans. 97
3.2.2.6. Calcium. 98
3.2.2.7. Pyridinoline. 98
3.2.3. Experimental. 99
3.2.3.1. Response of osteoblasts to pSi-PCL composites *in vitro.* 99
3.2.3.1.1. Scanning electron microscopy (SEM). 100
3.2.3.1.2. Light microscopy. 100
3.2.3.2. Osteoblast response to silicic acid in media. 101
3.2.3.3. Osteoblast response to pSi, pSi-PCL and Bioglass®-PCL degradation products. 102
3.2.3.3.1. pSi-conditioned media. 102
3.2.3.3.2. Co-incubation of osteoblasts with pSi-PCL and Bioglass®-PCL composites. 102

**3.3. Results. 104**
3.3.1. Response of osteoblasts to pSi-PCL composites. 101
3.3.1.1. 54% porous pSi. 105
3.3.1.2. 66% porous pSi. 107
3.3.1.3. 70% porous pSi. 108
3.3.1.4. 82% porous pSi. 110
3.3.2. Osteoblast response to silicic acid in media. 111
3.3.2.1. osteoblast response to 100 – 1000 $ng.mg^{-1}$ Si. 111
3.3.2.2. osteoblast response to 1 – 5 $\mu g.ml^{-1}$ Si. 112
3.3.2.3. osteoblast response to 1 – 35 $\mu g.ml^{-1}$ Si. 114
3.3.2.4. osteoblast response to 25 - 3100 $\mu g.ml^{-1}$ Si. 115
3.3.3. Osteoblast response to pSi degradation products. 117
3.3.3.1. pSi-conditioned media. 117
3.3.3.2. pSi-PCL discs co-incubated with osteoblasts. 119
3.3.3.3. pSi-PCL and 45S5 Bioglass®-PCL discs co-incubated with osteoblasts. 123

**3.4. Discussion. 125**

**Chapter 4 pSi-PCL Composites for the Controlled Delivery of Pharmaceuticals. 128**

**4.1. Introduction. 129**
4.1.1. Bone stabilisers. 130
4.1.2. Analgesics and anti-inflammatories. 131
4.1.3. Antibiotics. 132
4.1.4. Porous silicon for drug delivery. 133
4.1.5. Polycaprolactone for drug delivery. 135
4.1.6. Loading and release of substance in pSi-PCL composites. 136
4.1.7. Substances tested. 137
4.1.7.1. Fluorescein. 138
4.1.7.2. Bovine serum albumin. 139
4.1.7.3. Alkaline phosphatase. 140
4.1.7.4. Gentamicin. 140
4.1.7.5 Nystatin. 141
4.1.7.6. Dexamethasone. 142
4.1.7.7. Bone morphogenic protein-7. 142
4.1.8. Aims. 143

**4.2. Materials and methods. 144**
4.2.1. Loading of substances into pSi and polycaprolactone. 144
4.2.2. Substances tested. 146
4.2.2.1. Fluorescein. 146
4.2.2.2. Bovine serum albumin and alkaline phosphatase. 147
4.2.2.2.1. Protein release. 147
4.2.2.2.2. Alkaline phosphatase activity. 148
4.2.2.3. Gentamicin. 148
4.2.2.4. Nystatin. 149
4.2.2.5. Dexamethasone. 150
4.2.2.5.6 Bone morphogenic protein-7 (BMP7). 151

**4.3. Results. 153**

4.3.1. Loading of substances into pSi and polycaprolactone. 153
4.3.2. Substance release. 153
4.3.2.1. Fluorescein. 153
4.3.2.2. Bovine serum albumin and alkaline phosphatase. 156
4.3.2.3. Gentamicin. 158
4.3.2.4. Nystatin. 159
4.3.2.5. Dexamethasone. 160
4.3.2.6. Bone morphogenic protein 7. 162

**4.4. Discussion. 165**

**Chapter 5 Characterisation of pSi-PCL Composites in Simulated Physiological Environments 169**

**5.1. Introduction. 170**
5.1.1. Protein adsorption. 171
5.1.2. Permeability of polycaprolactone to silicic acid and small molecules. 172
5.1.3. Composite behaviour in a dynamic perfusion model. 173
5.1.4. Bone tissue simulation. 174

**5.2. Materials and methods. 176**
5.2.1. Protein adsorption. 176
5.2.2. pSi encapsulation in PCL layers. 177
5.2.3. Dynamic perfusion. 178
5.2.4. Bone tissue simulation. 179

**5.3. Results. 181**
5.3.1. Protein adsorption. 181
5.3.2. Encapsulation. 182
5.3.3. Dynamic perfusion. 183
5.3.4. Bone tissue simulation. 185

**5.4. Discussion. 186**

**Chapter 6 Physical properties of pSi-PCL Composites. 189**

**6.1 Introduction. 190**
6.1.1. Particle dispersal. 191
6.1.2. Tensile strength. 191
6.1.3. Electrical conductivity. 194
6.1.4. Aims. 199

**6.2. Materials and methods. 200**
6.2.1. Particle dispersal. 200
6.2.2. Tensile strength. 200
6.2.3. Electrical resistance. 201

**6.3. Results. 203**
6.3.1. Particle dispersal. 203
6.3.2. Tensile strength. 204
6.3.3. Electrical resistance. 209

**6.4. Discussion. 211**

**Chapter 7 General Discussion 214**

**References 227**

**Appendix Applications. 263**

**1. Introduction. 264**
1.1. 3-Dimensional porous composites for tissue engineering. 265
1.2. Composite orthopaedic fixation screw. 268
1.3. Poly(methyl methacrylate) bone cement. 270

**2. Materials and methods. 275**
2.1. Fabrication of 3-D scaffolds. 275
2.1.1. Particulate porogens. 275
2.1.2. Porosification using soluble templates. 275
2.1.3. Porosification using caramelised sucrose templates. 276
2.2. Screw fabrication. 277
2.3. PMMA bone cement incorporating pSi. 278
2.3.1. Characterisation of pSi-PMMA in water. 278
2.3.2. Response of osteoblasts to pSi-PMMA composites *in vitro*. 278
2.3.3. Drug release from pSi-PMMA composites. 279

**3. Results. 280**
3.1. 3-D scaffold fabrication. 280
7.3.1.1. Particulate porogens. 280
7.3.1.2. Porosification using soluble templates. 282
7.3.1.3. Porosification using caramelised sucrose templates. 283
3.2. Mechanical testing of orthopaedic screws. 286
3.3. pSi-PMMA bone cement. 289
3.3.1. Characterisation of PMMA bone cement incorporating pSi. 289
3.3.2. Response of osteoblasts to pSi-PMMA composites *in vitro*. 291
3.3.3. Drug release from PMMA bone cement incorporating pSi. 292

**4. Discussion. 293**

**ACKNOWLEDGEMENTS**

I would like to thank the many people who have helped me in my research over the years and especially in the production of this thesis. Firstly I would like to thank Dr Susan Anderson for giving me the opportunity to undertake this research under her supervision and her advice and encouragement throughout the project. I am also very grateful to Professor Fran Ebling for his support and valued contributions to my written and presented work. I would like to thank Professor Leigh Canham for his considerable contribution to the underlying research on which I have based my research and for the opportunity to work with pSiMedica on this project.

I would like to thank all the staff at pSiMedica Ltd, particularly Dr Christian Barnett for help with the drug delivery aspects and Dr Armando Loni for help in preparing the pSi microparticles. I am very appreciative of the professional advice and friendship of my colleagues at the University of Nottingham, Ian Ward, Denise Christie, Marie Smith and Idris Sidique. I thank Dr Thomas Buss for his advice on mechanical testing techniques and the Medical Engineering team for their work in preparing mechanical testing moulds.

Discussions with consultant surgeons at the University of Nottingham's Institute for Clinical Orthopaedics, Miss Brigitte Scammell, Mr Ian McVickar and Dr Roger Bayston have been invaluable in the consideration of possible applications for this material. I am very grateful to Dr Julie Gough for provision of bioactive glass particles and to Dr Robert Layfield for his helpful assessment of my annual reports.

For their support and camaraderie I am indebted to all my friends, particularly Phil & Lynsey Lord, Jon McCrossan, Eoin Mount, Jonathan Alldis, Matthew Gascoyne, Matthew Jordan and Melanie Birkhead who ensured I took occasional breaks from my studies. I would like to thank my family, particularly my parents Tony and Lynn for their constant support, patience and understanding during the course of my education and especially during the period over which I have written my thesis.

## ABSTRACT

Silicon is an essential element in human nutrition, with the symptoms of a silicon-deficient diet being abnormal bone development (Carlisle, 1972). Similarly, animals and bone forming osteoblast-like cells *in vitro* show an increase in bone growth when supplemented with the soluble, bioavailable form of silicon, orthosilicic acid [$Si(OH_4)$] (Carlisle, 1988). Certain bioactive glass compositions can form a strong chemical bond with bone, doing so by dissolving to form a solution that includes orthosilicic acid which re-polymerises to form a hydrated silica gel layer that adsorbs growth factors, supports cell growth and acts a nucleation bed for bone mineral (Hench, 1980). Bioactive glass degradation products alone have also been shown to significantly enhance the activity of osteoblasts *in vitro* (Xynos *et al*, 2001).

Pure, crystalline silicon is not soluble in water or body fluids, but when electrochemically etched with hydrofluoric acid, nanoscale silicon hydride-lined pores are formed through the material which render it soluble in aqueous solutions, yielding orthosilicic acid (Canham, 1996). Porous silicon has therefore been proposed as a novel orthopaedic biomaterial, acting in a similar way to bioactive glasses. In addition, the long, narrow pores can be filled with pharmaceuticals, creating a dissolvable drug delivery material with release kinetics that are easily controllable by adjusting the pore morphology and drug loading density (Anglin *et al*, 2008).

This research aims to evaluate porous silicon (pSi) as a therapeutic biomaterial for bone tissue engineering applications in the form of a composite with the biodegradable polymer, polycaprolactone (PCL). pSi microparticles were incorporated into a polycaprolactone matrix and the composites characterised in terms of the ability to generate orthosilicic acids under various conditions. It was found that the composites released silicic acids at a rate proportional to the loading proportion of pSi, with 8% composites (20mg pSi in 230mg PCL) eluting ~400 $ng.ml^{-1}$ Si per day. At this composition, pSi increased the amount of calcium phosphate formed on the composite in a simulated body fluid and this had the morphology and molar ratio of biological apatite ($Ca:P \approx 1.5$).

The addition of 8% pSi to polymers enhanced the electroconductivity of hydrogels by two orders of magnitude and did not significantly affect mechanical strength. The release profiles of small molecules such as gentamicin and large hydrophobic proteins such as alkaline phosphatase were enhanced by pre-loading sample drugs into pSi rather than directly loading drugs into PCL. Crucially, the molecules retained their activity following release. Other proteins such as bovine serum albumin were adsorbed onto the surface silica gel layer, suggesting a method for localising growth factors onto biomaterial surfaces.

Osteoblasts responded well to 8% pSi-PCL composites, producing significantly more collagen and glycosaminoglycans *in vitro*. Collagen in the extracellular matrix (ECM) was also significantly more highly crosslinked as determined by the pyridinium content of ECM lysates and was more mineralised than the ECM on PCL alone. The breakdown products of pSi also significantly enhanced the osteoblastic phenotype of cells *in vitro*. This research demonstrates that porous silicon can be added to polymer-based materials to enhance their effectiveness as biomaterials for orthopaedic tissue engineering.

## ABBREVIATIONS

| | |
|---|---|
| **4-MUP** | 4-Methylumbelliferyl phosphate |
| **ALP / AP** | Alkaline phosphatase |
| **API** | Active pharmaceutical ingredient |
| **BMD** | Bone mineral density |
| **BMP / BMP7** | Bone morphogenic protein (7) |
| **BS** | British Standard, UK |
| **BSA** | Bovine serum albumin |
| **BSP** | Bone sialoprotein II |
| **C** | Tissue culture plastic control |
| **cDNA** | Complementary deoxyribonucleic acid |
| **CLSM** | Confocal laser scanning microscopy |
| **DEX** | Dexamethasone |
| **DMEM** | Dulbecco's modified Eagle's medium |
| **DMPT** | N,N-dimethyl-para-toluidine |
| **DNA** | Deoxyribonucleic acid |
| **EDX** | Energy-dispersive X-ray spectroscopy |
| **ESEM** | Environmental scanning electron microscopy |
| **FCS** | Foetal calf serum |
| **FDA** | Food and Drug Administration, US |
| **FGFR1** | Fibroblast growth factor receptor 1 |
| **GAG** | Glycosaminoglycan(s) |
| **GM** | Genetically modified |
| **HA** | Hydroxyapatite |
| **HEPES** | 4-(2-hydroxyethyl)-1-piperazineethanesulfonic acid |
| **HF** | Hydrofluoric acid |
| **HMDS** | Hexamethyldisilazane |
| **HOB** | Human primary osteoblast-like cells |
| **IGF** | Insulin-like growth factor |
| **IL-6** | Interleukin 6 |
| **ISO** | Organisation internationale de normalisation |
| **L32** | Ribosomal protein L32 |
| **MC-3T3** | Mouse calvarial osteoblast-like cells |

| | |
|---|---|
| **MMA** | Methyl methacrylate |
| **mRNA** | Messenger ribonucleic acid |
| **MW** | Molecular weight/mass |
| **OA** | Osteoadherin |
| **OC** | Osteocalcin |
| **ON** | Osteonectin |
| **OP** | Osteopontin |
| **PBS** | Phosphate buffered saline |
| **PCL** | Poly(ε-caprolactone) |
| **PDGF-Ra** | Platelet-derived growth factor receptor α |
| **PDLLA** | Poly(D,L-lactide) |
| **PGA** | Poly(glycolide) |
| **PGDF** | Platelet-derived growth factor |
| **PHA** | Polyhydroxyalkanoate |
| **PHB** | Poly(hyroxybutyrate) |
| **PHBV** | Poly(hydroxybutyrate-co-hydroxyvalerate) |
| **PLA** | Poly(lactide) |
| **PLGA** | Poly(lactide-co-glycolide) |
| **PMMA** | Poly(methyl methacrylate) |
| **pSi** | Porous silicon |
| **pSi-PCL** | Porous silicon – polycaprolactone composite |
| **PTH-R** | Parathyroid hormone receptor |
| **PTHrP** | Parathyroid-related protein |
| **PVA** | Poly(vinyl alcohol) |
| **ROS** | Rat osteosarcoma cells |
| **SA/V** | Surface area : volume ratio |
| **SBF** | Simulated body fluid |
| **SDV** | Silica deposition vehicles |
| **SEM** | Scanning electron microscopy |
| **T** | Thermanox |
| **TC** | Tropocollagen |
| **TGFβ** | Transforming growth factor β |
| **UHMWPE** | Ultra-high molecular weight polyethylene |

# Chapter One

-

# General Introduction

## 1.1. Bone biology.

The aim of the research presented here is to assess porous silicon as a bioactive agent which can be added to polymer-based implants to increase their osteoconductivity (bone-bonding ability). A supporting aim was to further elucidate the mechanisms and biochemistry of the effect silicon (in the form of silicic acids and silica) has on osteoblasts *in vitro* and determine a bioactive range of soluble silicic acids.

The following sections outline the normal structure and formation of bone *in vivo*, provide a brief history of orthopaedic biomaterials and summarise the emerging recognition of the importance of silicon in bone formation, repair and in functional biomaterials.

### 1.1.1. Bone structure – growth and repair.

Bone is a dynamic biological tissue comprising organic and inorganic matrix components, living cells and haematopoietic elements forming a functional and load-bearing structure for support of the body. Although a rigid composite material, through the combined action of osteoblasts (which deposit organic matrix) and osteoclasts (which degrade bone tissue), bone is continually reshaped and remodelled to increase strength in response to changing stresses throughout life. This remodelling action also allows fractures in bone to heal as damaged bone can be removed and replaced, reforming a strong structural tissue over a period of several weeks (Sommerfeldt & Rubin, 2001).

These repair mechanisms are very well documented and allow for physicians to enhance the rate and degree of bone repair through the inclusion of bone grafts or artificial strengthening materials during the healing process. As approximately 500,000 bone repair operations are performed annually in the United States, improvements in clinical treatment of complex fractures, incidents of bone loss and joint prostheses are continually being sought (American Academy of Orthopaedic Surgeons, 2009).

#### 1.1.1.1. Structure and biology.

Bone is a complex composite material which is structurally organised in several hierarchical levels during formation and exists in various forms depending on the material properties required. Two main types of bone, cortical (or compact) and trabecular (cancellous or spongy) bone comprise the majority of osseous tissue found in the adult body. A third type, woven bone, is found during development and in some areas of a restoring fracture site, as it is able to form quickly and *de novo* without a preliminary collagenous matrix on which to build (Sommerfeldt & Rubin, 2001). Woven bone is structurally weak, lacking the high orders of organisation found in other types of bone and is gradually replaced by compact or trabecular bone as the site matures (Sommerfeldt & Rubin, 2001).

Many bones are composed of combinations of these three types of tissue, depending on the location and stresses particular to the bone. Long bones, for example, consist of an outer layer or collar of cortical bone for strength with an inner medullary core of trabecular bone supporting the haemopoetic (bone marrow) matrix and allowing transfer of stresses such as those in the femoral head (**fig. 1.1**). Cranial and maxillo-facial bones are often plates, consisting of a sandwich of trabeculae surrounded by cortical-type bone (**fig. 1.2**).

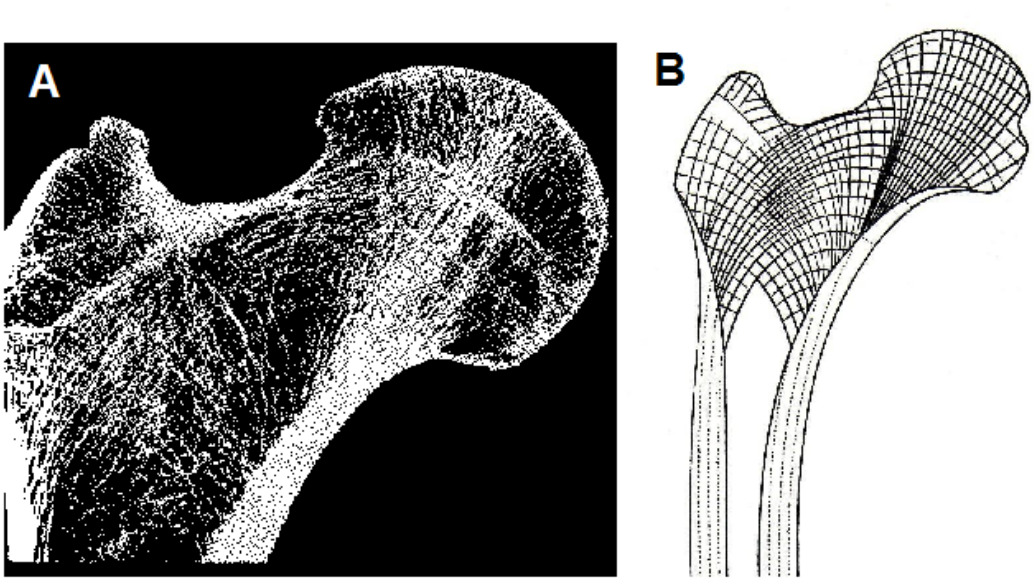


**Fig. 1.1. A**. Human femur in section revealing trabecular bone distributed along lines of tension and compression and, **B.** Stress trajectories in the human femur (from Thompson, 1992).

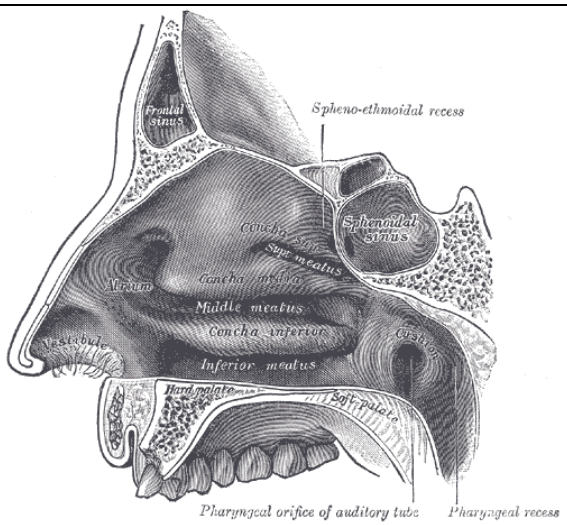


**Fig. 1.2.** Cross section of the maxilla, showing the typical arrangement of cranio-facial bones as dense, cortical-type plates with larger bones having trabecular cores (from Gray 1858).

Cortical bone is very dense, forming in sites where large loads are borne and providing support for locomotion and other motor functions. Cortical bone is arranged in osteons, a series of concentric rings surrounding the central Haversian canal, which contains blood vessels that are linked laterally by Volkmann's canals (**fig. 1.3**). Osteocytes surrounded by osseous matrix are found in lacunae (spaces) within these rings and are linked by long cellular processes through a series of pores known as canaliculae with an average diameter (in humans) of 259nm (Liyan *et al*, 2005), enabling the exchange of nutrients, growth factors and factors responsible for maintaining calcium levels within the body.

In contrast, trabecular bone density is only 5 - 60% and forms the inner core of most long bones and cranial plates. Trabeculae are rod or plate-like, in general no greater than 200 μm in thickness and about 1000 μm long. Although lacking the regular composition of cortical bone osteons, Jee (1983) denotes the trabecular packet as the basic structural unit of trabecular bone based on the fact that it is the basic remodelling unit, just as the osteon is the basic remodelling unit of cortical bone. Trabecular packets are regions of osteoclast activity, creating a lacuna typically 50μm deep and 1mm long which is re-ossified by osteoblasts. As a product of osteoclastic remodelling, trabecular packets only exist on the surface of secondary (mature) bone, are comprised of lamellae and joined to the adjacent bone by cement lines similar to those seen in cortical bone.

**Fig 1.3.** Images of cortical bone showing the concentric rings system surrounding longitudinal Haversian canals and interconnecting Volkmann's canals – osteocyte lacunae are visible as black dots. Narrow canaliculi connect osteocyte lacunae, allowing for exchange of nutrients, waste and extracellular messages (from Khoury & Esterhai, 2006).

Unlike osteons, trabeculae in general do not have a central canal with a blood vessel, although unusually thick trabeculae contain a blood vessel and some osteon like structure with concentric lamellae (Barou *et al*, 2002). Depending on the location and age of the bone, several types of trabeculae form, varying in thickness and interconnectivity and degree of anisotropy (**fig. 1.4**).

This latter characteristic - the formation of trabecular structures along lines of stress to add further support to bones bearing higher loads in certain directions such as vertebrae, demonstrates the ability for osteoclastic remodelling to enhance bone strength.

Both cortical and trabecular bone are surrounded by the periosteum - an envelope of fibrous connective tissue. In addition to providing blood supply and noinceptive (pain-sensing) innervation to the bone surface, the periosteum is the main store of osteoprogenitor cells and osteoblasts, thereby being particularly important in fracture repair.

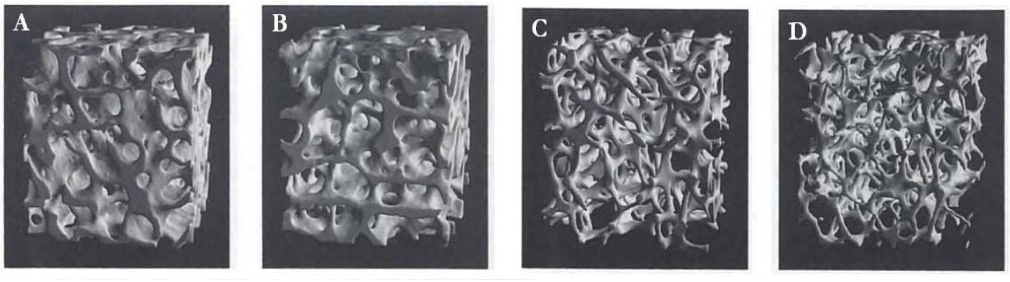


**Fig. 1.4.** Tomography models based on scans of trabecular bone from different sites (37 year old male), showing a) illiac crest, b) femoral head, c) Lumbar spine (LS4) and d) lumbar spine (LS2). These images illustrate the adaptability and anisotropic growth of trabecular bone in response to specific forces at each site (from Muller & Ruegsegger, 1997).

The periosteum is strongly bound to the bone matrix by strong collagenous Sharpey's fibers that penetrate the circumferential surface and interstitial lamellae (Kuroiwa *et al*, 1994). The inner medullary cavity of long bones is similarly lined by a thinner vascular layer, the endosteum, which also provides a source of osteoprogenitor cells and blood supply (Menton *et al*, 1982).

### 1.1.1.2. Cell types in bone metabolism.

Bone is a complex, highly ordered tissue which is dynamically remodelled by a variety of cell types throughout life. These cells can be classified into two main types, which have distinct lineages, and are responsible for a) bone deposition and homeostasis, or b) bone resorbtion. As a dynamic and continually adapted tissue, these cells are often both present and active concurrently, for example in a healing wound site or on either side of a trabeculum which is undergoing remodelling (**fig. 1.5**).

In addition to the cells responsible for bone metabolism, most long bones contain bone marrow which contains haemopoetic cells and adipocytes.

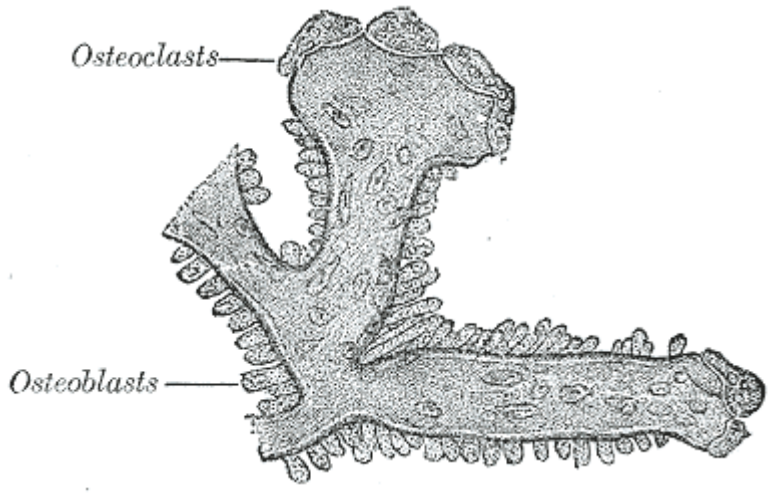


**Fig. 1.5.** Osteoblasts and osteoclasts on trabecula of lower jaw of calf embryo. From Gray's Anatomy, 1858.

#### 1.1.1.3. Bone formation and metabolism.

The cells responsible for deposition of bone matrix and homeostatic regulation of bone metabolism derive from osteo-progenitor cells of a mesenchymal lineage (Modder & Khosla, 2008; Liu *et al*, 2009). These pre-osteoblastic cells are found in large numbers, forming sheets in the inner part of the periosteum and the endosteum. Osteoprogenitor cells have been shown to attach to laminin-1, inhibiting the subsequent attachment of other cell types in rat calvarial *in vitro* cultures (Roche *et al*, 1999).

Osteoprogenitor cells and pre-osteoblasts are dividing cells, providing a source of osteoblasts for bone remodelling and repair following bone damage. Osteoprogenitor cells are also stimulated to differentiate into either osteoblasts or chondroblasts by the relative vascularisation of the tissue (Cormack, 1984). Upon receiving signals for differentiation, the pre-osteoblasts mature, losing the ability to divide and increasing the expression of osteoblastic markers such as Type I collagen and alkaline phosphatase (Leung *et al*, 1993).

Once differentiation initiates, osteoblasts begin to produce extracellular matrix components and allied substances involved in mineralisation of the osteoid, maturing into osteoblasts and potentially then osteocytes. The differentiation of

osteoprogenitor cells and pre-osteoblasts into mature, active osteoblasts is characterised by several morphological changes in the cell's structure and appearance, coupled to the expression of a variety of molecular markers, some of which are unique to the osteoblast (page 11). Mature osteoblasts are active secretary cells with prominent golgi apparatus and rough endoplasmic reticulum (Cormack, 1984) and are connected to each other and to underlying osteocytes via gap and adherens junctions (Cross, 1993).

Osteocytes are osteoblasts which become surrounded by osseous matrix and differentiate, changing from a bone deposition phenotype to one of bone homeostasis and maintenance of calcium levels (Teti & Zallone, 2009). After bone deposition, 10-20% of osteoblasts become encased in this way, becoming smaller and losing many of the intracellular organelles they possessed as osteoblasts - the remaining osteoblasts undergo apoptosis (Nijerwerde *et al*, 1996).

Osteocytes are well connected to each other and to osteoprogenitor cells and osteoblasts via extensive cellular processes which connect through tunnels in the osseous matrix known as canaliculi, such that nutrients, waste and intercellular messages can be exchanged via gap and adherens junctions. Osteocytes are sensitive to parathyroid hormone and calcitonin, indicating that part of their role is in maintaining plasma calcium levels and thereby governing the body's stores of this element (Billah, 1996).

The osteocyte lacuna is typically 10-20μm in diameter and both lacuna and canaliculi are filled with an annular fluid, thought to be a gel-like matrix composed of proteoglycans and other matrix molecules (**fig. 1.6**). This matrix resists fluid flow and assists in the osteocyte response to mechanical load which is though to be a major regulatory factor in bone remodeling (Weinbaum *et al*, 1994).

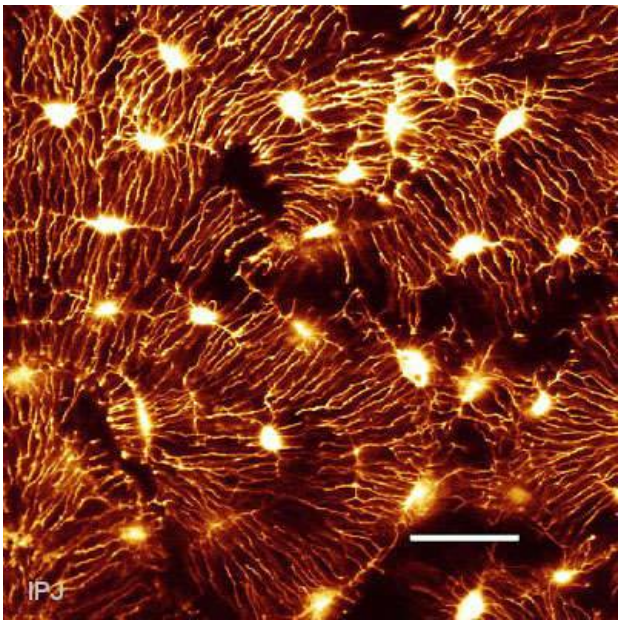


**Fig. 1.6.** Osteocytes in cortical bone after propyl-butadienylpyridiniumbromide dye (RH 414)-$H_2O$ staining and laromin C- embedding. Bar = 30 μm (from Meyle *et al*, 2002).

### 1.1.1.4. Bone resorbtion.

Osteoclasts are multinucleated cells that degrade and resorb bone and arise from haemopoetic cells of the monocyte/neutrophil lineage (specifically CFU-GM), rather than from the osteoprogenitor lineage (Vaananen *et al*, 2000; Billah *et al*, 1996). Osteoclasts can be histologically stained using acid phosphatase (Evans *et al*, 1980) and represent only a small percentage of the bone cell population, far fewer than osteoblasts (Nijerwerde *et al*, 1996).

Osteoclasts lie in small conical cavities called Howship's lacunae, formed from the digestion of the underlying bone and sealed by the attachment of the osteoclast's plasmalemma which is ruffled to increase surface area (Holtrop & King, 1977; **fig. 1.7**). The osteoclast releases hydrogen ions ($H_2O + CO_2 \rightarrow HCO_3^- + H^+$) into the cavity, acidifying and dissolving the mineralized bone matrix into $Ca^{2+}$, $H_3PO_4$, $H_2CO_3$ and $H_2O$. $H^+$ ions are pumped against a high concentration gradient by proton pumps, specifically a unique vacuolar-ATPase (Chatterjee *et al*, 1992). Additionally, several hydrolytic enzymes including collagenase and cathepsin K are released into the lacuna via lysosomes to degrade the organic matrix. Debris,

calcium and protease products are endocytosed by the cell allowing for processing of the vesicles in the cytoplasm before excretion. Regulation of osteoclastic differentiation and activity is by several hormones, including parathyroid hormone (PTH), calcitonin and interleukin 6 (IL-6) (Greenfield *et al*, 1999).

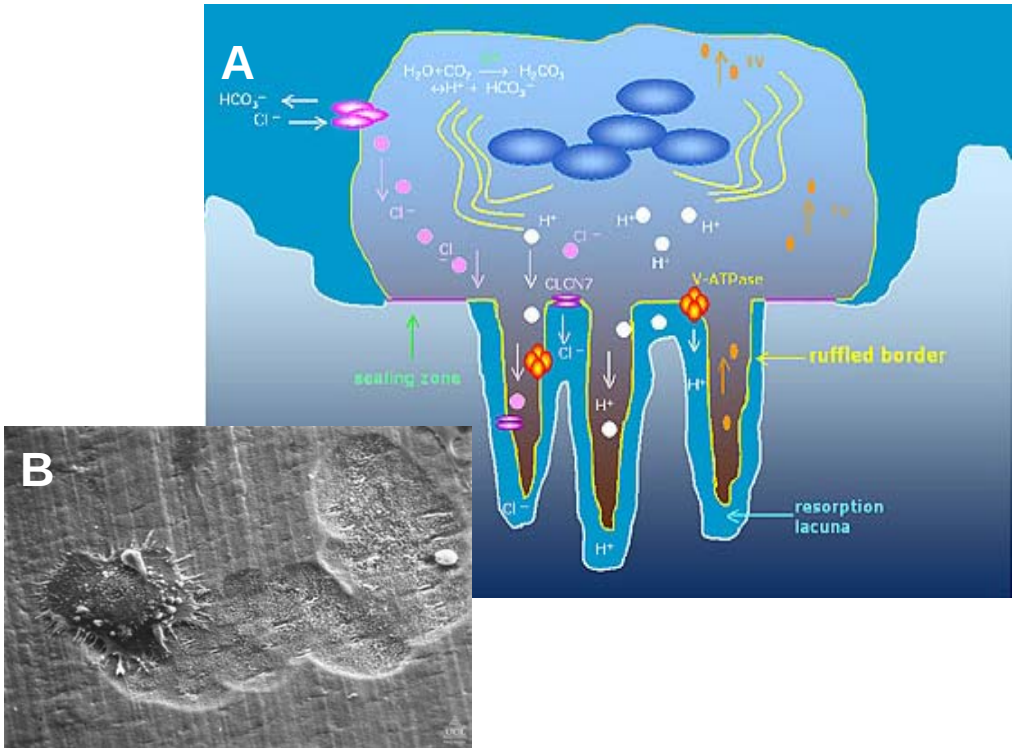


**Fig. 1.7. A**. Schematic of osteoclast action at a resorbtion lacuna. The sealing zone creates a border under which protons are pumped against a high concentration gradient to erode the inorganic phase of bone. The organic matrix is degraded by collagenases and other proteolytic enzymes (Vaananen *et al*, 2000). **B**. (*inset*) A resorbing osteoclast on bone showing distinctive phenotype and resorbtion trail (from the website of the Bone Research Organisation, 2008).

A familiar example of osteoclastic activity is in orthodontic tooth straightening using braces. Pressure exerted on the periodontal ligament of the tooth (by the braces) causes osteoclasts to absorb the bone which is then re-laid by osteoblasts to coincide with the reduced pressure on the opposite side of the tooth. Imbalances in osteoclastic activity can result in osteoporosis (osteoclast overactivity, reviewed in Liu *et al*, 2003), Paget's disease (Hasenhuttl, 1962) or osteopetrosis (insufficient activity, reviewed in Helfrich, 2003)

### 1.1.2. Molecular biology of the osteoblast.

Osteoblasts are characterised both by their morphology and by their expression of various unique molecular markers secreted in the formation of organic extracellular matrix (osteoid) and in regulating it's subsequent mineralisation. The expression of these molecular markers varies over time in response to the tissue site and exogenous mediators of activity. The differentiated and actively secreting osteoblast expresses the following proteins.

#### 1.1.2.1. Collagen.

Type I collagen is the most abundant type of collagen in the human body, being predominant in skin, lung and scar tissue and comprising ~90% of the organic component of bone (Nigg & Macintosh, 2000). The distribution and orientation of collagen is highly organised on several levels, reflected in the high tensile strength of bone (also see **fig 6.1**). The serially regulated structure of collagen is shown in **fig. 1.8.**

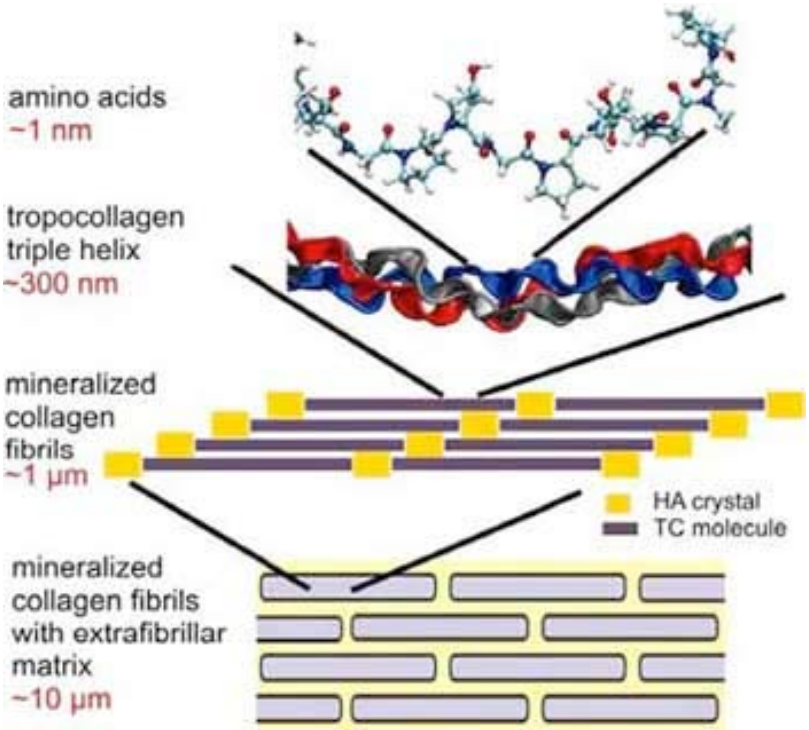


**Fig. 1.8.** Hierarchical organisation of collagen from the atomic scale to the microscopic, showing the beginning of mineralisation as the gaps between tropocollagen (TC) molecules act as nucleation sites for apatite crystals. From Buehler, 2007.

The tropocollagen superhelix is approximately 300 nm long and 1.5 nm in diameter and is comprised of three alpha polypeptide strands which individually are 'left-handed' and wind together in a right handed fashion to form a triple helix structure that is stabilised by extensive hydrogen bonding.

Collagen is rich is three particular amino acids: glycine, proline and hydroxyproline. Crucially to the structural role of collagen, glycine (the smallest amino acid with no side chain) is required as every third amino acid in the chain since the assembly of the triple helix puts this residue at the interior of the helix. Similarly, the side chains of proline and hydroxyproline always point out of the main axis of the helix, allowing for hydrogen bonding between adjacent helices.

Tropocollagen subunits spontaneously self-assemble into even larger macromolecules in the extracellular environment which are referred to as collagen fibrils (Hulmes, 2002), and are 10-300nm in diameter. Each tropocollagen subunit in the fibril is staggered from the next by 67nm (approximately a quarter of the length of a single subunit), giving the fibril a distinctive banded appearance when viewed using high-power microscopy (**fig. 1.9**). Fibrils can associate with various other proteins at this stage, including proteoglycans and other collagen types to form larger fibrillar bundles (fibres), which become increasingly covalently crosslinked as the tissue matures (Perumal *et al*, 2008).

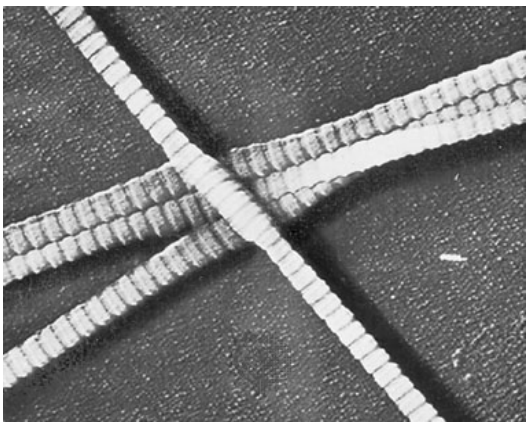

**Fig. 1.9.** A highly magnified electron micrograph of collagen fibrils stained with phosphotungstate, the cross striation can be resolved into several distinct bands due to the arrangement of the tropocollagen molecules within the fiber. From Encyclopedia Britannica (2009), micrograph by B.R. Olsen (Department of Cell Biology, Harvard Medical School, Boston, Massachusetts, USA**).**

Collagen fibrils can therefore be extremely heterogeneous in order to fulfil particular molecular and biomechanical roles, and so it is striking that type I collagen is bone is so highly organised.

#### 1.1.2.2. Bone sialoprotein II.

Bone sialoprotein II (BSP-II) is a large (72-80 KDa), flexible protein which is expressed during early matrix mineralisation, eventually comprising up to 8% of the organic mass of bone (Fisher *et al*, 1990). BSP is highly modified by post-transcriptional sulphation, phosphorylation and glycosylation, to the extent that up to 50% of the mature protein is comprised of these modifications, rendering the molecule highly heterogeneous. The function of BSP is not entirely clear, although Hunter and Goldberg (1996) propose that the protein acts as a nucleation site for apatite and mediates the extent of crystal growth along the collagen fibril depending on the particular post-transcriptional modifications.

#### 1.1.2.3. Osteopontin.

Osteopontin is a multifunctional 41 KDa protein secreted by numerous cells (such as myoblasts and macrophages, in a addition to osteoblasts and pre-osteoblasts) with roles in mineralisation and cell adhesion (Reinholt *et al*, 1990) particularly of osteoclasts in bone remodelling.

Osteopontin expression is stimulated by calcitriol, a modified form of vitamin $D_3$ and leads to the recruitment of immune cells, such as neutrophils (Koh *et al*, 2007) and autoimmune inflammatory responses in rheumatoid arthritis (Ohshima *et al*, 2002).

Osteopontin interacts with a large number of ubiquitously expressed cell surface receptors such as various integrins (Yokosaki *et al*, 2005) and CD44 (Weber *et al*, 1996) indicating an important role in both pathological and physiological processes involving leukocytes such as inflammation and bone remodelling.

### 1.1.2.4. Osteonectin.

Osteonectin is a 32.5 KDa protein which is post-translationally modified to become a 40-44 KDa glycoprotein with four distinct domains, two of which selectively bond calcium ions (Maurer *et al*, 1995).

Osteonectin binds strongly to hydroxyapatite (Romberg *et al*, 1986) and extracellular matrix proteins including collagens I, III, V, VIII (Sage *et al*, 1989), IV (Mayer *et al*, 1991), thrombospondin (Clezardin *et al*, 1988) and platelet-derived growth factors (PDGF-AB and PDGF-BB) (Raines *et al*, 1992). The role of osteonectin in bone remodelling therefore appears to be in initiating the calcification of collagen fibrils (Pacifici *et al*, 1990).

### 1.1.2.5. Osteoadherin.

Osteoadherin is a bone-specific keratan sulfate-containing 85 KDa glycoprotein that binds osteoblasts via their αvβ3 integrin (Wendel *et al*, 1998). In bone trabeculae, osteoadherin is found in a disulfide-bonded complex with osteonectin.

### 1.1.2.6. Osteocalcin.

Osteocalcin is a 5.8 kDa protein which is highly conserved between species, transcriptionally regulated by vitamin $D_3$ and modified (by γ-carboxylation) by vitamin K (Lee *et al*, 2000). Osteocalcin is the most abundant and well-studied of the non-collagenous proteins comprising osteoid (where it is adsorbed onto the mineral phase) and serves as a clinical marker for studies of bone metabolism, but despite this it's exact function and role in bone is slightly unclear (Lee *et al*, 2000).

Studies of osteocalcin knockout mice by Ducy *et al* (1996) exhibit a normal phenotype until about 6 months, after which bone production is markedly increased, suggesting osteocalcin has a role in maintaining bone turnover. Research on osteoclast recruitment and differentiation by osteocalcin-replete matrix particles (Glowacki *et al*, 1991) supports this, indicating that osteocalcin acts as a matrix-embedded signal for osteoclasts. In addition, studies in animal

models have shown that bone regulates glucose metabolism and fat mass via the uncarboxylated form of osteocalcin (Lieben *et al*, 2009)

Interestingly, plasma levels of osteocalcin are found to oscillate in a 24-hour period (Gundberg, 1985) with maxilla and mandible concentrations of osteocalcin varying the most over a day (Gafni *et al*, 2009) and indicating that bone remodelling occurs in a circadian pattern throughout the day.

**1.1.2.7. Alkaline phosphatase.**

Alkaline phosphatases are a family of widely expressed proteoglycan enzymes which exist in numerous tissues including liver and mucosa in addition to bone. Bone-specific alkaline phosphatase is identifiable by being post-transcriptionally modified to exhibit N-acetylglucosamine and N-acetylneuraminic acid Glycosaminoglycan motifs which can be precipitated by wheat lecithin to provide a measure of bone-specific alkaline phosphatase activity and therefore quantify bone metabolism for clinical applications (Leung *et al*, 1993).

Alkaline phosphatase is essential to the mineralisation of bone, recruiting inorganic phosphate from plasma to combine with calcium to form apatite crystals. As discussed later (page 18), alkaline phosphatase is secreted by osteoblasts in vesicles which accumulate high concentrations of inorganic phosphate and localise to the mineralisation front of the growing or repairing bone (Anderson, 1969).

### 1.1.3. Mineralization of bone matrix.

Extracellular matrices in all tissues are highly regulated and organised structures, and in bone the organisation of collagen, proteins and glycosaminoglycans forming the osteoid results in the tensile strength of the mature tissue.

Bone however is a composite material and derives its compressive strength and hardness from carbonated calcium phosphate crystals in the osteoid matrix. Sources give slightly differing values for this mineral proportion of bone mass, from 60% (Cormack, 1984) to 75% (Henrickson, 1997).

Phase pure hydroxyapatite (also referred to as apatite or hydroxyapatite, HA) is a crystalline mineral with the formula $Ca_5(PO_4)_3(OH)$, although the formula $Ca_{10}(PO_4)_6(OH)_2$ is more commonly used to acknowledge that two molecules comprise a single crystal, forming a hexagonal dipyramidal structure.

Apatites exist commonly in nature and are ranked at 5 in Moh's hardness scale, flanked by iron (4.5 – less hard) and titanium (6 – harder). Although bone mineral is almost universally referred to as apatite, the molecular ratios of hydroxyapatite and bone mineral differ. In bone, the molar Ca:P ratio is ~1.5, in contrast to 1.67 for crystalline HA (Landis and Glimcher, 1978). This is due to bone apatite being carbonated, with carboxyl groups substituting phosphate in the crystalline matrix.

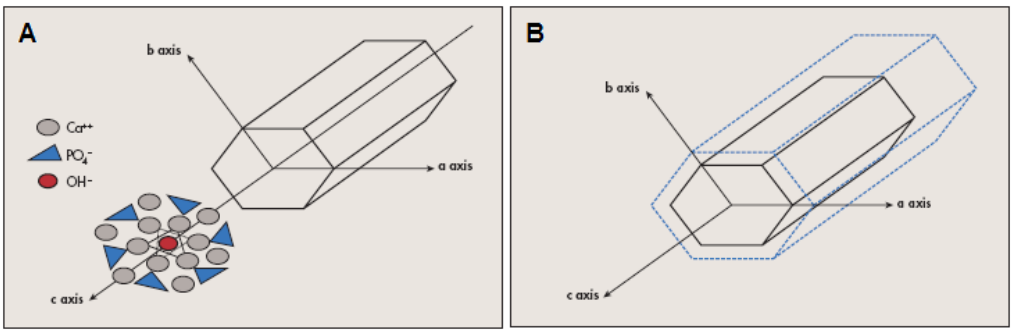


**Fig. 1.10.** Schematic illustration of the hexagonal bone HA unit cell found in bone (**A**) and the growth of the crystal (**B**), which is primarily along the c axis (longitudinally) but also along the a and b axes (width and thickness). (From Boivin, 2007).

In bone, hydroxyapatite crystals align along collagen fibrils, with the proposed nucleation site being the 35nm gap between N- and C- termini of the fibrils comprising the fiber (Buhler, 2007). However, it has been noted (Kristofferson *et al*, 2005) that a more primitive pattern of calcification is observed in juvenile epiphsyeal calcification, with crystalline deposits forming in a circle surrounding a central nucleation point. Bone mineralization in adults and non-woven types of bone is far more regular and organised, with a periodic distribution of 64-70nm and with the *c*-axis of the crystals being aligned (Robinson and Watson, 1952).

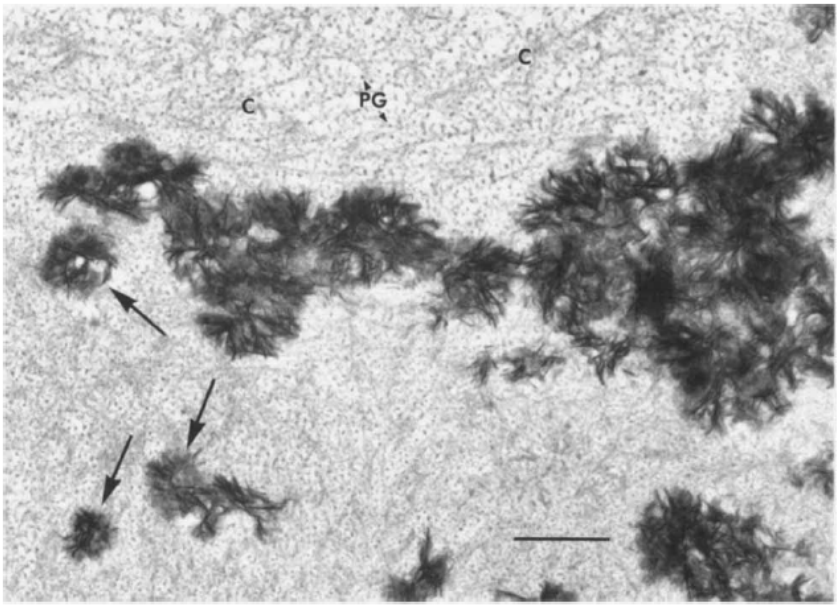


**Fig. 1.11.** A region of the extracellular matrix of growth cartilage from the tibia of a 3-week old adult chicken, showing the mineralisation of the matrix (arrows). Collagen fibrils (C) and proteoglycan aggregates (PG) are visible in this early stage of bulk epiphyseal mineralisation (bar = 500nm), from Christofferson and Landis, 1991.

Cortical and trabecular bone are shown to have some differences in mineral crystal organisation during development. Apatite crystals of 1-3 month old calves were shown by Kuhn *et al* (2008) to be larger (186 ± 3Å) than those found in trabecular bone (145 ± 5Å), with higher crystallinity and a correspondingly more apatite-like Ca:P ratio (1.61, cortical compared to 1.51, trabecular – hydroxyapatite is 1.66).

Whilst the organic osteoid is secreted by the osteoblasts, mineralization of the matrix is by the deposition of inorganic calcium and phosphate ions from the surrounding extracellular volume. It is thought that mineralisation is not a passive process and that extracellular vesicles have a role in the deposition of apatite crystals (Anderson, 2003).

These vesicles, first described by Anderson (1969), are 40-400nm in diameter, circular and trilammellar, with the main internal constituents being alkaline phosphatase and rod- or platelet-shaped particles of calcium phosphate and are localised in the mineralizing regions of bone. The role of the vesicles has not been fully elucidated but may form a mechanism for concentration of Ca and P ions.

In addition to the organic and mineral phase, bone is a highly hydrated tissue, with estimates of cortical bone being 10-20% water and trabecular bone being 30-50% water (in dogs) according to Boivin (2007).

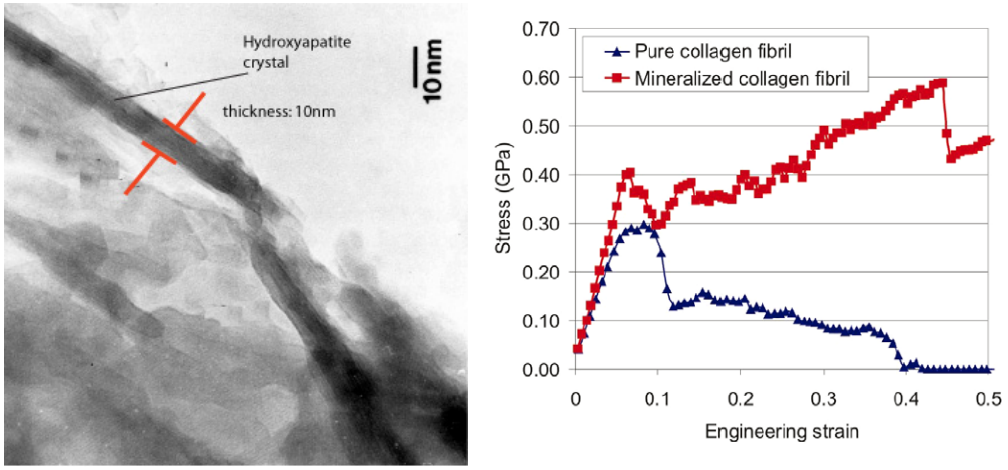


**Fig. 1.12. A**. High resolution electron micrograph showing a single bone apatite crystal (Hodgkinson, 1991). **B**. Stress-strain response of a mineralised collagen fibril and an unmineralised fibril (pure collagen) showing the much greater tensile strength of the mineralised collagen. The 'saw toothed' profile of the mineralised fibre results from intermolecular slip of tropocollagen in the fibril (From Bueler, 2007).

### 1.1.4. Mechanism of fracture repair.

Bone fractures heal naturally in the majority of cases due to the innate ability for bone to remodel itself and the mechanism of repair is a well-studied process. Following a fracture, healing progresses in four distinct stages:

1. Inflammation and hematoma formation
2. Neovascularisation and formation of soft callus (fibrocartiallge)
3. Hard callus formation (woven bone)
4. Remodelling

Immediately following a fracture, blood released from ruptured vessels in the bone and periosteum pools and coagulates, forming a haematoma. Over a period of several days, neovascularisation brings a new blood supply to the fracture site and macrophages invade the haematoma, endocytosing the damaged tissue. Concurrently, osteoclastic activity increases and fracture surfaces are abraded in a relatively large area surrounding the fracture site. Amongst the numerous cell types invading the site are fibroblasts which lay down type III collagen, providing temporary extracellular matrix for supporting neovascularisation – this network of blood vessels, fibroblasts, leukocytes and collagen in known as granulation tissue.

As the damaged tissue is endocytosed and removed from the site, fibroblasts, chondrocytes and osteoblasts begin formation of a callus. Composed of collagen and osteoid, the callus is very weak for the first 4-6 weeks and often requires support in the form of an external plaster cast or internal fixing pins, intramedullary nails or plates. Lacking the higher order ultrastructure of cortical/trabecular bone, this woven bone is generally much weaker, but as a temporary supportive structure serves to bind the outer surfaces of the fracture site during healing (Dutton, 2004).

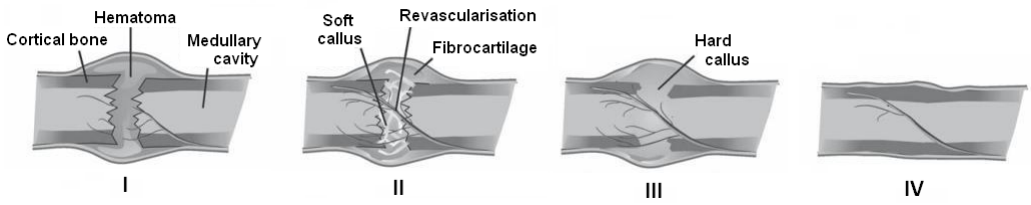


**Fig. 1.13.** Bone healing following a fracture proceeds through four distinct stages. Following inflammation, granulation tissue forms consisting of a fibrillar network and new blood vessels (I). A fibrillocartilagenous matrix forms to stabilise the wound (II) which subsequently becomes calcified, resulting in the formation of a bony callus (III). Over an extended period of time, the callus and surrounding bone are remodelled to restore the strength and function of the original bone. Redrawn from Sfeir *et al* (2005).

Once the fracture has been stabilised and is capable of bearing moderate loads, axial stresses caused by the bone's return to function cause osteoid to be laid down where it is needed and resorbed from the external callus. It is known that piezoelectric currents caused by compressing and decompressing bone matrix are somehow responsible for guiding remodelling, although the molecular biology behind this is presently unclear (Supronowicz *et al*, 2002).

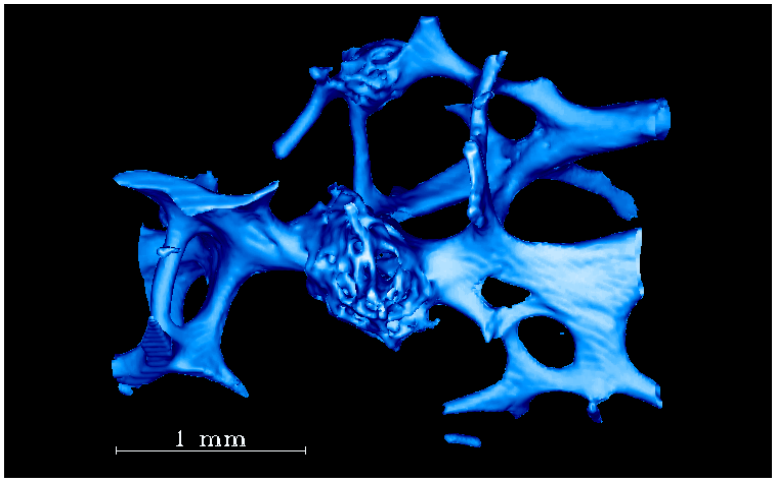


**Fig. 1.14.** Microtomography images of trabecular calluses. In trabecular bone microfractures caused by localised overloading, formation of a callus of woven bone allows the site to strengthen quickly and provides attachment sites for trabeculae and anastomosing spicules. From the University of Dortmund (2009).

## 1.2. Biomaterials and tissue engineering.

Throughout the history of surgery materials have been used in enterprising ways to solve medical problems and improve the quality of life for patients. In previous centuries materials were often chosen more for their familiarity or availability than for their biological compatibility, and so catgut and nylon sutures became predominant in surgery just as the use of stainless steel became universal in bone fixation.

Many modern and almost all historical biomaterials do not necessarily integrate fully with the body, examples including ivory tooth replacements, dental fillings, stainless steel bone prostheses and artificial heart valves. However, advances in the understanding of how materials function in the body and widespread investment in new technologies has revolutionised the opportunities for employing modern materials in novel functional roles.

Bioresorbable polymers have been particularly important in modern tissue engineering and surgical procedures, providing resorbable matrices for supporting tissue growth and allowing temporary fixation of medical devices without the requirement for surgical removal. Most resorbable polymers are aliphatic (open chain) polyesters with hydrolysable ester linkages which degrade to generate relatively non-toxic waste products such as carbon dioxide and water.

Tissue engineering encompasses the implantation of biomaterials to restore function to tissues following disease or injury. Biomaterials can be implanted as porous scaffolds to support tissue ingrowth from surrounding tissue, or cellularised *in vitro* prior to implantation. Uses for such materials are diverse, from vascular grafts (Kannan *et al*, 2005) to maxillo-facial reconstruction (Schliephake, 2009).

The need for advanced, biocompatible materials for tissue engineering becomes evident following an analysis of current techniques used for such treatments. Currently, most vascular grafts are performed using autologous (patient's own) saphenous veins (Dashwood & Loesch, 2009), but this technique has associated

complications following the necessary vein harvesting operation. A rise in the alternative use of Dacron (a resorbable polymer) mesh tubes for this operation has met with considerable clinical success (Kannan *et al*, 2005).

Similarly, maxillofacial and mandible reconstruction techniques often utilise bone harvested from three main sources: autologous bone, typically from the iliac crest; allograft bone from human cadavers; and xenografts from animal bone. Each of these procedures has associated difficulties, from the pain and morbidity of harvesting autograft bone to immune rejection and infection through using allografts and xenografts.

The use of non-toxic and resorbable materials which can be seeded with the patients own cells prior to implantation resolves these problems, but difficulties include a lack of surgical expertise in their usage, regulatory restrictions and issues regarding implant design and standardisation which are still unresolved for the majority of applications.

Examples of successfully applied tissue engineering are now appearing in the literature in greater numbers, including the artificial collagen-cell seeded bladder constructs (Atala *et al*, 2006) which have met with significant clinical success and raised public awareness of tissue engineering. Designs for the engineering of specific tissues share similar criteria, such as for supporting cell attachment and activity, but differ in terms of mechanical and morphological properties. Bone-specific materials for example must allow for osteoconduction (from surrounding tissue), osteoinduction (development of bone matrix throughout the implant) and neovascularisation to develop healthy bone. During this process, the material must also support mechanical loads as the bone returns to function.

Clearly substantial challenges remain for developing synthetic biomaterials for tissue engineering, but the advantages of using advanced materials for regenerative medicine are considerable. Technological advances in rendering polymeric materials more biocompatible through the inclusion of relevant bioactive agents such as Bioglass® and eluted or surface-bound growth factors have enhanced the ability for tissue regeneration (Chouzori & Xanthos, 2007).

### 1.2.1. Bioglass® and the response of osteoblasts to silicate biomaterials.

Since the discovery by Larry Hench in the 1960s that certain glass compositions can form a strong chemical bond to living bone, research has focussed on the properties of these materials which are responsible for their biocompatibility (Bosetti *et al*, 2001; Hench *et al*, 2000, 2001; Oliviera *et al*, 2002). 45S5 Bioglass® has a low silica content with a sodium flux and the calcium to phosphorous ratio of hydroxyapatite, the inorganic component of bone. This composition effectively induces the attachment and proliferation of osteoblasts around the implant site, leading to inclusion of the Bioglass® material into a callus of reconstructing bone supported by the implant, and strengthens the site against lateral movements and shearing forces. Further, as Bioglass® is bioresorbable, the implant is gradually dissolved and excreted as its ionic constituents.

Bioglass® is termed a class A bioactive material as it induces both extracellular and intracellular effects at the interface between implant and host tissue (class B bioactive materials illicit only extracellular responses, such as osteoconduction of bone growth along an interface). It has been established that twelve reaction stages are involved in the regeneration of bone by Bioglass®-based implants, including surface and genetic effects (Hench, 2001).

Implantation of a Bioglass® scaffold into a target site initiates the process of bone regeneration with stages 1-5 occurring at the material's surface within 24 hours of exposure to body fluids. Rapid release of soluble ionic species into the interfacial area results in the formation of Si-OH bonds and the formation of orthosilicic acid ($Si(OH)_4$). As this collects in increasing concentration around the surface of the implants, orthosilicic acid polycondenses into larger polymeric silicic acids, ultimately precipitating out of solution to form a hydrated silica gel (Hench, 2001).

Simultaneously, amorphous Ca, $PO_4$ and $CO_3$ ions are adsorbed out of solution onto the surface of the implant and crystallise into hydroxyapatite, $Ca_{10}(PO_4)_6(OH)_2$. The silica gel/hydroxyapatite layer adsorbs biological molecules from the surrounding tissue fluid, including growth factors, proteins and regulatory glycosaminoglycans, stimulating migration of macrophages and

osteoprogenitor cells into the region (Chai & Leong, 2007). Hydroxyapatite crystals in the silica gel reaction layer enhance attachment of filipodia and stimulate synchronised proliferation of osteoblasts which produce various growth factors and morphogens (Oliveira *et al*, 2008).

Osteoprogenitor cells have been found to colonise the surface of class A biomaterials within 48 hours and begin production of extracellular matrix components including type I collagen which quickly becomes mineralised, leading to maturation of osteocytes after 6-12 days of *in vitro* culture (Loty *et al*, 1999). Expression levels of insulin-like growth factor (IGF) axis system proteins, responsible for regulating certain key growth factors, are shown to increase by 300 to 500% over controls after only a few hours of exposure to the chemical extracts of 45S5 Bioglass® (Valerio *et al*, 2003).

Osteoblasts cultured *in vitro* on Bioglass® show a distinct morphology compared to cells grown on control substrates such as thermanox. As shown by Xynos *et al* (2001), osteoblasts grown on 45S5 Bioglass® for 2 days maintained a more compact shape, with numerous filipodia, dorsal ridges and microvilli, characteristic of cell activation and an osteoblastic phenotype. In contrast, cells grown on bioinert substrates for the same period were flattened, forming confluent sheets – features normally attributed to non-differentiated cell types. Analysis of cells cultured on Bioglass® reveals that the number of osteoblasts in the S and G2-M phases of the cell cycle (respectively DNA replication and cell division) were double that of cells grown on bioinert substrates (Hench, 2001).

Interestingly, cells grown on Bioglass® also exhibit much higher levels of apoptosis – typically between 5 and 7 times more cells being apoptotic after 2 days than control groups cultured on bioinert materials (Gough *et al*, 2003; 2004). This apparent regulation of cell cycle illustrates the effectiveness of Bioglass® as a biologically active material, capable of effecting the intracellular, genetic processes of osteoblasts. cDNA microarray analysis of 1,176 genes by Xynos *et al* (2001) demonstrated that the ionic products of 45S5 Bioglass® dissolution increased the levels of 60 transcripts twofold or more and reduced the levels of five transcripts compared to controls. Markedly up-regulated genes included RCL (a c-myc

responsive growth related gene), cell cycle regulators such as G1/S specific cyclin D1, and apoptosis regulators including calpain and DAD1. Other significantly up-regulated genes include the cell surface receptors CD44 and integrin β1, and various extracellular matrix regulators including metalloproteinases-2 and -4 and their inhibitors TIMP-1 and TIMP-2. In total Ca and Si ions in solution were shown to up regulate more than 200 genes by more than 150%.

Although cells grow more slowly on Bioglass® in the initial stages *in vitro*, cellular morphology and growth are much more osteoblastic in phenotype, indicating that these cells are responding in a similar way as they would in natural bone repair. This is supported by evidence that cells grown on Bioglass® synthesise alkaline phosphatase and osteocalcin, a non-collagenous extracellular matrix protein associated with the onset of mineralization, after 6 days in culture. After this period, osteoblasts have self-assembled into 3-dimensional structures known as bone nodules, comprised of cells and mineralised extracellular matrix – this is similar to the *in vivo* rate of nodule formation.

### 1.2.2. Silicon in biomaterials.

The importance of silicon incorporation in biomaterials has been appreciated for some time, particularly following studies of the dissolution products on osteoblasts directly *in vitro* by Xynos *et al* (2001). Despite this interest and numerous advanced techniques being employed to determine the inorganic crystallography of the silicon-hydroxyapatite interface and the reactions of silicon with cell and matrix components, no clearly descriptive theory exists. However, numerous theories have been tested experimentally and as none of these are exclusive, it could be that a combination of any or all of these explain the essentiality of silicon in osteogenesis and the enhancing effect silicon appears to have when incorporated into biomaterials.

The current theories can be broken down into those which suggest a role for silicon in adjusting the crystal microstructure of hydroxyapatite or its bioavailability and those which suggest that silicon affects the conformation and organisation of collagen and the osteoblast extracellular matrix.

### 1.2.3. Silicon substitution in hydroxyapatite.

Whilst bone mineral is generally referred to as hydroxyapatite, the molar Ca:P ratios found in bone are slightly different to phase pure HA (Landis and Glimcher, 1978). This results from the ionic substitutions for calcium and phosphate in the matrix with numerous other atoms and small molecules, such as magnesium and strontium for $Ca^{2+}$ (Ratner *et al*, 2004) with the majority of substitutions found in healthy bone being carbonate (0.79 $mmol.g^{-1}$), sodium (0.32 $mmol.g^{-1}$) and magnesium (0.17 $mmol.g^{-1}$) (Boivin, 2007).

In addition to carbonate, the hydroxyl residues can be replaced by chloride and fluoride (Boivin, 2007). This ionic substitution results from the relative instability of hydroxyapatite as a mineral and the large surface area of the crystal which is in contact with extracellular fluid (Boivin, 2007).

The mechanism of increased bioactivity of Si-substituted HA biomaterials has been studied extensively (Porter *et al*, 2004), yet no clear explanation exists. Frequent observations are made in the literature to the reduced grain size and solubility of Si-substituted HAs (Gibson *et al*, 2002), however, the grain size and solubility of carbonated HA is greater than Si-HA but shows much lower bioactivity (Porter *et al*, 2004).

Research has shown that increasing dietary silicon content in humans is associated with increased bone mineral density (BMD) in the cortical bone of hip in all subjects except post-menopausal women (Jugdaohsingh *et al*, 2004). Large differences in hip BMD (up to 10%) between the highest ($Si > 40$ $mg.day^{-1}$) and lowest ($Si < 14$ $mg.day^{-1}$) groups were observed, demonstrating both the importance of silicon in bone and showing the concentrations of bioavailable silicon that physiologically stimulate bone growth.

### 1.2.4. Silicon function in the osteoid.

In addition to silicon being substituted into the mineral phase of bone, research by Schwarz (1973) demonstrated that silicon is essential to the normal development of the glycosaminoglycan network, helping to stabilise the complex polysaccharide structures and forming crosslinks via silanolate (R-O-Si-O-R and R-O-Si-O-Si-O-R) bonds which regulate the structure and function of these molecules.

Almost concurrently, Carlisle demonstrated that silicon-supplemented embryonic chick bones showed a 100% increase in collagen content over silicon-low bones after 12 days in culture (Carlisle, 1974), whilst more recently Reffitt *et al* (2003) demonstrated that type I collagen synthesis increased in osteoblastic cells cultured in the presence of orthosilicic acid concentrations of 10 and 20 μM. Type I collagen mRNA has also been shown to increase significantly in osteoblasts seeded with orthosilicic acid concentrations from 5 to 50 μM (Arumugram *et al*, 2004).

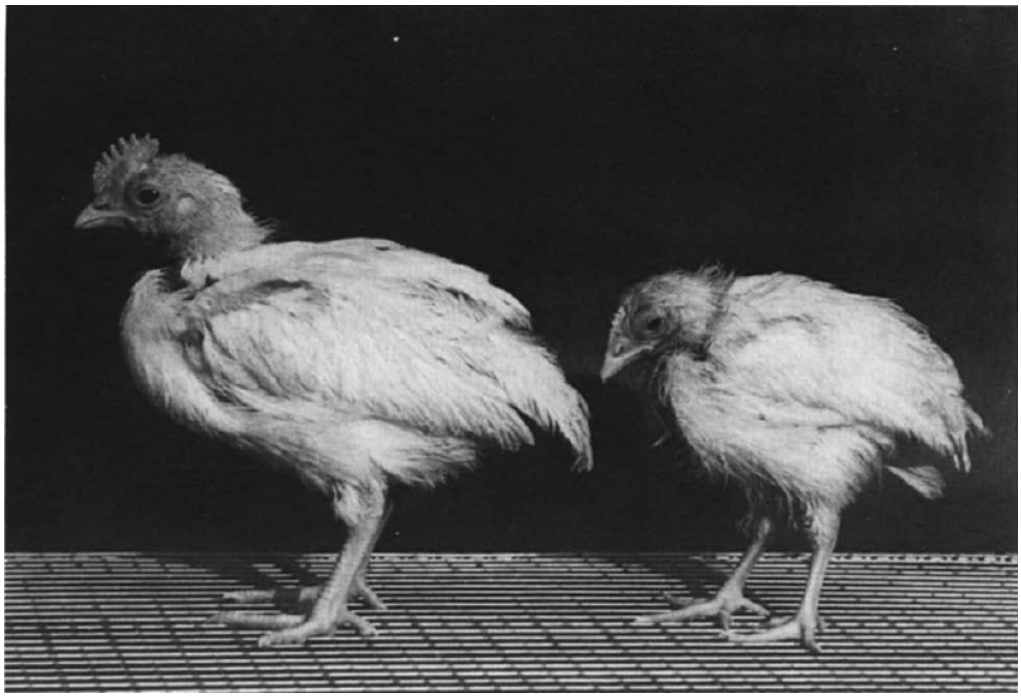

**Fig. 1.15.** Four-week old chicks showing normal growth with silicon-replete diet (left) and abnormal growth following a silicon-deficient basal diet (right), from Carlisle (1988).

Symptoms of silicon deficiency have been targeted by several researchers as a method for identifying biological processes with an apparent requirement for Si. Of these, abnormalities in skeletal development and adult brain diseases emerge as the most silicon-dependant mechanisms (Birchall, 1995). Studies of skeletal development in Si-deficient chicks reveal reduced circumference of leg bones with thinner cortex and reduced flexibility (Elliot *et al*, 1991). **Fig. 1.15** shows four-week old chicks fed a silicon-replete diet and a silicon-deficient diet, illustrating the profound physiological effects on development of Si-deficiency. Deficient chick skulls are abnormally shaped (also true of Si-deficient rats - Schwarz *et al*, 1973) with the cranial bones appearing flatter than normal, lacking the typical striated trabecular matrix and instead having a less organised, nodular pattern of growth characteristic of immature or woven bone.

Carlisle (1973) found that Si is localised in the active bone growth areas of young mice and rats (co-localised with osteoblasts) and increases together with the concentration of calcium in osteoid tissues. As bone matures, the level of (detectable) silicon diminishes as calcium levels approach those of fully mineralised bone. This indicates that silicon may have a role in development of organic matrix and the subsequent initiation of calcification.

This is further evidenced by the concentrations of glycosaminoglycans and collagen, which are depressed in Si-deficient animals whilst the mineral composition of bone is largely unaffected. Extracts of these glycosaminoglycans show that they are associated with silicon in several types of tissue (Shwarz *et al*, 1973), whilst other research has indicated that silicon is associated with organic phosphorus prior to calcification (Singh *et al*, 1985). These results indicate that silicon may have a role in co-coordinating glycoprotein phosphorylation reactions with collagen prior to growth of hydroxyapatite crystals.

**1.3. Silicon.**

Silicon is the eighth most abundant element in the solar system (Suess *et al*, 1956), and comprises 27.7% of the earth's crust by weight, second only to oxygen (46.6%) (Lutgens *et al*, 2000). In fact, silicon dioxide and silicates constitute the vast majority of minerals found on earth, in various crystalline, lithogenic forms being found as sand, amethyst, agate, quartz, rock crystal, chalcedony, flint, jasper, and opal in combination with other elements. Despite this abundance silicon is rarely found in biology, occurring as a trace element in higher animals and forming just 0.02% by weight of the human body (Emsley, 1998).

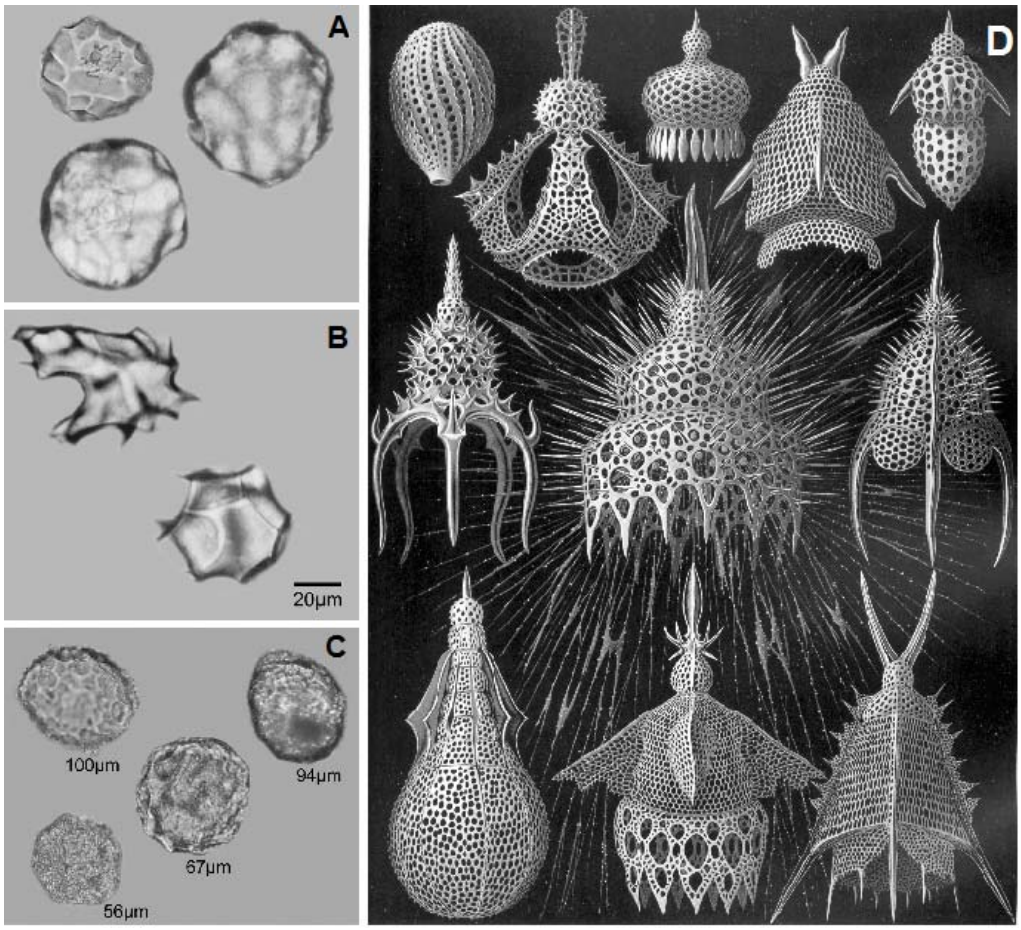


**Fig. 1.16.** Phytoliths from **A**. *Lagenaria siceraria* (bottle gourd), **B**. neotropical tree species and **C**. the squash *Cucurbita maxima* [from D. R. Piperno "Phytoliths: A Comprehensive Guide for Archaeologists and Paleoecologists" (AltaMira Press, Lanham, MD)]. **D** shows the 31st plate from Ernst Haeckel's *Kunstformen der Natur* (1904), depicting the silica frustules of radiolarians classified as *Cyrtoidea*.

Silicon in the form of silica is found in greater abundance in plants where it is used to strengthen cell walls in the form of phytoliths, and in the frustule surrounding marine algae, the diatoms and radiolarians (**fig. 1.16**).

### 1.3.1. The biogeochemical cycle of silicon.

Orthosilicic acid is the only form of silicon biologically available to higher animals (Sripanyakorn *et al*, 2005). It is formed by the action of acidified water on silica and silicate rocks exposed to terrestrial rain/groundwater or the action of seawater on marine rock and animal debris. The example mechanism of Albite (a simple feldspar) degradation by acidified water is illustrated in **fig. 1.17.A**. which results in the formation of silicic acid and Kaolinite (i), a mineral which can be further reduced to liberate more soluble silicic acid (ii). Silicic acid can also be produced by the action of water on pure silica such as quartz or glass as described in **fig. 1.17.B**.

**A** $2NaAlSiO_3O_8 + 2H^+ + 9H_2O \rightarrow Al_2Si_2O_5(OH)_4 + \mathbf{Si(OH)_4} + 2Na^+$
Albite → Kaolinite

$Al_2Si_2O_5 + 6H^+ \rightarrow 2\mathbf{Si(OH)_4} + 2H_2O$

**B** $SiO_2 + 2H_2O \rightarrow \mathbf{Si(OH)_4}$

**Fig. 1.17. A**. The reduction of albite by acidified water to kaolinite releases soluble orthosilicic acid. Kaolinite can react further with $H^+$ to produce more orthosilicic acid, illustrating a mechanism for silicic acid generation, from Worland (1997). **B**. The direct dissolution of silica in water to form orthosilicic acid.

Soluble silicic acids are absorbed by higher animals from four main sources:

1. Directly from silicic acid-containing drinking water.
2. From eating plants containing phytoliths.
3. From eating animals.
4. (In man) from drinking beverages made from plants.

The orthosilicic acid content of bottled mineral water is <10mg.l$^{-1}$ in the majority of samples tested (77%) by Giammarioli *et al* (1996), compared to an average of 19.2mg.l$^{-1}$ found in beer (Sripanyakorn *et al*, 2004). This is due to the brewing process involved in making beer in where plant phytoliths (which are found in large quantities in barley husks) spend some time macerated in contact with acidified, agitated water, allowing more silicic acid to pass into solution.

This effect is so great than in the average western diet beer (and bananas) forms the main source of bioavailable silicon for men (Jugdaohsingh, 2002). The silicon content of meat (food) animals is minimal, particularly as silicon in vertebrates is concentrated in the non-eaten tissues such as bone and aorta (Martin, 2007). The main routes by which silicon enters the human food chain are summarised in **fig. 18**.

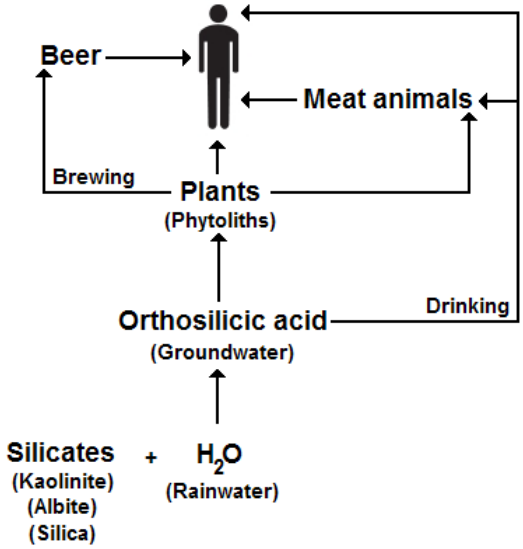


**Fig. 1.18.** Simplified schematic of part of the biogeochemical silicic acid cycle showing the main routes of bioavailable silicon ingestion for omnivorous humans.

### 1.3.2. Polymerisation of orthosilicic acid.

Orthosilicic acid remains in it's monomeric state for long periods in solution at 25°C when the concentration is lower than about 2x10$^{-3}$ M (Iler, 1979). At pH 8.5, 10% of orthosilicic acid is ionised which rises to 50% at pH 10. Polymerisation of

silicic acids is precipitated by the presence of hydroxyl groups when only fractional ionisation is present – high proportions of ionisation and therefore alkaline pH inhibits polymerisation of silicic acids (Al Mutaz *et al*, 2002).

Polymerisation occurs through condensation of silanol groups, formation of connecting siloxane bonds and partial dehydration as illustrated in **fig. 1.19** (Kashutina *et al*, 2008).

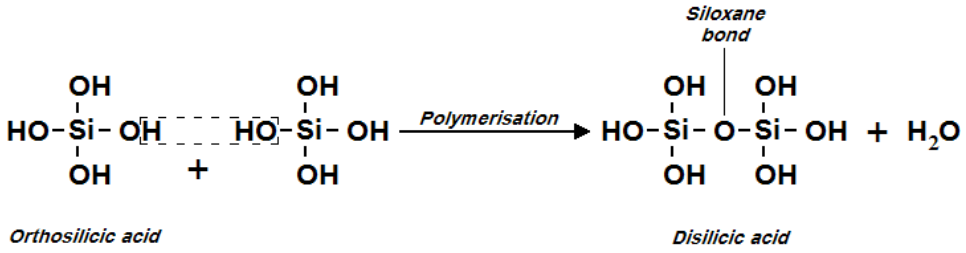


$$Si_mO_{(m-1)}(OH)_{(2m+2)} + Si_nO_{(n-1)}(OH)_{(2n+2)} \rightarrow Si_{(m+n)}O_{(m+n-1)}OH_{(2n+2m+2)} + H_2O$$

**Fig. 1.19. A**. Polymerisation of orthosilicic acid and, **B**. formation of polysilicic acids through condensation (from Kashutina *et al*, 2008).

Polymerisation continues following the formula $mSiO_2.nH_2O$ eventually forming colloidal particles of hydrated silica which can bond to organic molecules or form complexes with inorganic compounds such as aluminium and calcium oxide (Comb, 1996). As colloidal particles are formed, silanol groups dissociate to release $H^+$, leaving the silica colloid negatively charged (Kashutina *et al*, 2008).

In radiolarians and diatoms, silica frustules are formed by the organism increasing the concentration of aqueous orthosilicic acid [$Si(OH)_4$] in membrane-bound compartments known as silica deposition vesicles (SDVs) which polymerises to form biogenic silica. Transport of silicic acids against the concentration gradient into these compartments is by cell membrane-bound silicon transporters, such as those of the *sit* (silicon transporter) family in diatoms (Lopez & Coradin, 2003), which are shown to be sodium dependent. In addition, glycoproteins enriched with hydroxy amino acids are shown to associate with silica OH groups in the cell wall (Lopez & Coradin, 2003).

### 1.3.3. Technological applications of silicon.

Silicon is widely known as a semiconductor and through it's use in integrated circuits (microchips) forms the technological basis of the modern world. In addition, 55% of the world's total silicon production is used in aluminium-silicon alloy cast parts, particularly for the automotive industry, with a further 40% of total global consumption of silicon being turned into silicones for diverse uses, such as in waterproofing and in breast implantation.

The remaining 5% of elemental silicon is processed into high-purity monocrystalline wafers for electronics using the Czochralski method of pulling a growing crystal from a hot melt of silicon (**fig. 1.20.A**). Silicon produced in this way for electronics purposes is commonly 'doped' by addition of other elements (boron, phosphorus, arsenic or antimony) to produce n- or p-type wafers – even so, the purity of silicon in the wafer is 99.9999% (Widman & Dietrich, 2000).

Monocrystalline silicon wafers have a regular diamond cubic crystal structure with a lattice spacing of 5.430710 Å (0.5430710 nm). When cut into wafers (using a diamond-coated blade), the crystal surface is aligned in one of several orientations, defined by the Miller index with [100] or [111] faces being the most common (O'Mara *et al*, 1990) and which have a bearing on the wafer's anisotropic structural and electrical properties.

After cutting from a cylindrical block, a silicon wafer must be cleaned and polished with acids, and it is through experimental techniques in this process that porous silicon was first discovered.

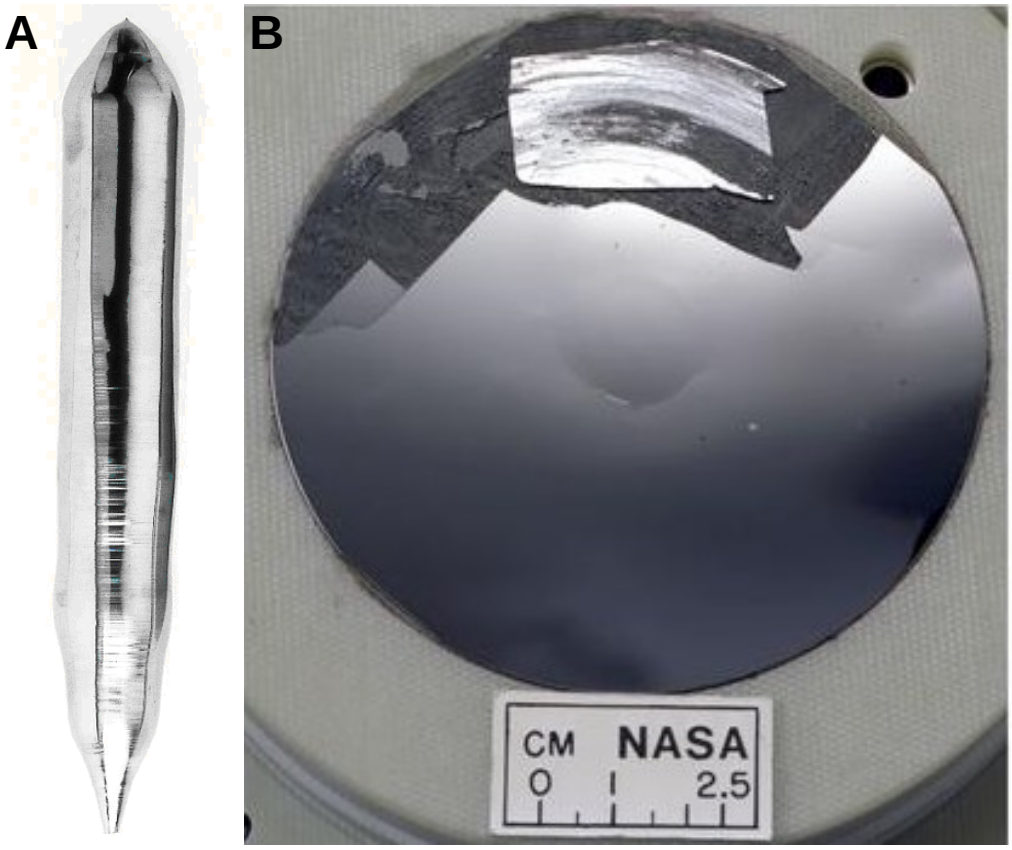


**Fig. 1.20. A.** Silicon monocrystal grown using the Czochralski method (© Dave King, Dorling Kindersley, From The Science Museum, London). **B.** Mirror finish silicon wafer (NASA Glenn Research Center).

### 1.4. Porous silicon.

Porous silicon was accidentally discovered in 1956 at the Bell laboratories in the US as an undesired product of experimental methods for polishing and shaping silicon surfaces for use as semiconductors (Canham, 1997). Under certain conditions the combination of acid etching under an anodic current resulted in the formation of a thick black, red or brown film on the material's surface. As this was regarded as a failure for the purposes of polishing wafer surfaces, the discovery was not further pursued until Leigh Canham reasoned that the resulting porous silicon may exhibit quantum confinement effects (Nash *et al*, 1994).

This effect occurs as the nano-scale holes in the acid-etched silicon wafer restrict the motion of electrons, particularly at the surface of the holes. As the size of the restricting hole decreases relative to the wavelength of the confined electrons, the energy of the electron increases. Coupled with the semiconducting properties which silicon naturally possesses, this leads to various unique physical properties that can be exploited for various applications, particularly in opto-electronic sensing (Parkhutik, 2000).

In addition to these novel electronic properties, the enormous surface area of silicon exposed by the pores relative to the volume (on the order of $500m^2/cm^3$) coupled with the covalently bonded hydrogen presented on the pore surfaces renders porous silicon soluble in water and aqueous media – a property which is unique for a pure silicon material (Canham, 1995).

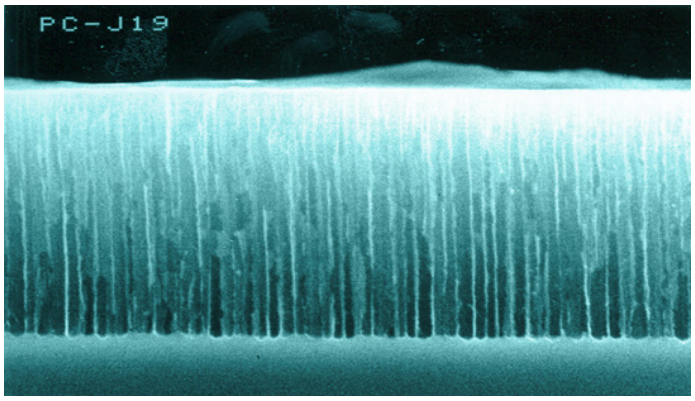


**Fig. 1.21.** Porous silicon surface of a silicon wafer (BioSilicon™, from pSiVida webpages).

### 1.4.1. Fabrication.

Several techniques for porosifying silicon are available, but the commonest method (used to produce pSi for this investigation) is through the anodisation of an '8 inch' silicon wafer (200mm diameter, 725µm thick). A platinum cathode and a silicon wafer anode are both immersed in a hydrogen fluoride electrolyte. A direct current is passed through the cell which corrodes the anode wafer, producing an even, porous layer (**fig. 1.22**). The addition of >15% ethanol to the electrolyte solution serves to dissolve hydrogen released during the reaction and homogenise the concentration of hydrofluoric acid within the developing pores, resulting in more uniform pore geometry (Halimaoui, 1997).

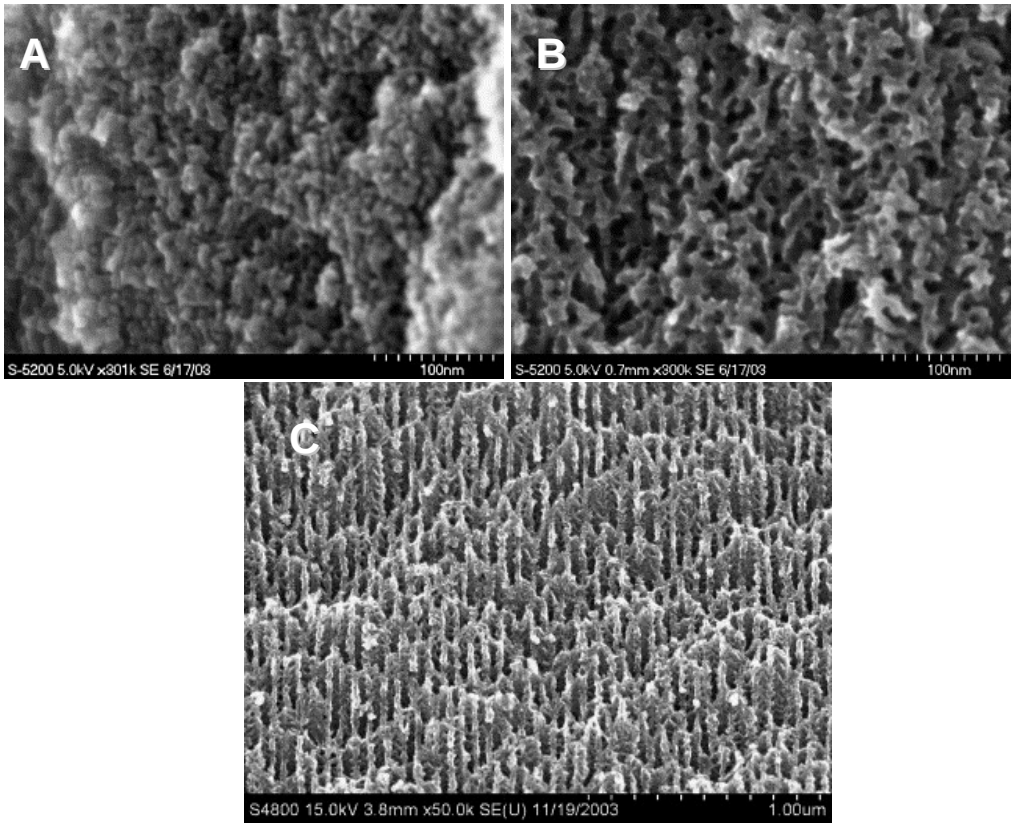


**Fig. 1.22.** The effect of etching current density on pore morphology in pSi. FESEM cross-section views of $n^+$-type silicon wafers made porous by anodization carried out at **A.** 18 $mA.cm^{-2}$ , **B.** 36 $mA.cm^{-2}$, **C.** 182 $mA.cm^{-2}$ in the dark in an ethanoic-HF bath. Channels vary from tortuous to straight with increasing current density, as does pore diameter from **A.** 6nm, **B.** 10nm, **C.** 30nm. From Pichonat & Gauthier-Manuel, 2006.

The pore diameter and depth can be controlled by HF concentration, with longer, narrower pores produced by concentrated HF solutions (Seo *et al*, 1994). Pore diameter is initially determined by the area of the surface oxide layer and so the $OH^-$ content of the electrolyte is also important (Seo *et al* 1994). Pore width is classified into three sizes, less than 2nm as nanoporous, between 2nm and 50nm as mesoporous and larger than 50nm as macroporous (Feng *et al*, 1994).

Once the wafer is fully etched the porous silicon must be dried by either supercritical drying, freeze drying or pentane drying. Water drying can be employed, although the high capillary stress forces incurred cause the porous wafer to crack, particularly when the wafer is etched beyond a certain critical thickness (Bellet, 1997). Although this is a major issue for opto-electronic applications, the microparticles required for biomaterials uses can be dried using water.

### 1.4.2. Degradation in water.

Due to the large surface area of Si-H ($500m^2.cm^{-3}$) on the surface and interior spaces of pSi, porous silicon is soluble in water and aqueous solutions, dissolving along the mechanism given in **fig. 1.23**.

$$Si + 4H_2O \rightarrow Si(OH)_4 + 2H_2$$

**Fig. 1.23.** Orthosilicic acid is liberated from the surface of the decomposing pSi in addition to hydrogen gas.

### 1.4.3. Biological activity.

Porous silicon has been shown to have good biocompatibility, supporting the growth *in vitro* of several cell types including osteoblasts (Whitehead *et al*, 2008), neurones (Johannsen *et al*, 2008) and hepatocytes (Alverez *et al*, 2008).

Low *et al* (2009) show that implantation of porous silicon under the conjunctiva of the rat eye results in the material becoming surrounded with a thin fibrous capsule after 8 weeks, with no erosion of surrounding tissue, inflammatory response or neovascularisation. When injected intravenously into mice, Park *et al* (2008) also demonstrated good *in vivo* compatibility: pSi particles were observed in liver, kidneys and spleen with normal tissue morphology. Macrophages were observed in liver at day one following injection implying that the small particles are endocytosed and naturally degraded, but after 4 weeks all tissues were normal.

Porous silicon is being studied by various groups for biological applications in drug delivery (Serda *et al*, 2009) and radioisotope intratumoral brachytherapy for treatment of inoperable cancers with a typically poor prognosis, such as pancreatic and hepatocellular carcinoma (Zhang *et al*, 2005). In this latter case, small particles of $^{32}$P-loaded porous silicon are injected into a tumour, which disperse to provide localised but very concentrated radiotherapy. pSi particles are cleared by degradation and excretion via the kidneys (Canham, 2001).

### 1.5. Aims of the investigation.

The overall aim of the research presented here is to assess porous silicon as a potential bioactive material which can be added as a bioactive agent to increase the osteoactivity of polymer-based prostheses for bone tissue engineering. A secondary aim was to further elucidate the mechanisms and biochemistry of the effect silicon (in the form of silicic acid and silica) has on osteoblasts *in vitro*.

Therefore, the research aims can be summarised as follows, each of which outline the themes for the following chapters:

1. Examine the behaviour of porous silicon-polymer composites in simulated body fluids in terms of degradation and rate of silicic acid release from the material.

2. Evaluate the response of human osteoblasts to pSi-PCL surfaces, degradation products and orthosilicic acid solutions *in vitro*.

3. Assess pSi-PCL composites as delivery vehicles for active pharmaceuticals.

4. Determine the physical, mechanical and electrical properties of pSi-polymer composites.

5. Characterise pSi-PCL behaviour in simulated physiological models.

6. Consider the potential applications of pSi-based biomaterials and test relevant examples.

Throughout this investigation, appropriate materials were used for outside reference, particularly bioactive glass – polymer composites and unmodified 'pure' polycaprolactone. These were used to compare pSi-composites to other biomaterials with existing applications in orthopaedics and tissue engineering.

# Chapter Two

-

# Characterisation of Porous Silicon – Polycaprolactone Composites

## 2.1. Introduction.

Porous silicon exhibits many of the same characteristics as Bioglass®, being able to release silicic acids into aqueous solution and form a surface layer of hydroxyapatite in simulated body fluid (Canham, 1996). Like Bioglass®, the mechanical properties of porous silicon are poor, and so a composite material was developed to exploit the bioactive properties of pSi within a strong but degradable polymer matrix.

The polymer that was ultimately chosen for this composite was polycaprolactone (PCL), a biodegradable aliphatic polyester which has existing uses in tissue engineering (Sahoo *et al*, 2002) and drug delivery (Sinha & Trehan, 1999), and is FDA approved for human *in vivo* use (Rohner *et al*, 2003). Alternative biodegradable polymers were also trialed, and are discussed in this chapter.

To test pSi – PCL composites for tissue engineering applications, a standardised method for manufacturing reproducable materials was required, with the following necessary design criteria:

- Fully homogenous pSi dispersal through polymer matrix.
- Similar proportions of crystalline/amporphous PCL phases for equivalent samples.
- Easily measurable surface area, volume and mass.
- Consistent high densities (lack of pores, voids or excessive surface topography).

Following the fabrication of reproducible composites, the prospective biomaterial was characterised via a number of accepted techniques relevant to the material. For pSi-PCL, this included quantification of silicic acid release (the proposed source of bioactivity) under varying simulated physiological conditions; measuements of biodegradation; and evaluation of calcium phosphate deposits on the material from acellular simulated body fluids.

This section of the research encompasses the initial tests for bioactivity performed on the composite. The aims of this chapter therefore were to:

- Develop a method for forming a pSi-polymer composite.
- Compare biodegradable polymer-pSi composites to determine the most suitable for the proposed orthopaedic applications.
- Evaluate pSi-degradation and silicic acid release from the composite.
- Evaluate calcium deposition on the matrix in acellular simulated body fluids.
- Compare the performance of the pSi composite to similar composites in the literature, eg. Bioglass®-polymer composites.

### 2.1.1. Choice of biodegradable polymer.

Research in materials science since the 1950s has focussed extensively on synthetic polymers derived from crude oil fractions, developing a huge array of plastics with diverse properties for numerous applications. Of these, a comparitively small number have so far been used for internal clinical applications – these generally being hard and unreactive plastics developed to act as removable sutures, casings for sensors, or as inert components of internal prostheses such as the ultra high molecular weight polyethylene (UHMWPE) acetabular cups used in total hip replacements.

However, certain synthetic plastics are more amenable to modern biomedical science, possessing properties which make them desirable for inclusion within the body. Of these, aliphatic polyesters such as polylactides (PLA), polyglycolide (PGA) and poly-ε-caprolactone (PCL) are being developed for therapeutic applications including biodegradable sutures, cranial burr plugs and also as devices for drug delivery (Sahoo *et al*, 2002). Another major class of biodegradable polymers under investigation are polyhydroxyalkanoates which are biologically synthesised naturally by bacteria and by genetically modified plants (Poirer *et al*, 1992).

### 2.1.1.1. Polylactic acid.

PLA is an aliphatic (open chain) polyester derived from lactic acid. It can be easily produced in a high molecular weight form through ring-opening polymerization using a stannous octoate catalyst.

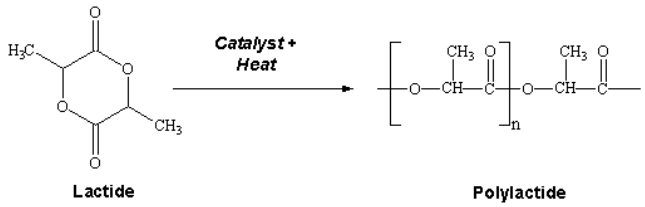


**Fig. 2.1.** Ring opening polymerization of lactide to polylactide.

Due to the chiral nature of lactic acid two distinct forms of polylactide exist: poly-L-lactide (PLLA) is the product resulting from polymerization of lactic acid in the L form. PLLA has a crystallinity of 13 - 37%, a glass transition temperature between 50-80° C and a melting temperature between 173-178°C (Park & Cima, 1996). The polymerization of a mixture of both L and D forms of lactic acid leads to the synthesis of poly-D,L-lactide (PDLLA) which is fully amorphous, possessing no crystalline regions (Ajioka *et al*, 1995).

Polylactic acid can be processed like most thermoplastics into fibre (using conventional melt-spinning processes, for example) and films. PLA is currently used in a number of biomedical applications, such as sutures, dialysis media and drug delivery devices, but it is also evaluated as a material for tissue engineering (Sahoo *et al*, 2002).

Importantly for these applications, polylactides are biodegradable by hydrolysis of their ester bonds under physiological conditions, generating decreasing-weight polymer fragments which, at a certain size limit, are able to move out of the material and be excreted (Wise, 1995). The rate at which these materials degrade in this way is related to their proportional crystalinity, with the more amorphous poly-D-lactides degrading more quickly. Therefore by varying the monomer ratios in the poly-D,L-lactide copolymers, the degradation rate can be controlled (Wise, 1995).

PLA is particularly attractive as a sustainable alternative to petrochemical-derived products, since the lactides from which it is ultimately produced can be derived from the fermentation of agricultural by-products such as corn starch or other starch-rich substances like maize, sugar or wheat. PLA is more expensive than many petroleum-derived commodity plastics, but its price has been falling as more production becomes available.

### 2.1.1.2 Polyglycolide.

Dimerisation of glycolic acid into glycolide forms the monomer for polymerisation of polyglycolide, the simplest linear aliphatic polyester. The resulting polymer has a glass transition temperature between 35-40°C and melting point of 225-230°C (Chujo *et al*, 1967). It is highly crystalline (around 45-55%) and thus insoluble in most common organic solvents except for highly fluorinated solvents such as hexafluoroisopropanol (HFIP; Hariharan & Pinkus, 2006).

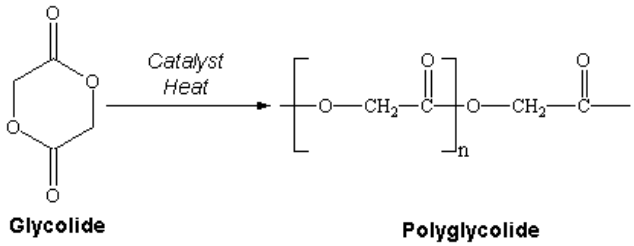


**Fig. 2.2.** Ring opening polymerisation of glycolide to polyglycolide.

PGA was the first material to be used as a synthetic, absorbable suture (marketed as Dexon in the 1960s by Davis and Geck, Inc.) and has been authorized for the production of implantable medical devices including mesh for wound closure in severely ruptured spleen (Vandershot *et al*, 1993; Louredo *et al*, 2005). Due to the high degree of crystalinity, pure PGA homopolymers have a high elastic modulus (~7 GPa) and are too stiff for use as sutures unless braided or co-polymerised with other monomers.

Degradation of the homopolymer occurs rapidly *in vivo*, with 50% loss of strength after 2 weeks and 100% loss of strength after 4 weeks, although the material is not fully absorbed until 4-6 months post-implantation (Kim *et al*, 2005). Degradation results in the production of glycolic acid which is non-toxic and easily broken down into $CO_2$ and water.

PGA/Polylactide co-polymers have been researched extensively as a way of tailoring the physical properties of the material. Vicryl, a 90/10 PGA/PLA co-polymer was marketed by Ethicon as a braided absorbable suture which degrades completely in 3-4 months. This is shorter than polyglycolide homopolymer and the material is slightly stronger initially (Bourne *et al*, 1988). The differences in degradation rate are considered to be due to the greater vulnerability to hydrolytic attack of the amorphous regions than the crystalline regions – co-polymers containing 25-70% mole percentage PGA are fully amorphous. A 70/30 L-lactide/glycolide copolymer is marketed as Lactomer (injection moulded surgical staples) by US Surgical (Hirashima *et al*, 1985).

### 2.1.1.3. Polycaprolactone.

PCL is a biodegradable polyester with a low melting point of around 60°C and a glass transition temperature of about -60°C (Sinha *et al*, 2004). PCL can be prepared by ring opening polymerization of ε-caprolactone using a catalyst such as stannous octoate.

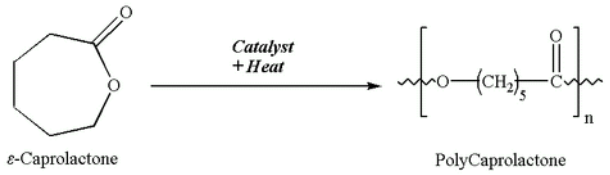


**Fig 2.3.** Ring-opening polymerisation of ε-caprolactone to polycaprolactone.

Polycaprolactone is used as an absorbable suture material in Europe and is under evaluation as a drug delivery device in the form of porous microspheres (Williams *et al*, 2005; Venugopal *et al*, 2005; Quinn *et al*, 2004; Sinha *et al*, 2004). PCL is semi-

crystalline with a low modulus (0.4GPa) and degrades slowly (>2 years for full absorbtion), although this can be dramatically reduced by inclusion of co-polymers such as poly-D,L-lactide (PDLLA). PCL co-polymerised with glycolide is marketed as a monofilament suture by Ethicon, Inc. (Somerville, NJ), under the trade name Monacryl. Co-polymers of ε-caprolactone and L-lactide are elastomeric when prepared from 25% e-caprolactone, 75% L-lactide and rigid when prepared from 10% ε-caprolactone, 90% L-lactide.

As with other biodegradable aliphatic polyesters, PCL degrades via hydrolytic cleavage of ester linkages within the polymer, forming smaller oligomers which results in the weakening of the material. Studies have demonstrated that polymer fragments with $W_M$ more than 8 KDa are unable to diffuse out through the semicyrstalline matrix, accounting for the slow rate of PCL absorption *in vivo*. As the average molecular weight of PCL used for tissue engineering research is 65-80 KDa, each oligomer must be cleaved several times before diffusible lengths are generated. The sole metabolites of PCL are ε-hydroxycaproic acid, water and $CO_2$, although small polymer fragments are removed from the implant site by macrophages and giant cell phagocytosis (Lam *et al*, 2008).

#### 2.1.1.4 Poly-3-hydroxybutyrate.

Polyhydroxyalkanoates (PHA) are a family of polyesters first isolated and characterised by the microbiologist Maurice Lemoigne in 1926. Poly-3-hydroxybutyrate (PHB) is produced by several bacteria including *Ralstonia eutrophus*, a gram negative, non-spore forming bacterium which thrives in millimolar concentrations of heavy metals. Capable of growing chemo-lithotropically by using molecular hydrogen as an energy source and $CO_2$ as a carbon source, *R. eutrophus* can also store carbon and energy as PHB which is subsequently used as a metabolite.

Although chemically different to polypropylene, the physical properties of PHB are similar, being stiff and brittle but having high crystallinity and a melting point of 180˚C. Although currently prohibitively expensive compared to other

biodegradable polymers, extensive research is being conducted in both academic and industrial institutions to biotechnologically manufacture PHB (and other PHAs) for commercial and medical applications.

In 1992, a team at the DoE Plant Research Laboratory, Michigan State University successfully introduced the three PHB forming genes into cress, thereby creating a harvestable method for producing biodegradable plastics from a renewable resource; without affecting the plant's growth, 14% of the dry weight of the leaves were PHB although did not exhibit quite the same stereoregularity as naturally occurring PHB (Poirier *et al*, 1995; Coghlan, 1992).

Monsanto, which now markets PHB (co-polymerised with hydroxyvalerate, another PHA) as Biopol have purchased all patents for making the polymer from ICI/Zeneca, although current adverse public opinion and media attention to GM crops have delayed news of Monsanto's plans for future marketing of PHAs.

In 2005, the US Environmental Protection Agency presented their 2005 Green Chemistry Small Business Award to Metabolix, a company involved in developing and commercialising a cost-effective method for manufacturing PHAs in general (and PHB in particular) using bacterial biotechnology.

#### 2.1.1.5. Choice of polymer.

Following these considerations, it was decided that polycaprolactone should be employed as the polymer component in the composite for the following reasons:

- Mechanical stability over a long time period (more than 6 months).
- Mass produced in standardised bulk volumes.
- Inexpensive (£46.80/100g, Sigma Aldrich, February 2009).
- Soluble in a range of solvents (including low-toxicity acetone).
- Low melting point (~60°).
- Existing use as a biomaterial.
- Existing use as a drug delivery vehicle.

As a means of validating this choice, comparisons between PCL, PLGA and PHB –pSi composites were made experimentally in this investigation.

### 2.1.2. Degradation of the composite in acellular fluids.

The dissolution of pSi in polymer composites into a surrounding volume is by hydrolysis of S-H bonds to generate free $Si(OH)_4$ which disperses into solution (Canham, 2000) or polycondenses onto the surfaces of the pSi, composite or reaction vessel walls. The degradation of PCL and pSi and the rate of silicic acid polymerisation are therefore respectively governed by hydrolytic and condensation reaction rates and so the chemical nature and conditions of the dissolution medium are important in determining silicic acid release rates and potential bioactivity.

Simulated body fluid (SBF) was developed by Kokubo *et al* in 1990 and is widely used to simulate the *in vivo* conditions to which a biomaterial is exposed by closely replicating the ionic composition of human blood plasma (see **table 2.5**). This approach is biologically relevant and allows for calcium deposition from the solution to be monitored, but due to the metastability of the solution, ionic and pH changes caused by the presence of hydroxycaproic and silicic acids, and precipitated calcium and phosphates can alter the balance of the solution in an unpredicatable and complex way (Rhee & Lee, 2007).

Phosphate buffered saline (PBS) is used widely in biochemistry and molecular biology to provide a non-reacting buffer solution in which to perform studied reactions at a buffered pH (typically pH 7.0). By comparing the degradation of pSi and pSi-composites in SBF and PBS, an analysis can be made of the effect of non-interacting (PBS) versus chemically active solutions (SBF).

More simply, using $dH_2O$ as the dissolution solution allows the chemistry of silicic acid degradation, condensation and polymerisation to be studied in effective isolation, with the formation of silicic acids and silica gel the only product of degradation.

The effect on porous silicon of the amount of fluid it is allowed to dissolve in has not been studied in depth, particularly smaller physiologically relevant volumes (<10ml). Whilst it is known that silicic acids polycondense in a concentrated solution to form insoluble silica, thereby establishing a dynamic dissolution-saturation-condensation flux in fluids, it has been reported (pSiMedica internal report, unpublished) that highly concentrated solutions inhibit further dissolution of the original porous silicon, with a putative 100 $\mu g.ml^{-1}$ threshold determining the upper concentration of orthosilicic acid which is metastable.

### 2.1.3. Comparison to other bioactive composites.

pSi-PCL composites are currently being studied by only one other group, affiliated with pSiMedica (Whitehead *et al*, 2008) at the Texas Christian University, USA). Consequently, comparison to the literature must be via similar materials such as Bioglass®-PCL composites. Studies of such composites have been reported by two groups, Chouzori and Xanthos (2007) at the New Jersey Institute of Technology, USA and Jiang *et al* (2005) at the University of Nottingham, UK.

Chouzouri & Xanthos report lower than expected bioactivity for composites containing up to 30% *w/w* Bioglass® particles, with an increased rate of polymer degradation following addition of Bioglass® particles to the polcaprolactone matrix. Other Bioglass®-polylactide composites have been studied, such as 40% Bioglass®-polylactide foams (Blaker *et al*, 2003) which act as a useful reference. Other biodegradable composites containing an inorganic phase such as silica, silicates and hydroxyapatite (Venugopal *et al*, 2008) are a useful comparison, but these are generally less bioactive than Bioglass® and the ionic dissolution products (cheifly silicic acid) do not reach the high concentrations in solution achieved by either Bioglass® or porous silicon.

Interestingly, the above mentioned composites have high proportions of the inorganic component, from 30% (Bioglass®) to 50% (hydroxyapatite), with correspondingly weaker mechanical properties as the strengthening polymer phase is reduced and subsequently degraded (Chouzouri *et al*, 2007; Jiang *et al*, 2005).

## 2.2. Materials and Methods.

### 2.2.1. Forming the composite.

Polycaprolactone (MW 65,000; Sigma, UK) was dissolved in acetone at 40°C in a 1:1 ratio (g/ml) and stirred thoroughly. pSi microparticles (10µm, 70% porous; pSiMedica, Malvern, UK) if being used were also added at this stage and stirred thoroughly to mix. After removal of the solvent by air drying at room temperature for 1-2 hours, the composite was cut into small sections and placed into the body of a 5ml polypropylene syringe (Becton Dickinson, UK). The syringe nozzle was sealed with adhesive tape and the mould placed upright in an incubator at 65°C to allow the sections to fuse together into a cylinder without voids.

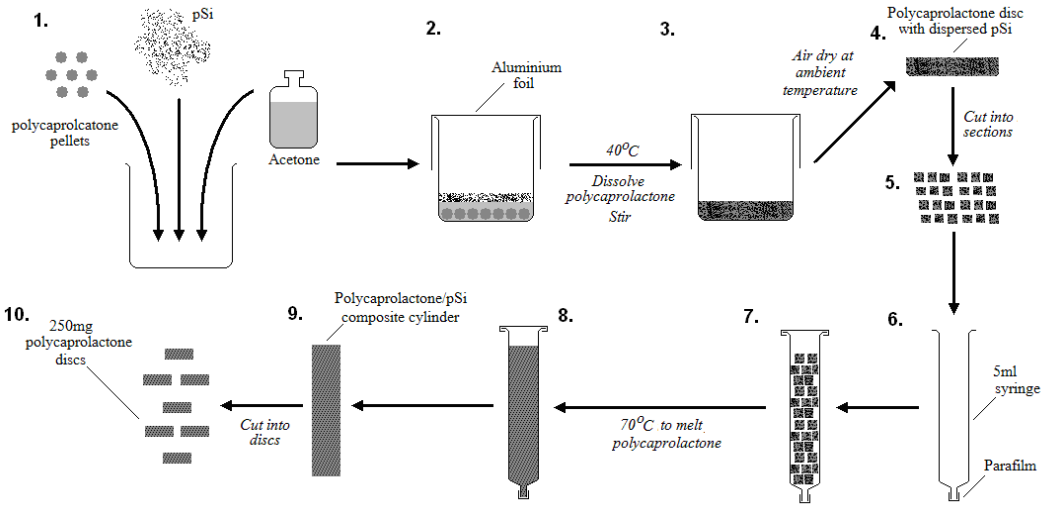


**Fig. 2.4.** Schematic for forming composite discs for testing. **(1)** Polycaprolactone and pSi microparticles were mixed with acetone, covered **(2)** and incubated at 40°C until PCL was fully dissolved and pSi dispersed. **(3)** The mixture was stirred thoroughly and the acetone evolved at room temperature **(4)** to create a solid composite which was cut into sections **(5)** and placed in a 5ml polypropylene syringe body **(6,7)**. After heating to ~70°C to melt together the composite **(8)** the cylinder was cooled and once solid was removed from the syringe body to evolve residual acetone **(9)**. The 10mm diameter cylinder was then cut into 250mg discs which were used for testing **(10)**.

Once melted together the composite cylinder was left at room temperature overnight to enable the evaporation of residual solvent. The composite cylinder was cut using a single-edged razorblade into discs 10mm in diameter, weighing 250mg ± 15mg. Throughout the fabrication process, only polyproplylene labware was used.

### 2.2.2. Determining bioactivity.

The following assays and protocols were used in this part of the investigation to characterise the composite and so determine bioactive properties and behavior in acellular fluids.

#### 2.2.2.1. Simulated body fluid.

Simulated body fluid was prepared as described by Kokubo *et al* (1990) with the compounds listed in **table 2.5** added to 1 litre $dH_2O$ in the order and in the amounts given. All reagents were obtained from Sigma, UK and clean plastic labware was used throughout preparation and storage. pH was adjusted to 7.4 using NaOH and HCl and the solution stored at 4°C for up to one month.

| **A** | Ion concentration ($mmol/dm^3$) | | **B** SBF Formulation | |
|---|---|---|---|---|
| | SBF | Human plasma | Reagent | Mass (g/l) |
| $Na^+$ | 142.0 | 142.0 | NaCl | 7.995g |
| $K^+$ | 5.0 | 5.0 | $NaHCO_3$ | 0.353g |
| $Mg^{2+}$ | 1.5 | 1.5 | KCl | 0.224g |
| $Ca^{2+}$ | 2.5 | 2.5 | $K_2HPO_4.3H_2O$ | 0.174g |
| $Cl^-$ | 147.8 | 103.0 | $MgCl_2.6H_2O$ | 0.305g |
| $HCO^{3-}$ | 4.2 | 27.0 | $CaCl_2.2H_2O$ | 0.368g |
| $HPO_4^{2-}$ | 1.0 | 1.0 | $Na_2SO_4$ | 0.071g |
| $SO_4^{2-}$ | 0.5 | 0.5 | | |

**Table 2.5. A.** Comparison of ion concentrations in 1x simulated body fluid and typical human blood plasma (Kokubo *et al*, 1990) and, **B**. the mass of reagents used to formulate the solution.

**2.2.2.2. Quantifying silicic acid.**

Silicic acid release from the composite was measured by placing discs into a specified volume (see **2.2.3**) of either $dH_2O$, 1x PBS or 1x SBF and fitting a screw-cap to ensure the volume was sealed. Samples of the incubating solution were taken at fixed intervals, measuring 20 – 400µl, dependant on the total volume of the medium and the incubation time.

Analysis was by a molybdenum (molybdate) blue assay, in which ammonium molybdate in solution reacts with silicic acid in the sample to form β-silicomolybdic acid (yellow) which is subsequently reduced to form a molybdate blue complex with a peak absorbance at 810nm.

Up to 400µl of the incubation solution was removed to a 1.5ml eppendorf tube and the volume made to 400µl with $dH_2O$. 100µl of a solution containing acidified ammonium molybdate (1g ammonium molybdate (IV) tetrahydrate and 3ml concentrated (17M) hydrochloric acid in 50ml total volume) was added and allowed to stand for 10 minutes. 500µl of a reducing solution (4g oxalic acid dihydrate,1.33g 4-(methylamino)phenol sulfate, 0.8g anhydrous sodium sulfite, 20ml concentrated sulfuric acid, total volume 200ml with $dH_2O$) was then added, the solution allowed to develop a blue coloration for 2-4 hours and the absorbance read at 810nm using a spectrophotometer zeroed using $dH_2O$.

Calibration of this assay was by a standard curve obtained using known concentrations of sodium metasilicate, from which absorbance at 810nm could be directly compared to Si in solution. Throughout this work, silicic acid is represented as mass units of silicon to avoid confusion between ortho- and polysilicic acids in solution.

**2.2.2.3. pH.**

pH changes in water and buffered solutions incubating porous silicon composites were analysed using a calibrated Hannah HI 120 pH meter and measured to three decimal places.

**2.2.2.4. Assessing silica gel formation.**

The presence of a hydrated silica gel was initially determined by measuring the changes in mass of composite discs incubated solely in $dH_2O$. Discs were weighed accurately to 0.1 mg before incubation and at time points throughout the experiment by being removed from solution and dried in a slide drying oven at 37°C for 24 hours prior to weighing.

Silica deposition was then estimated by subtracting the starting mass of the composite from the end point mass. The presence of the silica gel was confirmed using EDX, see below.

**2.2.2.5. Quantifying calcium.**

Polycaprolactone / composite discs that had been incubated in SBF were rinsed carefully in $dH_2O$ and stained for calcium using 1ml staining solution comprising 1% (*w*/*v*) alizarin red S (Sigma, UK) in $dH_2O$. The red-stained calcium was imaged using a bifocal dissecting microscope and then the calcium-alizarin complex solubilised with 2-5ml 2% (*w*/*v*) solution of cetylpyridinium chloride monohydrate (Sigma, UK) in $dH_2O$ to provide a purple solution with peak absorbance at 562nm which was measured using a spectrophotometer.

**2.2.2.6. SEM, ESEM and EDX.**

PCL / composite discs were removed from solution and dried thoroughly in a drying oven at 37°C overnight before being mounted onto aluminium stubs for scanning electron microscopy. As the discs were acellular, no further fixation or dehydration was required. The discs were gold coated for 3-6 minutes in a sputter coater and imaged using a Jeol JSM840 scanning electron microscope.

Discs were also imaged using a Phillips XL30 FEG-ESEM in which case no processing/coating was required. Samples were imaged using the auxiliary mode which allowed for energy dispersive X-ray spectroscopy to be performed on target regions of interest and the elemental composition of surface layers to be mapped.

### 2.2.3. Experimental.

The following sections detail the individual experiments that were performed.

#### 2.2.3.1. Composite formation.

pSi-PCL composites were fabricated as detailed in section **2.2.1**. A sample of the composite was removed at stage 5 (**Fig. 2.4**) and at stage 10 to compare the microtopography of the composites at each stage. The discs were gold coated in a sputter coater and imaged using a Jeol JSM 840 scanning electron microscope.

Silicic acid release from the stage 5 (termed 'freeze-cast') composite and the finished stage 10 (termed 'melt cast') discs was analysed by incubating 250mg ± 10mg discs of each in 20ml $dH_2O$ in screw-capped polystyrene tubes at 37°C for 10 days, with three repeats for each composite stage.

After 10 days the silicic acid concentration of a 400µl sample of the solution was determined using the molybdenum blue assay.

#### 2.2.3.2. Porous silicon – porosity and particle size.

Silicon wafers were porosified at pSiMedica (Malvern, UK) with porosities ranging from 49% to 82% and milled by hand for 15 minutes in a pestle and mortar in a fume hood. The resulting particles were seived using a series of graded meshes into fractions containing particles less than 38µm in size, 39 – 38 - 150µm and more than 150µm in size. The mass of each fraction was recorded.

The 38 - 150µm fraction was used to create 8% w/w composites with polycaprolactone, with a standardised 70% porous silicon (11µm particle size) used as a control. 1.0g ± 10mg PCL was heated to ~50°C with 1ml acetone in a polypropylene beaker until melted/dissolved and 80mg ± 2mg pSi microparticles were added. A further 1ml acetone was added to suspend the particles and the mixture stirred for 1 minute until homogenous.

The composite was cast in a 5ml polyproplyene syringe body at -20°C for 30 minutes and weighed to ensure full evaporation of the solvent. The 1.08g composite was cut into four 250mg ± 10mg discs which were pre-wetted in ethanol and placed in wells of a 24-well plate. 2ml freshly prepared simulated body fluid was added, the plate sealed and incubated at room temperature for 72 hours.

The silicic acid concentration of the SBF was measured using the molybdenum blue assay and calcium phosphate deposition on the disc measured using the alizarin red assay.

**2.2.3.3. Polymer type – PCL, PHBV and PLGA.**

A comparison was made between the behaviour of native polycaprolactone, poly(hydroxybutyrate-co-hydroxyvalerate) and poly(D,L lactic-co-glycolic acid) and their composites with pSi (using 8% *w/w* pSi).

PCL (MW 80,000, Sigma, UK) and PLGA (85:15, LA:GA, MW 50-70,000, Sigma, UK) were formed into 250mg discs and 250mg composite discs as described above. PHBV (8% hydroxyvalerate, MW 272.2, Sigma, UK) was formed into composites by melting the polymer in a glass beaker on a hotplate at ~180°C and mixing pSi microparticles into the molten polymer. 250mg discs of PHBV and PHBV-pSi were the made by melting small sections on top of each other on glass slides on a hotplate.

The resulting 250mg ± 10mg discs were accurately weighed and then incubated in 50ml $dH_2O$ at 37°C for 24 weeks in 50ml polypropylene screw-capped tubes. 400µl of the incubation solution was removed, replaced and tested for silicic acid using the molybdenum blue assay every week for 8 weeks and again at 12 weeks.

At 4, 8, 12 and 24 weeks the discs were removed from the solution and allowed to air dry overnight at room temperature before being observed and reweighed to assess mass loss/gain. At 4 and 8 weeks the pH of the solution was measured using a Hannah 120 benchtop pH meter.

#### 2.2.3.4. Relationship of composite mass to silicic acid release.

A quantity of 8% pSi-PCL was made and cut into twelve discs with accurately weighed masses ranging from 37mg to 157mg. The discs were incubated in 20ml $dH_2O$ in screw-capped tubes at 37°C for 10 days, at which point the solution was tested for silicic acid content using the molybdenum blue assay.

#### 2.2.3.5. Dissolution buffers and solution volume.

To compare the effects of using a metastable solution (SBF) to a pH buffered solution, PBS was used as a comparison. SBF was prepared as described in (2.1.2x) and PBS was prepared by dissolving one buffer solution tablet (Sigma, UK) in 100ml $dH_2O$. The water used in this investigation was millipore processed and all solutions were stored at 4°C for no longer than 4 weeks.

250mg ± 10mg 8% pSi-PCL composite discs were placed in 25ml screw-capped polystyrene universal tubes (10, 5 & 2.5ml samples) or 5ml polystyrene screw capped tubes (1ml samples) with three replicates per condition (n=3). 1x PBS or 1x SBF were added to each tube, with volumes of 1ml, 2.5ml, 5ml and 10ml.

These were incubated in a shaking water bath (70rpm) at 37°C and each solution was removed and replaced every 24 hours. The removed solution was tested for silicic acid using the molybdenum blue assay.

#### 2.2.3.6. Comparison of pSi-PCL to 45S5 Bioglass®-PCL.

45S5 Bioglass® particles were provided by Dr Julie Gough (University of Manchester) and used as a direct comparison for equal amounts of pSi in PCL composites. Bioglass®-PCL composites were produced in an identical manner to pSi–PCL composites containing 8% Bioglass® particles or 8% pSi (20mg per 250mg PCL) and cut into 250mg ± 10mg discs.

Bioglass®-PCL and pSi-PCL composite discs were placed in 20ml polystyrene screw-capped tubes, 20ml $dH_2O$ added and incubated at 37°C for 42 days. 400µl

of the incubation volume was removed and replaced every 14 days with the removed solution tested for silicic acid using the molybdenum blue assay.

#### 2.2.3.7. Long-term incubation.

250mg discs were created using PCL and 1 – 30mg pSi (70% porous, 11μm particles) using the method described above. The discs were incubated in 500ml $dH_2O$ at 37°C for 360 days with samples of the solution taken at 30, 210, 290 and 360 day intervals and measured for silicic acid content. The solution was changed completely at 4 and 8 months at which time the pH was measured and the discs dried overnight at room temperature and re-weighed.

#### 2.2.3.8. Morphology and composition of apatite formation.

250mg discs containing 0, 1mg, 10mg or 20mg of pSi were incubated in SBF for 28 days and the calcium phosphate layer analysed by ESEM and EDX. Seperately, 20mg pSi-PCL and PCL-only discs were co-incubated in 20ml $dH_2O$ in order to test how readily a silica gel layer forms on surrounding surfaces.

## 2.3. Results.

### 2.3.1. Forming the composite.

Polycaprolactone is highly viscous at temperatures below 100°C, but is soluble at room temperature in a range of organic solvents, including acetone, dichloromethane and chloroform. Of these it was determined that acetone was preferable for dissolving the polymer due to its low toxicity and high volatility, enabling the solvent to be quickly extracted from the composite at temperatures below the 60°C melting point of the polymer.

This method proved successful in forming composites by allowing a fully homogenous composite to be produced, but the mechanical properties of the material were poor and the composites often deformed after drying due to the micropores formed by evolving a large volume of acetone from the matrix (**fig. 2.6.A**). To overcome this a two-stage process was developed, with the first phase being dissolution of the polymer and mixing with pSi microparticles. At this stage the acetone in the composite was frozen at -80°C to allow the microporous morphology of the composite at this stage to be imaged using SEM (**fig. 2.6.A**).

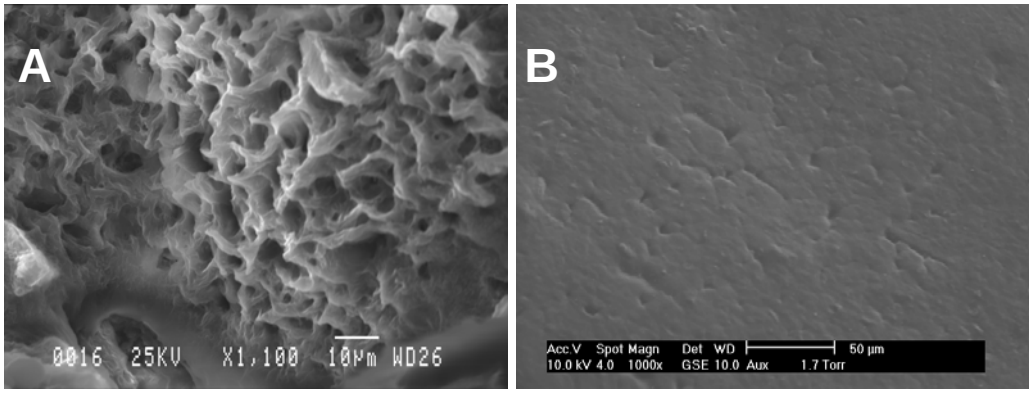


**Fig. 2.6.** Comparison of two methods of casting composites, each showing a 10mg composite. **A**. Composite produced by freezing an acetone-containing cylinder at -80°C to cast an open-textured microporous polymer. **B**. Composite produced by allowing the acetone to evolve at 70°C during the two-stage process outlined in **fig. 2.4** and following drying the construct at room temprature overnight.

The second phase of fabrication was to cut the composite into fragments followed by melt-casting into shape at 60°C. This method was found to produce a dense composite with high resistance to deformation (identified subjectively by manual handling of the material) with an approximately four-fold lower silicic acid release rate (for comparable composites, **fig. 2.7**) and is outlined in methods, section **2.2.1**.

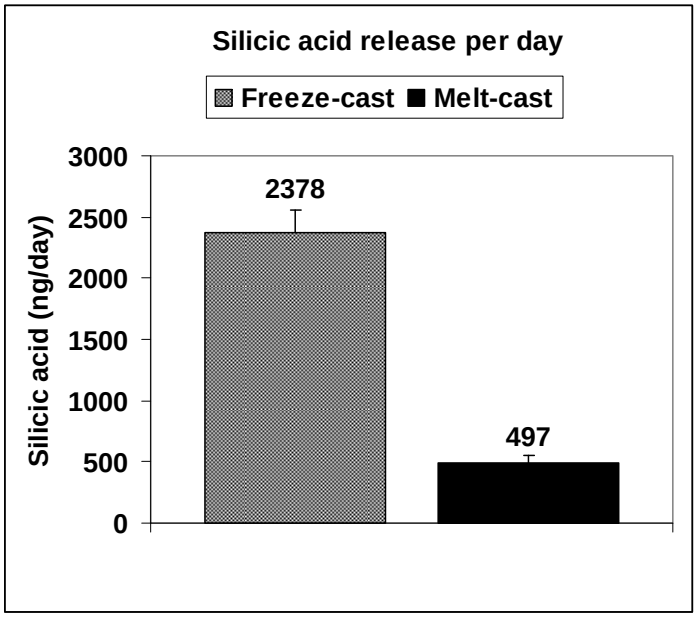


**Fig. 2.7.** Silicic acid release from freeze-cast (microporous) or melt-cast (dense) composite discs containing 20 mg pSi incubated in 20ml $H_2O$ for 10 days at 37°C. Bars show standard error of the mean, n=3.

### 2.3.2. pSi particle size.

Porosified silicon wafers were produced at pSiMedica (using the electrochemical etching process described above) in a range of porosities from 49.0% to 66.4% porous and ground in a pestle and mortar in a ventilated fume hood for 10-15 minutes. The resulting particles were seived using graduated mesh filters to obtain particle size fractions of ≤ 38μm, 38 - 150μm and ≥ 150μm. The mass of each fraction is shown in **fig. 2.8**.

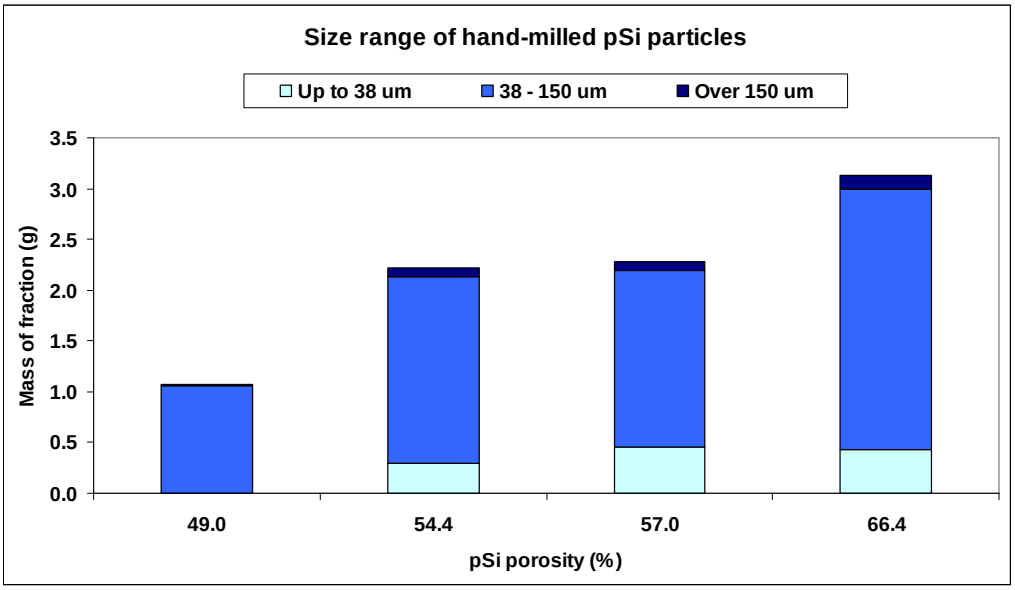


**Fig. 2.8.** Mass of particle size fractions resulting from hand-milling of porosified 9" silicon wafers. The percentage of the total mass comprising the intermediate (38 - 150µm) fraction was between 76.2% (for 57% porous silicon) and 99.1% (for 49% porous silicon).

The 38 – 150 µm particles were used for this investigation to evaluate specific pSi porosities, but were considered both too large and the size range too broad for optimal applications (**fig. 2.9.A**). At pSiMedica a standardised size range of 11µm (**fig. 2.9.B**) is used for most applications which has a very small distribution in particle sizes and small enough to allow uniform dispersal of the particles throughout the polymer phase (see **fig 6.7**).

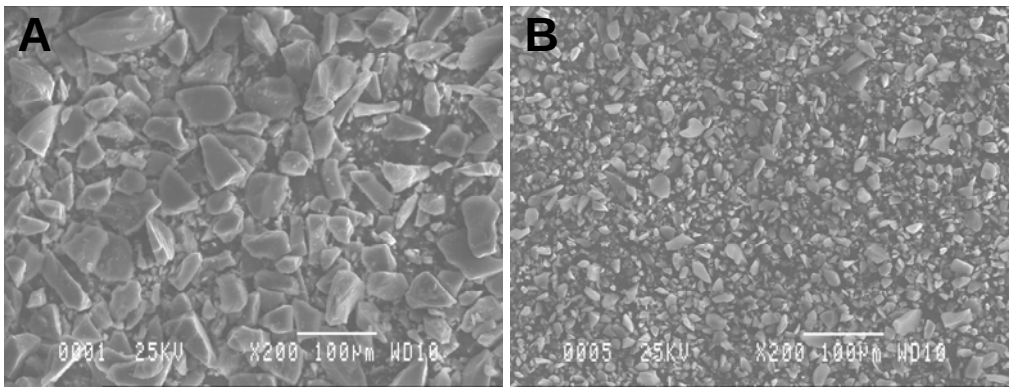


**Fig. 2.9.** SEM images of **A**. 49% pSi particles (38-150µm) and **B**. 70% (11µm) particles.

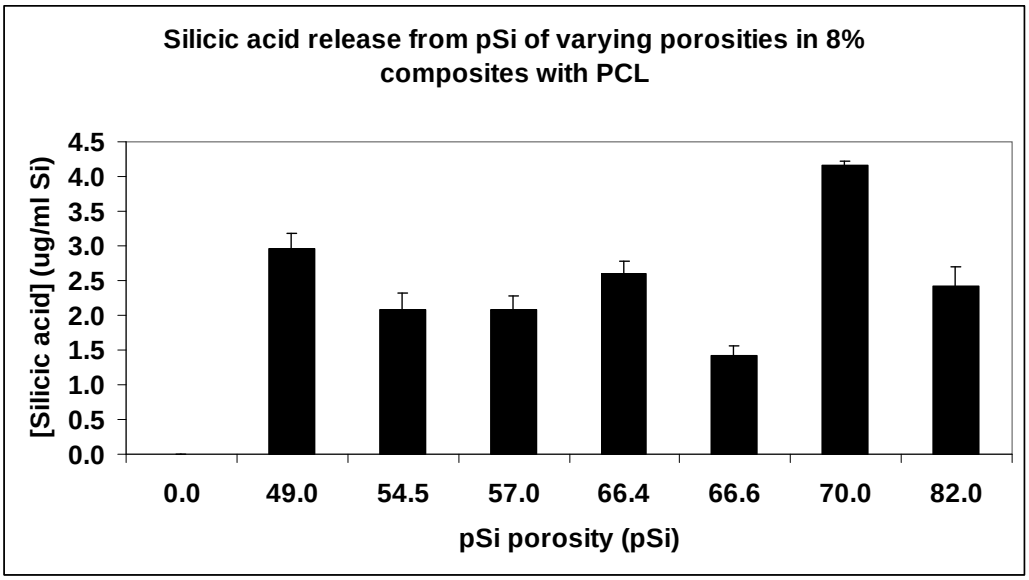


**Fig. 2.10.** Silicic acid release from 8% w/w (20mg pSi per 250mg disc) composites containing pSi microparticles of varying porosity. 70% porous silicon was obtained from pSiMedica and had a smaller average particle size (11µm) than the other porosities, which were hand-milled and seived. pSi release was evaluated over 72 hours in 2ml SBF at room temperature. Error bars are standard error of the mean, n = 4.

In addition, it was observed that pSi porosity does not have a linear relationship with silicic acid release rate when the particles are not of comparable sizes (**fig. 2.10**), with a linear regression coefficient ($R^2$) of 0.4996 ([silicic acid]/pSi porosity (%). Smaller particles of 70% pSi generated more silicic acid over 3 days in SBF than 82% porous silicon particles of a larger size, indicating that particle size (available surface area) has a greater effect on degradation rate/silicic acid release than porosity of the particles when the pores may be blocked/filled with polymer.

### 2.3.3. PLGA, PHBV and PCL.

The silicic acid release profiles and degradation rates of the three polmer-composites were somewhat different. **Fig. 2.11** shows the release of silicic acid from the composites over the initial 8 weeks of the experiment, and illustrates three different profiles for silicic acid release: sigmidal (PCL), exponential (PLGA) and linear, but erratic (PHBV).

Despite the differences in the trend lines, the concentrations of the two aliphatic polyesters PCL and PLGA were similar at each time point, whereas PHBV released consistently less silicic acid into solution. Analysis of the masses of each composite in comparison to the basic polymer (**fig. 2.12**) illustrates the differences in degradation rate which partially describe the difference in silicic acid release.

All basic polymers showed a loss in mass over 24 weeks: PCL lost ~0.4% of the original mass after 24 weeks, PHBV lost ~1.0% and PLGA lost 80-100% of original mass by this time. During the initial period of the experiment (up to 8 weeks), PLGA increased in mass – this was discovered to be due to a hydrated layer inside the material which remained following drying at 40°C for 24 hours.

PCL-pSi and PHBV-pSi composites showed an increase in mass despite the combined losses from polymer and pSi degradation, which is thought to be through the deposition of hydrated silica gel on the surface of the material, adding to its overall mass. The mass increase due to silica formation was greatest for PHBV-pSi despite the lower solution concentrations of silicic acid for these samples, indicating that condensation of silicic acid to silica occurred within the material prior to release of silicic acids into solution.

PLGA-pSi was discovered to degrade extremely rapidly, with two out of the three sample discs degrading completely within 8 weeks and all discs totally degraded within 12 weeks. Mass loss was also consistent for these samples with no hydrated layer inside the material, possibly due to the porous nature of the composite at the 10μm particles of pSi were dissolved into solution.

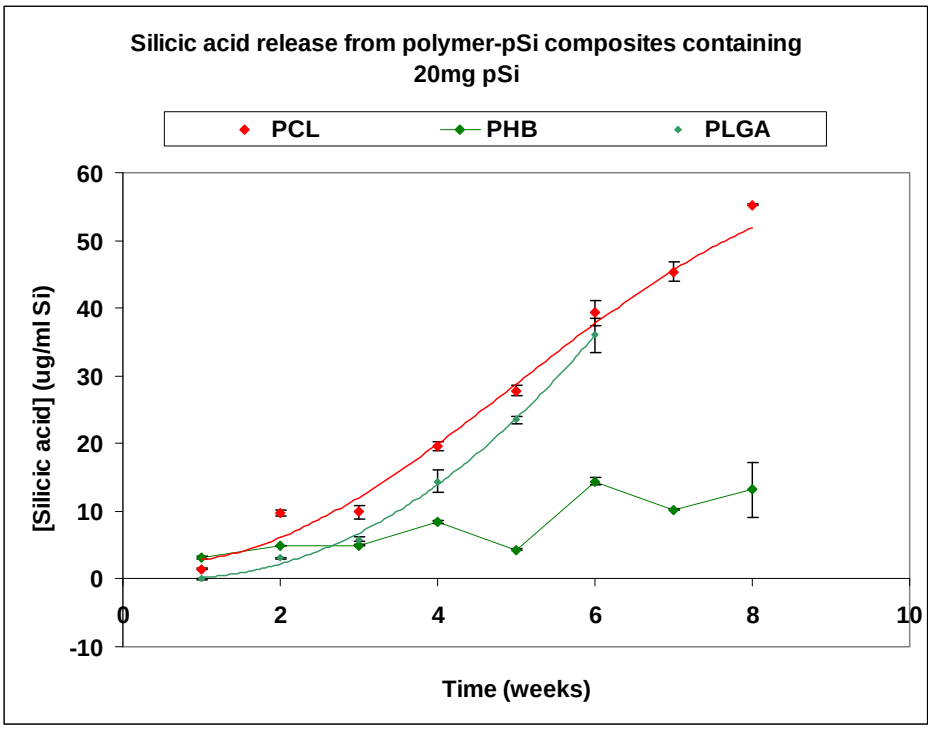


**Fig. 2.11.** Silicic acid release profiles of 8% *w/w* pSi-composites showing polycaprolactone (**red**), poly(lactic-*co*-glycolic acid) (**blue**), and poly-3-hydroxybutyrate (**green**) composite summed silicic acid release over 8 weeks into 50ml $dH_2O$. PLGA data only shown to 6 weeks as two out of three discs had totally degraded by 8 weeks. Bars show standard error of the mean, n=3; $R^2$ for trendlines > 0.99.

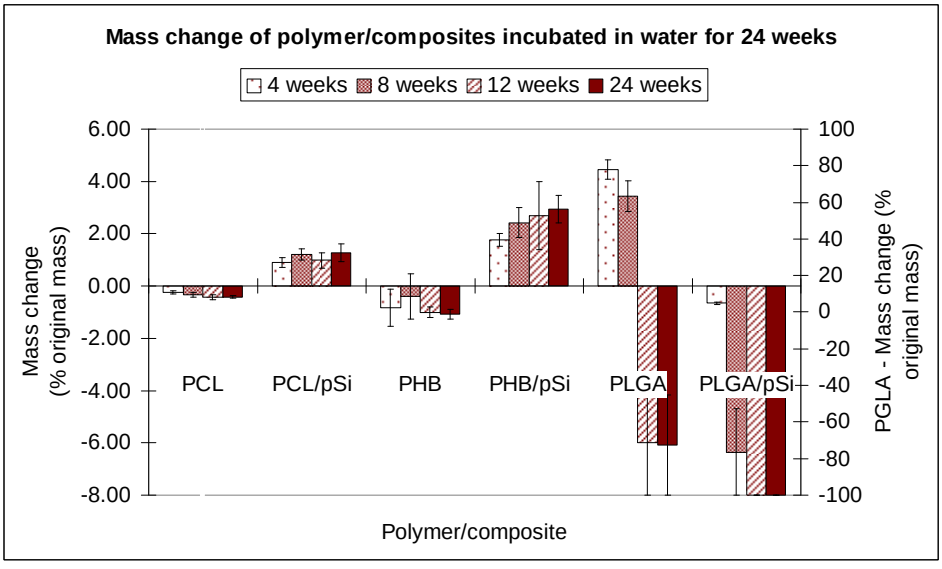


**Fig. 2.12.** Changes in mass of pure-polymer and 8% *w/w* pSi-composites with polycaprolactone, poly(lactic-co-glycolic acid), and poly-3-hydroxybutyrate expressed as a percentage of original mass. PLGA percentage mass loss is shown on the 2nd Y-axis.

The pH of the solutions was similar for both basic polymer and composites, with composites acidifying solutions by an additional pH 0.53 – 0.63 at 8 weeks over the acidification caused by polymer hydrolysis which generates carboxylic acids (**fig. 2.13**). The change in pH of solutions between 4 and 8 weeks shows that the degrading polymers continued to acidify the solution, whereas the additional chemical interactions of the composites resulted in an increase in pH from 4 to 8 weeks (**fig. 2.14**).

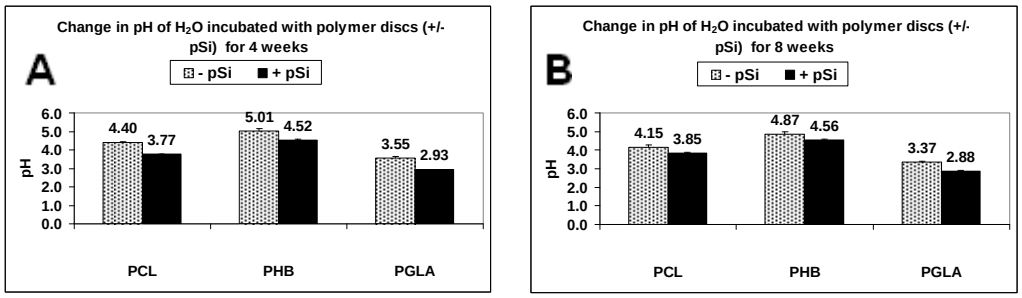


**Fig. 2.13.** pH of dissolution volume ($dH_2O$) after **A**. 4 weeks incubation. **B**. 8 weeks incubation. (Bars show standard error of the mean, n=3).

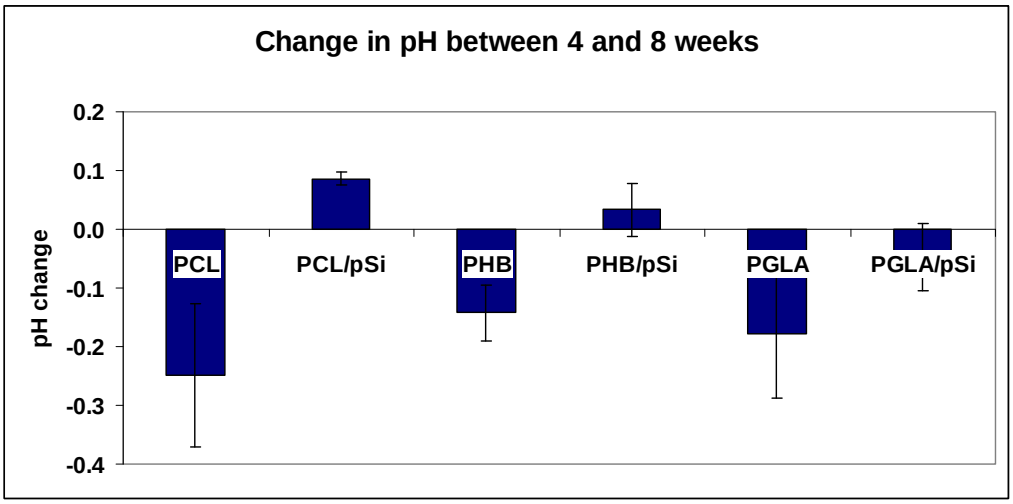


**Fig. 2.14.** Subtracting the pH of the solutions at 4 weeks from the pH at 8 weeks shows that the acidification caused by polymer degradation was offset by silica formation in the composite samples, resulting in a lowering of acidity over time for PCL and PHB composites. The enhanced degradation of PLGA-pSi resulted in further acidification of the solutions and importantly the pH generated by all composites was lower than basic polymer (see **fig. 2.13**). Bars show standard error of the mean, n=3.

### 2.3.4. Composite mass.

**Fig. 15** shows the silicic acid release from 8% melt-cast composites (20mg per 250mg PCL) with masses ranging from 37 – 157 mg and incubated in $dH_2O$ for 10 days, and shows that silicic acid release is proportional to composite mass.

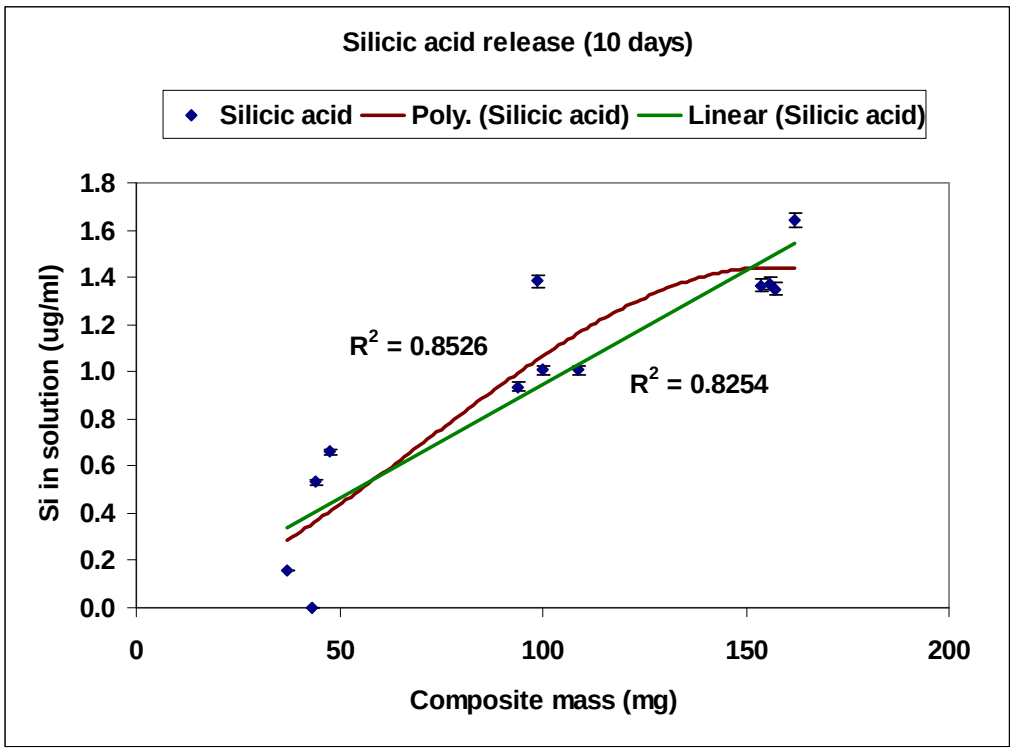


**Fig. 2.15.** Silicic acid release from 8% *w/w* pSi-PCL composites of varying size (37mg - 157mg) incubated in $dH_2O$ for 10 days. Lines of best fit for linear regression (green) and second order regression (red) are shown with accompanying coefficients, $R^2$ (Bars show standard error of the mean, n=3).

The linear and second order lines of best fit show a slight effect of composite thickness on dissolution rate, indicating that pSi is able to elute from deep within the construct. This suggests that the polymer phase of the composite is largely amorphous (non-crystalline), allowing for water ingress and silicic acid elution throughout the bulk of the composite without being obstructed by the matrix.

### 2.3.5. Solution and volume.

Dissolution of pSi-PCL in small (1 – 10ml) volumes of PBS followed a linear regression ($R^2$ = 0.9875) over these volumes, indicating that PBS does not interact with the dissolution of pSi in solution. Interestingly, pSi dissolution in SBF was non-linear and instead followed a second order regression ($R^2$ = 0.9875), implying that SBF interacts with pSi and silicic acid in solutions, particularly when the silicic acid concentration is abouve ~ 500μg.ml$^{-1}$.

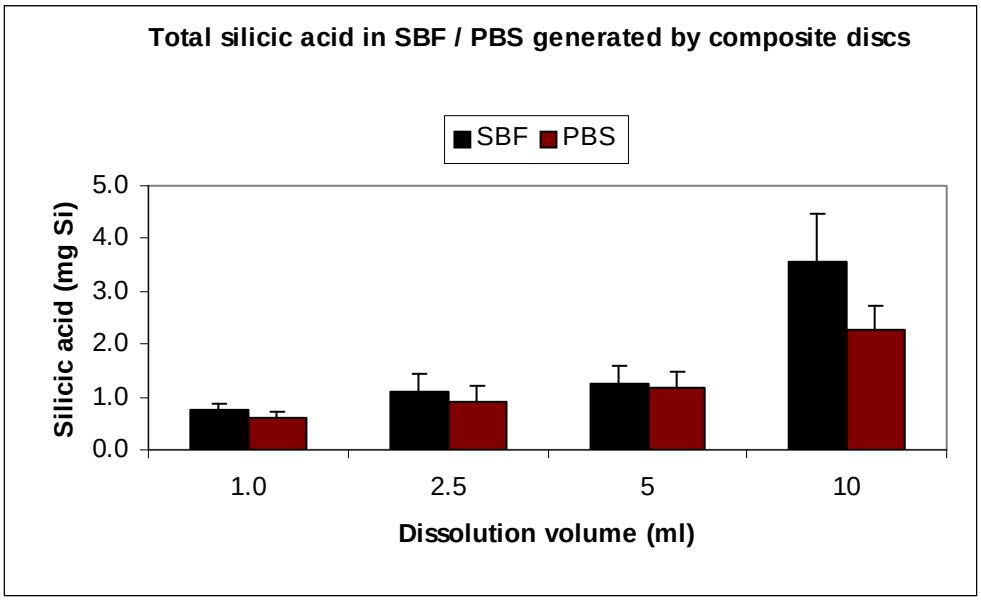


**Fig. 2.16.** Total silicic acid released into solution by 8% composite discs in 1 – 10 ml volumes of SBF or PBS after 28 days. Bars show standard error of the mean, n=3.

### 2.3.6. Comparison of pSi to Bioglass® in PCL composites.

Composites made from PCL with 8% (*w*/*w*) either 45S5 Bioglass® particles or 70% pSi both released silicic acids into solution. Over 42 days the release of silicic acids was linear for both composites (Bioglass®, $R^2$ = 0.8592; pSi, $R^2$ = 0.8556). pSi-PCL was shown to release significantly more silicic acid than Bioglass®-PCL ($p \leq 0.001$ at each time point, detemined by Student's T-test), with pSi releasing an average of 2.5 times more silicic acid than Bioglass® in comparable composites (**fig. 2.17**).

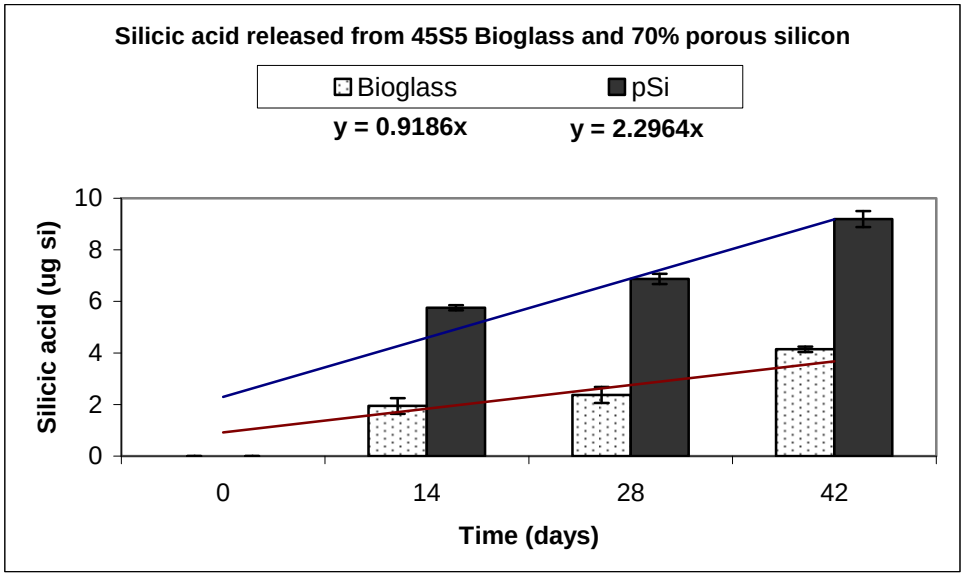


**Fig. 2.17.** Silicic acid release into 20ml $dH_2O$ from 8% *w*/*w* pSi-PCL and 8% 45S5 Bioglass®-PCL. (Bars show standard error of the mean, n=3). Linear regression for silicic acid release (per day) from each composite is shows silicic acid release (y in µg Si) to be 0.9186x for Bioglass®-PCL and 2.2964x for pSi-PCL, where x is time (days).

### 2.3.7. Long term study.

Silicic acid was released from all composites in quantities that were detectable within 24 hours (for 15-30 mg discs) but not until day 28 for discs containing lower amounts of pSi (1-5 mg), (**fig. 2.18**). In this static, non-agitated system, silicic acid levels did not exceed 500 $ng.ml^{-1}$, equaivalent to a total mass of Si in 500ml of 0.25mg. For a 30mg pSi-composite disc this is equivalent to 0.83% of the total pSi present and is similar for all discs tested (**fig. 2.19**).

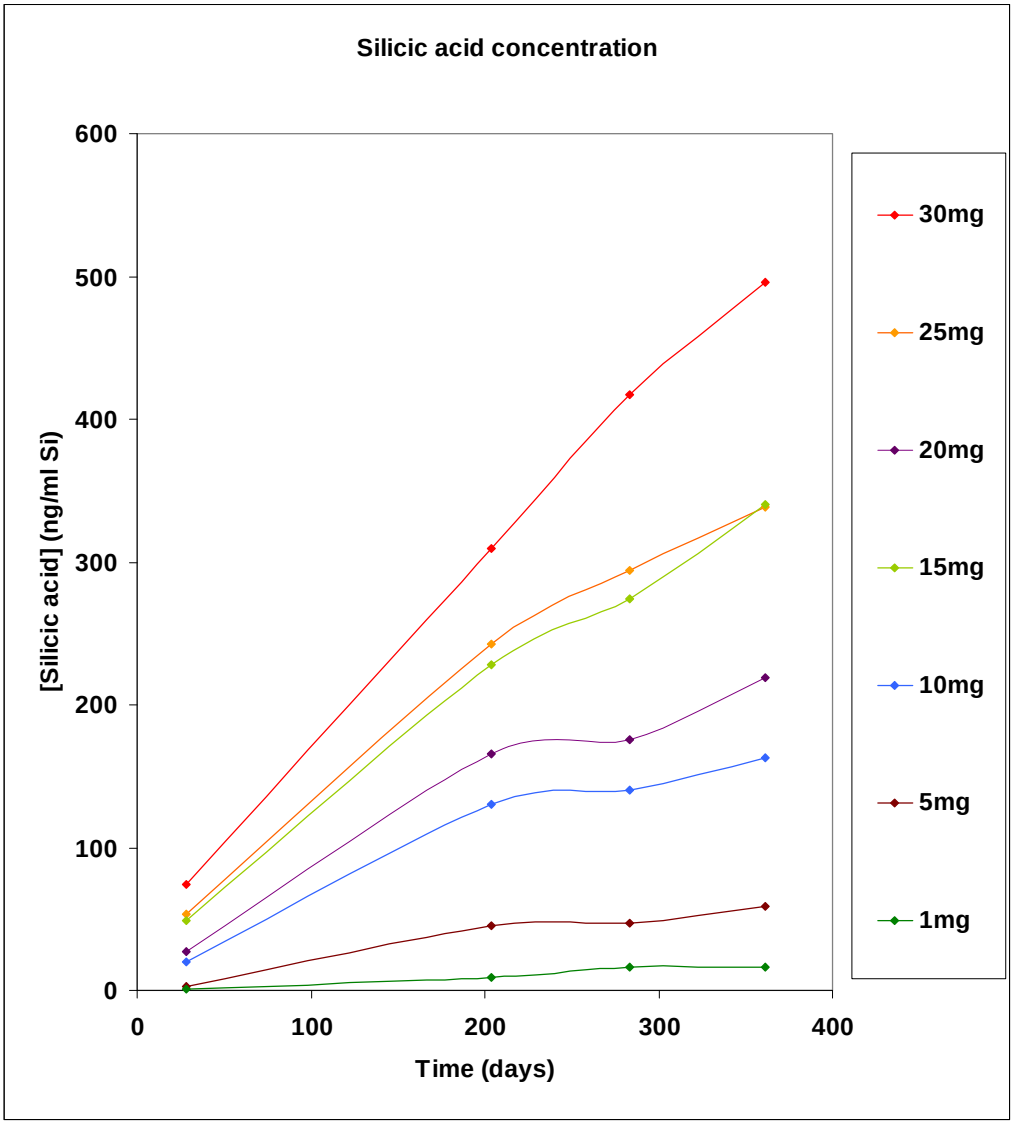


**Fig. 2.18.** Silicic acid release for pSi-composite discs incubated in $dH_2O$ for 360 days at 37°C. Error bars ommitted for clarity, see **fig 2.20**.

For all composite discs, silicic acid was released continuously through the experiment, although the rate becomes lower over time for composites with less pSi, silicic acid release from 30mg discs was almost linear over 360 days ($R^2$ = 0.997, compared to 10mg discs with linear $R^2$ = 0.933). From this data, the amount of silicic acid released per mg pSi in a 250mg disc when the system is not subject to fluid flow (see **section 5.1.2.**, page 173) can be determined as 0.299 ± 0.004 $ng.day^{-1}$.

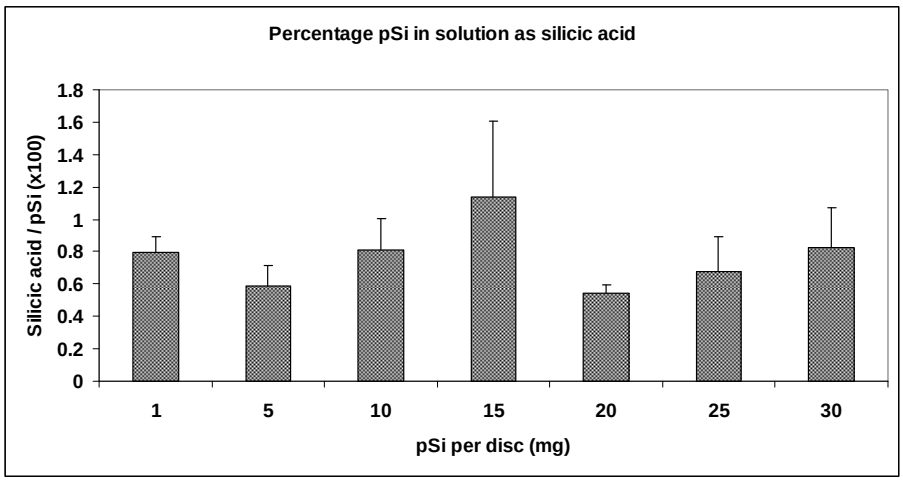


**Fig. 2.19.** Percentage of Si originally added (as pSi) present in solution as silicic acid after 360 days. Error bars are standar error of the mean, n=3.

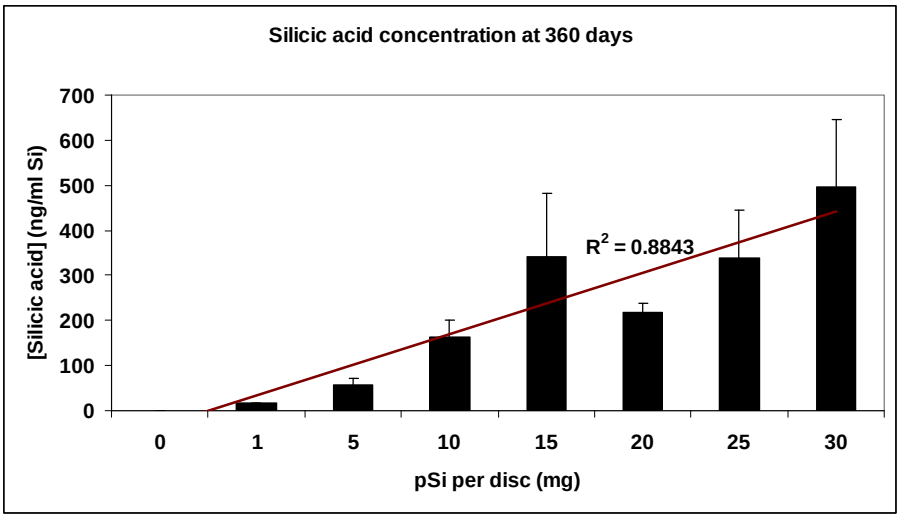


**Fig. 2.20.** Silicic acid concentrations at 360 days for each ratio pSi-PCLcomposite. Trend line (linear) shows silicic acid release per disc, $R^2$ = 0.8646 when plotted on scatter graph. Error bars are standard error of the mean silicic acid concentration at day 360, n=3.

Polycaprolactone discs without pSi lost 6-8% initial mass within 90 days which did not change for the remainder of the experiment and was attributed to the loss of residual solvents and small molecular weight polymers which were able to disperse from the matrix. 1mg discs lost <1% mass whereas discs containing more pSi increased in mass, peaking at a 4% mass gain for 20mg discs. 25mg and 30mg discs did not increase in mass to the same extent and some replicates showed a net loss in mass. The loss in mass from 280-360 days was observed in all composite discs regardless of initial weight gains corresponding to the increase in mass loss from polymer decomposition at this time.

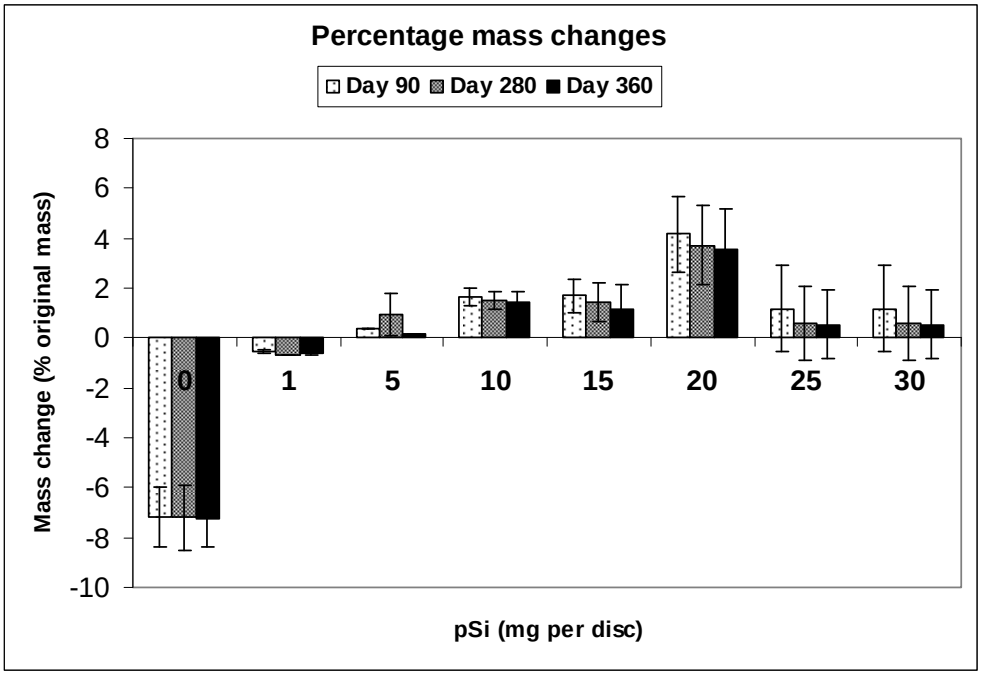


**Fig. 2.21.** Mass changes of pSi-PCL over 360 days showing the decrease in mass of PCL and the relative increase in mass of pSi-composites due to the build up of a hydrated silica gel layer on the surface of composites and oxidisation of pSi in the matrix. Error bars are standard error of the mean, n=3.

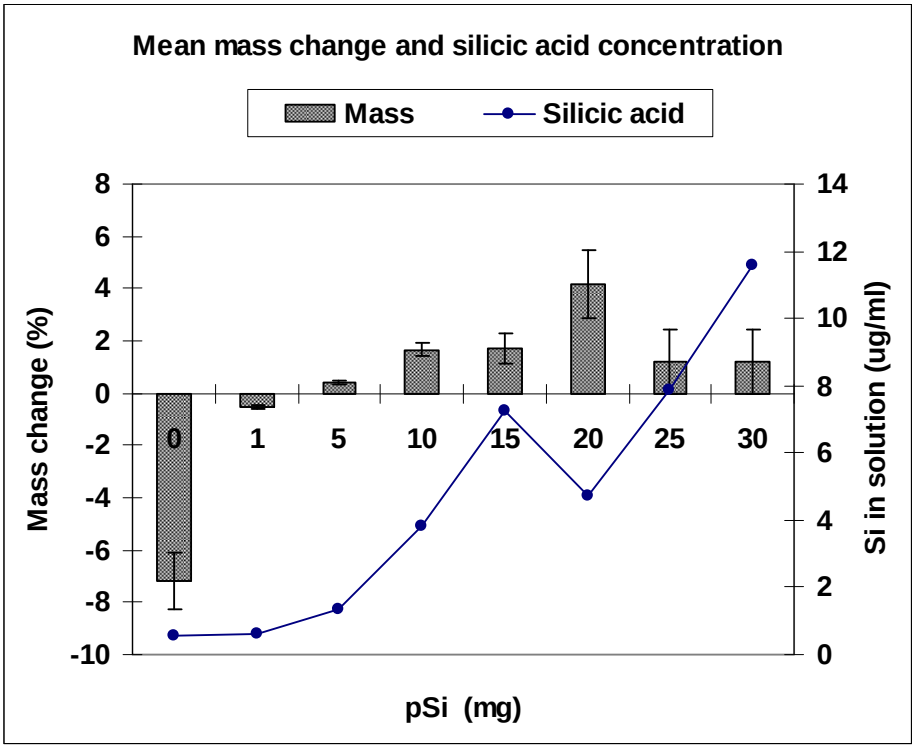


**Fig. 2.22.** Mass change against mean silicic acid concentration in solution at 90 days. Error bars for mass change are standard error of the mean at day 90, n=3. Error bars ommited from silicic acid line for clarity (see **fig. 2.17.**)

Solution pH after 120 days was lower for all composites than PCL-only and was inveresly proportional to pSi content of the composite, with a coefficient of linear regression ($R^2$) of 0.939 (**fig. 2.23**).

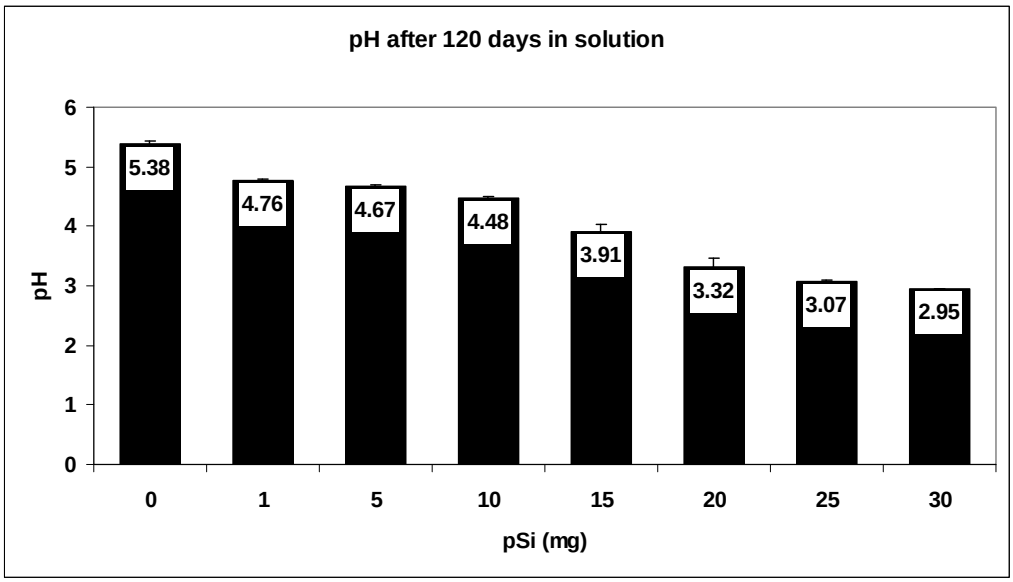


**Fig. 2.23.** pH of initial solution after 120 days incubation. Error bars are standard error of the mean, n=3.


**Fig. 2.24.** Discs removed from solution and dried after 360 days (One third of each disc has been removed for analysis), showing reduction in composite disc diameter compared to PCL. Image was taken using a Brother DCP -560CN scanner. Bar shows 10mm, initial diameter at Day 0 for all discs was 11.5mm.

### 2.3.8. Morphology and composition of silica and apatite formation.

Scanning electron microscopy of composites incubated in $H_2O$ shows the formation of a silica gel layer with a pronounced surface togography on composite discs. As the PCL and composite discs in **fig. 2.25.** were co-incubated, the silica gel formed on the surface of the PCL-only disc results from condensation of silicic acids from solution, demonstrating that pSi can condition peripheral surfaces with a silica gel layer.

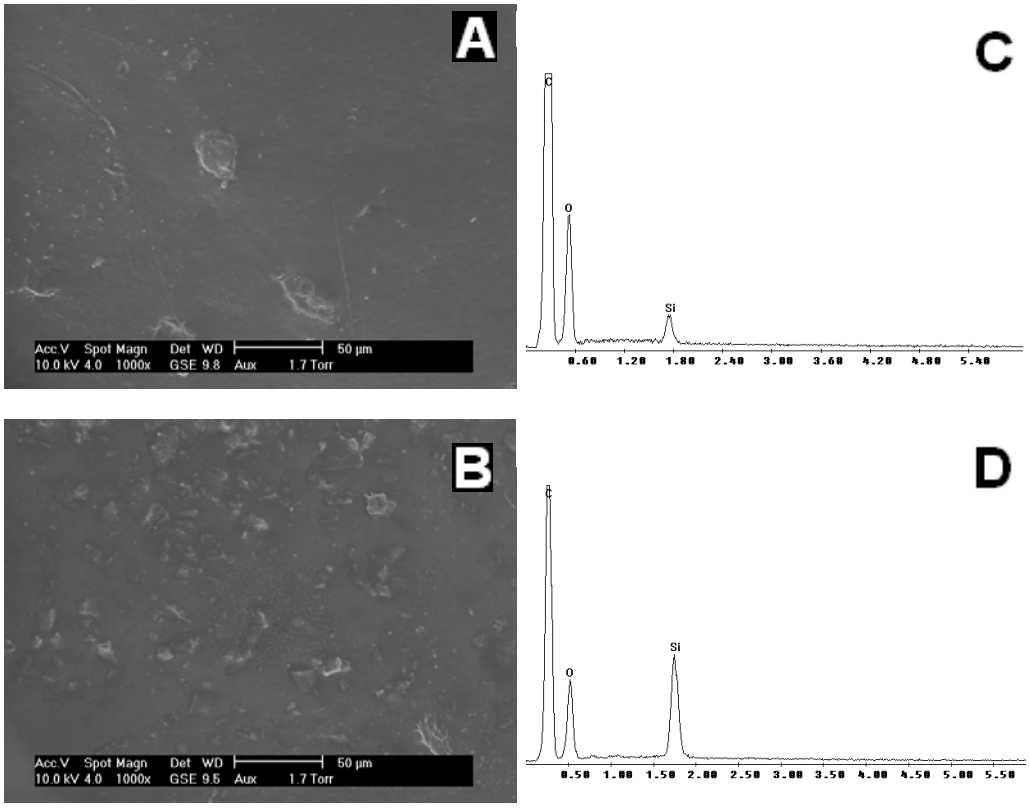


**Fig. 2.25**. ESEM images of **A**. PCL and **B**. 20mg (8%) pSi-PCL composites co-incubated in the same volume (50ml) $dH_2O$ for 14 days, and EDX spectra (**C.** PCL. **D.** pSi-PCL) showing the deposition of silica occurs across all surfaces exposed to the degradation products of pSi.

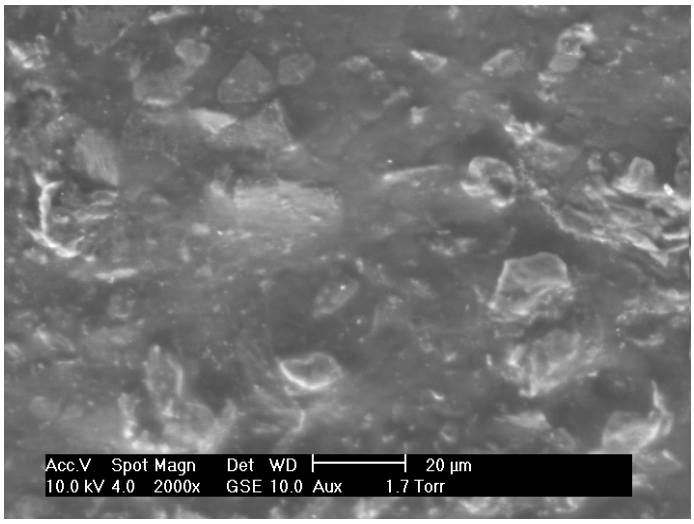


**Fig. 2.26.** Magnified ESEM image of **Fig. 2.25.B** showing the surface morphology of the silica gel layer is highly contoured surrounding pSi particles.

Incubation of 0.4% (**fig. 2.27**), 4% (**fig. 2.28**) and 8% (**fig. 2.29**)composite discs in SBF for 4 weeks results in the formation of a calcium phosphate layer in addition to the silica gel layer. This calcium phosphate layer has the morphology of biological apatite seen in Bioglass® studies. Analysis of the surface using X-ray dispersive spectroscopy shows that the calcium/phosphate ratio is closer to biological apatite (1.5) than phase-pure hydroxyapatite (1.67).

In some regions, the cracked surface is perpendicular to the disc, allowing a cross-section of the layer to be imaged. This shows a 'sandwich' of silica, with an inner and outer cortex surrounding an inner region which appears less dense (**fig. 2.27.B & C**)

Further analysis of calcium phosphate layers on increasing concentrations of pSi show that the calcium deposits become increasingly large and more continuous. In addition, EDX reveals that the calcium/phosphate ratio of the mineral is proportional to silicon content (**fig. 2.30**). That is, increasing pSi in the matrix or [silicic acid] in solution results in increased substitutions in the apatite crystal for phosphate, or possibly reduced substitution for calcium.

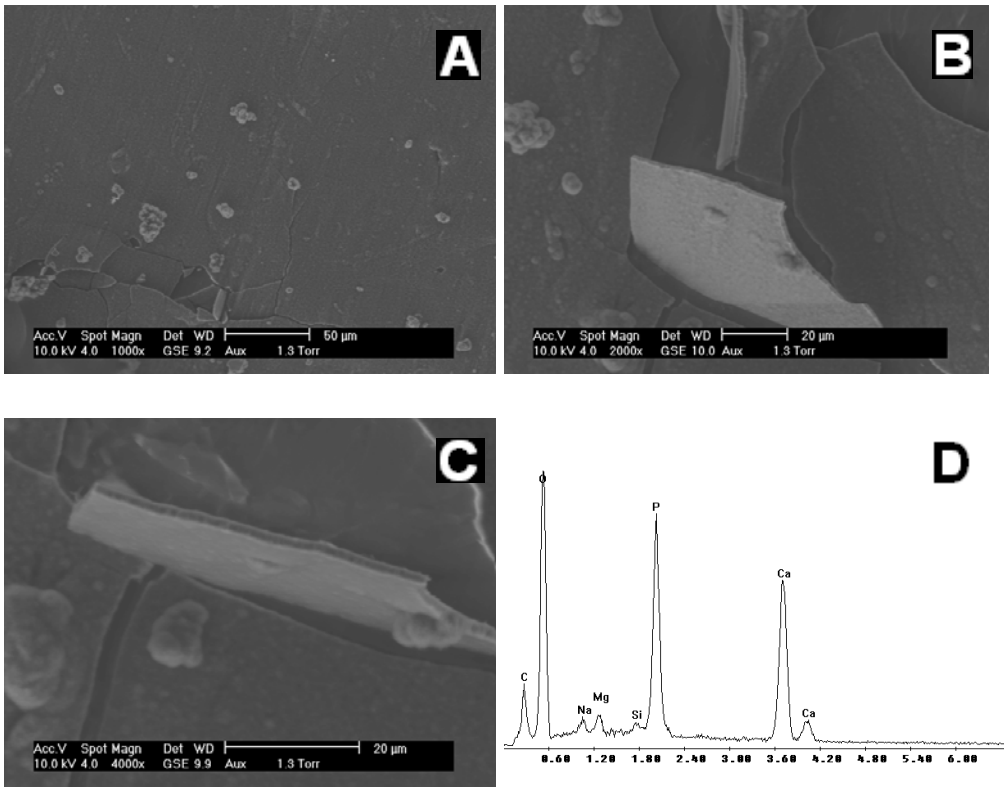


**Fig. 2.27.** ESEM images of 1mg (0.4%) composite discs incubated in SBF for 4 weeks, showing the build up of a calcium- and phosphate-containing surface layer. (**D**) This layer is shown to have a Ca/P ration of 1.487. In this spectrum, silicon represents only 0.7% of the atoms present in the target region, (**A**). **B**. and **C**. show a section through this layer which appears to contain an interior architecture of lower density. The Ca/P ratio in this spectrum is 1.487.

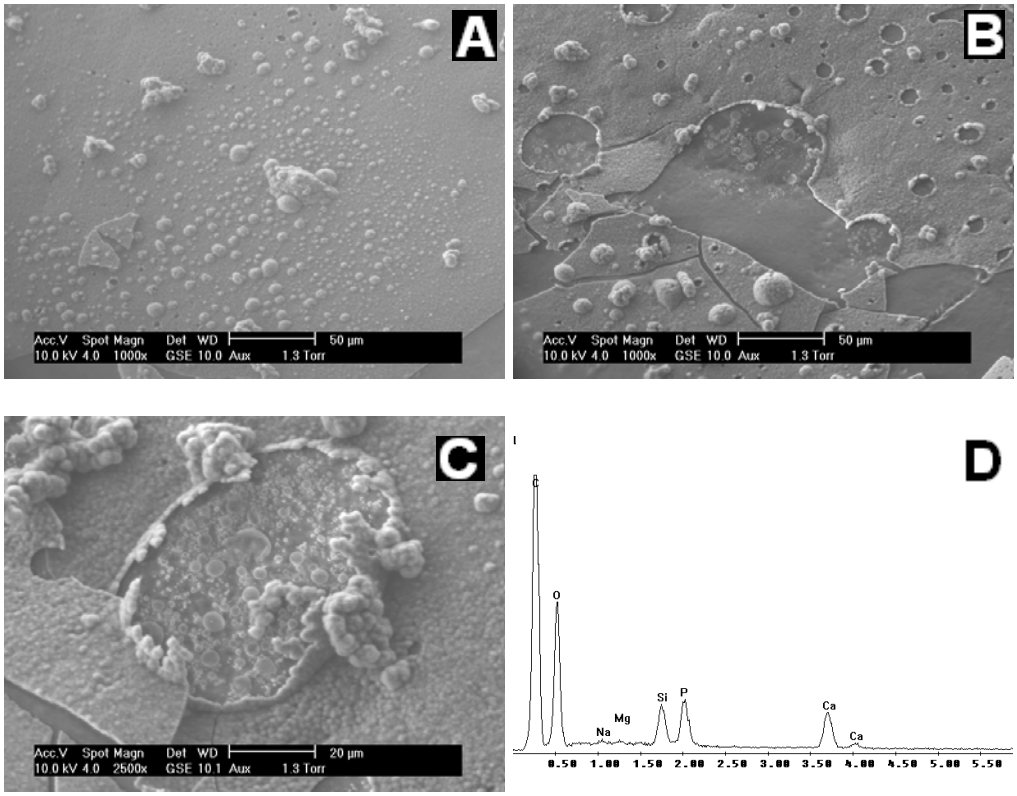


**Fig. 2.28.** ESEM images of 10mg (4%) composite discs incubated in SBF for 4 weeks, showing the build up of a calcium- and phosphate-containing surface layer (**A**). This surface layer is contiguous but was fractured during the drying process to reveal separated plates approximately 2µm in thickness (**B**). Distinctive biological apatite formations are observed on this surface layer (**C**) with an overall Ca/P ratio of 1.498 (from **A**).

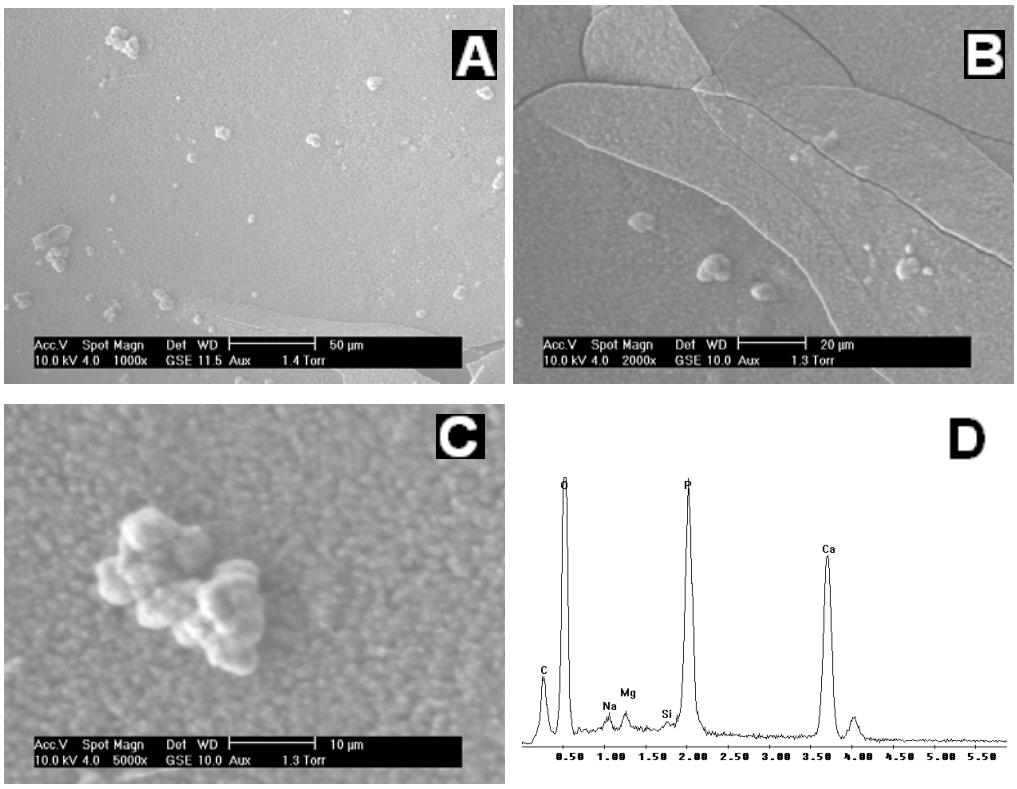


**Fig. 2.29.** ESEM images of 20mg (8%) composite discs incubated in SBF for 4 weeks, showing the build up of a calcium- and phosphate-containing surface layer with a distinctive apatite-like morphology.

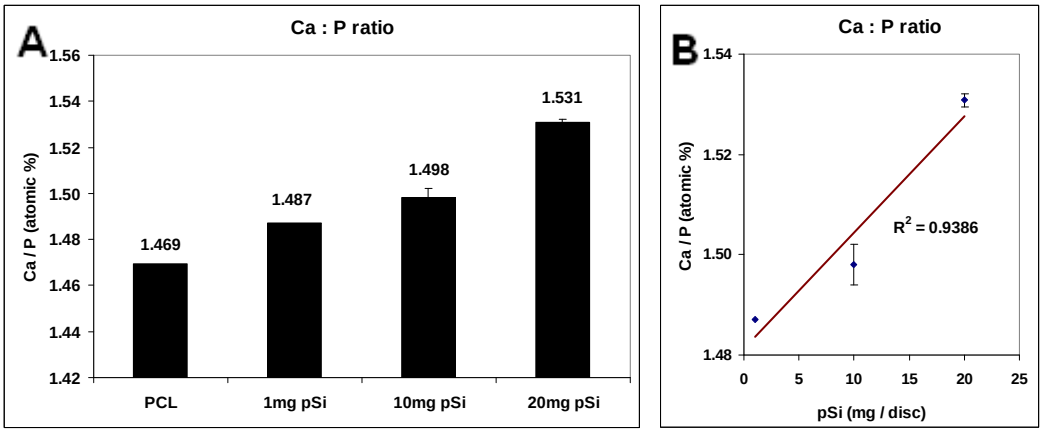


**Fig. 2.30. A**. Calcium/phosphorus ratios of the surface layers deposited on the composite surfaces after 4 weeks in SBF. Increasing the pSi content of the composite correlates to a decrease in phosphate content of the mineral layer. **B**. This effect is linear over the composite range tested (0.4 – 8% *w*/*w*), $R^2 = 0.9986$.

**2.4. Discussion.**

This section of the work describes the initial trials that were performed in order to assess the effect of adding porous silicon to biodegradable polymers in terms of biodegradation rates, silicic acid release and the enhancement of calcium phosphate deposition from acellular simulated body fluids.

The method developed for forming the pSi-polycaprolactone composite involved first combining pSi microparticles with a solution of polycaprolactone in acetone to create a homogenous, microporous composite. The mechanical properties of this composite appeared to be enhanced (by subjective analysis: the mechanical properties were not measured directly) by then melting the composite at >60°C to eliminate most of the micropores and residual solvent. The final composites for testing were cast in the body of a polypropylene syringe, which allowed a cylinder of uniform, consistent diameter to be produced, which could be easily cut into discs with regular size and weight, standardised to 250mg ± 10mg.

In this investigation, the pSi content of the composite is presented in two ways, either as a mass value indicating the amount (in mg) of pSi in a disc (which were almost always 250mg in total) or as a percentage composition. Thus 10 % composites contained 25mg pSi for every 250mg PCL. It is important to note that due to the large surface area and volume to mass ratio, composites containing 10 % by mass of porous silicon contained a much larger proportion by volume. The typical density of monocrystalline silicon is 2.33 $g.cm^{-3}$, but for 70% porous silicon this density is only 0.7 $g.cm^{-3}$. Therefore the volume percentage of this composite would theoretically be closer to 33%.

In practice, the method used for creating the composite using a solution of the polymer in acetone would allow some of the internal pore spaces of the pSi to become filled with polymer, particularly after recasting using heat as the molten polymer was compressed into the pores. Some groups have exploited this effect by sing pSi pores as a template for producing 'male' casts of pSi pore architectures for various applications (Kim *et al*, 2007).

At the beginning of the investigation several porosities of pSi were evaluated, from 49% porous to 82% porous. These were produced by pSiMedica Ltd at the company laboratories in Great Malvern, Worcestershire, and milled by hand on the premises using a pestle and mortar. This generated pSi particles of varying sizes, with the main fraction (~80%) of particles being in the 38 – 150μm size range. These particles were used for initial trials, but it was decided that greater uniformity and a smaller size range was required and so in later experiments a standardised 70% porous silicon was obtained from pSiMedica with 11μm particles in a narrow size range. In this part of the investigation, all experiments (unless stated otherwise) utilised the 70% 'standard' pSi to allow direct comparison between experimental conditions to be made. Alternative porosities were utilised for *in vitro* testing of osteoblasts as will be discussed in chapter three.

The proposed bioactive properties of porous silicon result from the material's release of orthosilicic acid, which was detected and quantified throughout this investigation using the molybdenum (molybdate) blue assay. In this assay, ammonium molybdate in solution reacts with silicic acid in the sample to form β-silicomolybdic acid (yellow) which is subsequently reduced to form a molybdate blue complex with a peak absorbance at 810nm. The assay was highly adjustable as up to 40% (400μl) of the reaction volume comprised the tested solution, allowing for very dilute samples to be successfully assayed, with a lower limit of detection at 1 $ng.ml^{-1}$ of the test solution. The assay worked equally well using PBS and SBF as incubation/buffer solutions as with water and was linear over the concentration ranges tested, with typical coefficients of linear regression for calibration (using sodium metasilicate standards) being $R^2 > 0.99$.

Silicomolybdic acid is formed rapidly from the interaction of the molybdate with orthosilicic acids, and increasingly slowly for larger weight di- and poly-silicic acids. Colloidal silica and solid silica gels do not form silicomolybdic acids at all, but do exist in dynamic equilibrium with soluble silicate species in solution (Alexander *et al*, 1954). The time allowed for the formation of silicomolybdic acid in this assay was fixed at 10 minutes, which allows all of the orthosilicic acid in the solution to react, but minimises the amount of polysilicic acids detected by the assay. This was done to allow a measure of control and standardisation over the

complex and dynamic chemistry of silicic acid polycondensation occurring in the system.

Microporosity caused by acetone evolution had a large effect on the rate of orthosilicic acid release, increasing the rate of silicic acid release into solution almost five-fold. This indicates a surface area/volume effect, allowing small weight silicic acids to diffuse out of the matrix rapidly. All of the experiments in this part of the investigation were performed on 'two-dimensional' discs without significant or designed interior architecture apart from some micropores as illustrated.

In this investigation, porous silicon composites were made from the addition of pSi microparticles to biodegradable polymers. The choice of biodegradable polymer was made early in the project based on the considerations outlined in the introduction to this chapter, but a selection of relevant biodegradable polymers were also included in the trial to determine the effect of the polymer phase on composite behaviour in terms of degradation, silicic acid release and calcium phosphate nucleation.

It was observed that silicic acid release was not equal for polycaprolactone, poly(D,L lactide-co-glycolide) or poly(hydroxybutyrate-co-valerate) and the release kinetics also differed. Composites based on PCL show a sigmoidal pattern of silicic acid release with an increase in release rate after one week which stabilises and gradually decreases over time. It can be surmised that these changes result from changes in surface chemistry of the composite over this time, with water ingress through the matrix and wettabilty increasing due to reduction of water contact angles through the hydrolysis of hydrophobic S-H motifs to more hydrophilic Si-O (Tolstoy *et al*, 2003). The deposition of a silica gel layer on the surface of the composite then inhibits both further water ingress and elution of orthosilicic acid from the material. This silica gel layer was observed and recorded in electron micrographs. Additionally, it should be noted that the continuing degradation of pSi in solutions of orthosilicic acid under the silica layer increases the rate of silicic acid polymerisation as the reaction is concentration dependent, leading to a reduction in the concentration of dispersible, detectable species.

Degradation of pSi in PLGA and PHBV occurs via the same mechanism, but release profiles of silicic acid were different. Rather than sigmoidal, PLGA released silicic acid in an exponential way, with the degradation rate of porous silicon in the matrix increasing at a steady second order rate over the 8 week period but generating similar concentrations of silicic acid at each time point as PCL composites. PHBV degradation was slower than both PCL and PLGA and more erratic, following a linear profile over 8 weeks but with a coefficient of linear regression ($R^2$) of only 0.68.

The differences in the behaviour of these three biodegradable composites derive from three parameters: polymer degradation rate, relative hydrophilicity / hydrophobicity and percentage crystallinity of the native polymer.

The hydrolytic degradation of polycaprolactone occurs slowly, taking up to two years for substantial mass loss, whereas PLGA degradation occurs much more quickly, within 3 months. PHBV degrades over 200-300 days under physiological conditions (Muhamad *et al*, 2006). In this investigation it was noted that the addition of porous silicon to the polymer matrix increased the rate of polymer degradation (determined from total mass loss) in PLGA significantly, causing two out of the three samples to completely decompose after 8 weeks, with complete degradation occurring for all samples within 12 weeks.

Hydrophobicity and crystallinity of the native polymers/co-polymers affect the behaviour of all aqueous solutions in contact with the material. Water contact angle is used as a measure for hydrophobicity, and is 82° for PCL (Tan & Teoh, 2006), 78° for PLGA (Wan *et al*, 2004) and 72.5° ± 5.6 for PHBV (Wang *et al*, 2006), interesting illustrating that the more hydrophobic polymers show greater solubility/degradation of pSi from the composite. Crystallinity for native polymers is cited as being ~50% for PCL (Goldberg, 1995), 51.1% for PHBV (Muhamad *et al*, 2006) and considerably lower for PLGA co-polymers. Polymer crystallinity therefore does not appear to have a bearing on the degradation rate of pSi in the matrix in this case, although it is noted that the percentage crystallinity of composites may be different to that of native polymer.

Acidification caused by the presence of polymer degradation products is a concern in orthopaedics that has been a major factor limiting their use, particularly in ischemic conditions that surround many orthopaedic wounds and implant sites. Acidosis inhibits bone formation and stimulates osteoclastic resorbtion of bone (Frick and Bushinsky, 2003), and so limiting the acidification of orthopaedic wounds is important in designing degradable implants. As a material designed to elute orthosilicic acid, this was a concern from the beginning of the investigation.

Whilst composites of PCL, PHBV and PLGA with pSi lowered the pH of incubating solutions, the composites were shown to stabilise the solutions over time, with volumes incubating composites increasing in pH after 8 weeks rather than decreasing. This is through the formation of silica which eliminates silicic acid from solution as described in simplified formula:

$$\mathbf{Si(OH)_4 + Si(OH)_4 \rightarrow 2SiO_2 + 4H_2O}$$

In addition to porosity and concentration of pSi microparticles in the polymer, other factors which effect silicic acid release were the size of the composite and the volume of medium in which the material was incubated. Composites containing the same percentage of pSi (8%) but with varying sizes released silicic acid in an almost linear way, indicating that the material is fully permeable to water and demonstrating that, at least for small-sized composites, the mass of the composite is directly proportional to the amount of silicic acid eluted. The slightly better fit of a second order trend line to the graph demonstrates that release of silicic acid from larger composites may be slightly inhibited by the mass of the material.

The volume of the surrounding solution into which the porous silicon degrades was shown to have a linear relationship to the amount of silicic acid detected in PBS. Larger volumes supported higher concentrations of orthosilicic acid, either by stimulating enhanced degradation of pSi or inhibiting condensation of polysilicic acid. Interestingly, the $[Si(OH)_4]$/volume was non-linear when SBF was

used as the dissolution solution, with significantly higher concentrations of silicic acids detected in 10ml SBF than either 10ml PBS or 2 x 5ml SBF.

The proposed bioactivity of porous silicon results from it's degradation in aqueous solutions to yield soluble silicates and form a hydrated silica gel on the materials surface. This mechanism has been extrapolated from studies of Bioglass® bioactivity, in which the glass dissolves in solution to liberate it's ionic constituents, chiefly comprising silicon (Reffit *et al*, 2003; Keeting *et al*, 1992). The class A bioactivity of this type of biomaterial therefore can be reasonably related to the generation of silicic acids, therefore, and so a comparison of the silicic acid release rate of both pSi-PCL composites and 45S5 Bioglass®-PCL composites was performed in order to evaluate pSi activity in relation to a well-documented and well-known example.

8% w/w composites of pSi or Bioglass® in PCL were made and incubated in $H_2O$ for a period of 6 weeks. Over this time, release of silicic acids from both composites was linear, but pSi generated 2.5 times more silicic acid than Bioglass®. As a measure of potential bioactivity therefore, this suggests that pSi-PCL will outperform Bioglass®-based composites in subsequent *in vitro* tests, based on silicic acid acting as the main bioactive component of both materials.

The polymer chosen for the composite in this investigation, polycaprolactone, degrades slowly, with substantial mass loss occurring only after 6-24 months. Therefore it was decided that a long-term degradation study covering one year should be performed to evaluate the behaviour of the composites over this time scale. Silicic acid release in this system was proportional to the pSi-content of the composite, and linear over the first 200 days, after which the silicic acid release plateaued in lower compositions (up to 25mg, 10% *w/w*) but 30mg (12% *w/w*) continued to release silicic acids into solution at the same constant rate of ~1.4 $ng.ml^{-1}.day^{-1}$.

Despite the continued release of silicic acids over 360 days, at the end of this time, the mass of silicon in solution was less than 1% of the mass of pSi originally added into the system. Free pSi degrades rapidly in solution (pSi data), so the low

rate of degradation suggested by this data in incongruous with the predicted results. However, silicic acids polymerise rapidly in solution, with the rate proportional to the concentration, which becomes high peripheral to the surface of the composite and within the matrix, particularly in the static system used here with little solution flow around the material.

This polymerisation results in the formation of large molecular weight silicic acids and solid silica, which condense on the surfaces of the composite and the walls of the incubation vessel. In this investigation, the silica formation on the composites was measured by comparing the original mass of the discs to the mass of the discs at set intervals during the experiment. The weight gain due to the presence of silica was easy to determine in this simple system, as the baseline mass loss due to polymer degradation could be determined from the PCL-only control, any mass increase therefore was due to silica deposition.

Gain in mass due to silica deposition is pronounced in this system. One mole of Si (or pSi) masses 28.09 g whereas one mole of silica ($SiO_2$) is 60.08 g, therefore the full dissolution and conversion of 20mg pSi would generate 42.78g $SiO_2$, a percentage increase in mass of the composite of 9.11%. In the investigation, the maximum mass gain achieved by a composite disc was ~5%, indicating condensation of silica occurs on other surfaces in the reaction vessel and that larger, undetectable polysilicic acids are present in solution.

Electron microscopy of composite discs incubated in just water shows a pronounced surface layer which was attributed to a hydrated silica layer, possibly containing polymer fragments resulting from the combined dissolution of both polymer and silicon in the material. A cross section through this layer shows it to have a pronounced internal architecture, with perpendicular striations between solid outer layers.

Calcium phosphate was detected in composites incubated in acellular simulated body fluid and shown to be proportional to the amount of silicic acid released by the material. This calcium phosphate was shown using SEM to have the characteristic morphology of biological apatite, with a Ca:P ratio of ~1.5,

supporting this conclusion. Interestingly, the Ca:P ratio was proportional to the pSi/[silicic acid] in the system, with increasing pSi in the disc resulting in a lower proportion of phosphate in the crystal. Due to the higher amount of silicates in the system here, it is proposed that the apatite in these cases is silicate substituted (for some phosphate and carbonate).

In summary, these initial investigations demonstrate that porous silicon microparticles can be added to biodegradable polymers to create a silicic acid acid-eluting material which forms a silica/calcium phosphate layer autonomously in acellular simulated body fluid. Silicic acid release rates can be finely controlled by varying the percentage porosity and amount of microparticles added, and pSi-PCL composites outperform comparable 45S5 Bioglass®-PCL composites in terms of silicic acid release.

Further and more detailed physical characterisation of the composites is discussed in chapters 5 and 6 and in the appendix.

# Chapter Three

-

# Osteoblast Response to Porous Silicon – Polycaprolactone Composites *in Vitro*

### 3.1. Introduction.

*In vitro* cultures of osteoblast-like cells are a useful means of analysing cell biology and interactions with biomaterials in effective isolation from other cells. Using such cultures allows the molecular biology of large populations of similar cells to be quantified, enabling statistical significance to be determined and enhancing the reproducibility of experimental data. In addition, current trends in tissue engineering have been towards the development of *in vitro* cellularised scaffolds – three-dimensional porous materials which can be seeded with the autologous cells and cultured in the laboratory prior to implantation (Wang *et al*, 2009).

#### 3.1.1. Osteoblasts *in vitro*.

Osteoblasts derive from a pluripotent mesenchymal lineage, sharing common progenitor cells with fibroblasts, chondrocytes, myoblasts and adipocytes (Aubin *et al*, 1995) as illustrated in **fig. 3.1**.

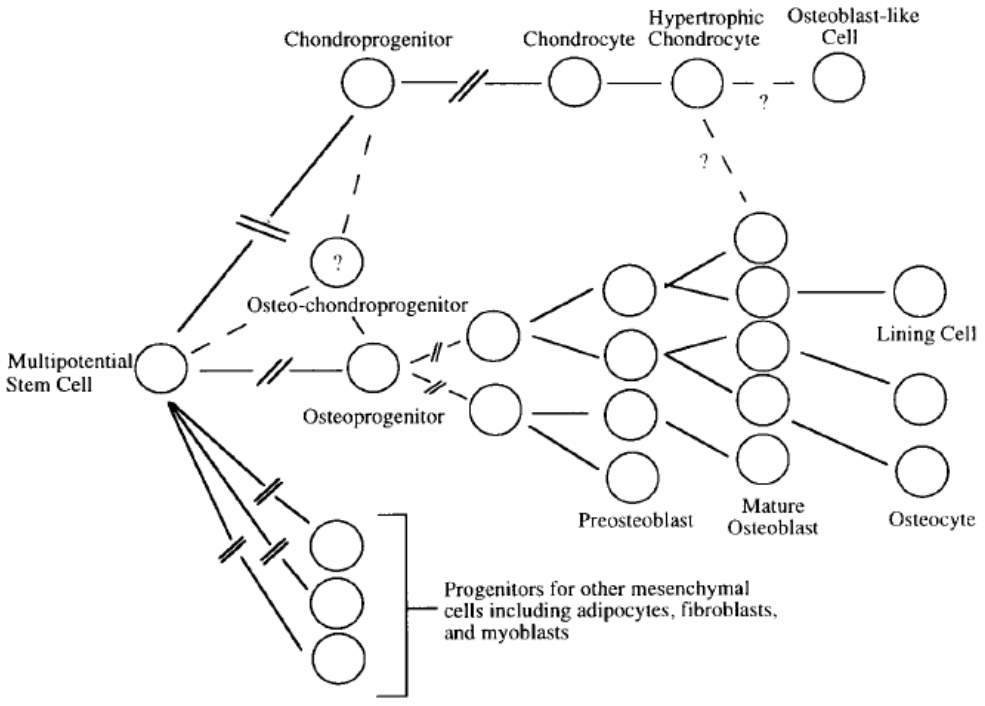


**Fig. 3.1.** Osteoblast ontology proposed by Aubin *et al*, 1995. Osteoblasts derive from a pluripotent mesenchymal lineage.

Differentiation of progenitor cells into osteoblasts is triggered by several physiological factors, including the relative vascularisation of the tissue (Cormack, 1984) and numerous autocrine and paracrine cell signals such as bone morphogenetic proteins (BMPs) - chiefly acting through the hedgehog signaling cascade - and the transcription factor, core-binding factor -1 (Yamaguchi *et al*, 2000; Soltanoff *et al*, 2009). Upon receiving signals for differentiation, the pre-osteoblasts mature, gradually losing the ability to divide and increasing the expression of mature osteoblastic markers such as type I collagen and alkaline phosphatase (Leung *et al*, 1993).

Methods for isolating and culturing osteoblasts have been developed, beginning with Peck *et al* (1964) and utilising cells from a variety of sources. Commonly used sources of primary osteoblast-like cells for research purposes are neonatal mouse or rat calvaria and human femoral head trabecular bone (**fig. 3.2**), which is removed from patients undergoing total hip arthroplasty and is therefore relatively easy to obtain.

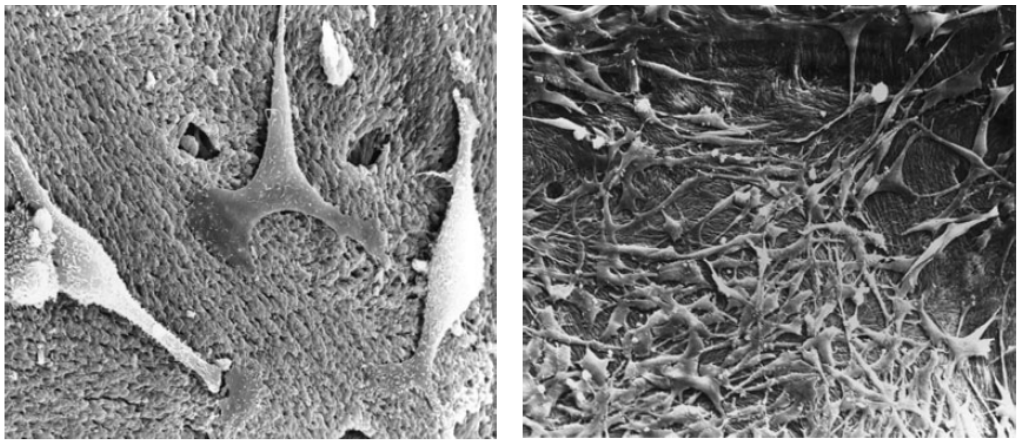

**Fig. 3.2.** Mouse calvarial MC3T3-E1 cells (**A**) and primary human osteoblasts (**B**) cultured *in vitro* on sintered hydroxyapatite showing distinctive morphology: cells appear superficially similar to fibroblasts with a ruffled plasmalemma and numerous filipodia. From Trentz *et al* (2003).

Alternatively, cell lines exist which are derived from osteosarcomas, including rat osteosarcoma (ROS) and human MG-63 cells and these exhibit a constant phenotype, although being immortalised and adapted to *in vitro* conditions these

cells may not be fully representative of normal osteoblast behaviour (Majeska, 1996). It is thought that primary cultures are more representative of the natural behaviour of osteoblasts *in vivo*, and therefore are more useful to studies of response to biomaterials *in vitro*. Cell lines established from normal cells, such as MC3T3-E1 from mouse calvaria, show that these primary cultures of normal cells can be passaged for long periods and stored in liquid nitrogen, retaining their expression of markers of osteoblastic differentiation and activity (Sudo *et al*, 1983).

Proliferation *in vitro* continues until a confluent cell layer is formed (**fig. 3.3**). At this point the collagenous matrix matures, containing non-collagenous bone-specific proteins, becoming crosslinked and calcified (Hasegawa *et al*, 2008). Osteoblasts become encased in nodules – cell multilayers in which the microenvironment is controlled by the osteoblasts and which form the nucleation points for mineralisation. Cells entrapped in the calcifying matrix can be said to behave from this point as osteocytes, with a proportion of the cells undergoing apoptosis (Nijerwerde *et al*, 1996).

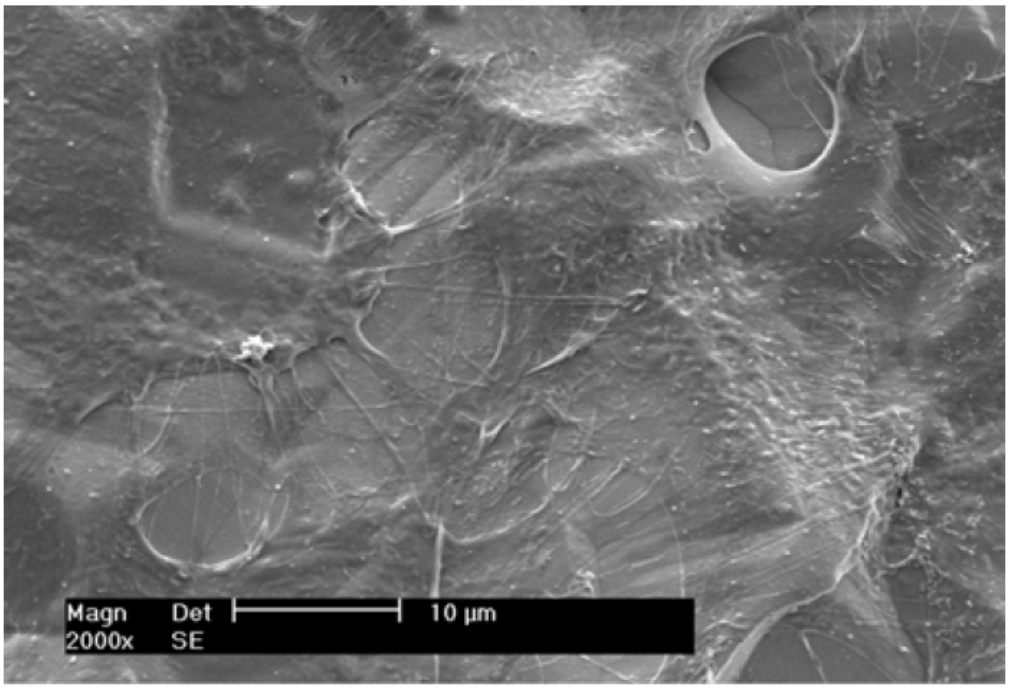


**Fig. 3.3.** Osteoblasts cultured *in vitro* on titanium surfaces for 7 days form a confluent cell layer. From Ramires *et al* (2002).

*In vitro*, osteoblasts express a number of molecular markers, some of which are unique to the osteoblast. These markers are expressed at different times during maturation of the osteoblast, from the proliferation of osteoprogenitors and pre-osteoblasts to mature secretory cells which regulate a maturing and finally mineralising extracellular matrix (Aubin *et al*, 1995).

These stages are accompanied by changes in the relative expression of both collagen and other non-collagenous matrix proteins (**fig. 3.4**). As described by Aubin *et al* (1995), collagen formation is high following differentiation and decreases over time, as does alkaline phosphatase activity once mineralisation is well progressed. Expression of osteopontin precedes the expression of bone sialoprotein and osteocalcin, which is first detected with the onset of mineralisation (Liu *et al*, 1994). Therefore, primary human osteoblasts *in vitro* are well characterised both by their molecular biology and by their morphology.

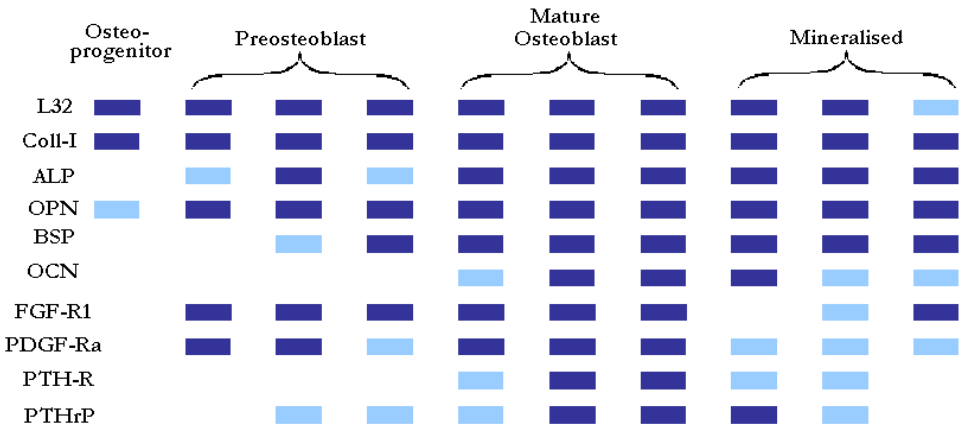


**Fig. 3.4.** Schematic representation of Southern blots from maturing osteoblasts *in vitro* showing the stages at which RNAs for various extracellular matrix components are expressed. Shading shows: Low expression. High expression. Probes were for ribosomal protein control (**L32**), Collagen-I (**Coll-I**), Alkaline phosphatase (**ALP**), Osteopontin (**OPN**), Bone sialoprotein (**BSP**), Osteocalcin (**OCN**), Fibroblast growth factor receptor 1 (**FRF-R1**), Platelet-derived growth factor receptor α (**PDGF-Ra**) Parathyroid hormone receptor (**PTH-R**), Parathyroid-related protein (**PTH-rP**). Redrawn from Aubin *et al* (1995).

### 3.1.2. Practical *in vitro* culture of osteoblasts.

Eukaryotic cell culture was pioneered in the late 19th Century by both Sydney Ringer and Willhelm Roux who developed salt solutions which allowed tissue explants to survive and function for several days. The methodology of tissue and cell culture was further developed during the 20th Century, particularly during the 1940's and 1950's to support research in virology and the production of vaccines (Norrby, 2008).

In modern times, effectively all mammalian cell types can be supported *in vitro*, but the conditions for the culture of specific cells varies in terms of their individual requirement for salts and molecules which ensure the normal behaviour of the cell, maintain a phenotype or stimulate physiological activity, proliferation or maturation.

Osteoblasts *in vitro* require several additions to the basic salts solution, including foetal calf serum (containing macromolecular proteins, albumins to aid protein solubility, hormones and cell-attachment factors) and ascorbic acid (for collagen crosslinking; Majeska, 1996). In addition, supplements such as the steroid hormone dexamethasone and sodium β-glycerophosphate help maintain an osteoblastic phenotype and provide a source of inorganic phosphate for matrix mineralisation respectively (Yamanouchi *et al*, 1997; Luriya *et al*, 2004).

In this investigation, osteoblasts were isolated from human femoral head trabecular bone and characterised by Di Silvio (1995), Gough & Downes (2001) and Anderson *et al* (2001). These cells exhibit a typical osteoblast morphology, express relevant molecular markers such as alkaline phosphatase and osteocalcin and form multilayered nodules which mineralise within 4 weeks without the addition of either dexamethasone or sodium β-glycerophosphate.

### 3.1.3. The effect of silicon on osteoblasts.

Silicon was determined to be an essential element for normal development by Carlisle (1972) and by Schwartz and Milne (1972), with the effects of silicon-deficient diets being abnormal bone formation. Similarly, Carlisle also demonstrated that chicks fed a silicon-supplemented diet (28 $\mu g.ml^{-1}$ silicon as sodium metasilicate) had enhanced bone growth.

Several decades later, the role of silicon in bone metabolism has been further elucidated. Electron microprobe analysis has revealed that silicon is concentrated in the growth areas of developing bone, such as the epiphyseal growth plates (Carlisle, 1980; Landis *et al*, 1986): the sites of greatest osteoblastic activity. Within the osteoblast, silicon is present in similar amounts to magnesium and phosphorus (Carlisle, 1976) and may be localised to mitochondria and other intracellular organelles (Carlisle, 1975), particularly during the early stages of mineralisation.

In the extracellular matrix (mineralising osteoid) silicon has been shown to be essential to the normal development of the glycosaminoglycan network, helping to stabilise the complex polysaccharide structures and forming crosslinks via silanolate bonds which regulate the structure and function of these molecules (Schwartz, 1973).

Carlisle demonstrated that silicon-supplemented embryonic chick bones showed a 100% increase in collagen content over silicon-deficient bones after 12 days in culture (Carlisle, 1974), whilst more recently Reffitt *et al* (2003) demonstrated that type I collagen synthesis increased in osteoblastic cells cultured in the presence of orthosilicic acid concentrations of 10 and 20 $\mu M$ (280 $ng.ml^{-1}$ – 560 $ng.ml^{-1}$ silicon). Similarly, Arumugram *et al* (2004) demonstrated that type I collagen mRNA increases significantly in osteoblasts supplemented with orthosilicic acid concentrations from 5 to 50 $\mu M$ (140 $ng.ml^{-1}$ – 2.8 $\mu g.ml^{-1}$ silicon).

### 3.1.4. The effect of silicic acid-eluting biomaterials on osteoblasts *in vitro*.

Bioglass® and silicate biomaterials such as silicon-substituted hydroxyapatite have been studied for several decades under *in vitro* conditions, and the effects on osteoblasts of both biomaterial surface substrates (Anderson *et al*, 2001; Gough *et al*, 2003) and their degradation products (Xynos *et al*, 2001) have been extensively analysed.

Osteoblasts cultured on 45S5 Bioglass® produce collagen-I which quickly becomes mineralised, leading to maturation of osteoblasts into matrix-encased osteocytes after 6-12 days of *in vitro* culture (Loty *et al*, 1999). The expression of insulin-like growth factor (IGF) axis system proteins, responsible for regulating certain key growth factors, are shown to increase by 300 to 500% over controls after only a few hours of exposure to the chemical extracts of 45S5 Bioglass® (Valerio *et al*, 2003) – implying that osteoblasts are rapidly able to sense changes in the calcium and or silicon content of their environment.

Osteoblasts cultured *in vitro* on Bioglass® also show a distinct morphology compared to cells grown on control substrates such as thermanox or tissue culture plastic. As shown by Gough *et al* (2003), osteoblasts cultured on 45S5 Bioglass® for two days maintained a more compact shape, with numerous filipodia, dorsal ridges and microvilli, characteristic of actively secreting cells exhibiting an osteoblastic phenotype. In contrast, cells grown on bioinert substrates for the same period formed flattened confluent sheets – features normally attributed to non-differentiated cell types.

### 3.1.5. Aims.

The aims of this section of the work were to evaluate the effect of silicon on osteoblasts, particularly the effect of porous silicon – polycaprolactone composites as a bioactive substrate to support cell growth. In addition, by evaluating the response of osteoblasts to the degradation products of pSi and pSi-PCL and to a range of orthosilicic acid concentrations in media comparable to the concentrations eluted by the materials, the relative effects of soluble silicon species and biomaterial surfaces on cell behaviour can be determined.

Several markers of osteoblastic activity were quantified at set intervals, including DNA as a measure of cell proliferation, collagen as an indicator of relative osteoblastic activity, alkaline phosphatase activity as a time marker of the onset of mineralisation and glycosaminoglycans as a measure of extracellular matrix composition and stability. The morphology of cells cultured on both PCL and pSi-PCL was also observed using conventional light microscopy and scanning electron microscopy.

## 3.2. Materials and Methods.

### 3.2.1. Osteoblast *in vitro* culture.

Osteoblasts isolated from human femoral head trabecular bone (removed during total hip arthroplasty) were cultured to passage 30 - 35 in DMEM supplemented with 10% FCS, 2mM L-glutamine, 1% non-essential amino acids, 0.2mM HEPES, 150 $\mu g.ml^{-1}$ ascorbic acid, 2% penicillin/streptomycin and with 10mM sodium β-glycerophosphate and $10^{-7}$M dexamethasone (all Sigma, UK). Cells were seeded at a density of ~$10^5$ $cells.ml^{-1}$ directly onto the PCL or composite disc surface or well surface in either 12- or 24-well plates (Nunc).

Media was replaced as dictated by the experimental set up (see below) and the osteoblasts incubated at 37°C in 5% $CO_2$. At set time points during the experiment plates were analysed for osteoblastic activity.

### 3.2.2. Analysis.

At the required time point, the media was removed from the well which was then rinsed carefully in three changes of PBS. The cells and extracellular matrix were prepared into a homogenous lysate by rapidly freeze-thawing the plate with 1 ml $H_2O$ per well for three cycles between -80°C and 20°C. DNA, collagen, glycosaminoglycan and calcium content of the lysate were quantified and alkaline phosphatase activity was measured at each time point. A measure of glycosaminoglycan and protein crosslinking was provided by quantifying pyridinoline in the cell lysate.

Statistical significance was determined by Student's T-Test compared to control populations – PCL for comparing substrates and Si-unsupplemented media for comparing Si-supplemented and conditioned media. Both conventional light microscopy using histological staining and scanning electron microscopy were used.

### 3.2.2.1. Silicic acid content of media.

The silicic acid content of media incubated with pSi-PCL or Bioglass®-PCL was determined by analysing a 50µl sample of the incubating culture media. This was added to 350µl $dH_2O$ and 100µl of a solution containing acidified ammonium molybdate (1g ammonium molybdate (IV) tetrahydrate and 3ml concentrated (17M) hydrochloric acid in 50ml total volume) was added and allowed to stand for 10 minutes. 500µl of a reducing solution (4g oxalic acid dihydrate, 1.33g 4-(methylamino)phenol sulfate, 0.8g anhydrous sodium sulfite, 20ml concentrated sulfuric acid, total volume 200ml with $dH_2O$) was then added, the solution allowed to develop a blue coloration for 2-4 hours and the absorbance read at 810nm using a spectrophotometer zeroed using $dH_2O$.

Calibration of this assay was by a standard curve obtained using known concentrations of sodium metasilicate prepared in fresh DMEM, from which absorbance at 810nm could be directly compared to Si in solution. Silicic acid is represented as mass units of silicon to avoid confusion between ortho- and polysilicic acids in solution.

### 3.2.2.2. DNA.

DNA was quantified by the intercalation of the fluorophore bisbenzimide (Hoechst 33258) between adenine-thymine residues and the analysis was performed from a commercially available kit (Sigma, UK). 200µl of the sample was added to wells of a 96-well transparent plate and 100µg.ml$^{-1}$ bisbenzimide in the supplied fluorescent assay buffer (1x in $dH_2O$) was added. The cell lysate samples were allowed to incubate for 20 minutes and the fluorescence measured at an excitation wavelength of 360nm and an emision wavelength of 460nm. A stock solution of 100µg.ml$^{-1}$ calf thymus DNA was supplied with the kit and diluted to provide a standard curve for calibrating the assay between 30µg.ml $^{-1}$and 100µg.ml$^{-1}$ DNA.

### 3.2.2.3. Collagen.

Collagen was quantified using the collagen stain sirius red (Direct red 80, Sigma UK), an anionic dye with sulphonic acid side chain groups which interact with the side chain groups of the basic amino acids present in collagen. Specific affinity of the dye for collagen under the assay conditions is due to the elongated dye molecules becoming aligned parallel to the long, rigid structure of native collagens that have intact triple helix organisation. 200µl of the cell lysate was added to a 1.7ml microcentrifuge tube and 1ml 1% *w/v* sirius red S in $dH_20$ added.

The solution was incubated at room temperature for 20 minutes and centrifuged at 10,000 rpm for 15 minutes to form a pellet. The supernatant was decanted and the tube walls carefully dried using cotton buds. The pellet was resuspended in 1ml 0.5M NaOH and the dye dissociated, the absorbance of the solution at 540nm was measured in a spectrophotometer. The assay was calibrated against a standard curve of 12.5µg.ml$^{-1}$ - 100µg.ml$^{-1}$ rat tail collagen (type I collagen from rat tail, Sigma, UK).

### 3.2.2.4. Alkaline phosphatase activity.

Alkaline phosphatase activity was determined by the ability of the cell lysate to cleave the substrate 4-methylumbelliferyl phosphate (4-MUP) into the fluorescent product 4-methylumbelliferone. 4-MUP liquid substrate system (Sigma, UK) contains 0.6mM 4-MUP in a pH 10.0 buffer solution. 200µl of this was added to wells of a 96-well plate containing 50µl cell lysate and the fluorscence measured with excitation at 360nm and emission at 440nm within 5 minutes of the reagent solution being added. The results were presented as units of activity derived directly from the fluorescence.

### 3.2.2.5. Glycosaminoglycans.

Glycosaminoglycans (GAGs) were quantified using Alcian Blue 8GX (Sigma, UK), a cationic dye which forms strong but reversible electrostatic bonds with anionic groups on the polysaccharide. 50µl cell lysate was placed into a 1.3ml

microcentrifuge tube and acidified by the addition of 100µl 8M guanidine hydrocholoride. After 15 minutes, 500µl 0.3% sulphuric acid (with 0.75% triton x-100, in $dH_2O$) was added to the tube followed by 500µl 200µg.ml$^{-1}$ Alcian blue 8GX and the mixture incubated at room temperature for 15 minutes. The tube was centrifuged at 15,000 rpm for 10 minutes and the supernatant carefully decanted and discarded. Residual supernatatant was carefully removed with a cotton tip and the pellet resuspended in buffer (4M guanidine hydrochloride, 33% 1-propanol, 0.25% triton x-100). The absorbance of the solution at 620nm was measured and compared to known concentrations of chondroitin-4-sulphate (from bovine trachea, Sigma, UK) from 50 - 200µg.ml$^{-1}$.

**3.2.2.6. Calcium.**

Calcium is chelated by alizarin red S in aqueous solution, forming a complex which can be subsequently dissociated. A 1% *w/v* solution of alizarin red S in $dH_2O$ was prepared and adjusted to pH 10.0 using ammonium hydroxide, 1ml of this solution was added to the empty well or disc and allowed to incubate for 10 minutes. The unbound calcium stain was carefully removed in several changes of $dH_2O$ and allowed to dry before the addition of 1ml 2% *w/v* cetylpyridinium chloride monohydrate. The absorbance of the resulting solution at 562nm was measured and expressed directly as units of absorbance.

**3.2.2.7. Pyridinoline.**

Mature type I collagen is crosslinked by pyridinoline and deoxypyrodinoline which are formed by the enzymatic action of lysyl oxidase on the amino acid lysine (Delmas, 1995; Seibel *et al*, 1992). Pyridinoline was quantified using a commercial 'sandwich' ELISA fluorescent immunoassay (MetraSys PYD ELISA, Technoclone, UK) designed for studying PYD concentration of human serum.

50µl of each cell lysate was pipetted into anti-PYD coated wells of the provided ELISA strip alongside serially diluted known concentrations of pyridinoline isolated from human urine (0 – 750 nmol.l$^{-1}$). 100µl prepared enzyme conjugate was added (murine monoclonal anti-pyridinoline antibody conjugated to alkaline

phosphatase in non-ionic detergent buffer) and incubated for 3 hours in the dark at 4°C. 150µl substrate solution was added (20mg p-Nitrophenol phosphate in 10ml diethanolamine and magnesium chloride buffer) and incubated for 1 hour at room temperature. 100µl stop solution (0.5M NaOH) was added and the absorbance (optical density) of the solution measured at 405nm. Sample values were compared to a calibration graph of the standard solution.

### 3.2.3. Experimental.

A series of experiments were designed to evaluate the response of osteoblasts to porous silicon – polycaprolactone composites containing a range of porosities of pSi in a range of quantities per disc. The effect of pSi-PCL degradation products on osteoblasts *in vitro* was determined and compared to the effect of 45S5 Bioglass®-PCL degradation products. A range of silicic acid concentrations were prepared from 100 $ng.ml^{-1}$ to 100 $\mu g.ml^{-1}$ using sodium metasilicate rather than porous silicon as a source of bioavailable silicon and used to supplement osteoblasts *in vitro*.

#### 3.2.3.1. Response of osteoblasts to pSi-PCL composites *in vitro*.

A range of 250mg composite discs were manufactured as described in chapter two (**fig. 2.4**, page 50) containing polycaprolactone and porous silicon with porosities of 54%, 66% and 82% which were milled by hand at pSiMedica and seived to provide particle sizes of 37 - 150µm, and the standardised 70%, 11µm particles that were used in all later experiments. These were made into composites with pSi the following ratios:

| Experiment | pSi porosity | pSi per 250mg composite disc (mg) | | | | | |
|---|---|---|---|---|---|---|---|
| **3.3.1.1.** | 54% | **1** | **5** | **10** | **-** | **25** | **50** |
| **3.3.1.2.** | 66% | **0.5** | **5** | **10** | **20** | **-** | **30** |
| **3.3.1.3.** | 70% | **1** | **-** | **-** | **20** | **-** | **-** |
| **3.3.1.4.** | 82% | **1** | **5** | **10** | **20** | **-** | **30** |

**Table 3.5.** Range of compositions tested for each porosity of pSi.

Composite discs were sterilised in 70% ethanol for 24 hours at room temperature before being dried completely overnight in 24-well plates (Nunc) in a sterile fume hood. Osteoblasts at passage 30 - 35 were seeded at a density of ~$10^5$ cells.ml$^{-1}$ directly onto the tissue culture plastic well, PCL or composite disc surface. 1ml DMEM supplemented with 10% FCS, 2mM L-glutamine, 1% non-essential amino acids, 0.2mM HEPES, 150 μg.ml$^{-1}$ ascorbic acid, 2% penicillin/streptomycin and with 10mM sodium β-glycerophosphate and $10^{-7}$M dexamethasone (all Sigma, UK) was added which was exchanged every 48 hours.

**3.2.3.1.1. Scanning electron microscopy (SEM).**

Osteoblasts cultured on PCL and composite discs were dehydrated and coated for SEM as follows. Media was removed from cells and the disc washed in PBS thoroughly but gently to avoid damaging cell layer. In a fume hood, cells were fixed in 3% glutaraldehyde for 1 hour and rinsed with $dH_2O$ twice. Osmium tetroxide was added and left to incubate for 30 mins and then rinsed off in three x 1ml $dH_2O$.

A series of ethanol rinses was performed to dehydrate the sample: 2 x 5 mins in 50% ethanol, 2 x 5 mins in 70% ethanol, 2 x 5 mins in 90% ethanol, 3 x 10 mins in 100% ethanol. Finally the discs were incubated for 5 mins each in 2 changes of 1ml hexamethyldisilizane (HMDS). All HMDS was removed and air dried in fume hood completely. The dry discs were gold coated for 3-6 minutes in a sputter coater and imaged using a Jeol JSM840 scanning electron microscope.

### 3.2.3.2. Osteoblast response to silicic acid in media.

Silicic acid was added to DMEM using known concentrations of a sodium metasilicate (Sigma, UK; $Na_2SiO_4.5H_2O$) stock solution to generate desired silicic acid concetrations as shown in the table below (**table 3.6**). Sodium metasilicate was added to the media as a concentrated solution in 10ml $dH_2O$ which was sterilised by filtration using a 0.2µm syringe filter.

Control media (0 $\mu g.ml^{-1}$) and DMEM for dilution of stocks contained no supplemented silicon or sodium metasilicate and were produced at the same times as those conditioned and stored under identical conditions (4°C for up to 7 days or -20°C for long-term storage). Silicic acid concentrations are presented as ng or µg silicon [Si] per ml media.

Osteoblasts at passage 30 - 35 were seeded in DMEM onto the well surfaces of 24-well plates (Nunc) at a density of ~$10^5$ cells per well and once attached (~4 hours) the media was replaced with 1ml silicon-supplemented media or control media (unsupplemented). The media was replaced every 48 hours for up to 28 days.

| Experiment | Silicic acid concentrations (per ml) |
|---|---|
| **3.3.1.** | 100ng 250ng 500ng 750ng 1000ng |
| **3.3.2.** | 1µg 2 µg 3 µg 4 µg 5 µg |
| **3.3.3.** | 1 µg 5 µg 10 µg 15 µg 20 µg 25 µg 30 µg 35 µg |
| **3.3.4.** | 25µg 50µg 100µg |

**Table 3.6.** Silicic acid concentrations used in the investigation achieved by the addition of sodium metasilicate to DMEM.

### 3.2.3.3. Osteoblast response to pSi, pSi-PCL and Bioglass®-PCL degradation products.

Media was conditioned with the breakdown products of pSi in two ways – by incubating pSi microparticles in a stock solution of cell culture medium or by co-incubating pSi-PCL composite discs in a cell-culture plate, seperated from osteoblasts by a semi-permeable (size exclusion) membrane.

#### 3.2.3.3.1. pSi-conditioned media.

1g microparticles of porous silicon were sterilised in 2ml 70% ethanol for 24 hours and added to 550ml DMEM supplemented with 10% FCS, sodium β-glycerophosphate and 10mM dexamethasone. The media was assayed for silicon content after 28 days and found to contain 45 $\mu g.ml^{-1}$ Si, which was diluted with pSi-free media (produced at the same time ad stored at 4°C to produce silicic acid concentrations of 1 – 5 $\mu g.ml^{-1}$ Si which were used for culturing osteoblasts.

Osteoblasts at passage 30 were seeded onto the well surface of 24-well cell culture plates (Nunc) at a density of $\sim 10^5$ cells per well and 1ml media added. The media was replaced every 48 hours for 20 days; one plate was analysed every 5 days for DNA and collagen content.

#### 3.2.3.3.2. Co-incubation of osteoblasts with pSi-PCL and Bioglass®-PCL composites.

Bioactive glass microparticles (batch code PM0126) were obtained from Dr Julie Gough (University of Manchester, UK) and composite discs were formed as described for pSi-PCL containing:

**A.** 1mg or 20mg 70% porous pSi per 250mg disc

**B.** 20mg Bioglass® or 20mg 70% porous pSi per 250mg disc

The composites were sterilised in 70% ethanol for 24 hours and dried overnight in a fume hood together with PCL-only discs. The discs were placed in transwell inserts (12mm diameter, 3.0μm pore size polycarbonate membrane; Corning, US) which were then fitted into 12-well plates. Controls used were empty inserts.

Osteoblasts at passage 30 were seeded onto the well surface at a density of ~$10^5$ cells per well and 3ml media was added to cover the disc in the transwell completely. Care was taken to ensure that no cells were introduced to the transwell and that all osteoblast growth was on the tissue culture well bottom.

1ml media was removed and replaced daily for 25 days, with time points at 1 day and every 5 days at which point the transwell inserts were removed, the plate carefully rinsed and freeze/thawed and lysates analysed for DNA, collagen and glycosaminoglycan content and alkaline phosphatase activity.

## 3.3. Results.

### 3.3.1. Response of osteoblasts to pSi-PCL composites.

Composite discs were made containing porous silicon in polycaprolactone and formed into discs 250 ± 10mg in weight, approximately 11.5mm in diameter. Four porosities of porous silicon were used as outlined in the methods section and in Chapter Two, including 54% porous, 66% porous and 82% porous microparticles that were milled and seived by hand (38 - 150µm particle size), and the 70% particles that were provided in a smaller size fraction (11µm particles).

Composites were manufactured containing 1 – 50mg pSi per 250mg disc (up to 20% *w/w*) and the silicic acid release rates of each material ascertained by measuring the silicic acid content of cell culture media. Silicic acid release was shown to be proportional to the percentage porosity of the silicon, particle size and porous silicon content of the disc (**fig. 3.7**), with 54% and 66% porous silicon releasing similar quantities of silicic acid into the culture medium but leveling off from 10mg to 50mg to elute less than 200ng.ml$^{-1}$ Si per day. 70% porous silicon inclusion in the disc showed a more linear relationship with silicic acid concentration of incubating media. 82% porous silicon released significantly more silicic acid and it's degradation caused effervesence of the culture medium, producing a foam on the surface of the medium in the culture well.

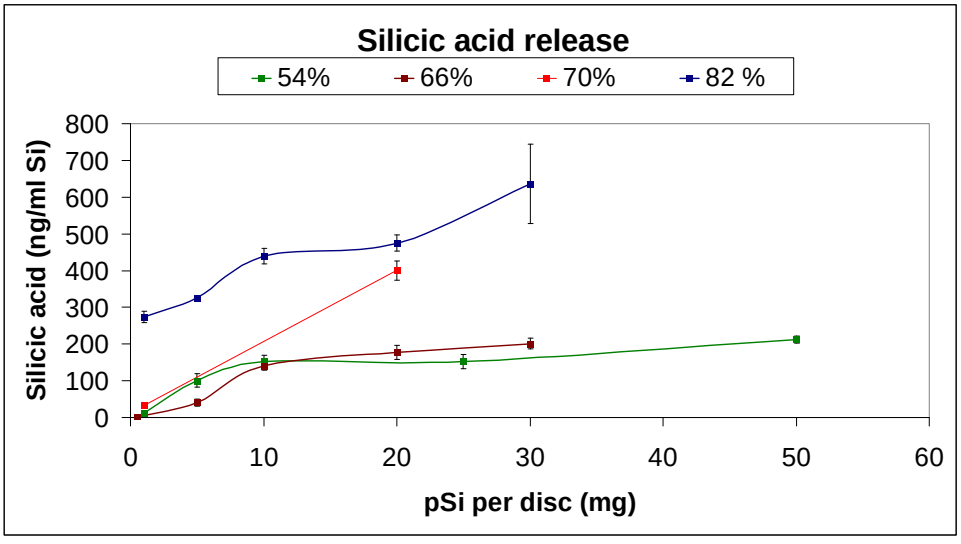


**Fig. 3.7.** Silicic acid release per day into media. Error bars are standard error of the mean, n = 3.

**3.3.1.1. 54% porous pSi.**

Scanning electron microscopy of cultured osteoblasts shows that the cell morphology is similar when cultured on PCL or 50mg pSi (20% *w*/*w* pSi) at 7 days (**fig. 3.8**). Substantial numbers of rounded cells were observed on both PCL and composite materials, but it was not determined if these were apoptotic or undergoing cell division.

Osteoblast proliferation on 54% porous silicon-containing composite discs was similar across the range of compositions and lower than tissue culture plastic controls (**fig. 3.9.A**). Collagen production was also similar, with an increase in total collagen on the 50mg composite at day 21 (**fig. 3.9.B**).

When normalised for cell number (μg collagen / μg DNA) however, the amount of collagen produced per osteoblast at day 21 is higher in the high-pSi composites and higher than tissue culture plastic controls, but not higher than PCL-only (**fig. 3.9.C**). Calcium deposition at day 21 (**fig. 3.9.D**) was also significantly greater than PCL only discs for composites containing ≥ 10mg pSi ($p < 0.05$).

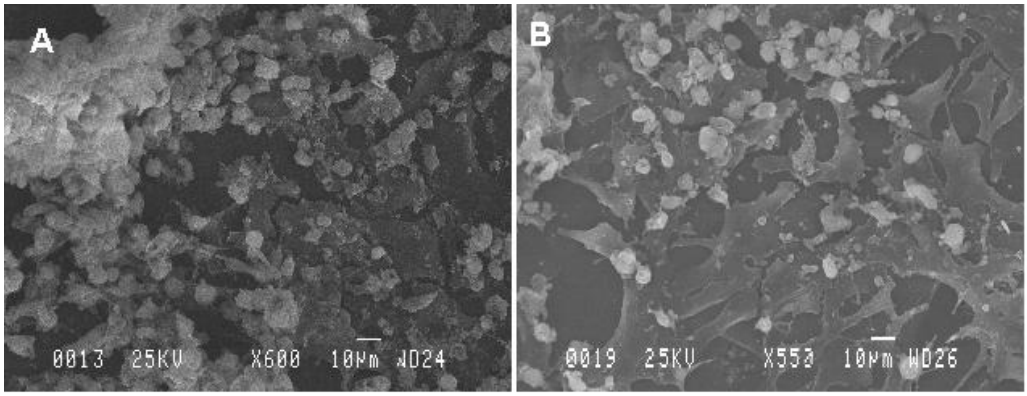


**Fig. 3.8**. Osteoblasts cultured on the surfaces of **A**. PCL or **B**. 50mg pSi composites (54% porous) for 7 days.

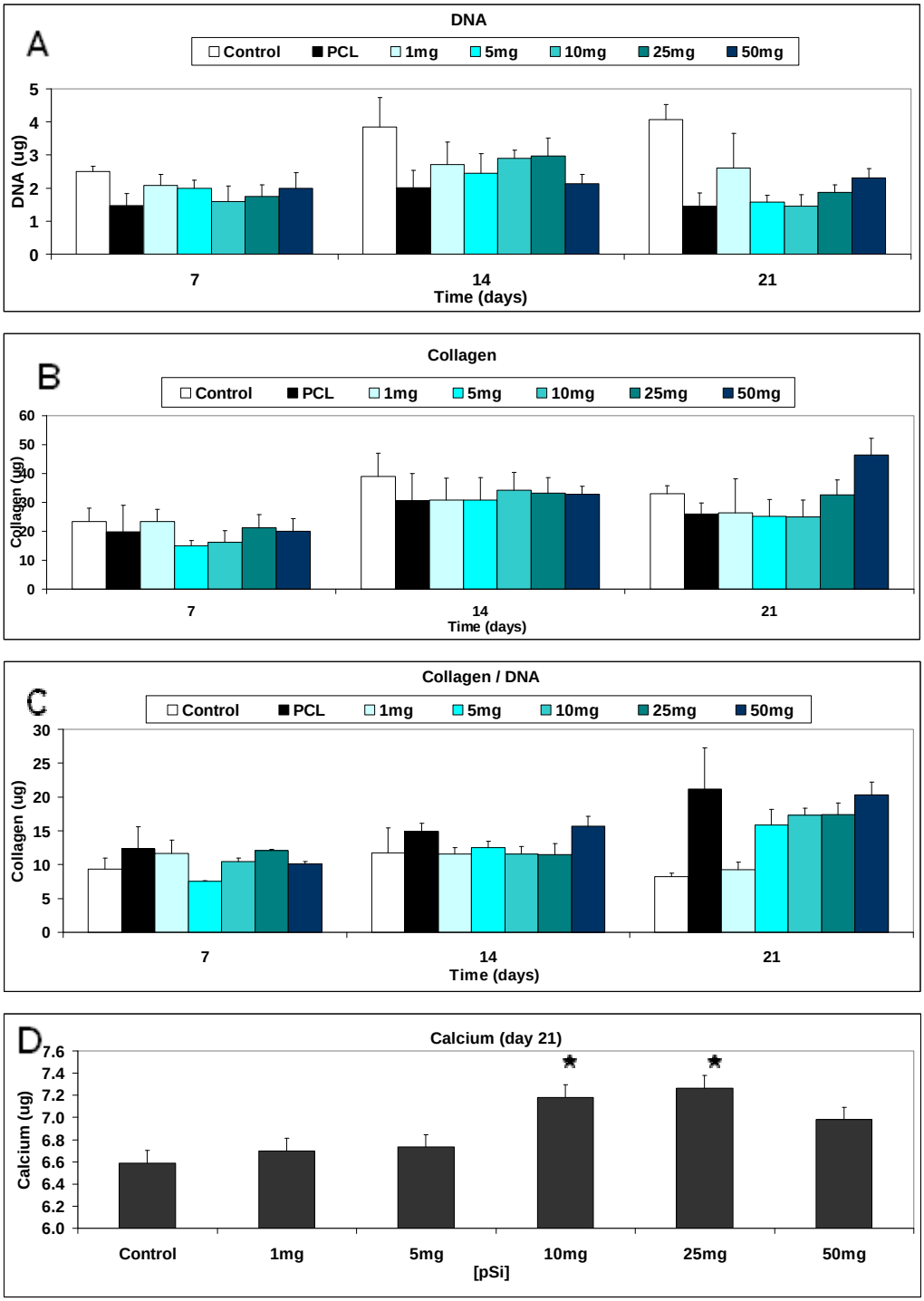


**Fig. 3.9.** Osteoblasts cultured on composite discs containing quantities of 54% porous silicon. **A**. DNA content of cell lysate. **B**. Collagen (total). **C**. Collagen normalised for cell number (collagen/DNA, µg/µg). **D**. Calcium deposition at day 21. Bars show standard error, n=3. Statistical significance was determined by Student's T-Test compared to PCL as the control population. Significant increase $p < 0.05$ ( ★ ).

### 3.3.1.2. 66% porous pSi.

Addition of 66% porous silicon to PCL did not markedly affect the growth of osteoblasts cultured on the surface, although higher pSi concentrations showed lower cell numbers at each time point than tissue culture plastic controls. Total collagen and collagen per cell (DNA) were also similar across all compositions with osteoblasts growing on PCL producing as much collagen as those on composites, and more per cell than tissue culture plastic controls (**fig. 3.10**).

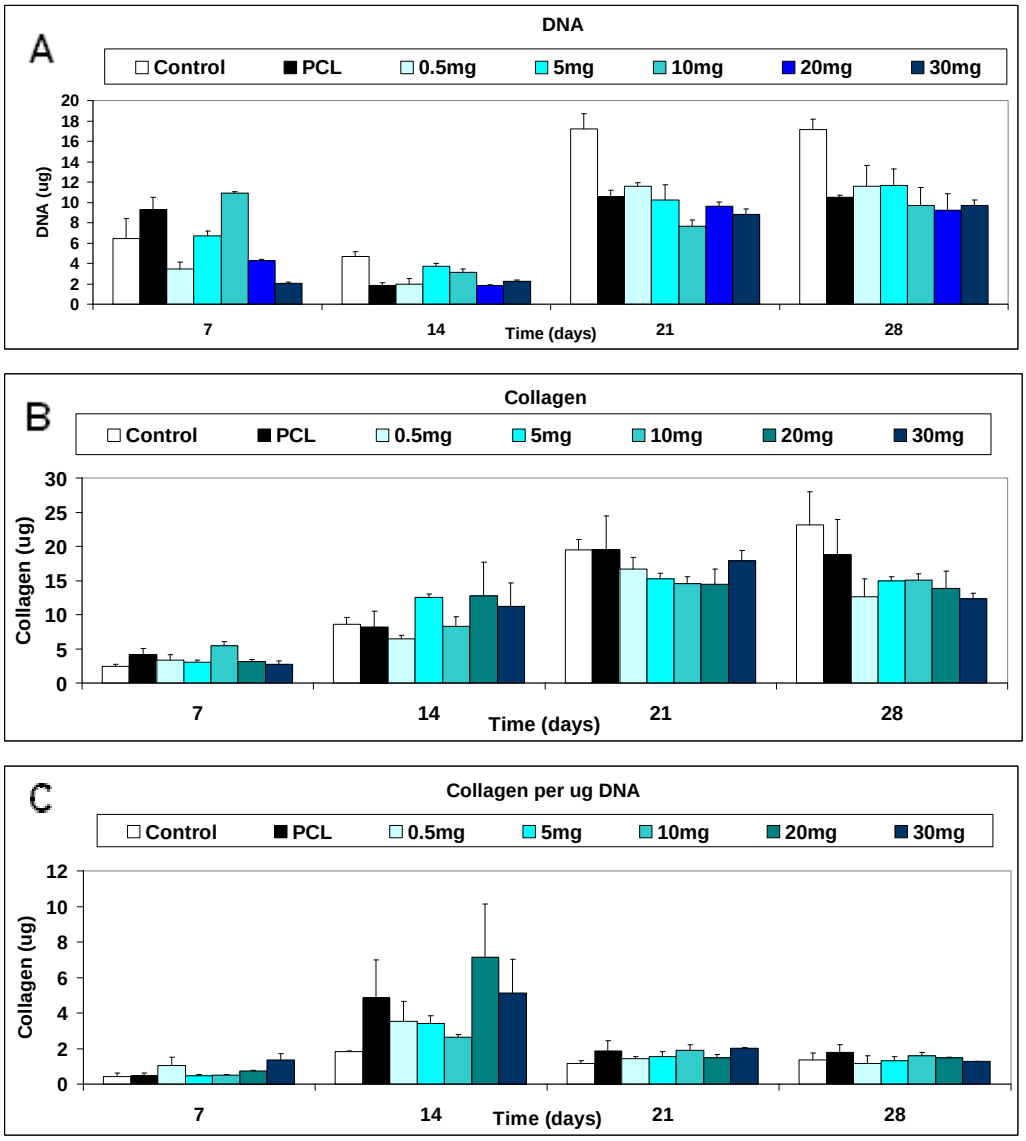


**Fig. 3.10.** Osteoblasts cultured on composite discs containing quantities of 66% porous silicon. **A**. DNA content of cell lysate. **B**. Collagen (total). **C**. Collagen normalised for cell number (collagen/DNA, µg/µg). Bars show standard error of the mean, n=3. No statistical significance was observed as determined by Student's T-Test compared to PCL as the control population.

### 3.3.1.3. 70% porous pSi.

The osteoblast response to 1mg and 20mg composites containing 70% porous silicon at 10 days *in vitro* culture was evaluated. In previous studies osteoblasts were shown to exhibit the greatest difference in behaviour between PCL and composite substrates at day 10 *in vitro* and so a large repeat number (n = 12) was used for a thorough statistical analysis of the effect of pSi on osteoblasts proliferation and activity.

Osteoblasts at day 10 displayed similar levels of DNA (**fig. 3.11**) when cultured on tissue culture plastic, PCL or 1mg pSi-PCL, but with significantly lower cell populations on the 20mg composite ($p$ = 0.0027) than PCL-only. Alkaline phosphatase activity was significantly higher for osteoblasts cultured with 20mg pSi than either PCL alone or 1mg pSi at day 10 (**fig. 3.12**). Collagen production was higher for the 20mg composite than PCL ($p$ = 0.0070). Osteoblast production of glycosaminoglycans (total and per μg DNA) as determined by alcian blue was significantly higher on 20mg pSi-containing composites ($p$ < 0.001).

Osteoblasts cultured on thin discs of PCL or 20mg pSi-PCL showed different cell morphologies at 5 days *in vitro* culture (**fig. 3.13**). Osteoblasts on PCL-only are rounded and closely packed, whereas those on pSi-PCL appear to have more pronounced filipodia and cellular processes which are associated with collagen.

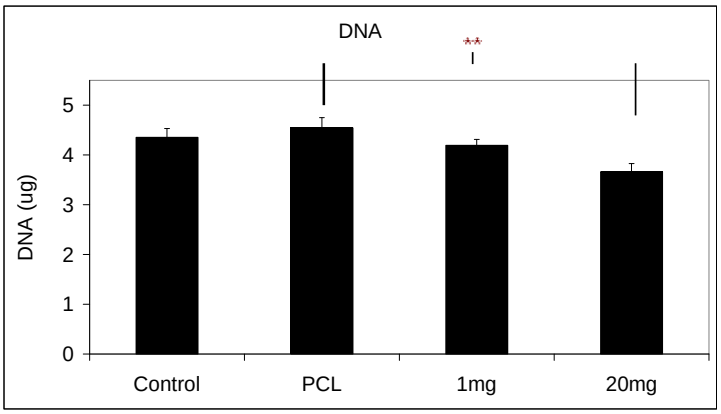


**Fig. 3.11.** Proliferation of osteoblasts cultured for 10 days on the surface of tissue culture plastic, PCL, 1mg pSi-PCL and 20mg pSi-PCL. Statistical significance was determined by Student's T-Test compared to PCL as the control population. Significant decrease p< 0.01 (★★).

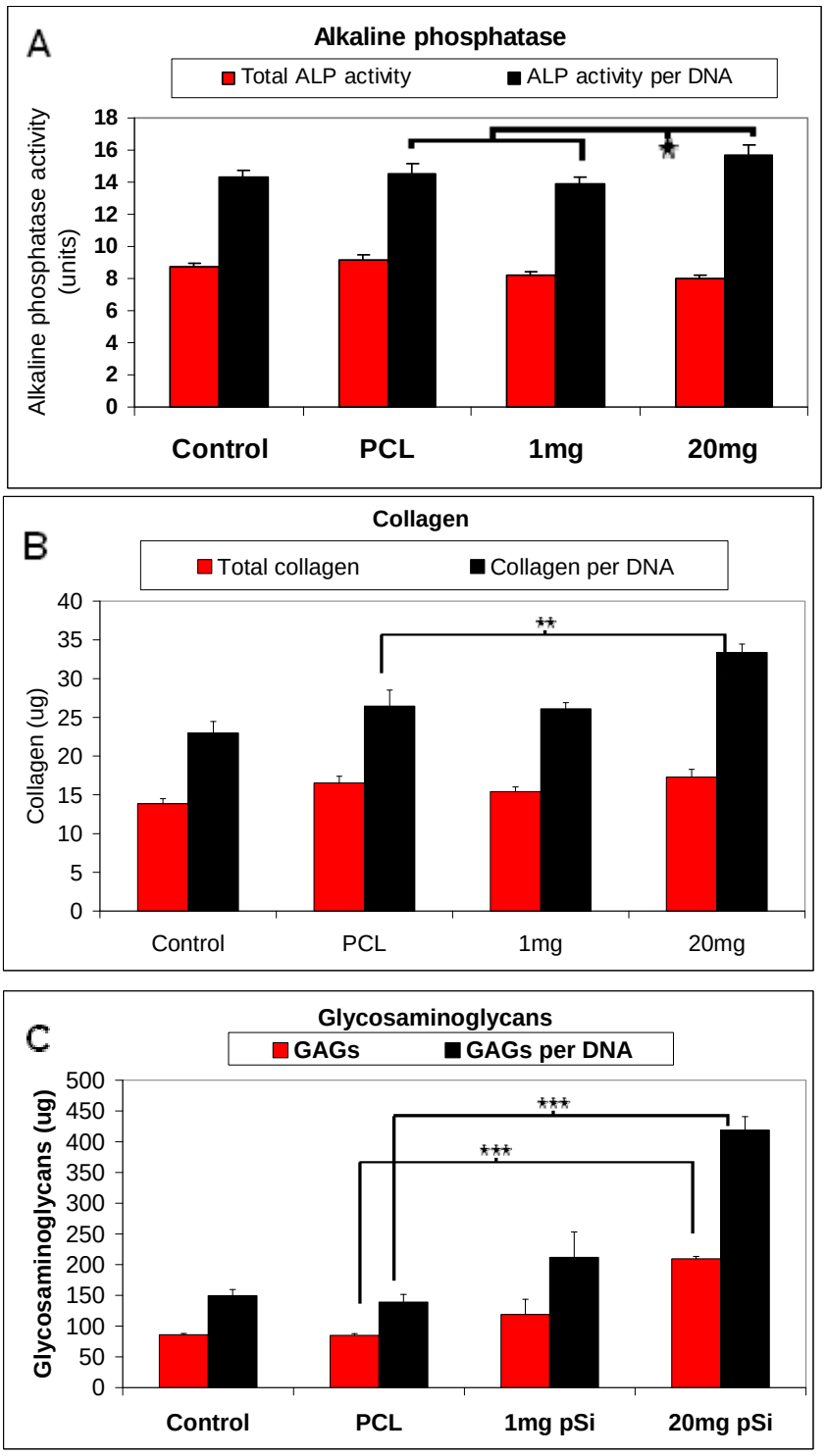


**Fig. 3.12.** Osteoblasts cultured for 10 days on the surface of tissue culture plastic, PCL, 1mg pSi-PCL and 20mg pSi-PCL. **A**. Alkaline phosphatase activity. **B**. Collagen (total) and collagen per µg DNA. **C**. Glycosaminoglycan content in total and GAGs per µg DNA. Bars are standard error of the mean, n=12. Statistical significance was determined by Student's T-Test compared to PCL as the control population. Significant increase $p < 0.05$ (★); $p < 0.01$ (★★); $p < 0.001$ (★★★).

### 3.3.1.4. 82% porous pSi.

82% porous silicon proved toxic to cells *in vitro*. Upon immersion in tissue culture medium, composites containing more than 5mg pSi effervesced, forming a foam which filled the well. No osteoblasts were observed surviving in the wells or on the discs after 24 hours.

## 3.3.2. Osteoblast response to silicic acid in media.

Osteoblasts were cultured *in vitro* on the well surfaces of 24-well cell culture plates. Media was DMEM containing 10% FCS and supplemented with sodium β-glycerophosphate and 10mM dexamethasone to maintain osteoblastic phenotype, and supplemented with sodium metasilicate to generate desired concentrations of soluble silicon species. Silicic acid concentration is represented as [Si] to cover the presence of mono- (ortho)-silicic acid and polysilicic acids in the solution.

Silicic acid concentrations were tested in four ranges:

**3.3.2.1.** 100 – 1000 $ng.ml^{-1}$

**3.3.2.2.** 1 – 5 $\mu g.ml^{-1}$

**3.3.2.3.** 5 – 35 $\mu g.ml^{-1}$

**3.3.2.4.** 25 – 100 $\mu g.ml^{-1}$

### 3.3.2.1. Osteoblast response to 100 – 1000 $ng.ml^{-1}$ Si.

The amount of silicic acid produced by 1-20% composite discs incubated in SBF is in the order of 50 – 500 $ng.ml^{-1}.day^{-1}$ [Si] which is reflected in the silicic acid range established in this experiment by supplementing media with sodium metasilicate.

Osteoblast proliferation as determined by DNA content of cell lysates was similar at each time point at all Si concentrations (**fig. 3.13.A**). Alkaline phosphatase activity per cell was highest at day 7 for all Si concentrations and showed a linear decrease over time for all conditions (**fig. 3.13.B**). Collagen per cell was also similar throughout all concentrations tested (**fig. 3.13.C**). No significant difference in any activity marker was observed at any time point, implying that this concentration range of silicic acid (when achieved by dissociating sodium metasilicate) does not have an effect on osteoblast activity *in vitro*.

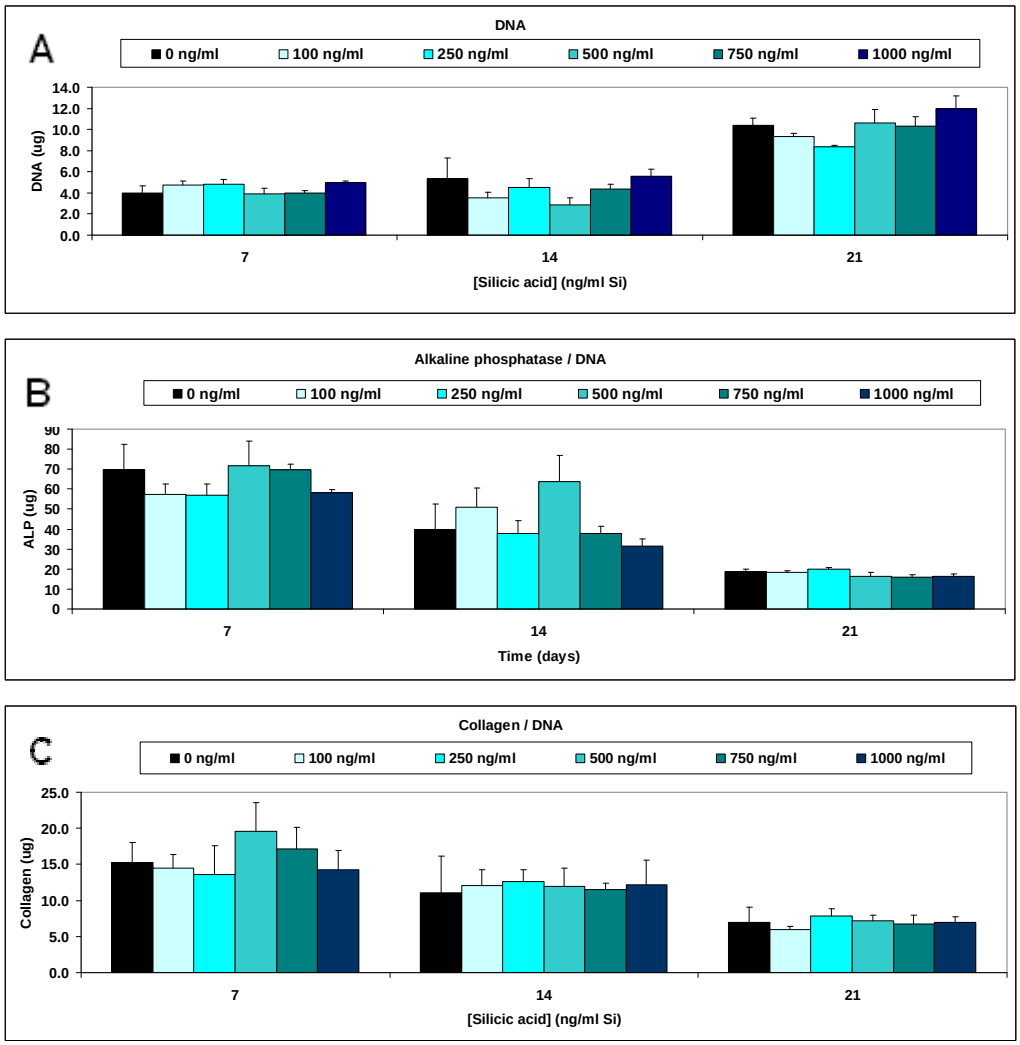


**Fig 3.13.** Osteoblasts cultured in media containing 100 – 1000 ng.ml$^{-1}$ Si. **A**. DNA content of cell lysate. **B**. Alkaline phosphatase activity per µg DNA. **C**. Collagen produced per µg DNA. Bars show standard error, n=3.

### 3.3.2.2. Osteoblast response to 1 – 5 μg.ml$^{-1}$ Si.

When cultured in media containing Si in the concentration range 1- 5 μg.ml$^{-1}$, osteoblasts proliferated at a similar rate to Si-unsupplemented controls (**fig. 3.14.A**), and cell populations were significantly higher at 1 and 4 μg.ml$^{-1}$ on day 15 days of the experiment ($p < 0.05$).

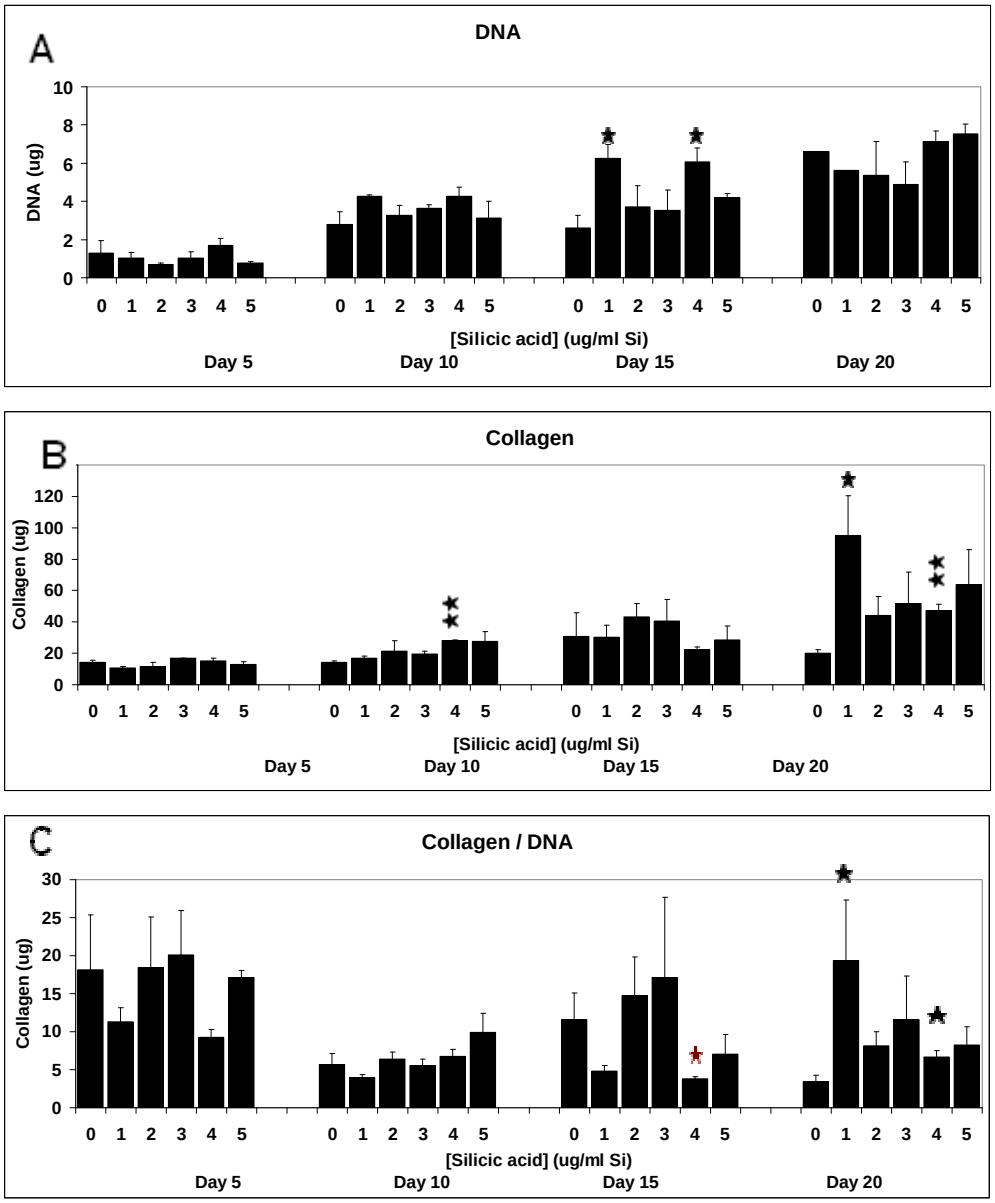


**Fig. 3.14.** Osteoblasts cultured in media containing 1 - 5μg.ml$^{-1}$ Si, from sodium metasilicate. **A**. DNA content of cell lysate. **B**. Total collagen per well. **C**. Collagen produced per μg DNA. Bars show standard error of the mean, n=3. Statistical significance was determined by Student's T-Test compared to 0μg.ml$^{-1}$ Si as the control population. Significant increase $p < 0.05$ (★ ), $p < 0.01$ (★★); significant decrease $p < 0.05$ (★).

The osteoblast production of collagen was similar for all conditions up to day 20, at which point cells cultured with 1 and 4 $\mu g.ml^{-1}$ Si produced more collagen in total than silicon-free controls (**fig. 3.14.B**). When collagen production was normalised for cell number, collagen per osteoblast at day 20 was significantly higher when cultured with 1 and 4 $\mu g.ml^{-1}$ Si than in unsupplemented controls (**fig. 3.14.C**).

### 3.3.2.3. Osteoblast response to 1 – 35 $\mu g.ml^{-1}$ Si.

Osteoblast growth rates in higher (> 25 $\mu g.ml^{-1}$) concentrations of Si are diminished for the first 21 days *in vitro* culture, with the reduction in cell population directly proportional to the amount of Si added – in concentrations greater than 20$\mu g.ml^{-1}$ Si osteoblast populations are significantly reduced ($p < 0.05$ for Si concentrations greater than 25 $\mu g.ml^{-1}$ for the first 21 days) although in all conditions cell numbers were similar by 28 days (**fig. 3.15.A**).

Collagen production per μg DNA was higher for osteoblasts cultured with more than 20 $\mu g.ml^{-1}$ Si than Si-unsupplemented media for the first 14 days, with some Si-supplemnted conditions being significantly increased (**fig. 3.15.b**). Calcium deposition was similar under all conditions, but significantly higher at day 7 for media containing 30 – 35 $\mu g.ml^{-1}$ Si ($p < 0.05$; **fig. 3.15.C**).

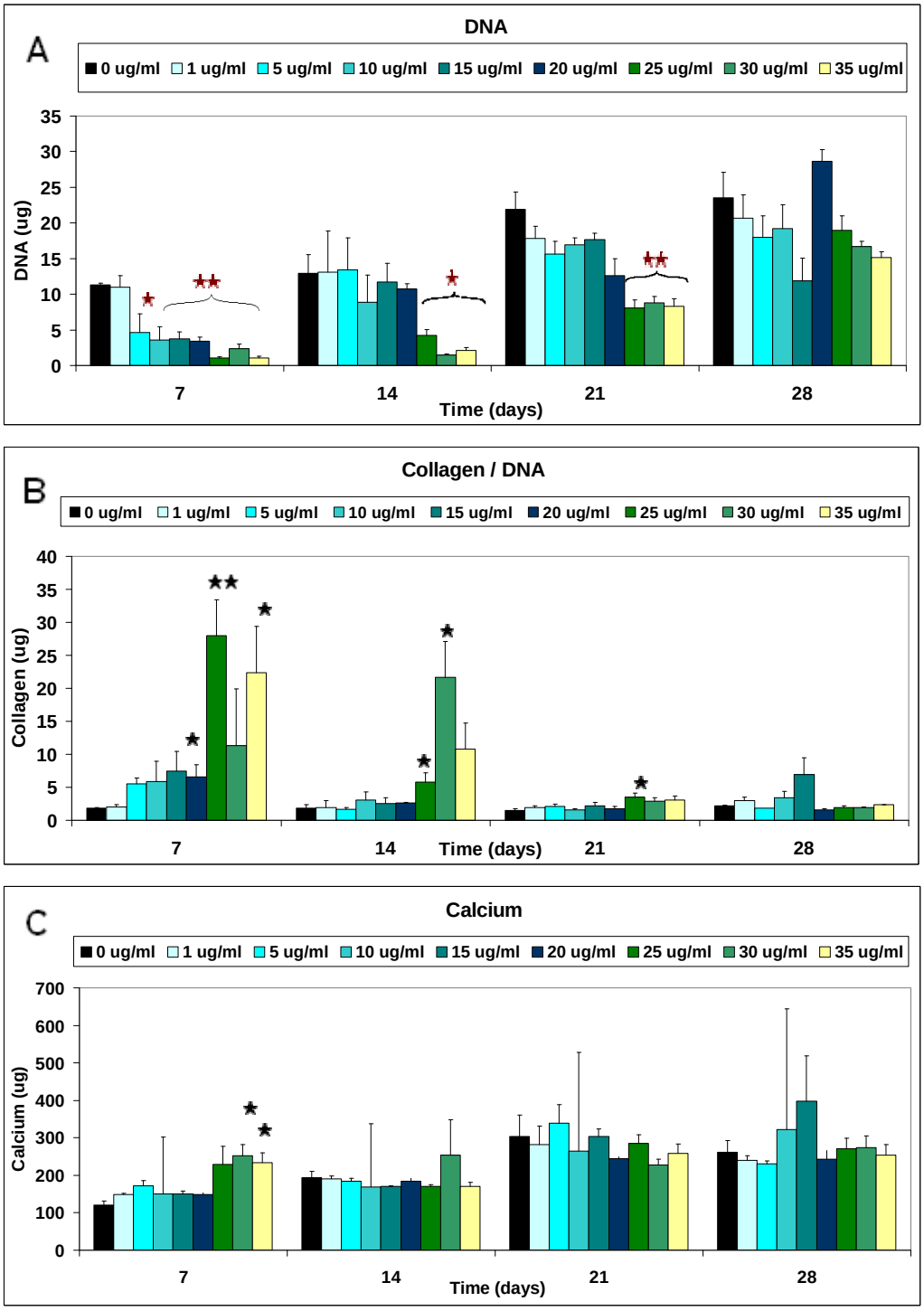


**Fig. 3.15.** Osteoblasts cultured in media containing 1 – 35 μg.ml$^{-1}$ Si. **A**. DNA, **B**. Collagen produced per μg DNA. **C**. Calcium deposition. Bars are standard error of the mean, n=3. Statistical significance was determined by Student's T-Test compared to 0μg.ml$^{-1}$ Si as the control population. Significant increase $p < 0.05$ (★), $p < 0.01$ (★★); significant decrease $p < 0.05$ (★), $p < 0.01$ (★★).

### 3.3.2.4. Osteoblast response to 25 - 100 μg.ml$^{-1}$ Si.

Osteoblasts cultured in media containing 100 μg.ml$^{-1}$ silicon showed significantly reduced growth rates ($p < 0.01$) compared to silicic acid-free media and media containing up to 25 μg.ml$^{-1}$ Si for the first 15 days (**fig. 3.16.A**). Media containing 50 μg.ml$^{-1}$ Si also inhibited osteoblast proliferation at 10 , 15 and 25 days ( $p < 0.05$).

Osteoblast production of collagen was significantly lower with 100 μg.ml$^{-1}$ Si than under control conditions and 25 μg.ml$^{-1}$ Si at 10 and 20 days ($p < 0.01$ at day 10 and day 20), whereas 25 μg.ml$^{-1}$ Si slightly increased the total collagen produced at 15 days (**fig. 3.16.B**). When normalised for cell population (divided by μg DNA, **fig. 3.16.C**), collagen production was higher at day 10 in 50 μg.ml$^{-1}$ Si and day 15 for 25 μg.ml$^{-1}$ Si ($p < 0.05$) than controls. However, collagen per osteoblast was significantly lower at day 20 for cells cultured with 50 μg.ml$^{-1}$ Si and 100 μg.ml$^{-1}$ Si ($p < 0.01$).

Osteoblasts cultured *in vitro* with more than 50 μg.ml$^{-1}$ Si in culture media showed diminished growth and collagen production compared to unsupplemented osteoblasts and those cultured in lower silicic acid concentrations.

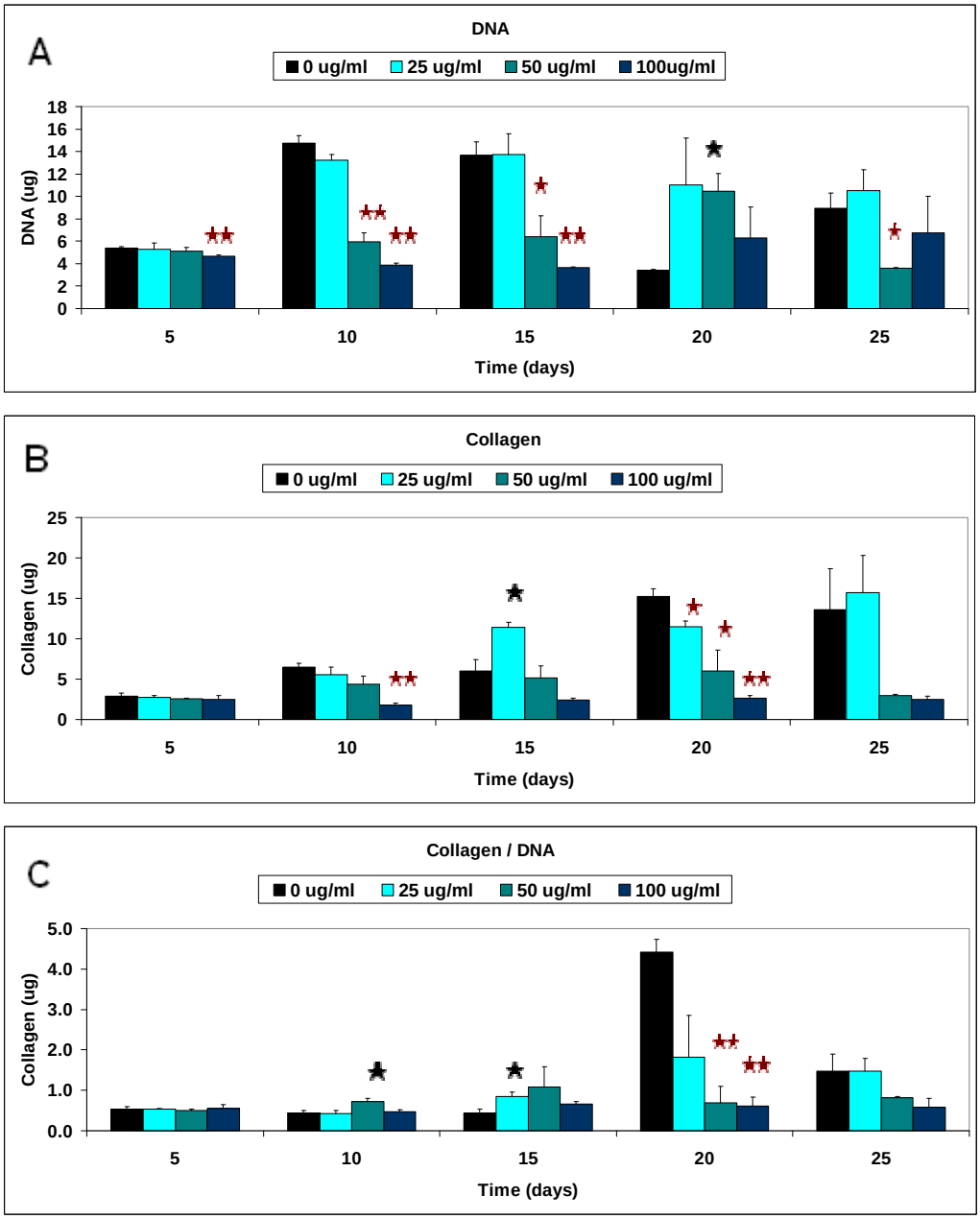


**Fig. 3.16.** The osteoblasts *in vitro* response to silicic acid concentrations of 25 – 100 μg.ml$^{-1}$ Si in culture media. **A**. DNA, **B**. Collagen, **C**. Collagen per DNA. Bars are standard error of the mean, n=3. Statistical significance was determined by Student's T-Test compared to 0μg.ml$^{-1}$ Si as the control population. Significant increase $p < 0.05$ (★ ), $p < 0.01$ (★★); significant decrease $p < 0.05$ (★), $p < 0.01$ (★★).

### 3.3.3. Osteoblast response to pSi degradation products.

Media was conditioned with the breakdown products of pSi in two ways – by incubating pSi microparticles in a stock solution of cell culture medium or by co-incubating pSi-PCL composite discs in a cell-culture plate, seperated from osteoblasts by a semi-permeable (size exclusion) membrane.

#### 3.3.3.1. pSi-conditioned media.

1g microparticles of porous silicon were used to condition 550ml DMEM supplemented with 10% FCS, sodium β-glycerophosphate and 10mM dexamethasone. The media was assayed for silicon content after 28 days and found to contain 45 $\mu g.ml^{-1}$ Si, which was diluted with pSi-free media to produce silicic acid concentrations of 1 – 5 $\mu g.ml^{-1}$ Si which were used for culturing osteoblasts.

Osteoblasts proliferated at a similar rate (**fig. 3.17**). Si-supplemented media stimulated cell growth up to day 15, with significantly enhanced proliferation in Si concentrations of 4 $\mu g.ml^{-1}$ Si (day 5 and 10), 5 $\mu g.ml^{-1}$ Si (day 10) and 1 $\mu g.ml^{-1}$ Si (day 15). At day 20 no difference was observed in cell populations under any condition (**fig. 3.18.A**).

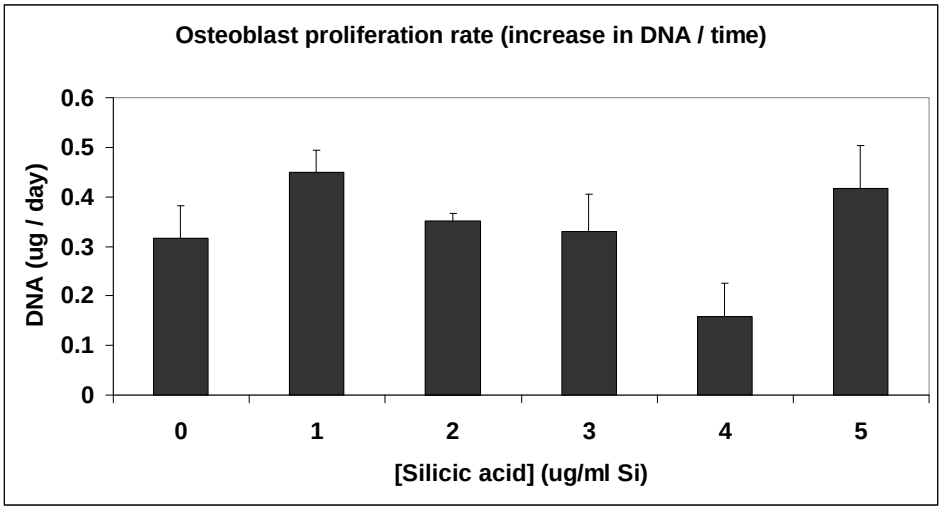


**Fig. 3.17.** Proliferation rate of osteoblasts as determined by increase in DNA content of cell lysate per day. Error bars show proportional deviation from linear regresssion coefficient, $R^2$ (n = 4).

Collagen deposition was significantly higher when osteoblasts were cultured with 3 - 5 μg.ml$^{-1}$ Si at day 10, 4 μg.ml$^{-1}$ Si at day 15 and 4 - 5 μg.ml$^{-1}$ Si at day 20 (**fig. 3.18.B**). When normalised for cell number, collagen per μg DNA was significantly greater only at day 20, for osteoblasts cultured with 3 – 4 μg.ml$^{-1}$ Si (**fig. 3.18.C**).

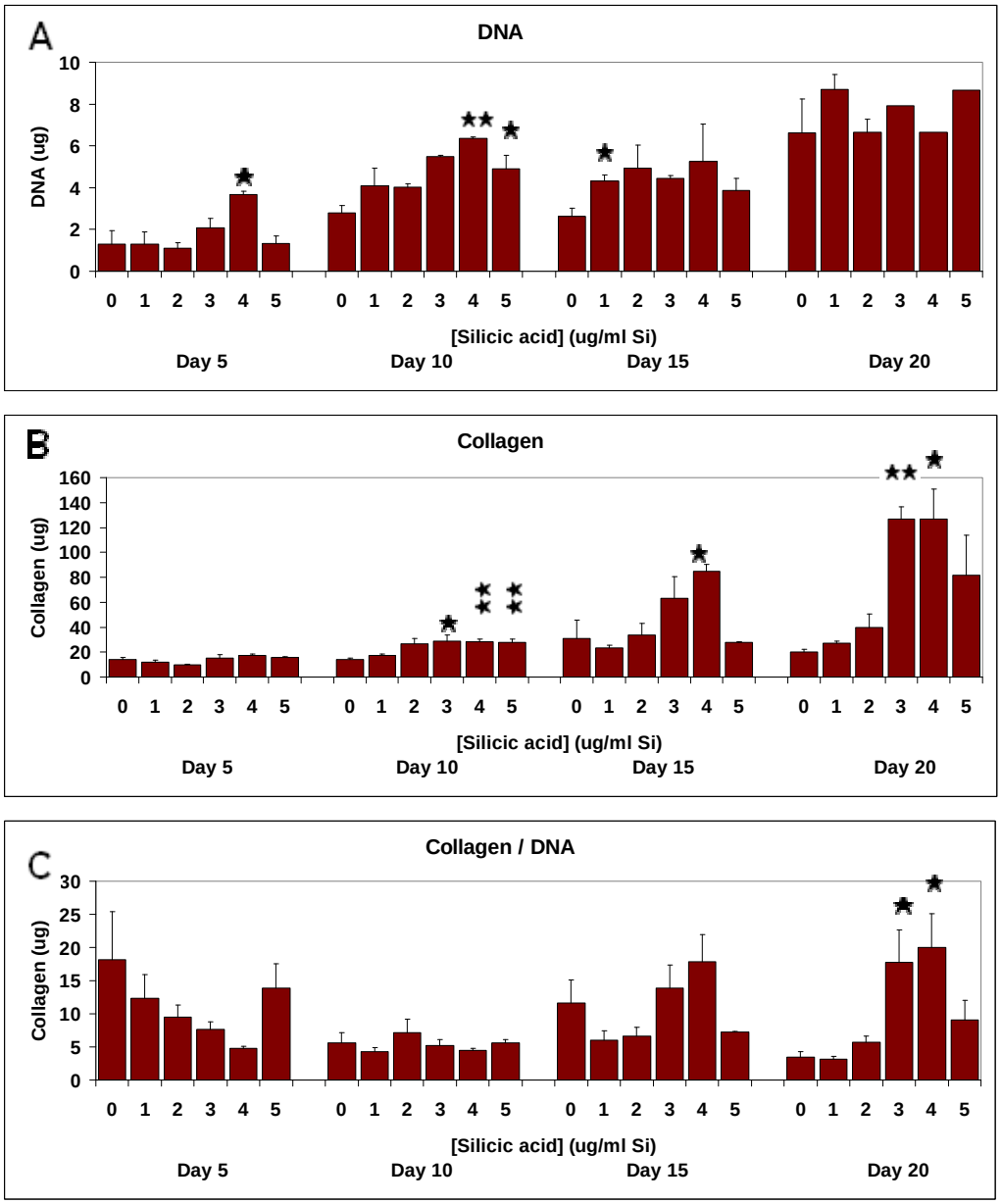


**Fig. 3.18.** Osteoblast response to media conditioned with porous silicon and diluted to provide 1 – 5 μg.ml$^{-1}$ Si. **A**. DNA, **B**. Collagen, **C**. Collagen per μg DNA. Bars show standard error of the mean, n=3. Statistical significance was determined by Student's T-Test compared to 0 μg.ml$^{-1}$ Si as the control population. Significant increase $p < 0.05$ (★), $p < 0.01$ (★★).

### 3.3.3.2. pSi-PCL discs co-incubated with osteoblasts.

PCL discs containing 0, 10 or 20mg pSi were placed in transwell inserts which were suspended in wells of 12 well plates such that the media covered both osteoblasts (on the well base) and composite disc (in the suspended insert), allowing the degradation products of the immersed disc to condition the media. 3ml media was contained in the well with 1ml exchanged daily for fresh media and assayed for silicic acid content (**fig. 3.19**).

Silicic acid was shown to elute from the discs at concentrations proportional to the pSi content of the disc and at concentrations similar to those observed when identical discs were incubated in SBF, PBS or $dH_2O$, demonstrating that the soluble degradation products of pSi-PCL passed into the cell culture medium.

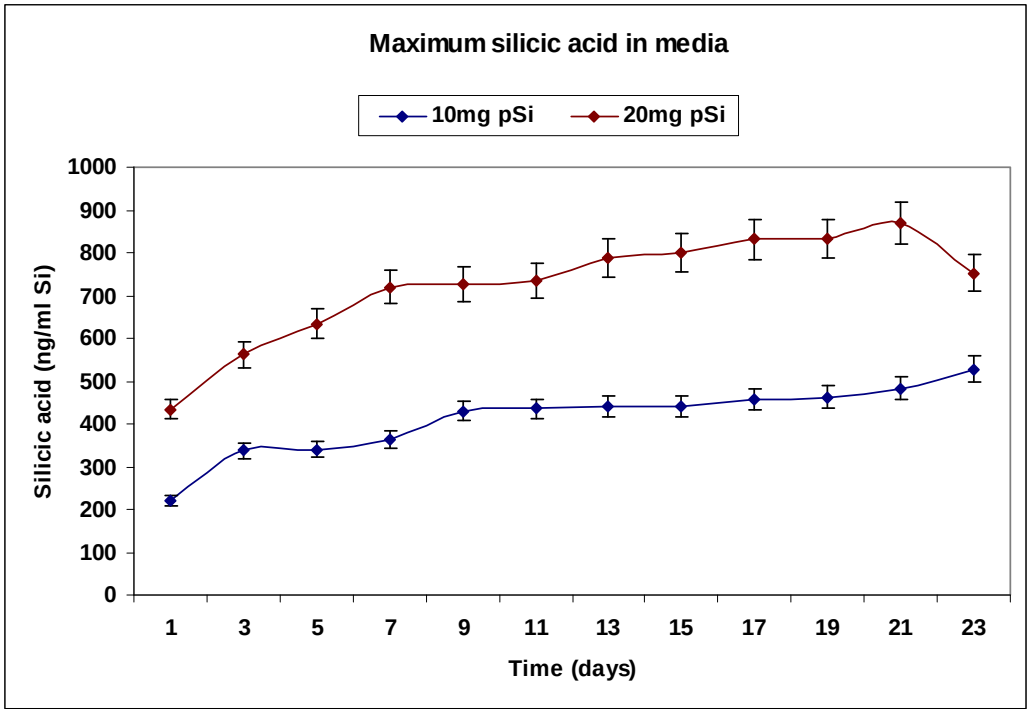


**Fig. 3.19.** Maximum silicic acid content of media incubating PCL-composite discs containing 10mg or 20 mg (4 – 8% *w/w*) pSi. Discs and osteoblasts were cultured in 3ml culture medium, 1ml of which was replaced daily for 25 days. Error bars show standard error of the mean, n = 3.

Osteoblast growth under these conditions was similar for all wells which contained PCL in the insert. Controls containing only empty inserts proliferated at a constant rate for 25 days, whilst all inserts containing PCL-based materials showed similar lower growth rates, although at no time point were these statistically significant (**fig. 3.20.A**).

As a marker of osteoblastic activity, alkaline phosphatase activity (normalised for cell number) peaked in control samples at day 10 and at day 15 for all conditions containing PCL or composites. Alkaline phosphatase activity was not significantly different at any point between PCL-only and composite discs (**fig. 3.20.B**).

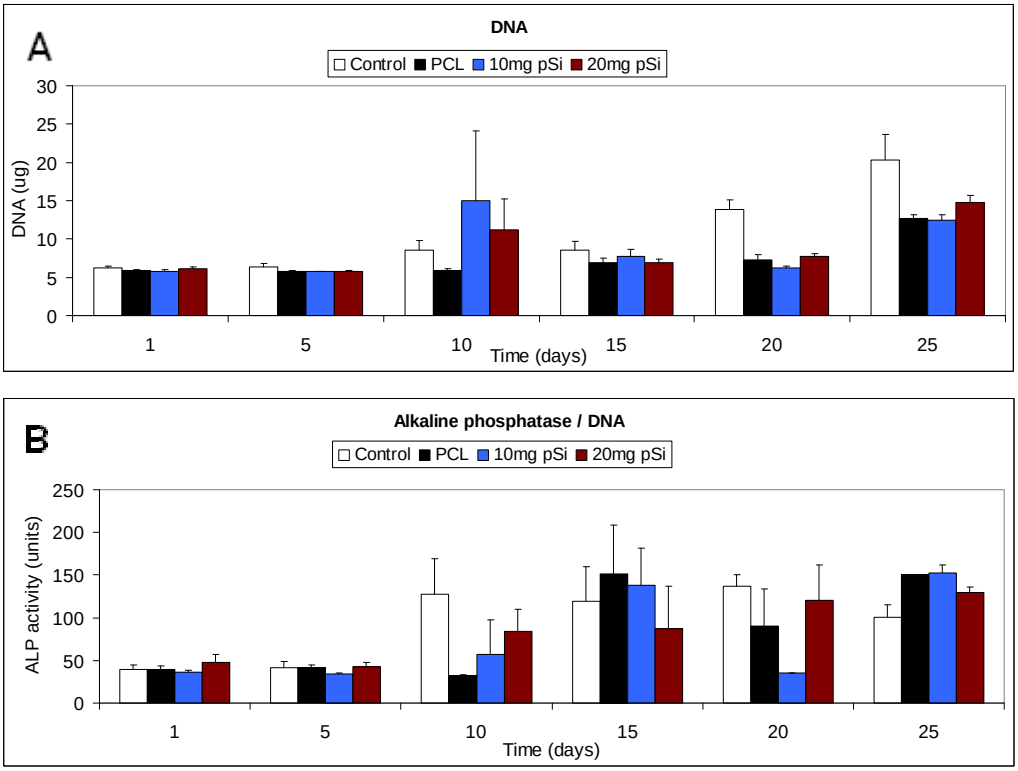


**Fig. 3.20.** Osteoblast proliferation on well bases cultured in the presence of PCL and pSi-PCL composite discs (**A**), and alkaline phosphatase activity as a marker of osteoblastic activity (**B**). Bars are standard error of the mean, n=3. Statistical significance was determined by Student's T-Test compared to PCL as the control population but no treatment was shown to be significantly different to PCL alone.

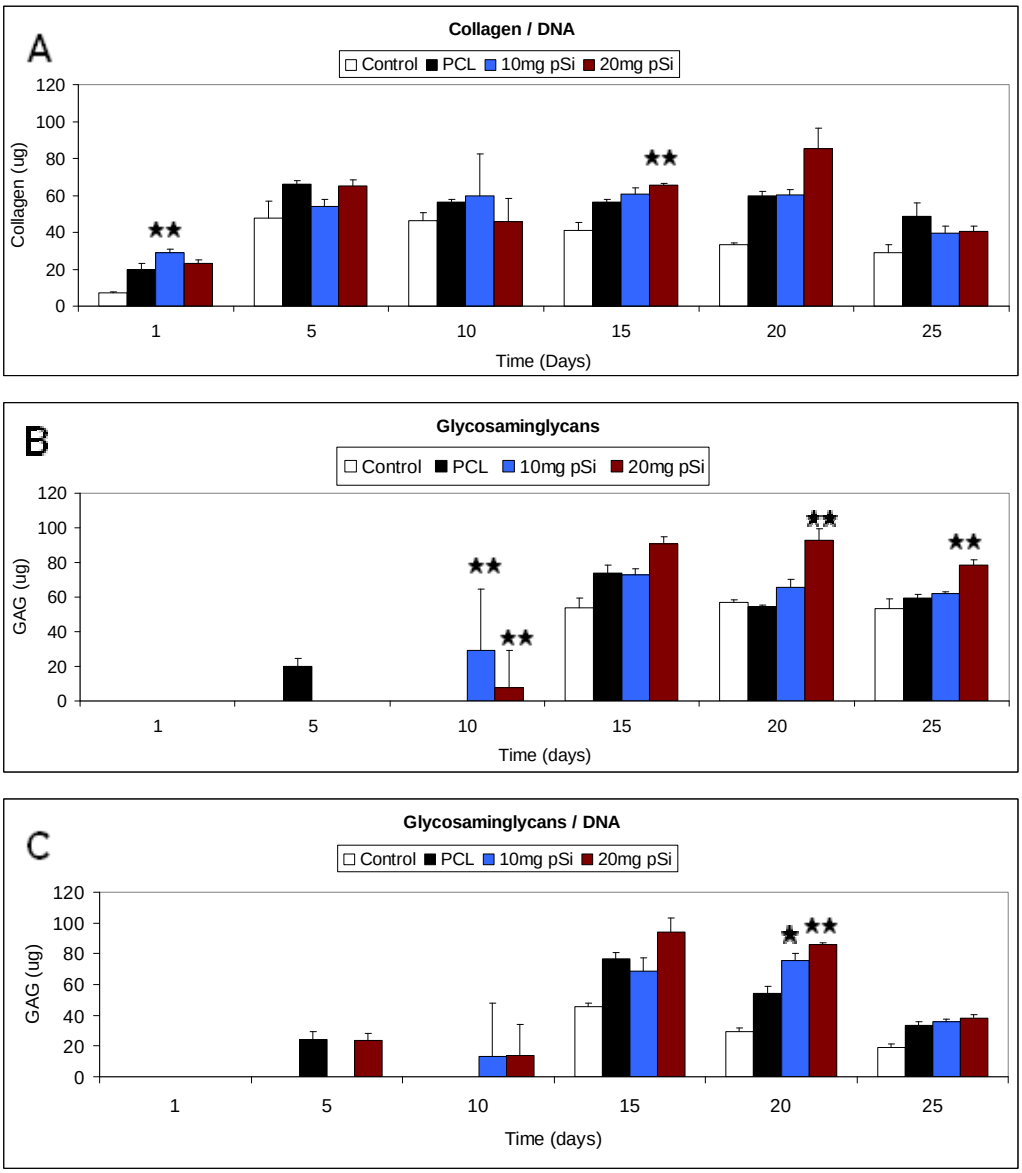


**Fig. 3.21.** Osteoblast formation of extracellular matrix components on well bases cultured in the presence of PCL and pSi-PCL composite discs. **A**. Collagen per µg DNA. **B**. Total glycosaminoglycans. **C**. Glyosaminoglycans per µg DNA. Bars show standard error of the mean, n=3. Statistical significance was determined by Student's T-Test compared to PCL as the control population. Significant increase $p < 0.05$ (★), $p < 0.01$ (★★).

Osteoblast deposition of collagen was higher for all conditions including PCL or composite than controls containing empty inserts throughout the investigation (**fig. 3.21.A**). Comparing PCL-only to 10mg or 20mg composite discs, collagen (per cell) was higher for 10mg at day 1 ($p < 0.01$) and 20mg at day 15 ($p < 0.01$).

Glycosaminoglycan content of the cell lysate and ECM was higher when osteoblasts were cultured with 20mg pSi-PCL discs (**fig. 3.21.B**), significantly so at day 20 and 25 ($p < 0.01$) and at day 10 for osteoblasts cultured with 10mg pSi-PCL discs. When normalised for cell number (**fig. 3.21.C**), glycosaminoglycans were significantly higher than PCL at day 20 for 10mg pSi ($p < 0.05$) and 20mg ($p < 0.01$).

Pyridinoline concentration of the lysate was used as a measure of GAG / protein cross-linking and showed an apparent increase in crosslinking for both 20mg pSi and 10mg pSi over PCL-only (**fig. 3.22**). This effect was significantly greater for 20mg pSi ($p < 0.01$) than for 10mg pSi ($p < 0.05$).

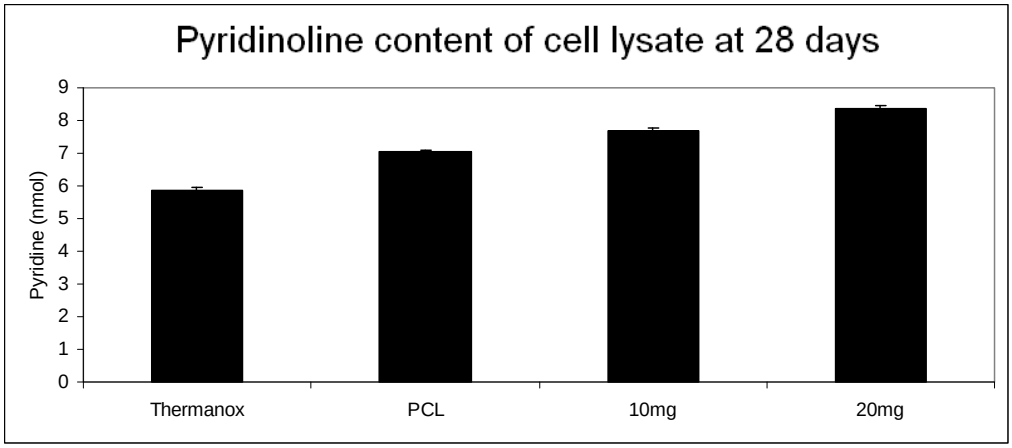


**Fig. 3.22.** Crosslinking of extracellular matrix components determined by assay for free pyridinoline in the cell lysate. Error bars show standard error of the mean, n = 3.

### 3.3.3.3. pSi-PCL and 45S5 Bioglass®-PCL discs co-incubated with osteoblasts.

The above experiment was repeated with 8% *w/w* 45S5 Bioglass®-PCL composite and compared to 8% *w/w* pSi-PCL composites. Osteoblast proliferation was similar under all conditions although PCL-free controls proliferated at a faster rate to reach higher cell populations at day 20 than either PCL- or composite-containing wells (**fig. 3.23.A**). Alkaline phosphatase activity per cell was slighly higher for Bioglass® and pSi-containing wells than PCL- containing wells up to 15 days (but not significantly so), and decreased at a similar rate to controls (**fig. 3.23.B**). The reasons for the decrease are unclear as this experiment was not repeated, but may result from the maturation of osteoblasts into osteocytes in the nodules *in vitro*.

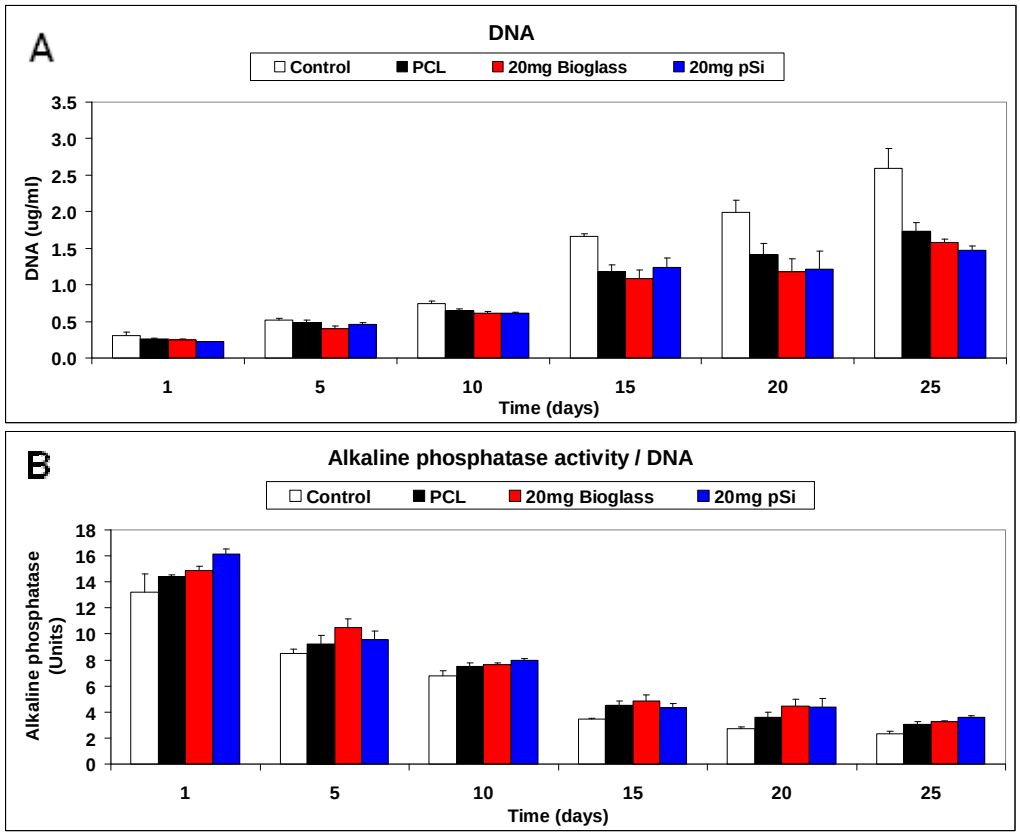


**Fig. 3.23.** Osteoblasts cultured on tissue culture plastic with composite discs containing quantities of 70% porous silicon or 45S5 Bioglass® suspended in the media in permeable transwell inserts. **A**. DNA content of cell lysate. **B.** Alkaline phosphatase activity per µg DNA. Bars show standard error of the mean, n=3.

Total collagen and collagen per cell was higher for both PCL-only and Bioglass®- or pSi-PCL conditioned media at day 10. No difference was observed in the osteoblast response to either Bioglass®-PCL or pSi-PCL in terms of collagen deposition, although at day 25 pSi-PCL produced significantly more collagen than Bioglass®-PCL (**fig. 3.24**).

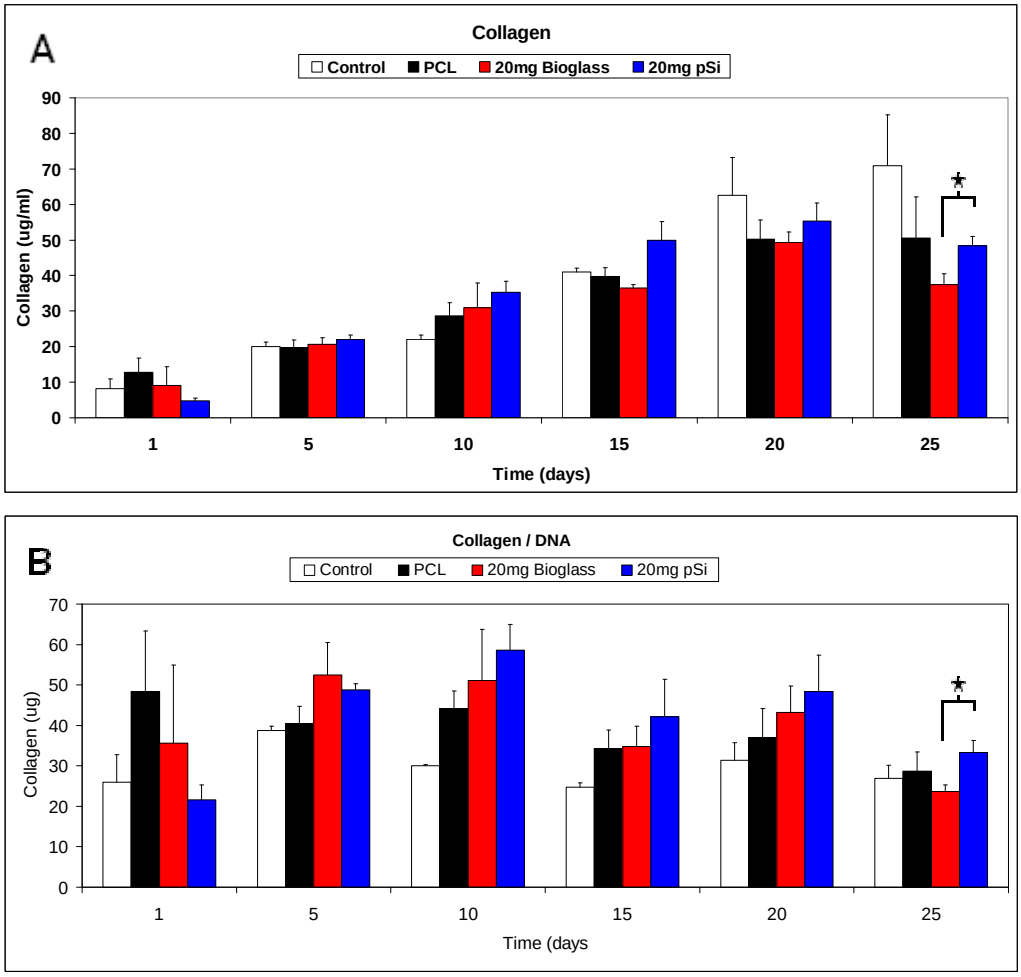


**Fig. 3.24.** Osteoblast formation of collagen on well bases cultured in the presence of PCL, Bioglass®-PCL and pSi-PCL composite discs. **A**. Total collagen per well. **B**. Collagen per μg DNA. Bars show standard error of the mean, n=3. Statistical significance was determined by Student's T-Test compared to PCL as the control population. Significant increase $p < 0.05$ ( ★ ).

**3.4.Discussion.**

In this part of the investigation, the response of human osteoblasts to silicon was evaluated by exposing the cells *in vitro* to porous silicon in a polycaprolactone matrix, the degradation products of both pSi and the composite and to a range of silicic acid concentrations in the growth media.

This approach was undertaken to attempt an understanding of the mechanisms which may underlie the potential bioactivity of porous silicon and further elucidate silicon's known role in bone metabolism *in vivo*. In the previous chapter it has been shown that the addition of porous silicon to polycaprolactone results in a material that elutes stable daily concentrations of soluble silicic acids over several weeks in simulated acellular body fluids. Further, these composites spontaneously form a silica gel layer on their surface in any aqueous environment and in SBF this gel layer increases the precipitation of calcium from the solution, forming crystals on the material surface with bone apatite like molar ratios and morphology.

As has been discussed (Chapter 1), the physiological requirement for silicon and the bone-bonding effects of Bioglass® are attributed to both stabilisation of the collagen and glycosaminoglycan components of the extracellular matrix and silicate substitution in the calcium phosphate crystalline structure in matrix mineralisation. In this investigation it was possible to test the effects of heavily silica-modified surfaces (pSi-PCL discs) and bioavailable silicon acid separately to some extent by providing composite substrates with silica gel layers and silicon-substituted calcium phosphate for osteoblast growth and separately culturing osteoblasts with the soluble silicon species available in media. The question of the relative importance of substrate chemistry and bioavailable silicon could therefore be addressed.

The first stage in this investigation was to determine the response of osteoblasts to a range of porous silicon – polycaprolactone compositions and to observe the effect of pSi-porosity/degradation rate on cells *in vitro*. The results of this analysis show that 54% and 66% porous silicon microparticles do not appear to

significantly enhance the proliferation or osteoblastic phenotype; whereas 82% microparticles degrade so rapidly the resulting accumulation of degradation products and effervescent hydrogen evolution is effectively toxic to cells.

70% porous silicon particles in a smaller particle size range (11μm rather than 38 – 150μm) proved to be more compatible with osteoblasts, stimulating the progression of the osteoblast from de-differentiated and dividing preosteoblast-like cells to mature secretory cells. Osteoblasts cultured on the surface of 8% *w/w* pSi-PCL composite discs produced significantly more collagen at 10 days *in vitro* than osteoblasts cultured on either PCL or tissue culture plastic. In addition, these cells were associated with a more than two-fold increase in glycosaminoglycan content of the extracellular matrix, which may be due to increased production of GAGs by the osteoblasts or by stabilisation of the ECM by soluble silicate species.

To examine the effect of these soluble degradation products on osteoblasts, porous silicon microparticles were added to cell culture medium to generate a solution containing known concentrations of silicic acid. When applied to osteoblasts, concentrations of silicic acids from 1 – 5 $\mu g.ml^{-1}$ appeared to increase the proliferation rate of cells and also their metabolic activity in terms of collagen production. Previous research has shown that silicic acid-releasing zeolite A has similar effect on osteoblasts, increasing the rate of proliferation in densely seeded cells by the autocrine TGF-β route (Keeting *et al*, 1992). Glycosaminoglycan content in the ECM was higher for osteoblasts grown with 20mg pSi-PCL indicating that pSi was having a positive effect on osteoblastic phenotype

Interestingly, osteoblasts cultured in media containing PCL-only discs suspended in inserts show almost identical, low rates of proliferation to discs containing pSi. Similarly, markers of osteoblastic activity such as alkaline phosphatase activity and collagen production are also comparable between PCL and pSi-PCL.

The reduction in osteoblast proliferation when exposed to the degradation products of PCL-only could derive from three sources: i) the breakdown products themselves – carboxylic acids and $CO_2$, ii) residual acetone being released from

within the polymer upon immersion in culture medium, iii) release of ethanol from the matrix which was used for sterilisation of the discs.

As the discs were prepared several days prior to use, it was expected that residual solvents would have evolved from the matrix before they were used. Also, both acetone and ethanol are highly volatile, and at least 12 hours was left between sterilisation and the immersion in media, with the interim period being inside a sterile fume hood with laminar air flow. In chapter two, it was observed that polycaprolactone discs lost up to 8% of their starting weight within 90 days which was attributed to small molecular weight polymer fragments eluting from the matrix.

It is concluded therefore that these polymer fragments have a significant effect on the growth of osteoblasts *in vitro*, both reducing their proliferation and slightly enhancing the osteoblastic phenotype. Ignatius and Claes (1996) demonstrated that the oligomeric breakdown products of polylactide biomaterials can prove toxic to cells by reducing mitochondrial activity and cell proliferation. In this investigation a slight increase in osteoblastic phenotype was observed (collagen production) for cells cultured with the breakdown products of PCL.

In summary, porous silicon can affect the growth of osteoblast-like cells *in vitro*. When cultured either on or in the presence of porous silicon, osteoblasts show reduced proliferation indicating cell maturation and an increase in the production of extracellular matrix components and calcium. The morphology of osteoblasts cultured on PCL containing pSi microparticles differs from those cultured on PCL only, being more 'osteoblastic', with numerous and extended filipodia which are strongly associated with collagen.

# Chapter Four

-

# pSi-PCL Composites for the Controlled Delivery of Pharmaceuticals

## 4.1. Introduction.

Fractures of the skeleton account for the majority of orthopaedic operations - with an estimated 6.8 million fractures coming to medical attention annually in the United States, the average person in a developed country can be expected to suffer two broken bones during their lifetime (American Academy of Orthopaedic Surgeons). The most common fractures are of the extremities in men under the age of 45, with the second most common being extremity fractures in women over the age of 45, due to loss of bone density post-menopause, particularly fractures of the wrist and hip (Singer *et al*, 1998). Additionally, ~600,000 articular joint prostheses (mainly hip and knee) are implanted annually in the US (Lentino, 2004).

In many cases, the breaking of a bone or replacement of a joint is accompanied by other pathologies, such as osteoporosis, severe trauma (such as car accidents), osteosarcoma or post-operative infection, many of which require medication. Bone fixation following either accidental breakage or surgical intervention also has associated pain, which is regulated intravenously in extreme cases and by oral medication in others (Duellman *et al*, 2009).

The total global market for orthopaedic drugs, implants and fixation devices stood at $44 billion in 2004 and is projected to reach $74.1 billion by 2009 (BCC Research, 2004 report). Of this, approximately three quarters constitutes drug sales, although sales of implants are increasing at a higher annual rate of 12.5% (against 10.5% for drugs). Additionally, the market for drug-releasing polymers currently stands at $28 billion per annum, with biomaterials encompassing a significant share (e.g. $5 billion P.A. for drug-releasing vascular stents).

Pharmaceuticals which are potentially relevant to bone implants and fixation devices can be fitted into three categories:

- Bone stabilizers (bone growth promoters & resorbtion inhibitors).
- Analgesics and anti-inflammatories.
- Antimicrobials.

### 4.1.1. Bone stabilisers.

Bone is a dynamic tissue which is remodelled continually through life. Osteoclastic bone resorbtion and osteoblastic bone matrix deposition are dynamically linked via a number of signalling pathways and are partially under central endocrine control (Karsenty, 2000). Disruption of these pathways leads most commonly to osteoporosis and results in a gradual weakening and loss of bone mass. As most hip and knee replacements are performed on patients over the age of 60, osteoporosis is a factor which must often be considered when implanting an articular prosthesis and care taken to avoid damaging the weakened bone matrix.

Bone turnover may be stabilised through inhibiting osteoclast activity or by stimulating pre-osteoblasts and osteoprogenitor cells to develop or enhance an osteoblastic phenotype. Osteoclast inhibition by bisphosphonates is the main route by which menopausal osteoporosis is managed, and the response to orally-delivered doses is well characterised and presents few side effects (Iwamoto, 2008). Additional bisphosphonate stabilisation following surgery may enhance the rate and extent of local bone healing and serve to reduce the need for or delay subsequent revisions, although intravenous use has been associated with jaw osteonecrosis (Ruggiero *et al*, 2004).

Bisphosphonates function by shortening osteoclast lifetimes (via apoptosis) and localise to bone mineral, thereby being endocytosed by the osteoclast during remodelling. Bisphosphonates already bound to bone therefore may continue to act in reducing bone loss for long periods after the oral dosing has stopped. The most commonly prescribed bisphosphonates are sodium alendronate (Fosamax, Merck) 10mg a day or 70mg once a week, risedronate (Actonel, Procter & Gamble) 5mg a day or 35mg once a week and ibandronate (Boniva) once a month.

Loading of bisphosphonates into drug-delivery vehicles has been attempted by several research groups with *in vitro* success (Shi *et al*, 2009; Faucheux *et al*, 2008), but is so far unreported *in vivo* or in clinical trials. Methods of conjugating proteins

to bisphosphonates have also been developed that provide a means to localise specific proteins to the bone mineral surface (Wright *et al*, 2009; Gittens *et al*, 2004). It is also apparent that preventing or reducing osteolysis and resorbtion of bone surrounding an implant may help to stabilise and improve the fixation of prostheses (Huolman & Ashammakhi, 2007). Stabilisation may alternatively be provided by treatment with promoters of osteoblast activity, such as bone morphogenic proteins or dexamethasone (see below).

### 4.1.2. Analgesics and anti-inflammatories.

Reducing post-operative pain and inflammation is essential to a patient's quality of care and may accelerate the rate of recovery and time in hospital. Most pain relief following surgery is given systemically by patient-controlled intravenous morphine drip, or by a multi-modal route which combinines several analgesics and anti-inflammatory drugs in order to improve efficacy and reduce side effects (Duellman *et al*, 2009). Topical pain relief is commonly by ibuprofen- or diclofenac-containing gels (Banning, 2008). Caterina *et al* (2001) have also suggested a use for topical doses of capsaicin post-operatively.

Release of analgesics and anti-inflammatory drugs from implanted materials has been studied in comparatively little detail considering the proven advantages of both topical pain relief and combined, multi-route methods for pain management. Analgesic-releasing bone cements have been patented (e.g. US patent numbers 6713527 and 6355705, both by Queen's University, Ontario, Canada) but clinical data is limited to one successful trial described in the patents using 5% lidocaine in poly(methyl methacrylate) bone cement in a total knee arthroplasty revision on a 68-year old female patient. Analgesic effects were described to increase to optimum levels over six hours and lasted for more than two days.

Release of this type of drug is therefore relatively untried when compared to antibiotic-releasing bone cements and materials (see below), but presents a potentially vast market for post-operative pain management.

### 4.1.3. Antibiotics.

In 1957, Elek and Conen demonstrated that the presence of a foreign body (such as an orthopaedic implant) significantly reduces the number of bacteria required to produce an infection. Approximately 1% of primary and 3% of secondary (revised) orthopaedic prostheses in the US become infected (Stocks *et al*, 2000), and most treatments require removal of the implant with associated morbidity and peripheral tissue destruction. The majority of these infections are bacterial in origin, but a small proportion (<1%) are produced by *Candida* (fungal) biofilms (Kojic *et al*, 2004).

In clinical practice, antibiotic-eluting polymers have been used for several years. Gentamicin- and other aminoglycoside- loaded bone cement was first used clinically in the late 1960s by Buchholz and Engelbrecht (see Wahlig *et al*, 1984), less than a decade after poly(methyl methacrylate) (PMMA) itself was first applied in prosthesis fixation. The loading ratios and release kinetics of aminoglycoside-bone cements have been well characterised over the last four decades and the mechanical properties of adding such substances evaluated.

Commercial products such as Depuy 1 Gentamicin Bone Cement (Depuy Orthopaedics) and Simplex™ (releasing tobramycin, Stryker Orthopaedics) contain 1g of the aminogycoside antibiotic mixed into the 40g powder component of the cement (approximately 1.5% final concentration, *w*/*w*). Clinicians may choose to add gentamicin separately to the PMMA bone cement and often favour a high-loading of gentamicin, commonly >9% *w*/*w* loading and up to 20% for treatment of active infections in revisions (Lautenschlager *et al*, 1976).

PMMA bone cement is not biodegradable, osteoinductive or permeable to water and consequently only a small percentage of the antibiotic is released into the wound site in a burst release following would closure. The primary clinical concerns with antibiotic-releasing cements are the potential for development of an immune response to high-doses and the possibility of gentamicin-resistant bacterial infections developing. A more detailed analysis of poly(methy methacrylate) bone cements in drug delivery is provided in the appendix.

### 4.1.4. Porous silicon for drug delivery.

Porous silicon exhibits numerous properties that make it desirable as a drug delivery vehicle: it can be manufactured with a range of pore architectures (width and depth) and the surface chemistry can be adjusted by various well-characterised technologies to aid both storage and release of specific molecules.

As pSi is biodegradable, its use as a delivery vehicle can provide a carrier for hydrophobic molecules which do not readily disperse using conventional means. pSi microparticles in suspension can distribute through a target area, organ or tissue, a property which has been exploited by pSiMedica in a radiotherapy treatment known as brachytherapy. In this technique, $^{32}P$ is loaded into porous silicon and injected percutaneously into a tumour, providing very high doses of localised radiation. This method is currently being explored as a method for treating tumours which are not treatable by conventional means, such as pancreatic and liver cancer (Zhang *et al*, 2005).

Conventional drug delivery has also been explored by several research groups with the release kinetics of various molecules including cis-platin (Coffer *et al*, 2003), dexamethasone (Anglin *et al*, 2004), ibuprofen (Charnay *et al*, 2004), and doxorubicin (Vaccari *et al*, 2006) being studied for drug delivery applications. A comprehensive review of pSi (and silica derivatives of the pSi matrix) for drug delivery applications is given in Salonen *et al* (2008).

Several methods to securely encapsulate molecules in a porous silicon matrix have been described, including covalently bonding drugs to the host silicon, although this may interfere with the structure and function of the API upon release (**fig. 4.1**). Alternatively, drugs may be attached to silicon via a cleavable linker, such as polyethylene glycol (Schwartz *et al*, 2005).

pSi loaded with pharmaceuticals may be subsequently oxidised which considerably decreases the internal diameter of the pores and so effectively locks the drug into place, releasing only as the silicon matrix degrades as described (for the release of iron oxide nanoparticles) in Dorvee *et al* (2008).

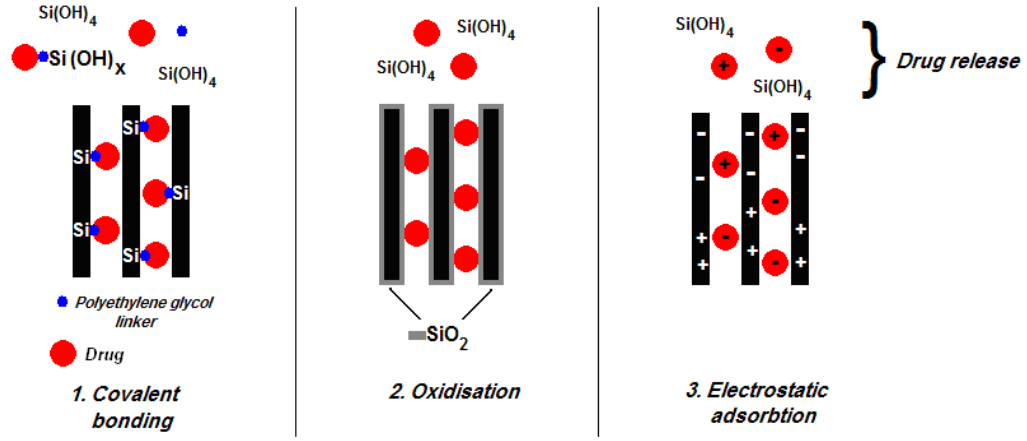


**Fig. 4.1.** Methods for incorporating pharmaceuticals into the pore spaces of pSi. **1.** Covalently bonding the drug to silicon via a polyethylene glycol linker, **2.** Oxidising the pSi after/during drug loading decreases pore diameter, trapping molecules in the oxide layer, **3.** Allowing the electrostatic forces between silicon hydride/oxide domains and charged/polar molecules to adsorb the molecules to the surface.

In this investigation, drug loading into pSi was achieved by filling the pore spaces with the sample substance, but even this simple method for containing drugs involves electrochemical interactions with pSi. As the surface of native pSi (presenting hydrides, Si-H) is initially highly hydrophobic it presents a net positive charge to the surrounding medium to which negatively charged molecules are drawn; conversely, oxidised regions of the pSi matrix present an overall negative charge and adsorb positively charged molecules (Anglin *et al*, 2008). In reality, pSi stored in atmospheric conditions and prepared in a standard laboratory possesses both Si-H and Si-O domains and so can attract ampiphilic molecules as readily as either negatively or positively charged species.

For advanced drug-delivery applications, electrostatic binding to the surface can be more finely controlled during pSi fabrication, helping to adsorb relevant molecules to the pore surface and effecting more rapid release (Arwin *et al*, 2000).

### 4.1.5. Polycaprolactone for drug delivery.

Polycaprolactone and polylactide blends or co-polymers are becoming increasingly popular as potential drug delivery vehicles in their own right, with a common application being the formation of a drug-polymer emulsion in a solvent which is subsequently formed into microspheres that can either be implanted into a target organ or wound site or injected (Sinha & Trehan, 2008).

Microsphere technology is well studied and patents cover numerous applications, but are currently commercially restricted due to several technical difficulties which range from the denaturing of proteins during formulation and encapsulation, processing or during prolonged release to overcoming burst release profiles, incomplete release and low encapsulation efficiency - factors which often have to be resolved simultaneously if the device is to be effective (Wu & Jin, 2008).

Targets for microsphere-encapsulated drugs have so far been in the sustained release of antibiotics such as gentamicin (Sinha *et al*, 2004), protein drugs (Wu & Jin, 2008), contraceptives (Dhanaraju *et al*, 2006) and various other molecules (reviewed in Varde & Pack, 2004). The aims of sustained drug release are to bypass issues in self-medication such as patient compliance, to increase the efficacy of drugs in tissues that are poorly vascularised or damaged, such as orthopaedic wound sites following prosthesis implantation and to provide a dispersible sustained dosage of drugs for cancer treatment.

The emulsion technology for producing microspheres lends itself equally to the formation of polymer-based tissue engineering scaffolds, and several groups have successfully produced tissue engineering scaffolds which elute therapeutic agents, particularly antibiotics such as gentamicin and amikacin (Prabu *et al*, 2006), and bone morphogenic proteins (BMP-2 and BMP-7; Kempen *et al*, 2008).

### 4.1.6. Loading and release of substances in pSi-PCL composites.

Substantial data exists at pSiMedica Ltd. for a range of pharmaceuticals which have been loaded into pSi microparticles and the release profiles they display. Prior to this investigation, however, the more complex release profiles of substances from pSi microparticles in a polymer composite had not been evaluated. pSiMedica data suggests that the degradation of pSi host matrices in aqueous media enhances the rate at which poorly soluble or hydrophobic molecules and proteins substances are carried into solution.

Loading of a substance into pSi is straightforward: a concentrated solution of the substance is made which is then added to pSi particles in suspension (in an organic solvent) and the solvents extracted by evaporation. The high surface area : volume ratio of pSi coupled with the capillarity of the pores ensures that the internal pore walls of the particles are lined with the substance. The particles are then mixed with the polymer in solution and the composite achieved.

The process of loading substances into pSi and releasing them from an actively degrading material involves exposing the active substance to several factors which may potentially degrade or inactivate pharmaceuticals:

**1. Loading:**

1. Dissolution in organic solvents
2. High temperatures as pSi oxidises

**2. Storage:**

3. Reducing conditions inside pSi nanopores
4. Polymer impurities, including:
    - Tin (<200ppm)
    - Toluene (~100ppm)

**3. Release:**

5. Localised high silicic acid concentrations
6. Associated composite degradation products include:
    - 5-hexanoic acid
    - $CO_2$
    - molecular hydrogen ($H_2$)

The activity of APIs following release from polylactide-only vehicles had been assessed (e.g. Park *et al*, 1995) and reviewed (O'Hagan *et al*, 1998) by several researchers to evaluate some of the concerns which relate to biodegradable drug carriers. Exposure of aqueous solutions of protein-pharmaceuticals to organic solvents results in the formation of an emulsion, minimising the effects of denaturing solvents except at the interface of the two solvents. Denaturation by this means can be minimised by using dried, powdered pharmaceuticals in suspension or by minimising the time spent in contact with the organic solvent (O'Hagan *et al*, 1998).

Exposure to acidic and reducing environments has only a minimal effect on protein structure, and it has been shown that even acid-sensitive proteins (cholera toxin B, O'Hagan *et al*, 1995) are released intact in both *in vitro* and *in vivo* trials from polylactide microspheres, although some hydrolysis does occur. Acidic conditions within larger materials have not been fully evaluated, but it would seem that the combination of fluid flow surrounding the material/microspheres coupled with the higher solubility of APIs in relation to the degradability of the polylactides allows the protein to escape the matrix with the native tertiary and quaternary structure intact.

No drug interactions with low level Tin or toluene contamination or degradation on exposure to molecular hydrogen or $CO_2$ are reported in the literature.

### 4.1.7. Substances tested.

For this investigation a number of substances were tested to simulate the wide range of APIs used, or potentially usable in orthopaedic pharmacy. It was the aim of this investigation to represent each class of API with a tested example, ranging from small hydrophilic compounds to large, dimerised proteins with limited solubility (such as alkaline phosphatase), as listed in **fig. 4.2**.

**Release kinetics studies** – To provide preliminary data on the release kinetics of molecules released from the material:

- Fluorescein — small, water-soluble molecule
- Bovine serum albumin — medium-sized water-soluble protein
- Alkaline phosphatase — large, membrane-derived glycoprotein

**Antimicrobial activity** – To test the efficiency of the material in releasing active concentrations of antimicrobial compounds:

- Gentamicin — broad spectrum antibacterial
- Nystatin — antifungal, used against *Candida* infections

**Effects on human osteoblasts *in vitro*** – To test the ability of the material to elicit biological responses to eluted substances:

- Dexamethasone — promotes alkaline phosphatase expression
- BMP 7 — promotes pre-osteoblast differentiation and calcification

**Fig. 4.2.** List of substances tested indicating the general class of pharmaceutical each substance was chosen to represent.

#### 4.1.7.1. Fluorescein.

Fluorescein is a small, water soluble molecule ($C_{20}H_{12}O_5$, 332 $g.mol^{-1}$) which was used in this investigation to represent a broad range of pharmaceuticals such as steroid hormones which share similar basic properties including molar mass, hydrophilicity and molecular structure. A comparison of fluorescein mass and molecular structure to several pharmaceuticals relevant to orthopaedics is given in **fig.4.3**.

Fluorescein was used in this investigation because of the relative ease and accuracy of determining concentrations in solution, allowing rapid and consistent analysis of solutions incubating fluorescein-containing polymer-composites. It was expected that similar molecules such as gentamicin and dexamethasone would elute in similar ways to fluorescein, a hypothesis which was subsequently tested.

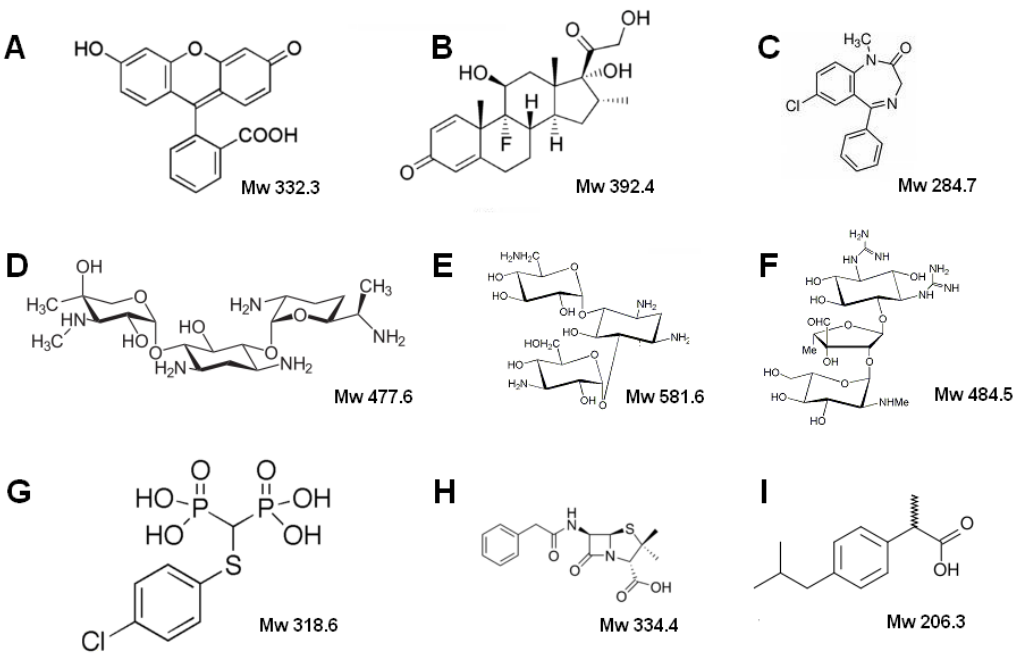


**Fig. 4.3.** Structures and molecular weights ($g.mol^{-1}$) for fluorescein and several similarly sized water-soluble pharmaceuticals: **A.** Fluorescein, **B.** Dexamethasone, **C.** Diazepam, **D.** Gentamicin, **E.** Streptomycin, **F.** Kanamicin (**D-F** are aminoglycoside antibiotics), **G.** Tiludronic acid, a bisphosphonate, **H.** PenicillinG, **I.** Ibuprofen. Images and data are from Sigma-Aldrich technical webpages.

#### 4.1.7.2. Bovine serum albumin.

Bovine serum albumin (BSA) is a 66 kDa protein which constitutes approximately 50% of the total protein in bovine serum. Serum albumins are responsible for maintaining osmotic pressure throughout body tissues and for binding to and aiding the solubility of numerous hydrophobic hormones and fatty acids in the blood (Bhattacharya *et al*, 2000).

In this investigation, BSA was chosen as an example of a medium-sized, water soluble protein which was easy to determine and quantify in solution using well-described colorimetric assay techniques such as the Bradford assay (Bradford, 1976).

### 4.1.7.3. Alkaline phosphatase.

Alkaline phosphatase from bovine intestinal mucosa is a dimeric, membrane-derived glycoprotein with a mass of ~160 kDa, representing a broad range of membrane-bound and partially hydrophobic proteins which can be used therapeutically. Active alkaline phosphatase dephosphorylates various molecules and in this investigation the enzyme was used to test the effect of loading and release of proteins on their activity in eluted solutions.

During the course of loading substances into pSi or PCL and casting the material into discs, molecules may experience high temperatures, exposure to organic solvents and various residual salts and experience a wide range of pH. The effect of this on enzymatic activity is crucial to evaluating pSi's suitability as a vehicle for pharmaceuticals.

### 4.1.7.4. Gentamicin.

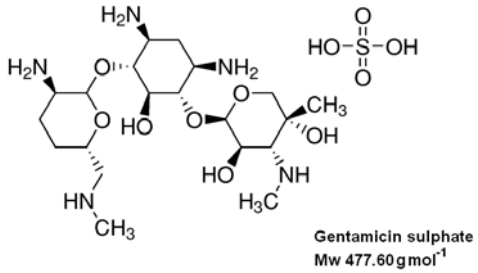


**Fig. 4.4.** Gentamicin sulphate.

Gentamicin (**fig. 4.4**) is an aminoglycoside antibiotic with a broad spectrum of antibacterial action, particularly against Gram-negative species, and is the most commonly used antibiotic following orthopaedic surgery (Dr Roger Bayston, personal communication). Gentamicin is also heat stable up to and exceeding autoclave conditions (Bourne, 2004), therefore presenting less of a problem in maintaining activity during loading into pSi / PCL.

**4.1.7.5. Nystatin.**

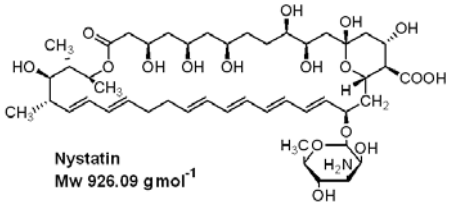


**Fig. 4.5.** Nystatin.

Nystatin (**fig. 4.5**) is a polyene antimycotic with a broad spectrum of antifungal activity, being effective against most cutaneous, mucosal and oesophageal *Candida* (yeast) infections. Polyenes associate with ergosterol in the fungal cell membrane, forming a channel which allows $K^+$ leakage resulting in cell death (Ghannoum & Rice, 1999).

As such, polyenes are fungi-specific and show only limited toxicity when delivered intravenously - polyenes are not absorbed across mucous membranes or the skin. Nystatin is not water soluble but forms an active suspension in solution and is thus also used as an example for this class of pharmaceuticals.

Fungal diseases of bone are rare, forming less than 1% implant infections (Kojic *et al*, 2004), but when presented are usually treated with a combination of debridement and topical treatment with a polyene antimycotic such as nystatin or amphotericin B (Kojic *et al*, 2004). Articular prostheses can become infected with *Candida* biofilms which are considerably more resistant to systemic treatment and require surgical intervention.

#### 4.1.7.6. Dexamethasone.

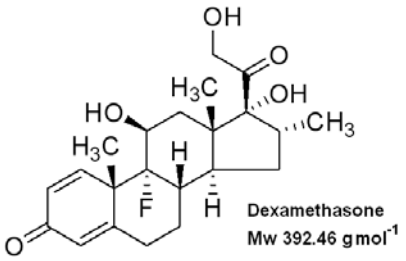


**Fig. 4.6.** Dexamethasone.

Dexamethasone (**fig. 4.6**) is a glucocorticoid steroid hormone with anti-inflammatory properties considerably greater than hydrocortisone (Jain & Srivastava, 1979). Dexamethasone also promotes the osteoblastic phenotype of human osteoblast-like cells and mesenchymal cells *in vitro*, stimulating alkaline phosphatase expression in responsive cell types (Yamanouchi *et al*, 1997; Yang *et al*, 2003).

#### 4.1.7.7. Bone morphogenic protein 7.

Bone morphogenic proteins (BMPs) are a group of cytokines and growth factors which mainly belong to the TGFβ family and have an ability to stimulate bone formation both *in vitro* and *in vivo* (Cheng *et al*, 2003). Bone morphogenic proteins have several clinical uses in treating non-union, with BMP2 and BMP7 having FDA approval in the US for human clinical applications and used in the UK for treating non-union and for spinal fusion.

Treatment programmes are expensive, however - typically in excess of £7,000 for treating tibial non-union in pilot studies (Dahabreh *et al*, 2008). BMP7 is a serum protein which binds to transmembrane proteins, signalling through the SMAD1 and SMAD5 signal cascade and inducing the transcription of several osteogenic genes including osteonectin, osteopontin and osteocalcin (Itoh *et al*, 2001).

### 4.1.8. Aims.

The aims of this part of the investigation were to evaluate porous silicon-polycaprolactone composites for sustained delivery of a range of molecules which have existing or potential orthopaedic applications. The objectives therefore were to:

1. Devise an appropriate method for loading substances into pSi microparticles, polycaprolactone and pSi-PCL composites.

2. Determine and compare the release kinetics of a preliminary range of small to large, hydrophilic and hydrophobic molecules.

3. Analyse the viability of biologically active molecules (such as enzymes) following release.

4. Investigate the antimicrobial effect of composites eluting gentamicin (anti-bacterial) and nystatin (anti-fungal).

5. Study the effect of composites releasing dexamethasone and BMP7 on osteoblast growth and activity *in vitro*.

Throughout this investigation, the release of substances from the composite was compared to the release from polymer-only vehicles prepared under identical or near-identical conditions and tested concurrently.

## 4.2. Materials and Methods.

### 4.2.1 Loading of substances into pSi and polycaprolactone.

Substance loading into porous silicon, polycaprolactone and the composite was achieved in the following way. A solubility study was performed on each substance in a series of organic solvents with a range of relative polarities and boiling points (**fig. 4.7**). A visual analysis was made to determine the level of solubility of 60mg of the substance in 150µl solvent in a glass vial (solution clarity).

**A**

| Solvent | Boiling point†(°C) | Dielectric constant†($\varepsilon_r$) |
|---|---|---|
| Water | 100 | 80 |
| Dimethylsulfoxide | 189 | 47.2 |
| N,N-dimethylformamide | 153 | 38.3 |
| Acetonitrile | 81 | 36.6 |
| Methanol | 68 | 33 |
| Ethanol | 78 | 24.3 |
| Acetone | 56 | 20.7 |
| 2-propanol | 82.3 | 20.18 |
| Methylene chloride | 40 | 9.08 |
| Tetrahydrofuran | 66 | 7.52 |
| Ethyl acetate | 78 | 6.02 |
| Chloroform | 61.2 | 4.8 |

**B**

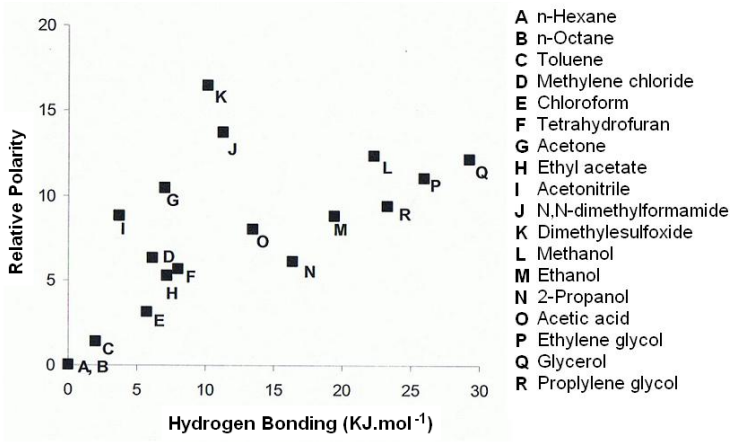


**Fig. 4.7. A.** Solvents listed in order of dielectric constant ($\varepsilon_r$), a measure of polarity. († source Sigma-Aldrich technical webpages). **B.** Scatter graph showing the relationship between polarity and hydrogen bonding for several common solvents (adapted from pSiMedica internal report by Dr. Christian Barnett).

In practice only three solvents were used: water, acetone and ethanol as all substances tested were soluble in either one or in combination, and which have a low boiling point to allow rapid extraction of the solvent. Substances which are only soluble in water were first fully dissolved in water and subsequently mixed with an equal volume of ethanol or acetone to aid loading into pSi. A table listing the solvents used for each substance is given below (**table 4.8**). High concentrations of the substance (solvent volume < 3ml) were used to minimise the loading time and subsequent solvent extraction.

| Substance | Primary solvent | Secondary solvent |
|---|---|---|
| Fluorescein | Water | Ethanol |
| Bovine serum albumin (BSA) | Water | Acetone |
| Alkaline phosphatase (AP) | Ethanol | Ethanol |
| Gentamicin | Water | Ethanol |
| Nystatin | Ethanol | Ethanol |
| Dexamethasone | Ethanol | Ethanol |
| Bone Morphogenic Protein 7 | Water | Acetone |

**Table 4.8.** Solvents used to dissolve substances used in this investigation. Secondary solvents were added to aid wetability (reduce contact angle) of porous silicon in the solution and enhance the uptake of the substance into pores.

Once dissolved in the solvent the solution was added to a measured amount of porous silicon (70% porous, 11µm particle size; pSiMedica) and agitated to fully disperse the silicon through the solution. The substance-loaded pSi was incubated at 4°C for 2 hours and then air dried in a mortar before being ground to redisperse the pSi microparticles and reweighed. If no pSi was to be used (i.e. direct release from PCL) the pSi loading stage was bypassed and the solution dried, ground in a pestle and mortar and added directly to PCL as follows.

The microparticles or ground substance were added to a 50:50 (*w*/*v*) solution of polycaprolactone in acetone at room temperature and dispersed through the polymer, which was immediately loaded into a 5ml syringe body and cast as a cylinder. The cylinder was allowed to dry overnight before being cut into 250mg discs for experimental use.

In this work the nomenclature used for the drug-loaded composites is:

(**mg pSi**) (polymer or composite) (***mg drug loaded***)

As an example, a standard 250mg composite disc containing 20mg porous silicon which has been loaded with 5mg fluorescein would be represented as **20** pSi ***5***. Similarly a 250mg polycaprolactone-only disc containing 5mg fluorescein would be represented as PCL ***5***.

### 4.2.2. Substances tested.

#### 4.2.2.1. Fluorescein.

Fluorescein (Sigma, UK - $C_{20}H_{12}O_5$ 332 $g.mol^{-1}$,) was loaded into polycaprolactone and into 20mg (8%) pSi composites in three different quantities: 1mg, 5mg and 10mg as shown in **fig. 4.9.** In addition, 20mg pSi microparticles were loaded with fluorescein and contained in a short piece of dialysis tubing by knotting the ends of the tubing.

| Sample | Polymer | pSi | Fluorescein |
|---|---|---|---|
| PCL | PCL | - | 1, 5 & 10mg |
| PCL+pSi | PCL | 20mg pSi | |
| PMMA | PMMA | - | |
| PMMA+pSi | PMMA | 20mg pSi | |
| pSi | - | 20mg pSi | |

**Fig. 4.9.** Polymer : pSi : Fluorescein ratios used in the investigation.

The 250mg discs and pSi-tubing were placed in the wells of a 24 well cell culture plate, with three discs per sample condition (n = 3). The discs were weighed down with a 5mm diameter rubber rings, 1ml PBS added and the plate lid secured. The PBS was removed every 24 hours, analysed and replaced - the well/disc was rinsed with PBS between solution changes.

The fluorescence at excitation 494nm and emission 521nm of 300µl of the released fluorescein solution was measured and quantified against known concentrations of 0.1 to 10 ng.ml$^{-1}$ fluorescein. Cumulative release was plotted against time for each loading concentration of fluorescein tested.

#### 4.2.2.2. Bovine serum albumin & alkaline phosphatase.

Bovine serum albumin (BSA fraction V, MW ~66 kDa, Sigma, UK) and alkaline phosphatase (AP Type VII-L from bovine intestinal mucosa, homodimer MW ~160 kDa; Sigma, UK) were loaded into porous silicon as described above in the ratios shown in **table 4.10.**

| Sample | pSi (mg) | BSA/AP (mg) | Polycaprolactone |
|---|---|---|---|
| PCL ***5*** | 0 | 5 | 250mg |
| PCL ***10*** | 0 | 10 | |
| **20** pSi ***5*** | 10 | 5 | |
| **20** pSi ***10*** | 20 | 10 | |

**Table 4.10.** Polymer : pSi : Protein ratios used in the investigation.

The discs were placed in the wells of a 24 well cell culture plate, with 4 discs per sample condition (n = 4). The discs were weighed down with a 5mm diameter rubber ring, 1ml PBS added and the plate lid secured. The PBS was removed every 48 hours for 8 days and analysed as described below; the well/disc was rinsed with PBS and 1ml PBS re-added to the well.

##### 4.2.2.2.1. Protein release.

Protein release was determined by a Bradford assay (Bradford, 1976). To 400 µl of the incubation media was added 100 µl pre-prepared Bradford reagent (Coomassie blue solution, Sigma, UK) and the absorbance measured at 595 nm. A calibration curve was established using known concentrations of BSA or alkaline phosphatase from 10 ng to 100 µg. The assay was optimised such that the calibration curve was linear for the concentrations determined in the experiment.

#### 4.2.2.2.2. Alkaline phosphatase activity.

Alkaline phosphatase activity was determined using 50 µl of the incubation media and 250 µl 4-methylumberiferyl phosphate substrate system (Sigma, UK). Alkaline phosphatase in the sample enzymatically cleaves phosphate from the 4-MUP, producing the 4-methylumbeliferone which can be quantified by its fluorescence (excitation 360nm, emission 460nm) and represented as relative units. To ensure the quantification was comparable for each time point, samples were immediately frozen at -20°C until the end of the experiment and assayed under identical conditions (5 minutes incubation time with substrate at room temperature).

#### 4.2.2.3. Gentamicin.

Gentamicin was loaded into polycaprolactone / pSi in the ratios shown in **table 4.11.** 250 mg discs were placed in wells of a 24-well plate (Nunc), n = 4. 1ml PBS was added and the covered plate incubated at 37°C for 21 days. Gentamicin in the solutions was quantified using an *o*-phthalaldehyde reagent which becomes fluorescent when conjugated to primary amines (Gubernator *et al*, 2006).

50µl of the incubating solution was pipetted into wells of a 96 well plate and 200µl pre-prepared cold *o*-phthalaldehyde reagent (1 $mg.ml^{-1}$ *o*-phthaldialdehyde with 2-mercaptoethanol, potassium hydroxide, methanol, boric acid and Brij 35 – pH 10.0, Sigma, UK) was added and the solution allowed to incubate at room temperatre for 10 minutes. The fluorescence of the solution was measured at λ 340nm (excitation) and λ 465nm (emisson) and compared to known concentrations of gentamicin sulphate in PBS (1 – 250 $\mu g.ml^{-1}$).

| Sample | pSi (mg) | Gentamicin(mg) | Polycaprolactone |
|---|---|---|---|
| PCL ***5*** | 0 | 5 | 250 mg |
| PCL ***10*** | 0 | 10 | |
| **20** pSi ***5*** | 20 | 5 | |
| **20** pSi ***10*** | 20 | 10 | |

**Table 4.11.** Polymer : pSi : Gentamicin ratios used in the investigation (n = 4).

**4.2.2.4. Nystatin.**

Nystatin was loaded into PCL and pSi-PCL in the ratios shown in **table 4.12**. An experimental set up was established to qualitatively (and semi-quantitatively) determine the amount of nystatin released from a static system. The polymer / composite disc was placed in the centre of a 10cm diameter polystyrene petri dish and 3ml 1% agarose (electrophoresis grade, Sigma, UK) added which contained a suspension of yeast cells (*saccharomyces cerivisiae*) such that only the upper surface of the disc was exposed (**fig. 4.13**). Once the gel was set, 2ml $dH_2O$ was added to the surface of the agarose/disc to act as a medium for nystatin release and the discs incubated at 37°C for up to 5 days.

| Sample | pSi (mg) | Nystatin (mg) | Polycaprolactone |
|---|---|---|---|
| PCL ***5*** | 0 | 5 | } 250 mg |
| PCL ***10*** | 0 | 10 | |
| **10** pSi ***5*** | 10 | 5 | |
| **20** pSi | 10 | 5 | |
| **20** pSi ***10*** | 20 | 10 | |

**Table 4.12.** Polymer : pSi : Nystatin ratios used in the investigation.

At 1 and 5 day time points the plates were analysed for the proportion of dead yeast cells by staining dead cells only with a 1% *w/v* aqueous solution of methylene blue (Kucsera *et al*, 2000). 1ml of the stain was applied and incubated at room temperature for 5 minutes before being thoroughly rinsed in several changes of PBS.

Controls used were agar discs containing no yeast cells to determine background staining and a plate containing heat-killed yeast cells with no nystatin which was irradiated by microwave radiation for 60 seconds to determine maximum staining for dead cells.

Analysis was by imaging the under surface of the plates using a Brother DCP-560CN scanner and quantification by transferring three circumferencial sections of the stained agarose/yeast to 1ml cuvettes by stamping the cuvette into the gel

to ensure identical volumes were tested. The absorbance of the agarose at 660nm was measured for each sample in triplicate and expressed as a percentage of the difference between background staining (0%) and maximum staining of irradiated cells (100%)

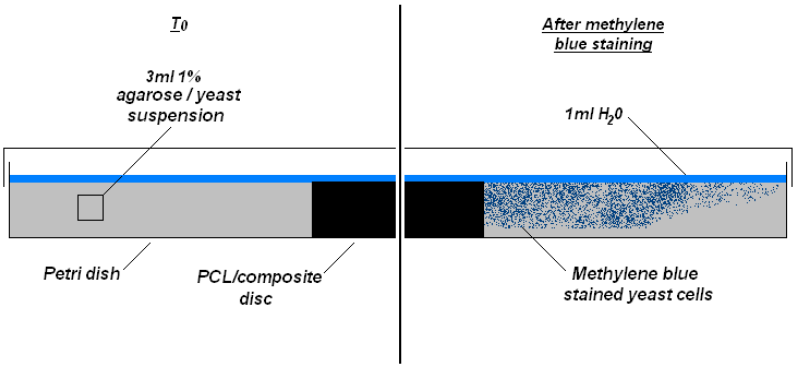


**Fig. 4.13.** Experimental set up for study of nystatin release.

#### 4.2.2.5. Dexamethasone.

Results from early experiments to determine fluorescein release rate (**4.3.2.1.**) allowed the release profiles of other small, water soluble compounds to be predicted [fluorescein $C_{20}H_{12}O_5$ 332g.mol$^{-1}$ dexamethasone $C_{22}H_{29}FO_5$ 392g.mol$^{-1}$]. Therefore, the initial loading concentrations of the substance into the material could be calculated to generate the required concentrations (see **4.3.2.1**).

Dexamethasone was loaded into polycaprolactone-only or a 20mg pSi (8%) composite in three concentrations based on the loading/release ratio of the similar molecule fluorescein. Yamanouchi *et al* (1997) suggests the optimum dexamethasone concentration for stimulating osteoblast activity *in vitro* is ~$10^{-7}$ M (39.2 ng.ml$^{-1}$). This was set as the intermediate (**Med**) release concentration maximum per day (± one standard deviation, ~50%) and achieved by loading 20mg pSi or PCL directly with 9.26 µg dexamethasone in ethanol (diluted from a 50 mg.ml$^{-1}$ stock solution).

Maximum daily concentrations of one order of magnitude lower and higher ($10^{-8}$ and $10^{-6}$ M) than this optimum were achieved by loading pSi or PCL with 926 ng and 92.6 μg respectively and designated **Low** or **High** Dex(amethasone).

Negative controls were unmodified tissue culture plastic wells, PCL discs and 8% psi-composite discs. Positive controls were replicates of these discs with $10^{-7}$M dexamethasone added to the culture medium, corresponding to the projected maximum daily release from PCL/pSi **Med** discs and equal to the concentration recommended for use in osteoblast supplementation *in vitro*.

Human osteoblasts extracted from femoral head trabecular bone were cultured in DMEM with 10% FCS, 2mM L-glutamine and 25mM HEPES. Osteoblasts at passage 30 were seeded at ~100,000 cells per well into a 48-well plates onto 250mg composite discs or into empty wells. 1ml media was added per well which was replaced every 24 hours for 15 days.

One plate was analysed every 5 days by rinsing each well carefully in PBS followed by freeze-thawing the plate with 1ml $H_2O$ per well for three cycles between -80°C and 20°C. DNA and collagen were quantified and alkaline phosphatase activity was measured as described in section **3.2.**: at day 15 the amount of calcium per well/disc was also measured.

#### 4.2.2.6. Bone morphogenic protein 7 (BMP7).

Human BMP7 (Monomer MW 15.7 kDa, Sigma UK) was loaded into pSi-PCL composites only in the ratios given in **table 4.14**. The discs were compressed between clean glass slides and removed once solid to produce a thin disc or film (~12mm x ~1mm) on which cells were seeded. Human osteoblasts at passage 30 were seeded at ~100,000 cells per well into a 12-well cell culture plate (Nunc) directly onto the well surface or onto the polymer/composite. 3ml culture media (DMEM with 10% FCS, 2mM L-glutamine, 25mM HEPES) was added which was exchanged every 5 days.

| Sample | BMP7 (μg) | pSi (mg) | PCL (mg) |
|---|---|---|---|
| Control | 0 | 0 | 0 |
| PCL | 0 | 0 | 0 |
| pSi | 0 | 2 | 25 |
| BMP7 | 2.5 | 2 | 25 |

**Table 4.14.** Loading concentrations of BMP7, pSi and PCL used in the investigation.

Three plates were set up which were analysed at 5 and 10 days for DNA and collagen content and alkaline phosphatase activity as described in section **3.2.2**. Calcium deposition was not measured due to the small repeat number (n=4). At the end of each time point the PCL, composite and BMP7-composite discs were removed from the wells and analysed seperately to determine the response of osteoblasts to growth directly on the eluting material (discs) and peripheral surfaces (wells).

## 4.3. Results.

### 4.3.1. Loading of substances into pSi and polycaprolactone.

The substance loading technique was optimised for this investigation to minimise the time substances were exposed to heat and solvent, therefore high concentrations of the substance in solvent were used (less than 3ml total solvent). Recovery of the pSi-substance was >98% by weight once the solvent was extracted with some loss experienced in transferring the pSi in slurry form to the mortar for drying and then again between the mortar and weighing boat/PCL solution. When water was used as the primary solvent some oxidisation (effervescence of the slurry) and heating was observed which was minimised by performing the loading stage at 4°C.

### 4.3.2. Substance release.

#### 4.3.2.1. Fluorescein.

1, 5 or 10mg fluorescein was loaded into 250mg polycaprolactone and 250mg 8% pSi-PCL composite discs. In addition, 20mg pSi microparticles (encapsulated in dialysis tubing) were loaded with the same amounts of fluorescein.

**Fig. 4.15.** shows the release rates observed for each loading concentration from the materials tested. At a loading of 1mg per material, the pSi microparticles in dialysis tubing are shown to release fluorescein rapidly (11.1 ± 1.84 $\mu g.day^{-1}$), corresponding with the high surface to area ratio of these particles.

PCL and PCL-pSi composite showed similar release rates (PCL: 5.78 ± 2.28 $\mu g.day^{-1}$; pSi-PCL: 4.20 ± 2.20 $\mu g.day^{-1}$). At this loading concentration the pSi microparticles became depleted of fluorescein after 9 days – it was noted that considerable fluorescein was lost in the washing steps between each media change. Both PCL and pSi-PCL eluted fluorescein at a consistent rate over 24 days.

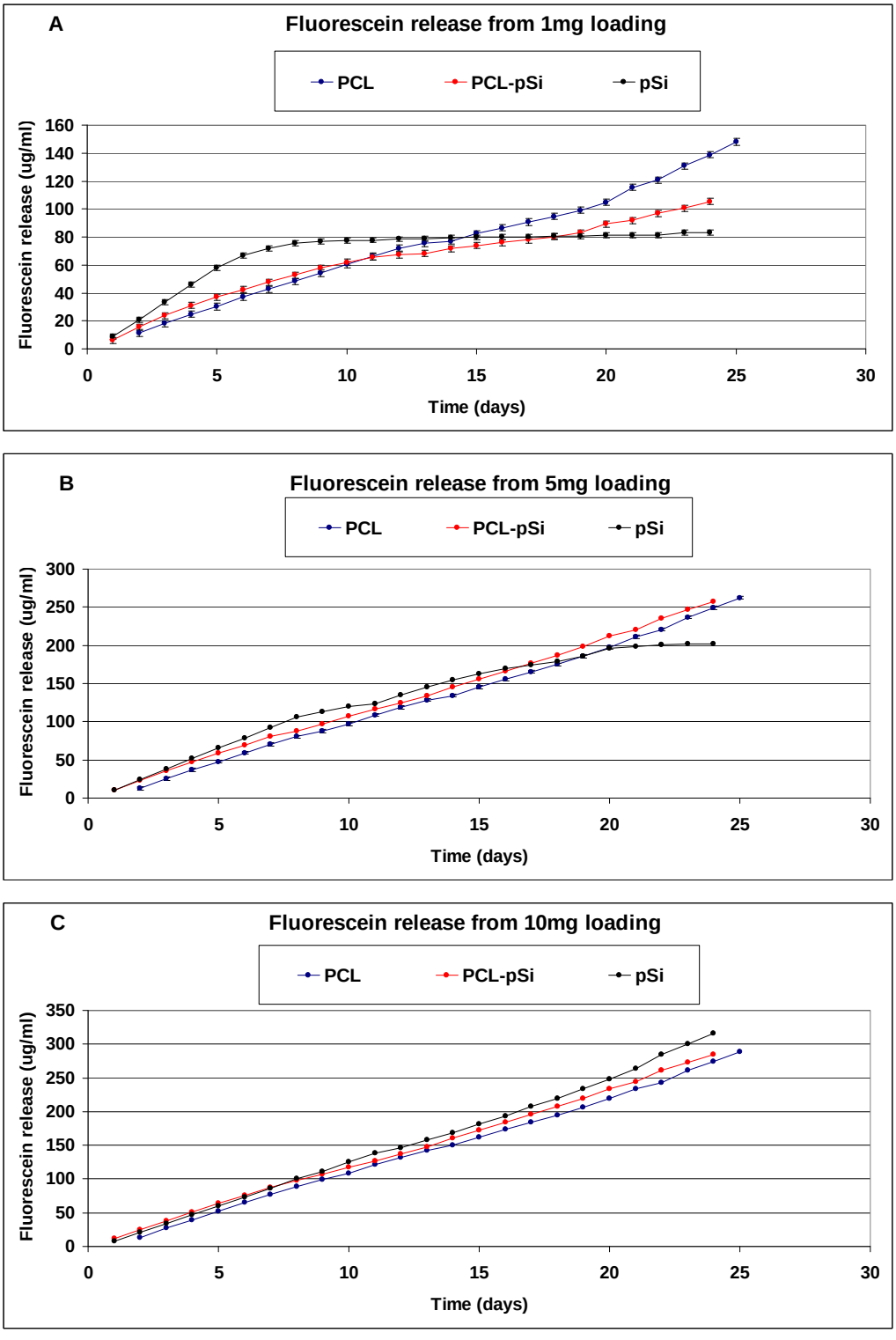


**Fig. 4.15.** Fluorescein release from polycaprolactone (PCL), 20mg (8%) pSi-PCL composites and tubing-contained pSi microparticles loaded with **A**. 1mg fluorescein; **B**. 5mg fluorescein; and **C**. 10mg fluorescein. Error bars are one standard deviation of the mean for daily release over 24 days.

At 5mg and 10mg loading, release was equivalent for pSi microparticles, PCL and the composite. For pSi microparticles the relationship between fluorescein loading and release was linear for the concentrations tested (**fig. 4.16**), whereas the PCL and PCL-composite relationship is second order, showing that the material inhibits the elution of fluorescein to some extent.

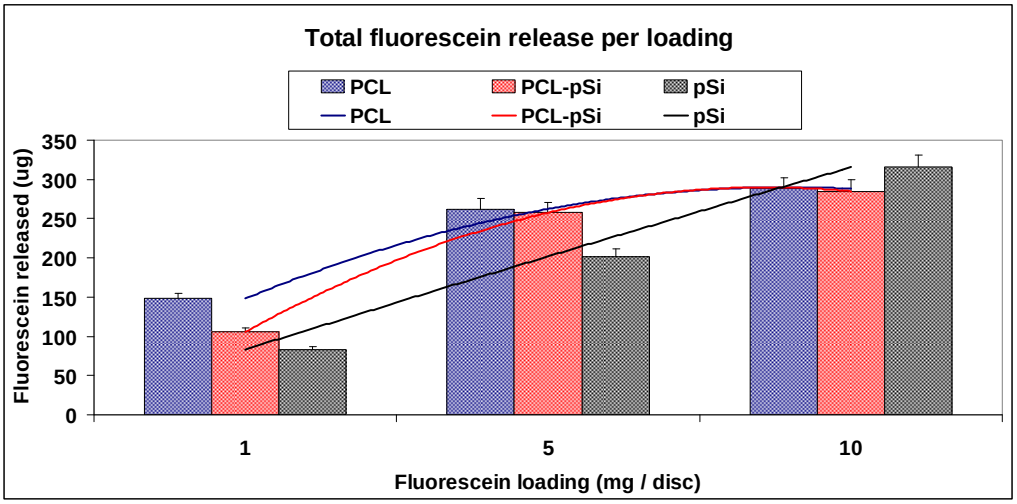


**Fig. 4.16.** Cumulative fluorescein released over 24 days at each concentration, showing a first order rate for pSi microparticles and second order rates for PCL and composite. Error bars are standard error of the mean.

| **Material** | **Release rate** | | | **Standard Deviation** |
|---|---|---|---|---|
| | **µg.day$^{-1}$** | **µM.day$^{-1}$** | **(%)$^{\dagger}$** | |
| PCL | 5.78 | 18.0 | 0.58 | ± 39.5 % |
| PCL-pSi | 4.20 | 13.0 | 0.42 | ± 52.4 % |
| pSi | 11.10 | 34.5 | 1.11 | ± 16.5 % |

**Table 4.17.** Fluorescein release per day for discs of PCL and PCL-pSi composite and pSi containing 1mg fluorescein. Release per day was similar for PCL and composite but fluctuated (standard deviation shown for data points across 24 days). pSi microparticles in dialysis tubing released significantly more fluorescein initially but became depleted (data shown for first 6 days of experiment during linear release). $^{\dagger}$ refers to fluorescein released per day/fluorescein loaded x 100.

#### 4.3.2.2. Bovine serum albumin and Alkaline phosphatase.

BSA was released from all polymer/composites but preferentially from PCL-only discs (**fig. 4.18.A**). Doubling the loading concentration (from 5mg to 10mg) increased the amount of BSA released into solution by an equal amount (107 ± 17 $\mu g.day^{-1}$ to 223 ± 7 $\mu g.day^{-1}$). Release of alkaline phosphatase into solution was lower than release of BSA but greatly increased when released from psi-composites (**fig. 4.18.B** and **fig. 4.20**)

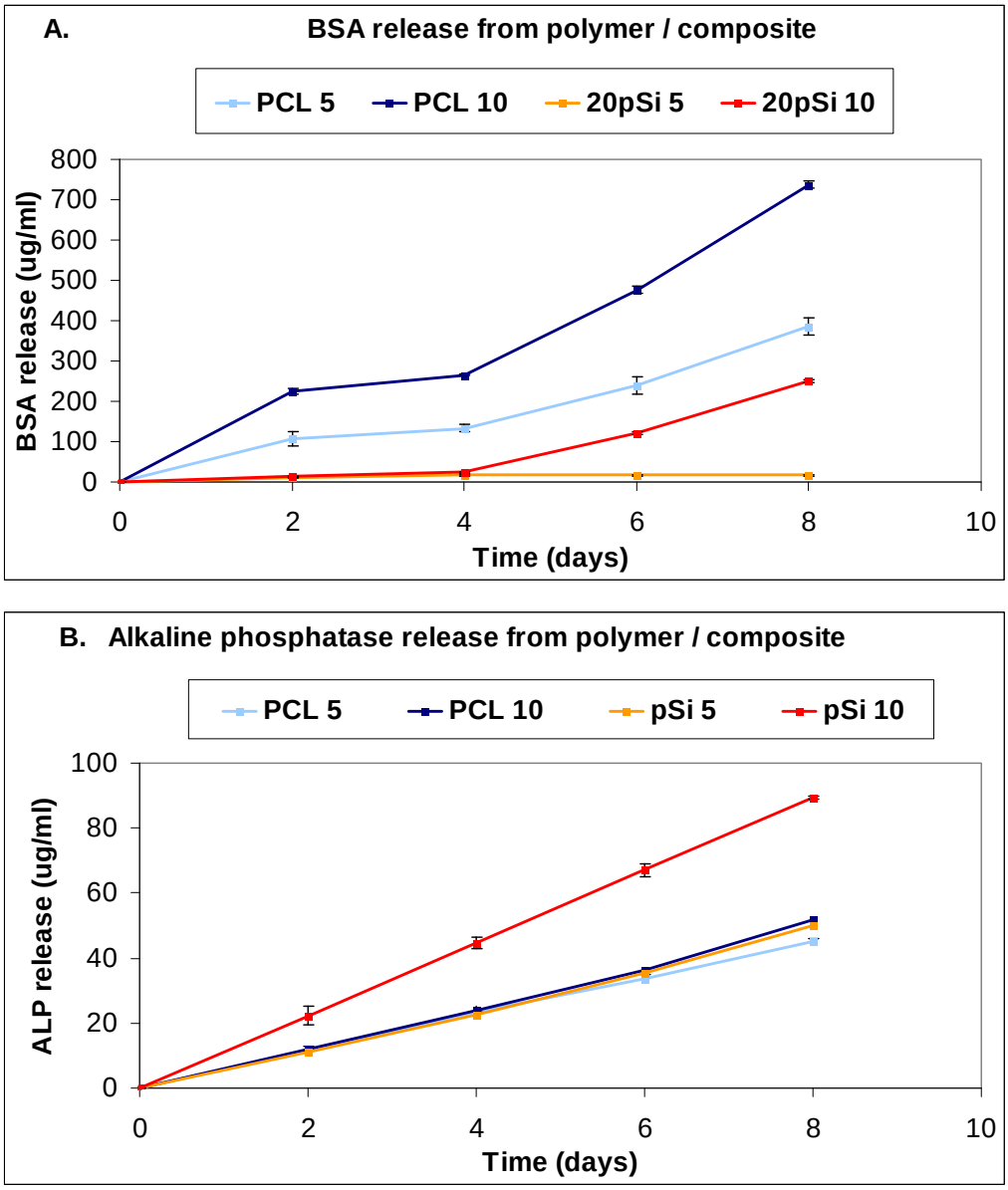


**Fig. 4.18.** Release profiles of BSA (**A**) and alkaline phosphatase (**B**). Error bars are standard error of the mean, n = 3.

Alkaline phosphatase activity per µg protein was highest across all samples at day 2 and decreased thereafter. Phosphatase activity was equally decreased across all samples at other time points (**fig. 4.19**) and appeared to further decrease over time in both PCL and pSi independently of loading vehicle.

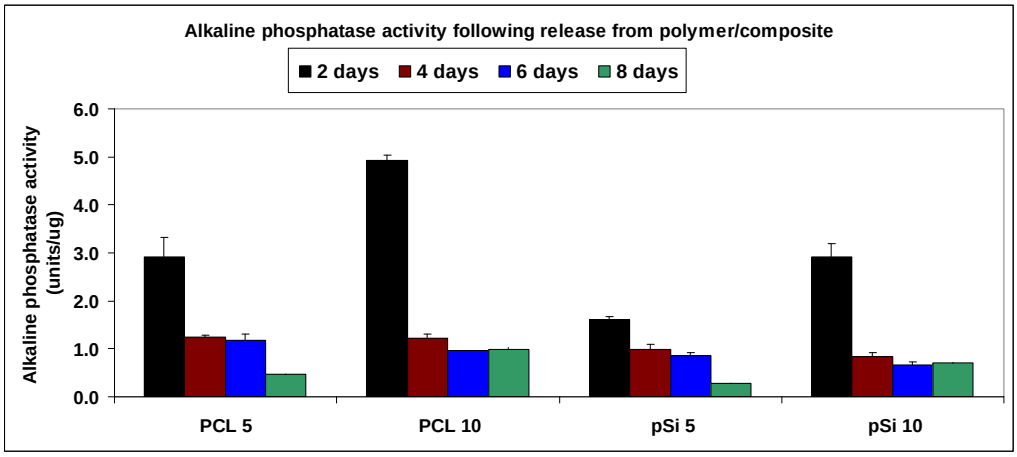


**Fig. 4.19.** The phosphatase activity per µg of alkaline phosphatase released from the polymer or composite at each time point. Error bars are standard error of the mean, n = 3.

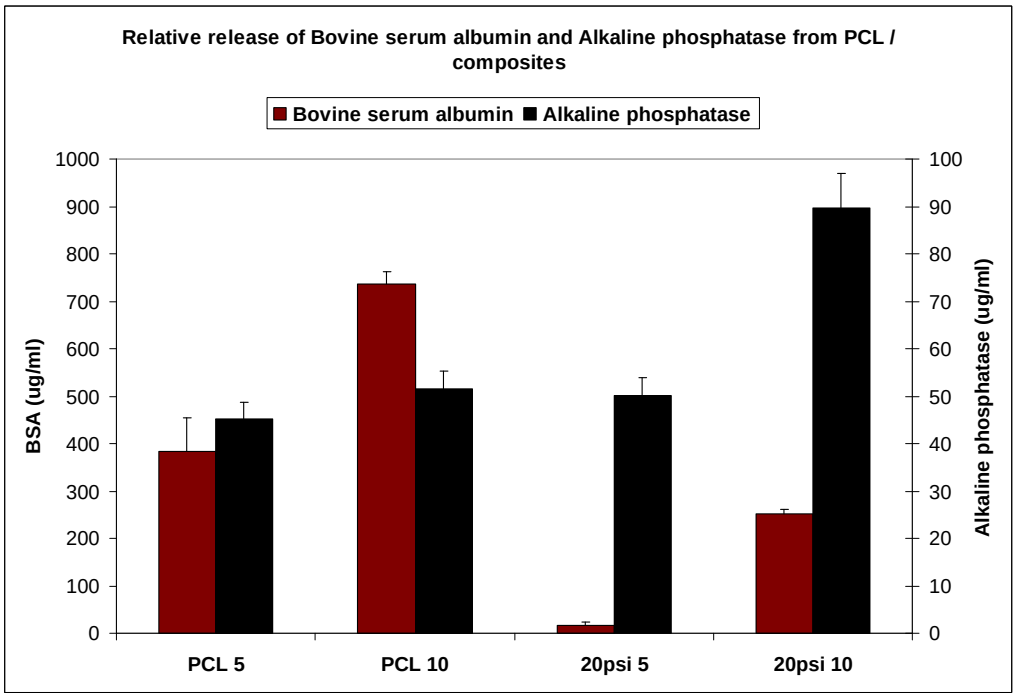


**Fig. 4.20.** Relative release rates of BSA and alkaline phosphatase from each material showing the enhanced released of alkaline phosphatase when loaded into pSi. Bars show standard error of the mean, n = 3.

#### 4.3.2.3. Gentamicin.

Gentamicin was released from PCL and from pSi in PCL into PBS. Gentamicin release from pSi was significantly higher than from PCL when 5mg was loaded ($p$ = 0.037) and when 10mg was loaded ($p$ = 0.005). In addition, release from pSi was proportional to loading concentration, but release from PCL was not significantly different at either 5 or 10mg loading ($p$ = 0.074).

Release of gentamicin (MW 447 g.mol$^{-1}$) from PCL and pSi-PCL was similar to the release of similar small, water soluble molecules such as fluorescein (MW 332 g.mol$^{-1}$) (4 - 5 µg.day$^{-1}$), supporting the hypothesis that such molecules have similar release kinetics.

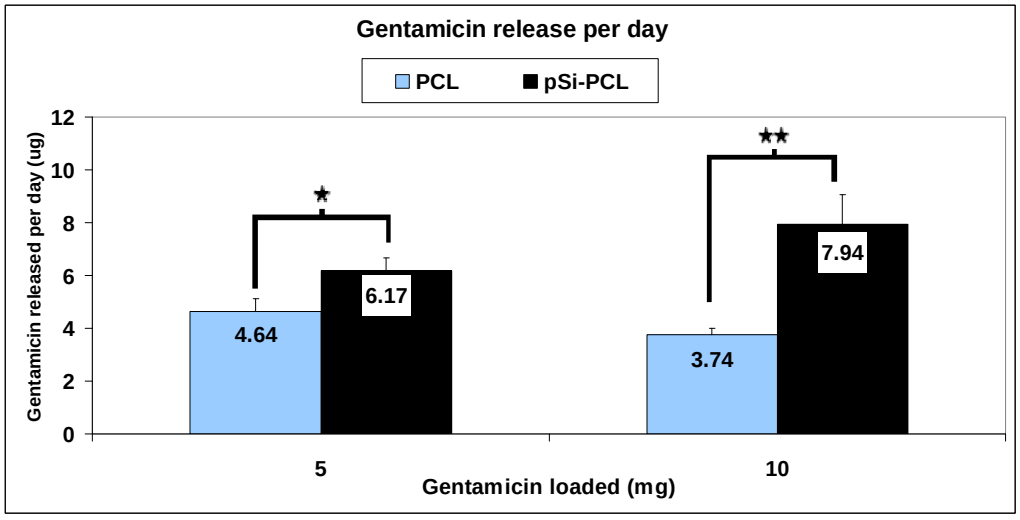


**Fig. 4.21.** Gentamicin release per day over 21 days from discs containing 5 or 10mg gentamicin in PCL or in pSi-PCL. Bars are standard error of the mean, n=4. Statistical significance was determined by Student's T-Test compared to PCL as the control population. Significant increase $p < 0.05$ (★); $p < 0.01$ (★★).

#### 4.3.2.4. Nystatin

Yeast cells were killed by nystatin released from all polymer and composite discs in a broad region throughout the agar plate (**fig. 4.22**). No gradient was observed from the central disc, indicating that the nystatin was released from the exposed upper surface into the aqueous surface layer and did not diffuse through the agar. **Fig. 4.23** indicates high release rates of nystatin from polymer-only discs and 10mg-loaded 8% composites with much reduced release from composites containing 5mg nystatin.

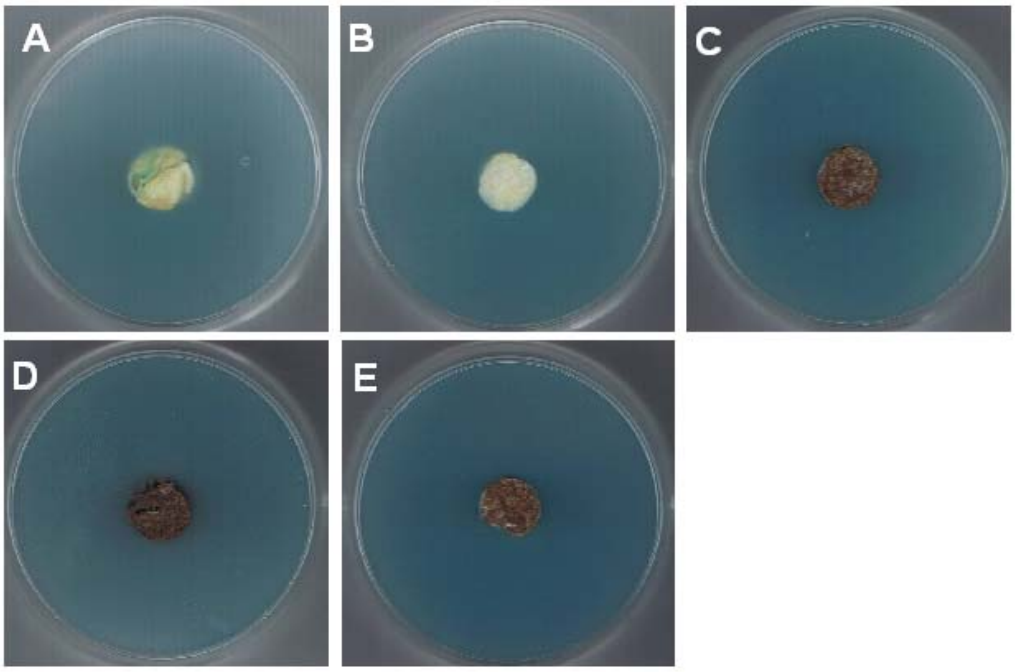


**Fig. 4.22**. Methylene blue staining of dead yeast cells at day 5. No gradient was observed in the area of effect and the region peripheral to the disc did not uptake more dye. **A**. PCL **5**; **B**. PCL **10**; **C**. **10** pSi **5**; **D**. **20** pSi **5**; **E**. **20** pSi **10**.

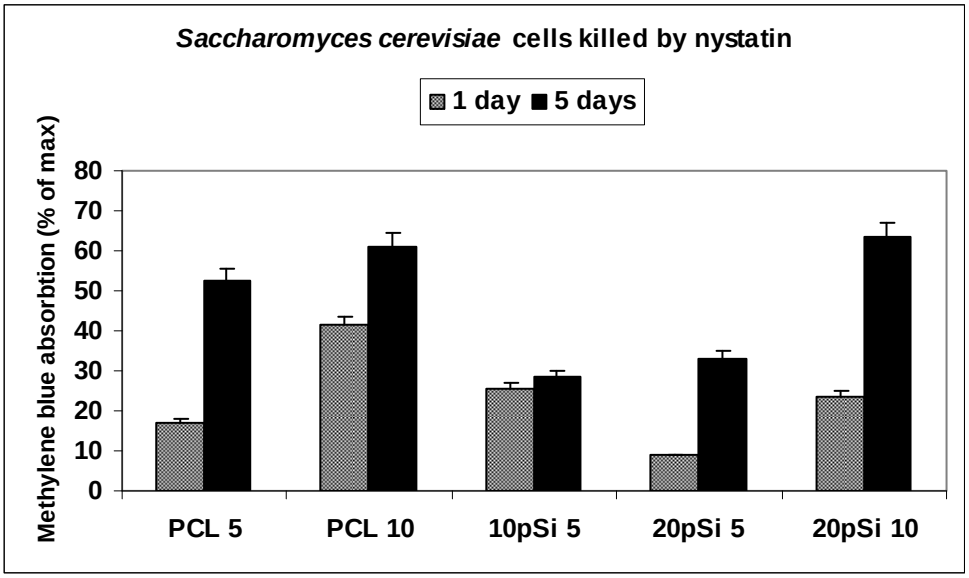


**Fig. 4.23.** Percentage of *S. cerevisiae* cells killed by nystatin as determined by methylene blue uptake. Bars show standard error of the mean, n = 3.

#### 4.3.2.5. Dexamethasone.

Dexamethasone was loaded into the PCL and pSi-PCL composite in concentrations designed to release a daily maximum of $10^{-6}$M, $10^{-7}$M and $10^{-8}$M ± 50% into solution. Controls show the response of osteoblasts cultured on tissue culture plastic (T), PCL and an 8% pSi-composite (pSi) without exposure to dexamethasone (labelled -) and also with $10^{-7}$M dexamethasone in the culture medium (labelled +).

Cultured with or without dexamethasone, osteoblasts grown on tissue culture plastic show higher cell populations but lower levels of collagen per cell and lower levels of alkaline phosphatase expression, indicating limited osteoblastic phenotype (**fig. 4.24.A**). Cells cultured on both PCL and composite produce more collagen and alkaline phosphatase at each time point than osteoblasts on tissue culture plastic (**fig. 4.24.B** and **fig. 4.24.C**).

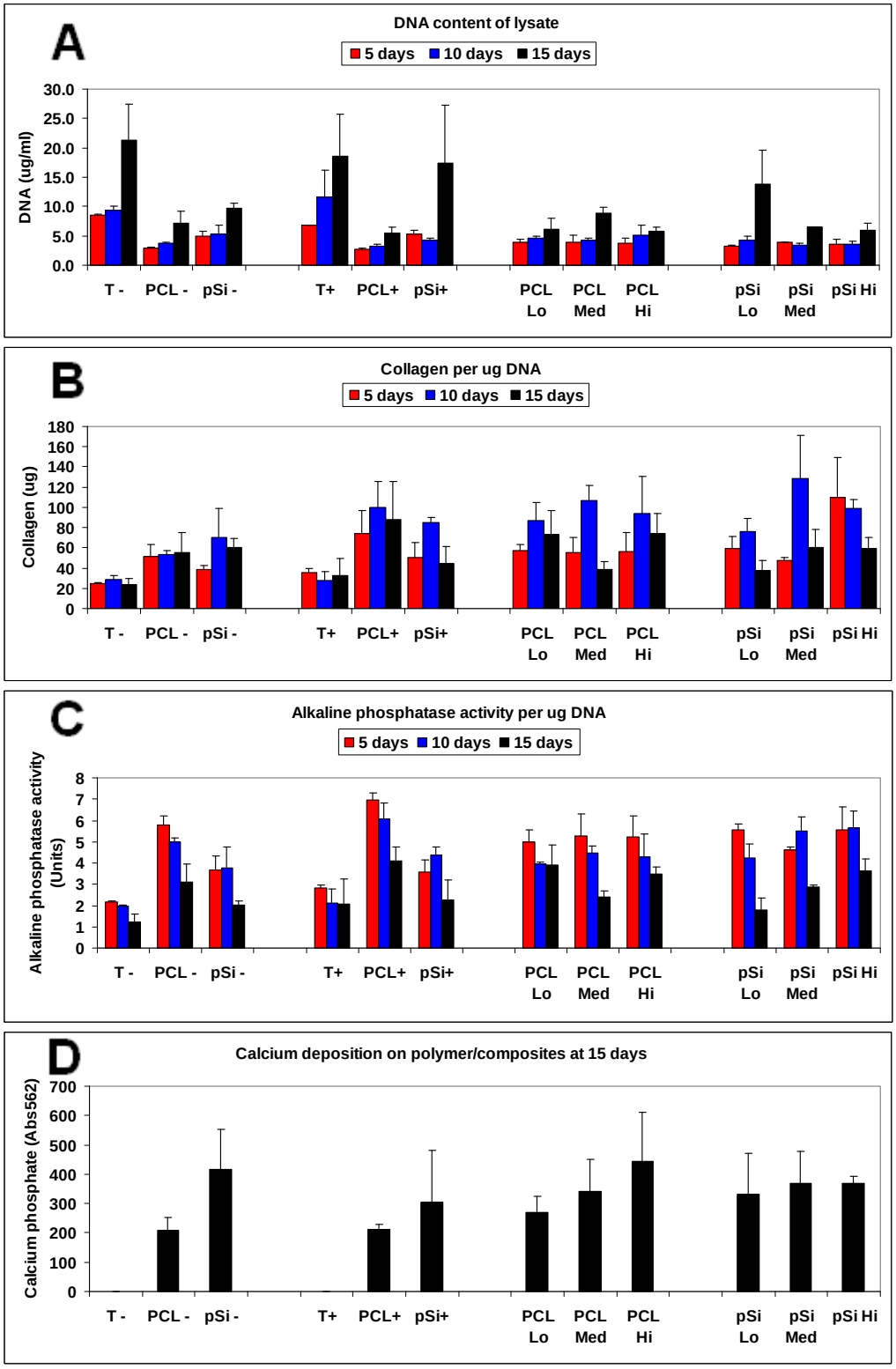


**Fig. 4.24.** Effect of dexamethasone release on human osteoblasts. **A**. DNA. **B**. Collagen normalised for osteoblast population (µg collagen / µg DNA). **C**. Alkaline phosphatase activity normalised for cell population (ALP / µg DNA). **D**. Calcium deposition on the disc surface. Bars show standard error of the mean, n = 3.

Osteoblasts cultured on dexamethasone-loaded PCL and composites showed alkaline phosphatase activity comparable to media-supplemented cells, and similarly high levels of collagen. No statistically significant difference was observed in collagen deposition or alkaline phosphatase activity at any time point for any of the material substrates (thermanox, PCL or pSi-PCL) with or without dexamethasone-supplemented media.

Similarly, the osteoblast response to PCL or pSi-PCL eluting dexamethasone was not significantly different to that of PCL or pSi-PCL with dexamethasone-supplemented media. No significant difference in calcium deposition at 15 days was observed in any condition.

#### 4.3.2.6. Bone morphogenic protein 7.

To examine the effect of the material surface on osteoblast activity from the behavior of osteoblasts on surrounding tissue culture plastic, the PCL, pSi-PCL and BMP-loaded pSi-PCL discs were removed from the wells and analysed seperately using the same techniques.

Osteoblast populations were significantly lower on the surface of PCL, composite and composite materials loaded with BMP7 (**fig. 4.25.A**) than on tissue culture plastic surrounding the material. Osteoblast populations on adjacent tissue culture plastic and control wells showed no significant difference across the conditions at each time point. Although control well populations appear higher, they were equivalent when compared to the sum of well plus composite.

Osteoblasts cultured on PCL, composite and composite-BMP surfaces exhibited significantly more alkaline phosphatase activity than tissue culture plastic ($p < 0.01$). Alkaline phosphatase activity was greater on composite and BMP7 than on PCL surfaces at day 5 ($p < 0.05$) but not at day 10. The addition of BMP to the composite did not significantly increase alkaline phosphatase activity.

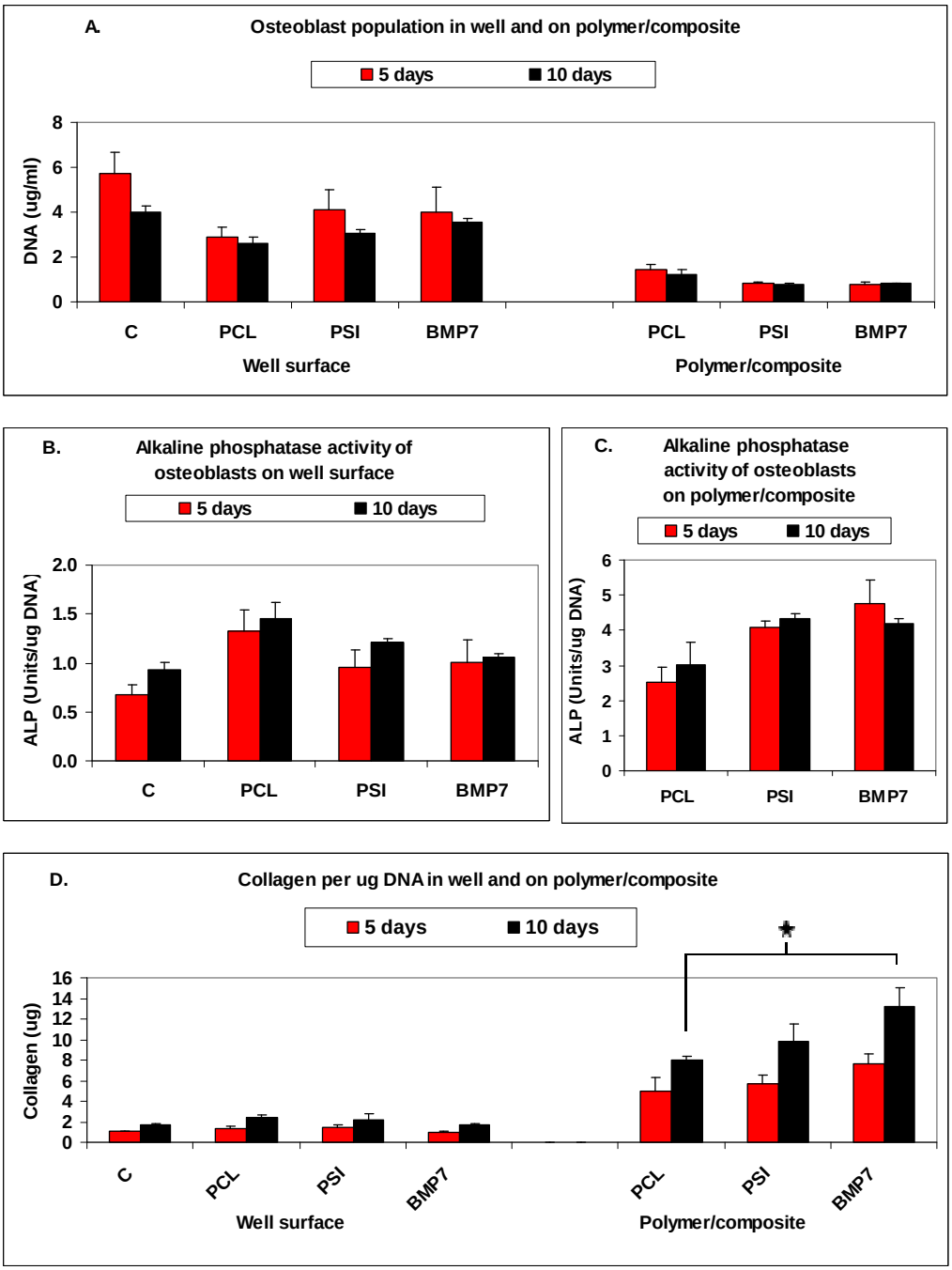


**Fig. 4.25.** Effect of BMP7 release on human osteoblasts. PCL, pSi-PCL and BMP-eluting pSi-PCL were removed from wells and analysed seperately to isolate the osteoblasts directly cultured on the material surface. DNA content (**A**) is shown as a measure of cell population on the well surface (*left*) including tissue culture plastic controls, and on the polymer / composite disc surface (*right*). **B** shows alkaline phosphatase activity on the well surface and **C** on the material discs. **D** shows collagen content on the well (*left*) and material (*right*) surfaces, per μg DNA to indicate collagen production (per cell). Significant increase $p < 0.05$ (★)

Total collagen per well was similar across all samples and slightly higher in pSi-containing composites. Collagen per cell was significantly higher on composite materials than on surrounding tissue culture plastic ($p < 0.01$). The addition of BMP7 to pSi-PCL significantly increased the osteoblast production of collagen at ten days over tissue culture plastic ($p < 0.01$) and PCL ($p < 0.05$) but not significantly more than pSi-PCL ($p = 0.119$).

**4.4. Discussion.**

The aim of this investigation was to assess porous silicon as a carrier for active pharmaceuticals in a polycaprolactone matrix for use in orthopaedic tissue engineering. In parts **4.2.1** and **4.3.1** a method is described for loading substances into pSi using a two-solvent technique whereby the drug in solution is mixed with a secondary solvent phase containing microparticles of porous silicon.

In this investigation it was important to determine that the substances were actually loaded into pore spaces of pSi and not simply precipitated out of solution with the microparticles before being cast into the polycaprolactone matrix. The large surface area to volume ratio of porous silicon (~500 $m^2.g^{-1}$) coupled to it's capillarity and electrostaically charged positive (silicon hydride) and negative (silicon oxide) surface regions suggest that substances would be drawn into the pore spaces and precipitate on internal (pore) surfaces.

Evidence for this is provided by the sustained release over 7 or more days of fluorescein from pSi microparticles which were contained in dialysis tubing. In this system, fluorescein continued to be released from the particles over a period of several days, even when the particles were thoroughly rinsed with water between solution changes. The pSi therefore prevented the fluorescein from being immediately washed out of the matrix during these rinses and allowed the fluorescein to elute from the material steadily over time in solution. Further evidence for this was subsequently provided by CLSM imaging of fluorescein-loaded pSi particles.

pSi-PCL composites have similar release profiles to drugs loaded into polycaprolactone-only for most of the substances tested in this investigation. Therefore the results of this research can be directly compared to the wealth of published data on polycaprolactone drug delivery devices, microspheres, screws and sutures (Wu & Jin, 2008; Varde & Pack, 2004).

The release of small, water-soluble molecules such as fluorescein and gentamicin were found to be similar, 6 -12 μg.day-1 for 10mg substance loaded into pSi-PCL,

allowing the amount of substance released to be broadly predicted from loading concentration. The release of proteins such as BSA and alkaline phosphatase from pSi-PCL was more dependent on protein mass and structure, with BSA (MW 66 kDa) being released into solution in concentrations an order of magnitude greater than the very hydrophobic dimer alkaline phosphatase (MW 160 kDa).

Sustained release of all tested molecules from pSi-PCL composites indicates that release is both stable and predictable over experimental timescales. Release of fluorescein was dependant on initial loading concentration, and was linear over time for loading concentrations of up to 50% *w/w* fluorescein into pSi (10mg fluorescein per 20mg pSi). The ability to achieve high loading densities of drugs into pSi without altering it's physical properties is an advantage of porous silicon for drug delivery applications.

The loading of drugs directly into a polymer can change the mechanical properties of the material - as described for PMMA bone cement by Lautenschlager *et al* (1976) - but the mechanical properties of pSi-PCL composites are not affected by the type or amount of drug loaded into pSi. Therefore, any combination or quantity of pharmaceuticals can be loaded into pSi (up to 50% of the pSi) whilst the mechanical properties remain the same, an important consideration for determining load-bearing, consistency and compliance with safety regulations set by the FDA and BSA standards commission.

A further advantage of using pSi carriers for pharmaceuticals is that they can be prepared and stored in advance and added to polymers to form composites which elute a combination of substances, such as antibiotics, steroid hormones, pain-killers and growth factors. The combination of drugs and dosages are therefore effectively bespoke and can be tailored by pharmacists or physicians to suit the patient. Surgeons familiar with preparing their own antibiotic bone cements currently use similar techniques as the antibiotic powders are mixed with the PMMA powder and formed into a dough. It is conceivable that mouldable or injectable polymers containing pSi-encapsulated drugs could be used by surgeons in a similar way.

Regarding the potential for pSi breakdown products to denature pharmaceuticals, the effects of reactive silicon species such as high concentrations of silicic acids, hydrated $SiO_2$ and silane on the stability of pharmaceuticals are not covered in the literature specifically, although silane is known to be a strong reducing agent. A major limitation of polylactide vehicles for drug delivery has been the acidic degradation products which are particularly damaging for protein drugs (Wu & Jin, 2008). This remains a concern for pSi-based polymer composites as the additional acidification caused by pSi dissolution into orthosilicic acid decreases the pH of incubating solutions.

The biocompatibility of pSi with organic molecules has been ascertained by several research groups (e.g. Bayliss *et al*, 2000). The effects of silicic acids on biological macromolecules have been studied, and as discussed elsewhere in this work, Bayliss *et al* (2000) showed that glycoproteins in the extracellular matrix may be crosslinked by siloxane bonds in the presence of silicic acids.

The effects of this on the enzymatic activity of a well-described glycoprotein (alkaline phosphatase, ALP) are studied in **4.3.2.2**. Activity per unit of eluted ALP was measured and found to decrease at a similar rate under all conditions, regardless of silicon content. It can therefore be concluded that crosslinking of the glycosaminoglycan chains by silicon species, if it occurs, does not adversely affect the activity of this glycoprotein in terms of enzymatic dephosphorylation ability. In *in vitro* conditions however, the precise tertiary and quaternary structural conformation of the protein may be more essential to it's function in ligand binding (e.g. Jefferis *et al*, 1995).

Bone morphogenic proteins are an important family of molecules for advanced orthopaedic applications and can be topically delivered to complicated wound sites, such as non-union and following substantial bone loss (Dahabreh *et al*, 2008). In this investigation, BMP7 was still active upon release from pSi-PCL composites and able to stimulate osteoblastic activity *in vitro*. Based on these results it can be concluded that in preliminary trials, protein drugs were not denatured by the breakdown products of porous silicon, including heavily glycosylated proteins (ALP) and proteins which are functional only as

homodimers (BMP7). The polyene antifungal nystatin was also anti-microbrially effective following release.

Interestingly, release of BSA from pSi-PCL appeared to be substantially lower in comparison to release from PCL alone. The Bradford assay used to detect protein in this investigation is also able to detect proteins which are denatured, demonstrating that BSA was either not released from pSi-PCL or was bound to the material following release. A further examination of this effect is given in chapter five (page 172), in which protein interactions with the material surface are investigated.

To conclude, porous silicon can be added to polycaprolactone to moderate the delivery of various drugs, and in combination with the proposed bioactivity of pSi may present a means for increasing the bioavailability and activity of several drugs for orthopaedic scaffolds. Based on the results from the present study however, the release kinetics from both PCL and pSi-PCL are similar. Advanced techniques for drug delivery such as staged release of various pharmaceuticals or easily tailored combination therapies may be developed which can make use of the advanced properties of pSi.

# Chapter Five

-

# Characterisation of pSi-PCL Composites in Simulated Physiological Environments

## 5.1. Introduction.

Characterisation of successful biomaterials progresses along well-developed routes, from initial studies of behavior in acellular simulated body fluids, to *in vitro* culture of relevant cell types and finally *in vivo* studies using experimental animal models.

Whilst animal models are useful for many applications and an essential prerequisite for clinical use and regulation, using animals for initial trials of biomaterials is costly, raises ethical issues and also limits the number of samples which can be tested. In addition, the reproducibility of the data is questionable, and so to overcome this, several groups have reported progress in developing simulated *in vivo* techniques. An example of this are the 4$^{th}$ generation composite femurs manufactured by Pacific Research Laboratories (Vashon, USA), which are similar in shape, mechanical characteristics, and material density to those of human femurs and are used for mechanical testing of hip arthroplasties (Zdero *et al*, 2008).

Such techniques are designed to mimic as closely as possible relevant factors in biomaterial testing and has considerable success in describing properties of biomaterials that previously would have been difficult to reproduce under controlled or *in vivo* conditions.

This section of the work encompasses the further acellular characterisation that was performed on the composite and includes:

- The dissolution of pSi-PCL in simulated static and perfusion bone models.
- The permeability of the composite to orthosilicic acid and small molecules.
- Evaluating protein adsorption onto pSi-PCL from simulated plasmas.

This work was performed in order to allow comparisons between features of pSi-PCL and other composite biomaterials in the literature.

### 5.1.1. Protein adsorption.

Part of the theory behind Bioglass® bioactivity is that the silica and hydroxyapatite layers accrued on the surface of the materials provides an adsorption bed for biological molecules. In a wound site, certain molecules such as IGF-I (Nakasaki *et al*, 2008), BMP-2, BMP-4, and PDGF-bb (Fiedler *et al*, 2002) are both localised and secreted, acting as chemotactic cues for osteoblast migration, differentiation and adhesion.

It has been proposed by several researchers (Kaufmann *et al*, 2000; Rosengren *et al*, 2003) that binding such molecules to a material surface enhances bioactivity by concentrating them on an implant surface and improving wound healing at the site. The activity of adsorbed proteins is crucial to their function in a wound site, and it has been shown (Lobell and Hench, 1998) that the activity of enzymes such as horseradish peroxidase continues following adsorption onto Bioglass®-silica-hydroxyapatite layers.

Misra *et al* (2008) showed that micro- and nanoparticles of 45S5 Bioglass® were capable of increasing the adsorption of proteins from foetal calf serum (FCS) onto poly(3-hydroxybutyrate). The study found that 20% *w/w* Bioglass® nanoparticles were required to significantly increase adsorption, and that this needed to be increased to 30% for microparticle-based composites. Soderling *et al* (1996) postulate that the surface energy and protein adsorption of biomaterials (specifically bioactive glasses) are directly proportional to their biocompatibility.

The type and function of proteins adsorbed also has a bearing on the effect on cell attachment. Whilst many of the proteins expressed in the extracellular environment *in vitro* are likely to be autocrine and paracrine signals from the osteoblasts stimulating aspects of activity and growth, other proteins such as adsorbed serum albumins may have a negative effect on cell attachment and profileration. The effects of protein adsorbtion *in vivo* in which a larger array of macromolecules are abundant may be expected to be considerably more complex.

### 5.1.1. Permeability of polycaprolactone to silicic acid and small molecules.

In this investigation, porous silicon microparticles are combined with polycaprolactone to form a biodegradable composite. Polycaprolactone is permeable to water, particularly in the non-crystalline amorphous phase (Stevens, 2001) but the permeability to silicic acid and loaded pharmaceuticals is unknown. This is relevant for a number of reasons, chiefly that the thickness and volume / surface area for many applications will vary and so the amount of silicic acid and loaded pharmaceuticals released should be predictable to enable the correct loading dosage to be achieved.

Goodwin *et al* (1998) report that the delivery of protein drugs from PCL is slow in comparison to other aliphatic polyesters. Lu & Lin (2002) attribute this to the poor diffusion of hydrophilic molecules through the hydrophobic polymer phase, coupled to the presence of non-permeable crystalline regions in the polymer and its relatively slow degradation rate.

Consequently, it was necessary to determine the dissolution mode of the pSi in the composite. This may be by either surface degradation in which the microporous exterior of the material only is permeable to water and dissolved molecules, or by bulk degradation if water ingress permeates throughout the polymer phase, allowing degradation equally throughout the material.

To investigate this, pSi was loaded with fluorescein and formed into a composite as described in Chapter 4. Successive encapsulating layers of PCL were added and the release rate of both silicic acid and fluorescein through these layers was measured.

### 5.1.2. Composite behaviour in a dynamic perfusion model.

Blood and tissue fluid flow around an orthopaedic implant depends largely on the implant type, site and the native physiology of the host tissue and is heavily modified by both behavior and pharmacological factors (McCarthy, 2006).

In bone, blood perfusion rates vary enormously due to the varied structure of the tissue: from intermedullary spaces and the periosteum in which arterial blood pressure determines fluid flow rates, to increasing pressure through narrower Haversian and Volkmann's canals. In the canaliculi linking osteocytes the pressure is high (and dependent upon variable mechanical loading), but interstitial fluid flow rate is relatively low and is regulated largely by the lymphatic drainage system in the periosteum (Hillsley & Frangos, 1993).

Therefore it is difficult to ascertain the perfusion rate which a bone implant or fixation device would experience *in vivo*, and also between test subjects, from scaling smaller experimental animals (chiefly rabbits) to human patients. From the limited literature available, it can be surmised that the flow rates in bone vary from 300 – 400 $\mu l.min^{-1}$ in rabbit tibial artery (Tu *et al*, 2000), $2.0ml.min^{-1}.100g^{-1}$ in rabbit tibial cortical bone (Larson *et al*, 2008) to 2.29 $ml.min^{-1}$ in the canine femoral periosteum and 6.5 $ml.min^{-1}$ in the canine ulnar endosteum (Li *et al*, 1989).

Whiteside *et al* (1977) also noted that the rate of blood flow in rabbit tibia is proportional to osteoblastic activity. Epiphyses with high osteoblastic activity ($283 \pm 53$ $\mu l.min^{-1}.ml^{-1}$) had significantly faster blood flow than that in epiphyses with minimal activity ($97 \pm 7$ $\mu l.min^{-1}.ml^{-1}$).

In this part of the investigation, the response of pSi-PCL composites was observed under conditions in which the dissolution volume was continually replaced, simulating an in vivo situation such as might be found surrounding a fixation screw head or the surface of a healing bone.

### 5.1.3. Bone tissue simulation.

Equal in importance to situations of high rates of fluid flow, the behaviour of an eluting biomaterial in a static bone matrix is crucial to its potential success or failure as an implant. In clinical situations, many implants are placed directly into the bone (screw bodies, bone fillers) where they immediately begin to degrade but in which the degradation products are not carried into the bloodstream and remain adjacent to the implant where the concentration becomes rapidly increased (Liu *et al*, 2006; Raghoebar *et al*, 2006).

The rate of clearance of the degradation products is related to the bone architecture, and as has been discussed, bone is a complex material with several levels of structure on both the macroscopic and microscopic scales. Trabecular bone is usually between 50% and 90% porous, with the interstitial spaces filled with haemopoetic cells and with a blood supply sufficient to rapidly perfuse the implant site with fluid. In this regard section **5.1.2.** (ample saturation and generally freely-flowing volumes) simulates trabecular and lamellar bone conditions.

Cortical bone, however, is much denser being typically only 5 – 10% porous. Nutrient distribution is effected in cortical bone by a network of inter-connected channels, from the longitudinal Haversian canals (20 - 150μm diameter) and radiating Volkmann canals (~25μm diameter) to the canaliculi (average diameter 259nm) that connect individual osteocytes.

Although lamellar and trabecular bone do not form Haversian systems, canaliculi are common to all types of mature bone, and represent the smallest and most frequent pore size in bone through which a small molecule must pass. Therefore, the model chosen to simulate a direct bone-implant interface was to have an average pore diameter of approximately 259nm.

To establish a simulated bone model, an agarose hydrogel was used. Agarose is a commonly employed hydrogel for molecular biology, used in size-exclusion electrophoresis of many molecules including DNA and proteins. This mechanism depends on the gelling of agarose producing nanoscale pores within a reasonably

narrow range of sizes, and which is furthermore directly related to the concentration of the gel (Pernodet *et al*, 1997).

Following the formula $a = C^{\gamma}$ [where **a** is average pore size; **C** is agarose concentration; **γ** is a constant -0.64] it can be derived that an agarose concentration of 3.78% will have a mean pore size of 259nm (**fig. 5.1**).

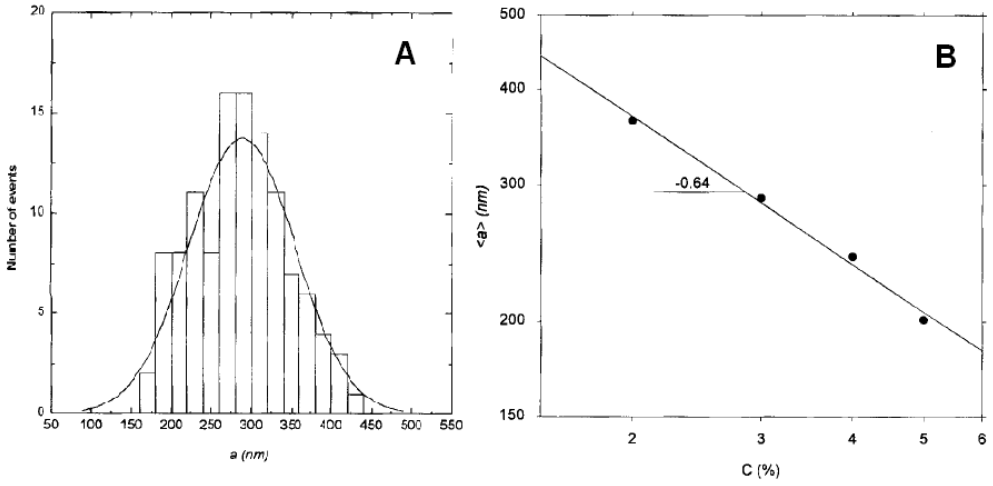


**Fig. 5.1. A**. Pore size distribution of 3.0% *w/v* agarose gels. **B**. Pore size as a function of agarose concentration (from Pernodet *et al*, 1997).

## 5.2. Materials and Methods.

### 5.2.1. Protein adsorption.

100mg discs of PCL and 8% pSi-PCL were melted on glass slides to produce flattened discs 12mm ± 1mm in diameter with a smooth surface. These were incubated (n = 4) in 4 ml of either 40 $mg.ml^{-1}$ bovine serum albumin (Sigma, UK) in water or 1 x foetal bovine serum (Sigma, UK) at room temperature for 72 hours in a sealed 5ml screw-capped polystyrene tube.

After 72 hours the discs were removed, carefully but thoroughly rinsed in $dH_2O$ and added to 1ml pre-prepared Bradford reagent (Sigma, UK) in a 24-well plate. After one hour the absorbance of the reagent at 595nm was read in a spectrophotometer. The amount of protein was established by comparison to a standard curve of known concentrations of BSA from 7 $\mu g.ml^{-1}$ to 120 $\mu g.ml^{-1}$, prepared in Bradford reagent.

Separately, four 8% pSi-PCL cylinders (500mg ± 50mg) were incubated in 4ml of 10mg.ml-1 alkaline phosphatase (bovine intestinal mucosa, Sigma, UK) at room temperature in screw-capped polystyrene tubes. After 72 hours the cylinders were removed, rinsed in $dH_2O$ and placed in wells of a 24-well plate. 1ml 4-methylumbelliferyl phosphate (Sigma, UK) was added and allowed to incubate at 37°C for 10 minutes.

5 x 200µl of the solution were removed to wells of a 96-well plate and the fluorescence measured at an excitation wavelength of 360nm and emission wavelength of 460nm. The cylinders were rinsed again in $dH_2O$ and the amount of protein per cylinder measured as above using the prepared Bradford reagent.

### 5.2.2. pSi encapsulation in PCL layers.

pSi was loaded with 50% fluorescein as described in Chapter 3 and added to 66% *w/v* PCL in acetone to produce an 8% composite. 100mg discs of the composite were cut and encapsulated in 1 – 4 layers of polycaprolactone (**fig. 5.2**).

Polycaprolactone beads (35-40mg) were melted at 100°C on glass slides using a hot-plate and pressed between another glass slide to produce a disc 0.7 mm in thickness. pSi-fluorescein/PCL composites were placed on the surface of the PCL on the slide and reheated until melted together and a second PCL disc added to encapsulate the composite discs – care was taken to ensure no air was trapped. The discs were cooled and the process repeated to create discs encapsulated in 1 to 4 layers of PCL.

Some discs were sectioned to determine the thickness of each layer using a dissecting microscope. Intact discs were placed in the wells of a 24-well plate and 1ml PBS added. The plate was incubated at 37°C for 8 days with the solution being changed every 2 days and assayed for silicic acid *via* molybdenum blue assay (section **2.2.2.2.**) and fluorescein content by measuring the fluorescence of 200µl of the incubation solution at excitation λ = 490, emission λ = 520.

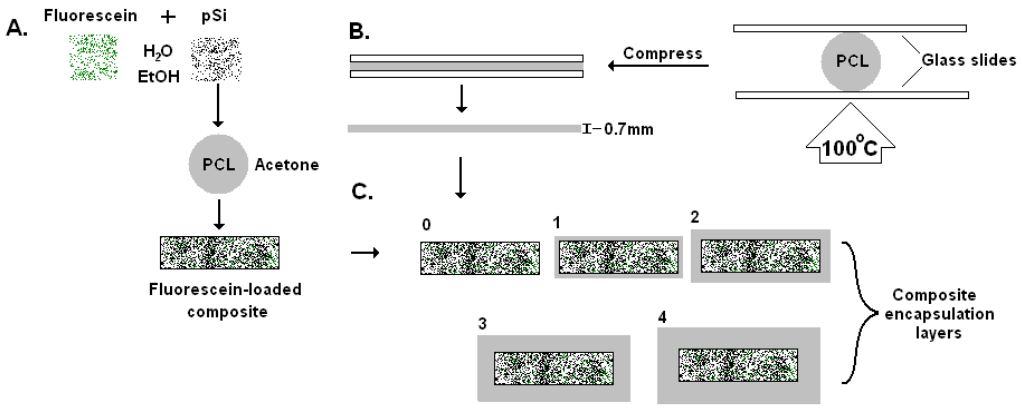


**Fig. 5.2.** Method for producing PCL-encapsulated fluorescein composite discs. **A**. 50% w/w fluorescein/pSi was prepared in 50:50 ethanol:water and loaded into PCL as described in section **2.2.1** (page 50). **B**. PCL beads (300-350 mg) were melted on a hotplate between glass slides and compressed to form 0.7mm thick discs. **C**. Composite discs were encapsulated between two PCL layers at 70°C. Encapsulation was repeated to produce discs with one to four surrounding layers.

### 5.2.2. Dynamic perfusion.

25 litres of simulated body fluid were prepared as described previously and stored at room temperature in a single reservoir. Six 1g discs were fabricated containing PCL or 8% pSi and placed in the base of 10ml syringe bodies which were arranged adjacently in a rack.

1mm diameter silicone tubing fed the SBF from the reservoir to the syringe bodies via a gravity siphon and the eluent solution was collected in 50ml graduated tubes which allowed the flow rate to be calculated (volume/time) and silicic acid release to be measured. After 24 hours the discs were removed from the tubes, rinsed carefully and assayed for calcium phosphate deposition using the Alizarin red S method as described in Chapter 2.

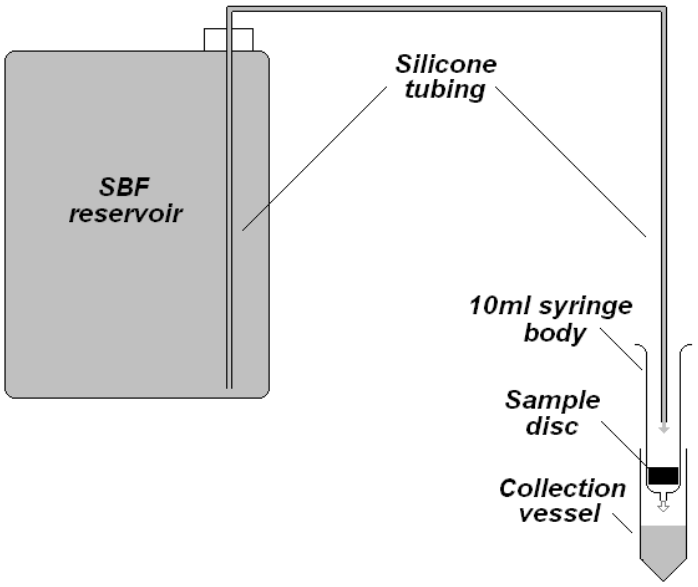


**Fig. 5.3.** System for testing dynamic perfusion of PCL and pSi-PCL with simulated body fluid. 1.0g PCL or 8% pSi-composites were placed in the base of a 10ml syringe body which was fixed vertically into a rack over a graduated 50ml collection vessel. A 25 litre reservoir of SBF was placed slightly above the syringe body and connected via a length of 0.1 mm (internal diameter) silicone tubing and a flow induced by siphoning the SBF via gravity. Flow rate was adjusted by varying the relative height of the syringe rack to be approximately 2.0 $ml.min^{-1}$.

### 5.2.3. Bone tissue simulation.

3.78g electrophoresis grade agarose was obtained and dissolved in 90ml by heating in a microwave oven before being cooled to ~30°C. 10ml penicillin/streptomycin solution (Sigma, UK) was then added and poured into 90mm diameter polystyrene petri dishes.

Three replicates were produced, with each dish filled to the top with agarose, (~5ml agarose). Whilst the agar was still liquid but <40°C, 250mg pSi-PCL discs were placed in the centre of the dish. To ensure full immersion, the discs were pre-wetted in 50% ethanol : water. When cool, the lids were replaced on the petri dishes and sealed with parafilm before being incubated at 37°C.

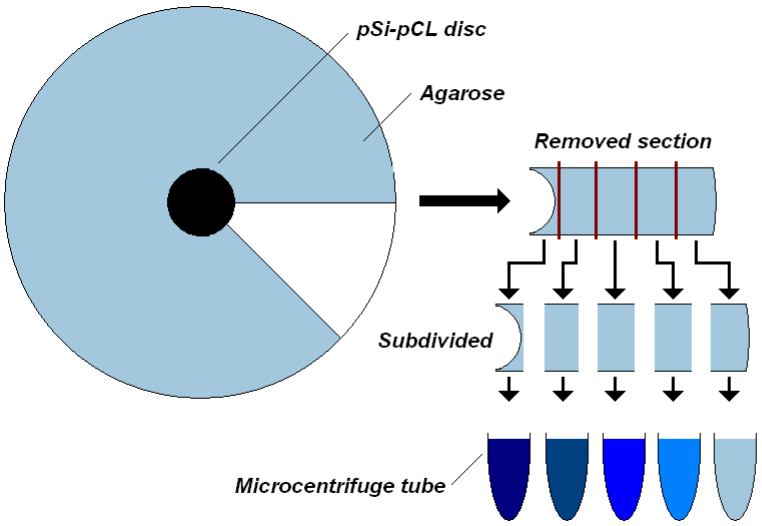


**Fig. 5.3.** Method for analysing silicic acid concentration in agarose gels. A 45° radial section is excised from the molybdenum-stained plate and subdivided into arcs 5mm in separation. The sections are melted using microwave radiation in microcentrifuge tubes and 1ml transferred to cuvettes for spectrometric analysis.

The agar was analysed after 7 days using a modified molybdate blue assay. 1 ml ammonium molybdate solution (3.5% ammonium molybdate (IV) tetrahydrate and 10% concentrated (17M) hydrochloric acid in $dH_2O$) was added to the surface of the agar and allowed to perfuse through the agar for 30 minutes at room temperature. 5 ml reducing solution (4g oxalic acid dihydrate,1.33g 4-(methylamino)phenol sulfate, 0.8g anhydrous sodium sulfite, 20ml concentrated sulfuric acid, total volume 200ml with $dH_2O$) was then added and left at room temperature for 2 hours.

After this time, the plate was imaged from underneath using a Brother DCP-560CN scanner. Secondly, a section of the agar was removed and subdivided into sections which were solubilised by heating and separated by centrifugation to yield a coloured supernatant that could be analysed spectrometrically at 810nm as with the standard molybdenum blue assay (**fig. 5.3**).

## 5.3. Results.

### 5.3.1. Protein adsorption.

Both polycaprolactone and 8% pSi-PCL adsorbed protein from BSA solutions and FCS which was not removed by washing in $dH_2O$. In both cases however, the amount adsorbed onto composites was significantly higher than PCL ($p < 0.05$) as shown in **fig. 5.4.** Adsorption of protein from either source was not significantly different per material (PCL, $p = 0.11$; pSi-PCL, $p = 0.28$), demonstrating that all proteins are adsorbed similarly, and allowing for further comparisons to published studies.

Adsorption of alkaline phosphatase onto pSi-PCL was lower than expected, although the SA/V of the cylinders was lower than for the discs used in BSA and FCS studies.

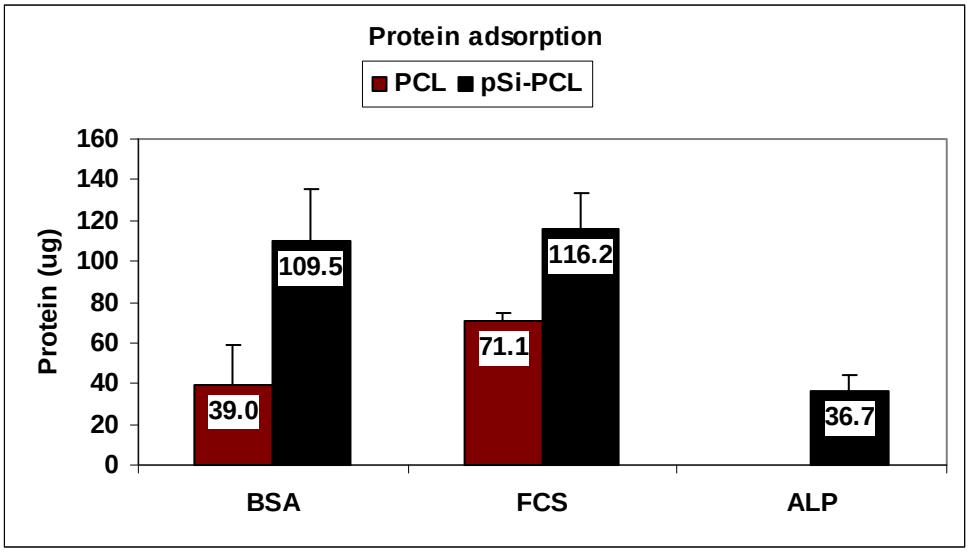


**Fig. 5.4.** Protein adsorption onto PCL and 8% pSi-PCL from solutions of BSA (40 µg.ml-1) and 1 x FCS after 72 hours. Protein adsorption is significantly higher on composites in both BSA ($p = 0.033$) and FCS ($p = 0.030$). Comparison was by Student's T-test (bars show standard error of the mean, n = 3).

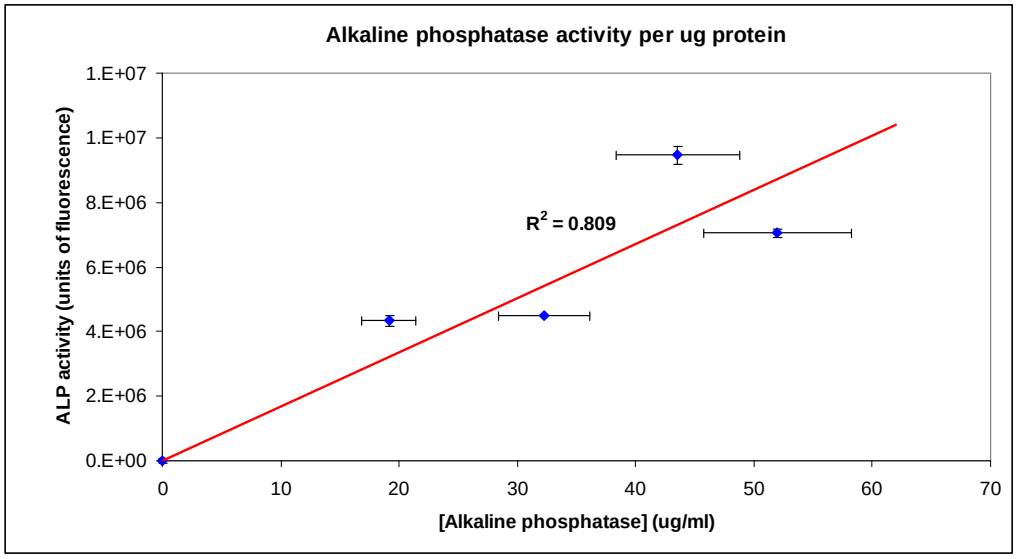


**Fig. 5.5.** Alkaline phosphatase activity per µg adsorbed protein. The relationship is linear (coefficient of determination, $R^2$ = 0.809) over the concentration range tested. Y-axis error bars are standard error of the mean (n = 5), X-axis error bars are standard error of the mean based on BSA concentration determination, 12% of value.

Alkaline phosphatase activity correlated with the mass of protein adsorbed onto the surface ($R^2$ = 0.809), indicating that the process of adsorption onto the silica gel does not denature the protein significantly (**fig. 5.5**).

### 5.3.1. Encapsulation.

Microscopy of the encapsulated discs showed no visible demarcation between layers and that the PCL layers were continuous with the central composite.

Silicic acid release for the unencapsulated disc was 125 – 180ng.ml$^{-1}$ per day, as predicted from previous studies. When encapsulated in PCL layers, silicic acid release is lower but does not decrease as further layers are added (**fig. 5.6**). Fluorescein release is proportional to the thickness of the PCL encapsulation layer with levels becoming undetectable when encapsulated in four layers of PCL (**fig. 5.7)**.

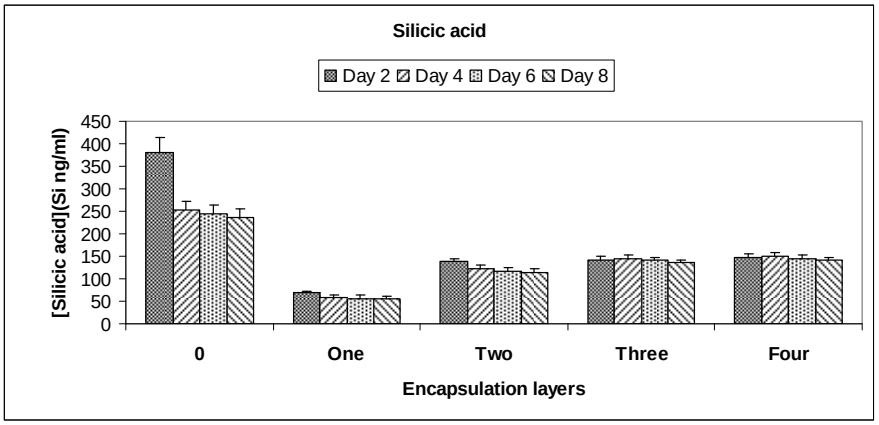


**Fig. 5.6.** Silicic acid release from pSi-PCL composites encapsulated in 1 – 4 layers of PCL (each layer 0.7 mm thick). Error bars are standard error of the mean, n=3

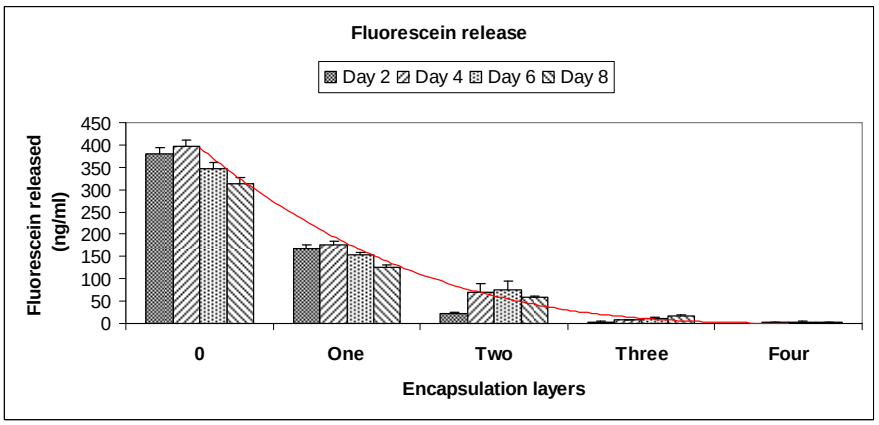


**Fig. 5.7.** Fluorescein release from pSi-PCL composites encapsulated in 1 – 4 layers of PCL (each layer xmm thick). Error bars are standard error of the mean, n=3

### 3.3. Dynamic perfusion.

The flow rate was measured throughout the 24 period and found to be 2.0 ± 0.1 $ml.min^{-1}$. Over 24 hours therefore, 2880 ± 288 ml SBF flowed across each disc with a volume of approximately 3ml covering the disc continuously. Silicic acid concentrations in the eluent were higher than expected based on data from previous 'static' studies with no fluid flow – at 4 hours silicic acid concentrations were 223 ± 0.8 $ng.ml^{-1}$ and slightly lower at 20 hours, 215 ± 0.6$ng.ml^{-1}$

After 24 hours and following drying, the masses of the discs had also changed more than expected – PCL discs had lost 0.56 ± 0.09mg (0.05% initial weight) and pSi-composites lost 1.2 ± 0.17mg (0.15%). The amount of silicon lost as silicic acid over 24 hours can be estimated from the silicic acid concentrations of the eluent at 4 and 20 hours, being 0.64 and 0.62 mg respectively. The average mass loss due to pSi dissolution (mean composite mass loss – mean PCL mass loss) was 0.63mg – approximately the same as can be accounted for by the silicic acid in solution.

Calcium deposition was found on both PCL and pSi-composite discs as determined by alizarin red staining, with markedly more calcium on discs containing pSi (17.5ug) than PCL-only discs (3.5ug).

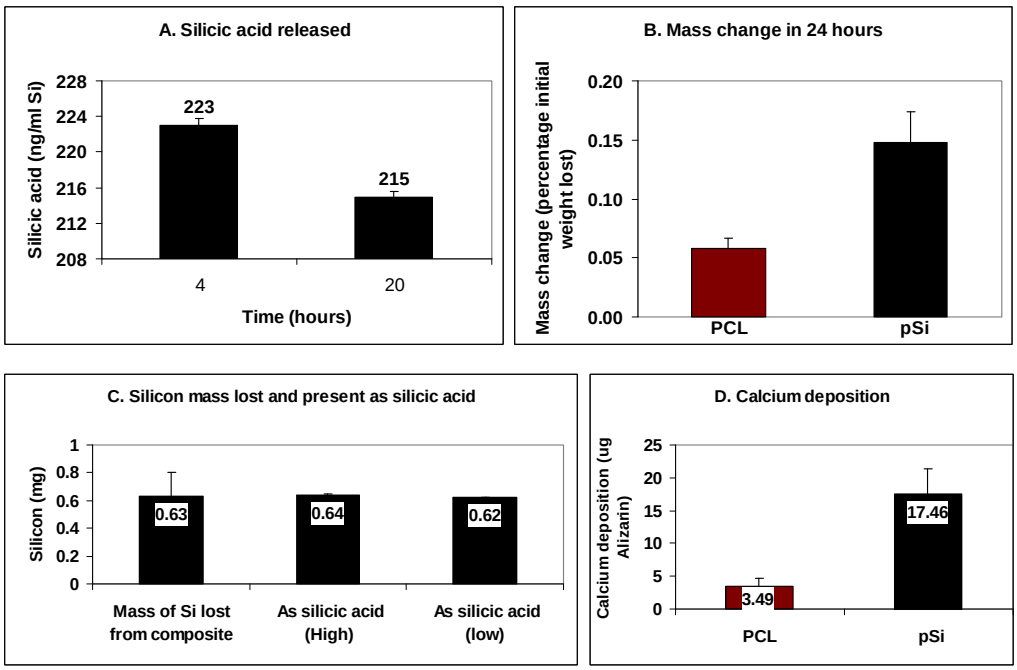


**Fig. 5.8.** Dissolution characteristics of PCL and 8% pSi-PCL in a continuously flowing volume. **A**. Shows the silicic acid concentration of the eluent collected following contact with the composite disc at 4 and 20 hours. **B** shows that after 24 hours and following drying, both PCL and composite discs lose mass, with a decrease in mass of approx. 0.11% due to silicon dissolution. **C** shows that the mass loss attributable to silicon dissolution is detected as silicic acid in the solution. **D** shows an increase in calcium deposition on composite discs over PCL.

### 5.3.3. Bone tissue simulation.

The bone tissue simulation model was partially successful in representing bone tissue. Determining the dispersion of silicic acid through the matrix showed that in a static environment (no fluid flow), silicic acid dispersed freely through agarose gels with an average pore diameter of 259nm as shown in **fig 5.9.** The concentration of silicic acid was found to be linear in regard to radius from the centre of the disc (coefficient of regression, $R^2 = 0.9129$) as shown in **fig. 5.10**.

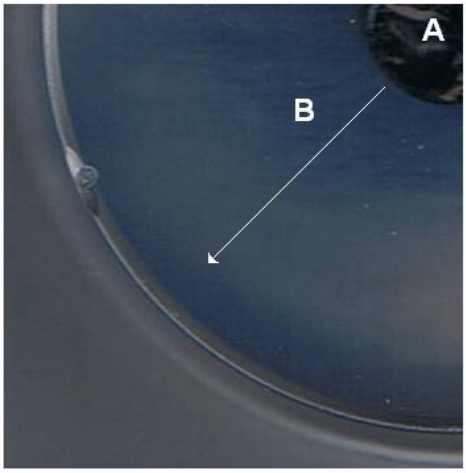


**Fig.5.9.** Dispersal of silicic acid through a static agarose gel with 259nm pores, stained with molybdenum blue reagent. Dissolution of the disc (**A**) in the hydrated gel is radial from the disc surface along vector, **B**.

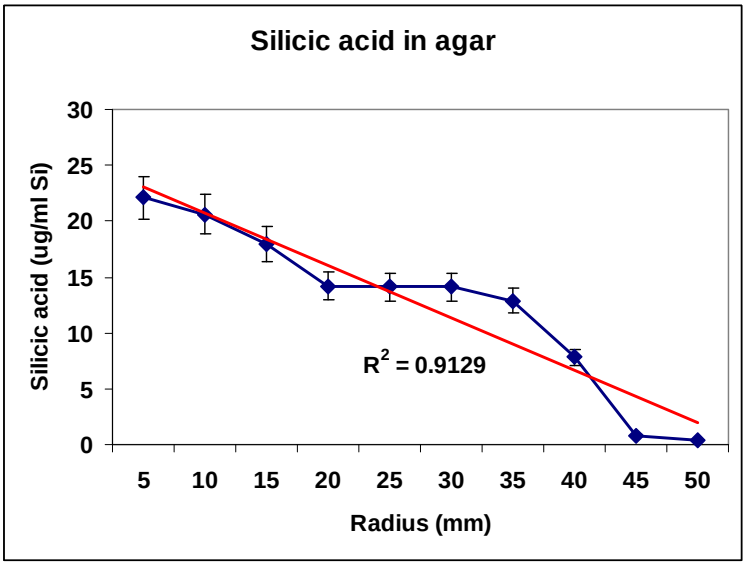


**Fig. 5.10.** Silicic acid concentration in the gel is inversely proportional to distance from the surface of the composite disc, measured in mm.

**5.4. Discussion.**

Adsorption of proteins onto the surface of Bioglass®-based biomaterials has been postulated as a key method by which they achieve bioactivity (Kaufmann *et al*, 2000; Rosengren *et al*, 2003). 8% pSi-PCL has been shown to significantly increase the amount of protein adsorbed from both concentrations of BSA at blood plasma concentrations (40 $mg.ml^{-1}$) and foetal calf serum over polycaprolactone-only controls. Further, the adsorption of alkaline phosphatase did not denature the protein's structure, allowing the complex homodimer to retain phosphatase activity when bound to the surface. The adsorption onto PCL-only materials is thought to be a result of surface energy or entrapment of the proteins in the surface layers of the polymer, and the washing process between incubation and testing demonstrated that the proteins were associated with the composite and strongly bound.

The behavior of pSi-PCL composites therefore is similar to the established data from Bioglass®-based composites, although it is again noted that statistically significant enhancement of bioactivity is achieved with a lower percentage inclusion of the bioactive phase (pSi vs. Bioglass®).

Encapsulation of the composite in PCL layers shows that both orthosilicic acid and small, water-soluble APIs can freely disperse from inside the composite and therefore degradation of the composite occurs throughout the material and not just at the surface. Release of silicic acid was lowest when encapsulated in one layer of PCL, which may be anomalous or possibly due to the way silicic acid releases and polymerises in this instance, as will be discussed. Release of fluorescein was proportional to the number of encapsulation layers.

As silicic acid is shown to elute freely through PCL, fluorescein was also expected to elute in a similar way. The differences between the release profiles for silicic acid and fluorescein may be attributed to the relative sizes and solubility of the molecules. A measure of solubility in water is the acid dissociation constant (pKa; Meissler, 1991), which for fluorescein is 6.4 (www.chemprep.com, 2009) orthosilicic acid 9.5 (Canham, 2007) and polysilicic acids >11.4 (Forgács &

Cserháti, 1997) which indicates that orthosilicic acid is less soluble than fluorescein, and suggests that solubility is not a key factor in the dissolution of molecules from within polycaprolactone-based materials.

The molecular weight of fluorescein (332.3 $g.mol^{-1}$) is considerably higher than that of orthosilicic acid (96 $g.mol^{-1}$), suggesting that molecule size is the limiting factor in impeding release from the composite. This is further supported by the finding that subsequent layers of PCL do not have a linear effect on the solution concentration of orthosilicic acid, as this small acid is freely able to diffuse through the layers, whilst larger polysilicic acids are less free to pass through the matrix and into solution.

As mentioned in the introduction to this chapter, many of the sites in which a bioresorbable device will be implanted exhibit characteristics including high flow rates for blood and interstitial fluid. This presents specific challenges to the design of the biomaterial, which must be able to tolerate the mechanical stresses of the site and potentially enhanced degradation rate and still maintain bioactive characteristics. For pSi-PCL composites, degradation rate is not expected to be problematic, as data in Chapter 2 demonstrated that pSi dissolution rate is largely independent of dissolution volume, and PCL in its native state is sufficiently resistant to hydrolytic attack to be stable over several times the projected time for which is will be required for mechanical reasons.

The challenge in this situation for pSi relates to the proposed theory of its potential for bioactivity, that is in establishing a silica gel / calcium phosphate layer on the surface of the material and surrounding tissues (Canham, 1995). In static situations, this is affected by the rapid dissolution rate of pSi coupled to the low flow rates at the surface of the material. As silicic acids rapidly condense into larger silicic acids and eventually precipitate out of solution, a gel is quickly formed. However, if the silicic acid solution is rapidly cleared from around the material, a silica gel may not form and so the associated bioactivity may be lost.

When compared to previous data obtained from discs incubated in a shaking water bath, it can be seen that the amount of silicic acid released from both

shaking and flowing systems are similar, 140 $ng.ml^{-1}$ for shaken solutions and 220 $ng.ml^{-1}$ when the solution is flowing. This experiment was designed to test the hypothesis using a continuously flowing solution of simulated body fluid and shows that even though the amount of silicon lost from the disc is high, calcium phosphate rapidly forms on the composite surface.

The amount of silicic acid detected in the eluent was far higher than had been expected. Comparable studies in static solutions suggested that a concentration of 1.4 – 2.0 μg per day would be generated by the discs tested, whereas a total of 630μg was recorded. This discrepancy shows that the actual amount of degradation undergone by pSi is far higher than previously estimated based on static studies, and that the polycondensation back into insoluble polymeric silica is similarly high.

Current theories of Bioglass® (and by extension, pSi) bioactivity rely on the formation of this silica gel to act as a nucleation bed for calcium deposition (Jones *et al*, 2007). Even though this flow-through experiment converted large quantities of silicon into soluble silicic acid and the polycondensation threshold was not reached (approx 100 $\mu g.ml^{-1}$; Canham 2007), formation of silica gel was implied by the increase in mass of the composite discs and the increase in calcium deposition. As a significantly greater quantity of calcium was deposited on the composite during this experiment, a silicic gel layer is assumed to have developed, acting as a nucleation bed for calcium phosphate.

The bone tissue simulation model using an agarose hydrogel was successful in demonstrating that diffusion of silicic acids occurs through hydrated porous structures. This is an important result, indicating that silicic acids are able to diffuse through bone tissue *in vivo*, even in a cortical setting with limited fluid flow and clearance of degradation products.

The methods developed here demonstrate that porous silicon-polycaprolactone biomaterials can be successfully evaluated using artificial approaches which simulate physiological conditions, and that the adsorbtion of proteins onto the surface of these materials are a key aspect of their bioactivity.

# Chapter Six

-

# Physical Properties of pSi-PCL Composites

## 6.1. Introduction.

The physical properties of most biomaterials are crucial to their useful function in an *in vivo* environment, from the essential low-friction surfaces of UHMW polyethylene acetabular cups to the supporting strength of a steel orthopaedic fixation pin or plate. Composite orthopaedic materials must also support biological tissues in a mechanical way even for non-load-bearing applications, and for polymer-based materials this can be a challenge due to the far lower strength of plastics in comparison to more traditional metal prostheses.

As an added complication, biodegradable materials must be designed to have sufficient mechanical strength to function during degradation and over a range of normal and excessive load conditions - reflecting the varying height, weight and lifestyle of patients - whilst normal tissue function is restored. For bone, this is typically considered to be 6-8 weeks (Ham & Harris, 1972) in normal circumstances during the formation of a natural callus, but for tissue engineering applications and treatment of bone non-union the timescale may exceed this nominal range.

Degrading composites therefore must be somewhat over-engineered and capable of bearing mechanical loads in excess of those that can be physiologically expected, and designed to maintain mechanical function beyond the formation of a callus whilst continuing to function as a reactive biomaterial, stimulating bone growth. As bone is a strong tissue with excellent mechanical properties, this is a complex challenge for material science and has to date limited the use of plastic orthopaedic devices to relatively non load-bearing regions such as cranial burr plugs, orbital floor supports and jaw fixation.

The application of porous silicon in this investigation also opens the possibilty of enabling a novel route for therapeutic electrical stimulation of bone, which has been suggested to aid the natural healing of this (Supronowicz *et al*, 2002) and other tissues (Zhao *et al*, 2006). The electrical and mechanical properties of pSi-PCL are therefore extremely relevant to this investigation and are reported in this section of the thesis.

### 6.1.1. Particle dispersal.

Composite materials derive strength from the combination of tensile strength from the polymer phase and hardness/compressive strength from the inclusion of microparticles, and so it is important for the material's properties that these two phases are correctly or homogenously dispersed (Supova, 2009). Natural composites such as bone are structurally highly regulated, and are arranged such that the tensile component, collagen, is aligned along stress lines and allow for mineral crystals to reinforce the matrix regularly throughout the matrix.

pSi-PCL composites are far less ordered structurally. It is proposed that due to the method on fabrication, PCL in the composite is non-crystalline and the amorphous phase is composed of polymer chains arranged randomly and without crosslinks. The inorganic phase, pSi, is large in comparison to the size of bone apatite crystals - 11μm for the pSi used in this investigation in comparison to 10nm x 0.3μm for bone apatite.

Because of these considerations, it is important that the pSi particles are both small in size and within a narrow range of sizes to maximise the distribution of pSi in the polymer phase and reduce the number of failure zones – large particles/aggregates which reduce the local mechanical properties and can act as points at which the material fails mechanically (Yaszemski *et al*, 2003).

### 6.1.2. Tensile strength

The mechanical properties of several common orthopaedic materials are shown in **table 6.1** in comparison to bone and cartilage. It is apparent that whilst metals and alloys are able to take large mechanical loads even when formed as small pins or plates, plastics have much lower tensile strength and are unsuitable for many load-bearing applications or act as failure points when employed, e.g. PMMA bone cement (Allgower & Perren, 1991).

| **Material** | **Ultimate tensile strength (Mpa)** | **Notes** |
|---|---|---|
| CoCr Steel | 735 | 28% Cr; 2% Ni; 7% Mo; |
| Stainless Steel | 600 | 18% Cr; 14% Ni; 2-4% Mo |
| Titanium alloy | 900 | Ti-6Al-4V |
| Cortical bone | 70 – 150 | |
| Trabecular bone[1] | ≤ 50 | |
| Mandible[a] | 96.2 ± 40.6 | Complete[2] |
| Mandible[b] | 56 ± 29.6 | Trabecular component[2] |
| Cartilage | 7 – 15 | |
| Bioglass® (45S5)[6] | 40-60 | Bulk |
| | 93.8 ± 8 | 193µm diamter fibres |
| | 82 ± 14 | 280µm diamter fibres |
| Monocrystalline Si[7] | 5-9,000 | |
| Hydroxyapatite[8] | 60-80 | Sintered at 800°C |
| PMMA | 35 - 50 | |
| Polyethylene | 23 - 40 | |
| PLA[6] | 10 – 70 | |
| PGA[6] | 55 - 58 | |
| Polycaprolactone | 5.17 – 29 [3] | Block/bulk |
| | 31.7 ± 4.0 [4] | Drawn fibre (150µm) |
| | 16.4 ± 3.9 [5] | Extruded (500µm) |
| PCL/HA (30% HA) | 14.2 ± 4.5 [5] | Extruded (500µm) |

**Table 6.1.** Tensile strength of some common orthopaedic materials, tissues and polymers/experimental composites. (from Ratner *et al*, 2004, and; [1]Hollinger *et al*, 2005; [2]Misch *et al*, 1999; [3]www.ides.com; [4]Williamson *et al*, 2002; [5]Kim, 2007; [6]De Deigo *et al*, 1999; [7]Howatson *et al*, 1991; [8]Ruys *et al*, 1995).

Polymers vary considerably in tensile strength, a property which is dependent on the composition of monomers, polymer molecular number/weight and the degree of anisotropy in fibre alignment. For bulk polymers, anisotropy is very limited but processing techniques can be employed to increase fibre alignment and tensile strength, such as fibre extrusion and electrospinning. Thomas *et al* (2004) showed increased tensile strength for polycaprolactone fibres electrospun onto a rotating collector to increase fibre anisotropy (**table 6.2**).

| Collector RPM | Average ultimate tensile strength (MPa) |
|---|---|
| 0 | 2.21 ± 0.23 |
| 300 | 4.21 ± 0.35 |
| 600 | 9.58 ± 0.71 |

**Table 6.2.** Increasing collecter RPM results in greater fibre anisotropy and causes an increase in tensile strength along the orientation of the fibres (from Thomas *et al*, 2004).

For the majority of biomedical applications, plastic and composite orthopaedic fixation materials are subject to tensile forces, particularly in screws and fixation plates. Larger orthopaedic devices such as hip or knee prostheses and long bone fixation plates are unsuitable for replacement by current polymer-based materials as the cyclic loads and high forces they must endure cannot be tolerated by polymers over the 10-20 year life of the implant (Granchi *et al*, 2006).

Polymer-based composites, therefore, are most usefully applicable as supports for tissue regrowth in maxillo-facial applications and as such the mechanical properties of the implant are of less concern, although should be sufficient to resist deformation under normal and occasional excessive loading forces. **Fig. 6.3.** shows a typical stress-strain curve for a polymer (or polymer-based composite), indicating the key aspects of response to strain by extension. The main indicators of resitance to deformation are elastic (Young's) modulus, the elastic limit and maximum load.

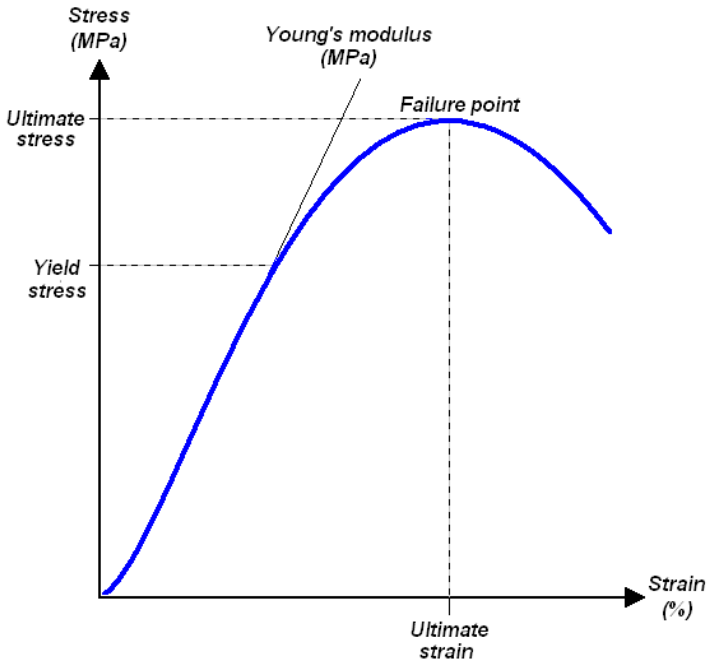


**Fig. 6.3.** Typical stress/strain curve for a polymer (or polymer-based composite) showing yield stress (point at which elastic deformation becomes plastic deformation), ultimate stress (the maximum stress the material can withstand), ultimate strain (the percentage strain at ultimate stress) and the Young's modulus (the linear component of the stress/strain coefficient below the yield point). Failure for polymers is typically by a process referred to as 'necking', in which the cross sectional area of the sample is reduced due to plastic flow of the material along the stress line (Considére, 1885).

The mechanical properties of currently described polymer-based biomaterials vary widely, depending on both the choice of polymer / non-polymer phase and the methods of fabrication and testing. Most commonly in the literature, biodegradable aliphatic polymers such as PLGA and less frequently PCL and PHB (polyhydroxybutyrate) are used as inert, degradable carriers for bioactive particles, such as HA microparticles or Bioglass® (Lee *et al*, 2008; Jukola *et al*, 2008; Papatheofanis, 1989).

Lee *et al* (2008) showed that the addition of 5% and 10% HA in the form of 100μm particles to PLGA increased the ultimate tensile strength from 1.89 (± 0.4) MPa to 3.4 (± 0.3) MPa and 3.9 (± 0.37) MPa respectively, whilst additions of HA

beyond this proved detrimental to yield strength, as 15% HA reduced ultimate yield strength to 1.77 ± 0.1 MPa.

Similarly, Papatheofanis (1989) showed an increase in the bone-bonding strength of isobutyl-2-cyanoacrylate (adhesive) from 8.33 (± 0.41) MPa to 12.03 (± 0.72) MPa upon the addition of 10% HA, decreasing to 7.89 (±0.58) MPa when 15% HA was added. This strengthening of a polymer fibre with an inorganic phase is similar to the enhanced tensile properties of minerilised against non-mineralised collagen fibrils (**fig. 1.12.B**).

Jukola *et al* (2008) demonstrated that by including Bioglass® fibres (diameter 31-43μm) to a 30:70 starch/PCL blend, the tensile strength can be increased from 16-18 MPa (without Bioglass®) to 26-29MPa with 10% *w/w* Bioglass®.

The mechanical properties of composites therefore can be made to exceed those of the components, although careful selection of particle size, shape and polymer anisotropy remain important considerations.

### 6.1.3. Electrical conductivity.

The tissues comprising a living organism naturally generate electrical fields as a product of chemical activity across membranes and through the transduction of mechanical forces. These electrical fields have been shown to play an important role in wound healing from the initial disruption of normal cellular interactions and leakage of tissue fluid electrolytes to the stimulating electro-mechanical forces which influence the extracellular matrix as the tissue returns to function (Zhao, 2008).

The mechanisms underlying this process are poorly understood but appear to be numerous, with several tissues reported to benefit from electrical stimulation during healing. Zhao (2008) indicates that the local electric fields vector towards an epithelial wound site, acting on epithelial cells via EGF receptors, integrins, V-ATPase proton pumps, and PI3 kinase/Pten (the 'cell compass' molecules which

determine polarity for chemotaxis) and stimulating migration to the wound site. Interestingly, it has recently been shown (Zhao *et al*, 2006) that electrical fields are capable of over-riding other directional cues for cell migration, including chemotactic gradients.

The electrical fields in wounds are caused by disruption of the transepithelial potential and vary in magnitude according to the site, being determined by the activity of the neighbouring cells in maintaining the surrounding potential. A corneal wound was observed by Chiang *et al* (1996) to generate 42 $mV.mm^{-1}$, whereas in guinea pig dermal wounds a steep, lateral voltage gradient falls from 140 $mV.mm^{-1}$ at the wound edge to 0 $mV.mm^{-1}$ just 3 mm laterally to the wound edge on the skin surface (Jaffe *et al*, 1984).

An additional factor is present in bone - as the tissue loads and unloads a pulsatile current is established through the tissue. This can be attributed to two sources: hydroxyapatite peizoelectricity, and more significantly the flow of electrons along hydrated collagen fibrils and through cannaliculi (streaming potentials). This mechanism has been proposed to be part of the mechanism by which Wolff's Law is effected in bone (Beck *et al*, 2002), and so has been a target for research into advanced treatments for bone repair. The electrical properties of bone have been shown to differ according to site and bone type, as demonstrated by the variation in skull plate morphology and resistivity in **table 6.4.** (Tang *et al*, 2008).

| **Skull morphology** | **Resistivity (Ω.m)** | |
|---|---|---|
| Standard trilayer | 79 | ± 17 |
| Quasi-trilayer | 144 | ± 30 |
| Standard compact | 265 | ± 53 |
| Quasi-compact | 198 | ± 32 |
| Dentate suture | 57 | ± 17 |
| Squamous suture | 127 | ± 41 |

**Table 6.4.** Tang *et al* (2008) show that electrical resistivity of skull fragments (flaps removed during surgery) varies according to bone structure.

*In vitro*, osteoblasts have been shown to respond favourably to alternating electric currents. Supronowicz *et al* (2002) showed a 46% increase in osteoblast proliferation after 2 days culture with 10 μA at 10Hz for 6 hours per day. A 307% increase in the concentration of extracellular calcium and upregulation of mRNA expression for collagen type-I was observed after 21 days.

Interestingly, similar enhancement effects in wound healing are shown for low-intensity pulsed ultrasound (LiPUS) such that the two techniques are often compared in the literature and used interchangably in clinical practices to treat non-unions. With a typical burst width of 200 microseconds, comprising a 1.5-MHz sinusoidal waveform with a repetition rate of 1 KHz and a spatial average temporal intensity of 30 $mW.cm^{-2}$ applied to bone non-unions for 20 minutes daily, LiPUS treatment has a similar profile to the application of alternating currents and is proposed to work via the same electromechanical route. Papthedourou *et al* (2009) show that using 1 MHz at a pulse repetition rate of 1 kHz and with 30 $mW.cm^{-2}$ for 20 min on rabbit tibial condyl, biglycan and collagen I mRNAs are significantly upregulated.

Artificial stimulation of bone to treat non-union by pulsatile electrical fields has been studied extensively, and is commonly performed at frequencies of 15 MHz (reviewed in Walker *et al*, 2007) and over long time periods, typically 12-16 hours per day for up to 4 months.

A literature review of clinical applications by Mollon *et al* (2008) shows that electrical stimulation has a positive benefit on quickening the onset of callus formation on but effects on treatment of non-unions do not show a significant benefit. Despite this lack of clinical evidence, numerous devices have been developed for employing electrical fields in wound repair, particularly for bone healing, with approximately 600 US patents covering this topic (February 2009).

Stimulation of osteogenesis by such devices has generally been performed by semi-invasive or transcutaneous methods, such as the direct current bone growth stimulator marketed by Zimmer of Warsaw (Indiana, USA) and licensed under US patent number 3842841. In this system, several needles are inserted through the

skin into a bone fracture, acting as cathodes. An anode pad is externally situated adjacent to the fracture and a direct current applied using an external power source.

Electrical stimulation of bone directly via conducting biomaterials is a promising way of exploiting the potential healing effect. As biomaterials act as support scaffolds for bone repair, they can be connected *in situ* to a current which can be applied directly or magnetically induced in a non-invasive way. However, as the majority of biodegradable polymeric and composite tissue engineering materials are non-conducting, research in this area has been limited. **Table 6.5.** provides a comparison of electrical resistivities for some common materials, showing the range of conductivity and that most orthopaedic biomaterials (bioactive glass, polymers, etc.) are electrically insulating.

| **Material** | **Resistivity (Ω.m)** |
|---|---|
| Gold[1] | $2.44 \times 10^{-8}$ |
| Iron[1] | $1.00 \times 10^{-7}$ |
| Bone (cortical)[3] | 876 |
| Polyurethane[4] | $10^{12}$ |
| Polyesters[4] | $>10^{18}$ |
| Silicon[1] | 640 |
| Glass[1,2] | $10^{10} – 10^{14}$ |
| $SiO^2$ (fused quartz)[1] | $7.5 \times 10^{17}$ |
| Carbon nanotube (single walled)[5] | $10^{-6}$ |
| Pyrrole co-polymers[6] | $10^4$ |

**Table 6.5.** Electrical resistivity (Ω.m) for a range of materials from good conductors (eg. Gold), to insulators (eg. Polyesters). From [1]Serway, 1998; [2]Griffiths, 1999; [3]Faes *et al*, 1999; [4]Warfield & Petree, 1961; [5]Frank *et al*, 1998; [6]Rivers *et al* (2002).

Silicon, however, is a semi-conductor with universal applications throughout electronics, and porous silicon has been evaluated by numerous groups

researching it's unusal electrical properties which diverge from bulk silicon (reviewed in Willoughby, 2006). Most carbon-based polymers are electrically insulating and so forming a composite from PCL with a porous silicon phase forms a material with unknown electrical properties. The potential therapeutic benefits of a conducting orthopaedic biomaterial in terms of generating a natural response from native bone cells are sufficient that research along these lines is worthy of pursuit.

### 6.1.4. Aims.

The aims of this part of the investigation therefore were to:

- Determine the dispersal pattern of pSi through the polymer phase of the composite.
- Measure the tensile strength of a range of composites.
- Determine the electrical resistance of a range of composites and determine if the addition of pSi enhances the conductance of the material.

## 6.2. Materials and Methods.

### 6.2.1. Particle Dispersal.

To determine the dispersal of pSi microparticles within the polymer matrix, pSi was loaded with 50% *w/w* fluorescein (in 50:50 water/ethanol) prior to incorporation into the polycaprolactone-based composite as described in chapter 4 to create final concentrations of 0.2% and 12% *w/w* pSi in PCL. Fluorescein-loaded microparticles and fluorescein powder were added to 2.5g PCL in solution with acetone (2.5ml acetone, 2.5g PCL) with either 5mg (0.2% *w/w*) or 150mg (12%) pSi in composites. 5mg fluorescein was also added to 2.5g PCL without pSi as a control.

The composite was formed into a 50 x 10mm cylinder and sectioned into five 10 x 10mm discs to enable both the size and dispersal pattern of the particles to be observed, and determine that dispersal is equal throughout the cylinder and that particles do not settle during casting. The discs were imaged using confocal laser scanning microscopy.

Images were processed using Volocity software (Improvision, Coventry, UK) to determine particle dispersion over a 5 -100% intensity threshold for background fluorescence, filtered using a 3 x 3 (x3) kernel filter (excluding objects smaller than 3 voxels) and expressed as volume ($\mu m^3$).

### 6.2.2. Tensile Strength.

Tensile strength of the composite was tested using either a) an I-shaped melt-cast specimen produced from a custom-made mould or b) a cylindrical specimen cast in a 1ml polypropylene syringe body (**fig. 6.6**).

Polycaprolactone-only casts were tested against 10mg (per 250mg PCL; 4%) and 20mg (8%) pSi-PCL composites (70% pSi, standard grade). Composites were produced by mixing pSi particles with melted PCL without solvent to avoid weakening the material and evolving solvent gases during casting. The composite

was milled and cast in either mould at 120°C by adding small quantities of solid to the melted surface to minimise the occurance of air bubbles and voids in the finished cast.

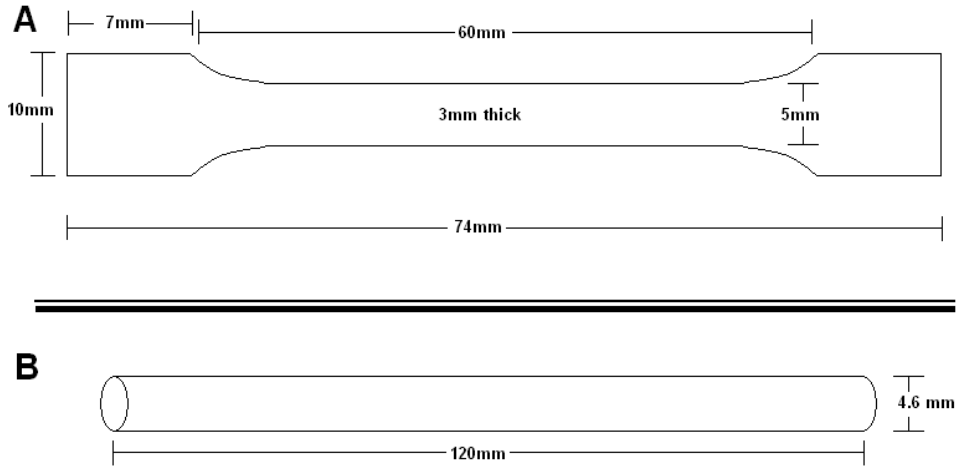


**Fig. 6.6.** Two specimen types were developed for testing mechanical properties: **A**. An I-shaped melt-cast specimen produced from a custom-made mould. **B**. A cylindrical specimen cast in a 1 ml polypropylene syringe body.

The cast samples were fitted into a 50 KN load cell in an Instron 5569 Tensile Testing System to test a 20mm region of the sample. Samples were fitted into grips which were moved apart at 2.0 $mm.min^{-1}$ until fail. Maximum load and tensile stress at maximum load were measured.

Elastic modulus was calculated from the stress-strain curve using the formula

$$E = \frac{F \cdot L_0}{A_0 \cdot \Delta L}$$

Where E is elastic modulus; F is Force (N); $L_0$ is sample length (m, at $T_0$); $A_0$ is cross sectional area ($m^2$, at $T_0$) and $\Delta L$ is the change in sample length (m)

### 6.2.3. Electrical resistance.

5ml of a 5% agarose gel were made by adding 250mg agarose (sigma, UK) to 5ml $dH_2O$ in a 50ml polyproplylene centrifuge tube. pSi was added in percentage quantities of 2, 4, 6, and 8% by weight (50mg = 1%) and the the vessels heated in a microwave until the agar had dissolved. Screw caps were replaced to minimise evaporative distortion of mass but not screwed tight.

After cooling for 20 minutes, the solution/suspensions were heated again and allowed to cool before being drawn into a 1ml polypropylene syringe. The syringes were layed horizontally and allowed to set at room temperature. The ends of the syringe were removed to leave the graduated section filled with the hydrogel, with the hydrogel dimensions being 4.6 mm (diameter) x 60.2 mm (length).

Electrodes of a handheld multimeter (Extech DM110) were inserted into each end to a uniform 5mm depth (marked on the electrode tip) and the resistance of the hydrogel measured over 50 seconds, with readings taken from the multimeter every 10 seconds to provide an average value.

Resistivity ($\varrho$) was calculated by the formula:

$$\varrho = \frac{R \times A}{l}$$

Where R is resitance (Ω), A is cross-sectional area ($m^2$) and $l$ is length (m). Polycaprolactone-pSi composites were tested for electrical conductivity in several ways, by fabricating thin sections and up to 20% *w/w* pSi-PCL composites. pSi-PCL composite cylinders measuring 4.6mm (diameter) x 60mm (length) in this [pSi] range were soaked in $dH_2O$ for 5 days and the resistance measured across the length of the cylinder.

Resistance of polycaprolactone was measured but was found to exceed the range of the multimeter.

## 6.3. Results

### 6.3.1. Particle dispersal.

pSi particles at the surface of 1mg composites were evenly distributed with a particle size of 5-20μm, particle aggregates were present but not of a large size (**fig. 6.7**). 20mg composites displayed a similarly well dispersed pattern, aggregates were present but appeared uniformly distributed between the top and bottom of the fabricated cylinder.

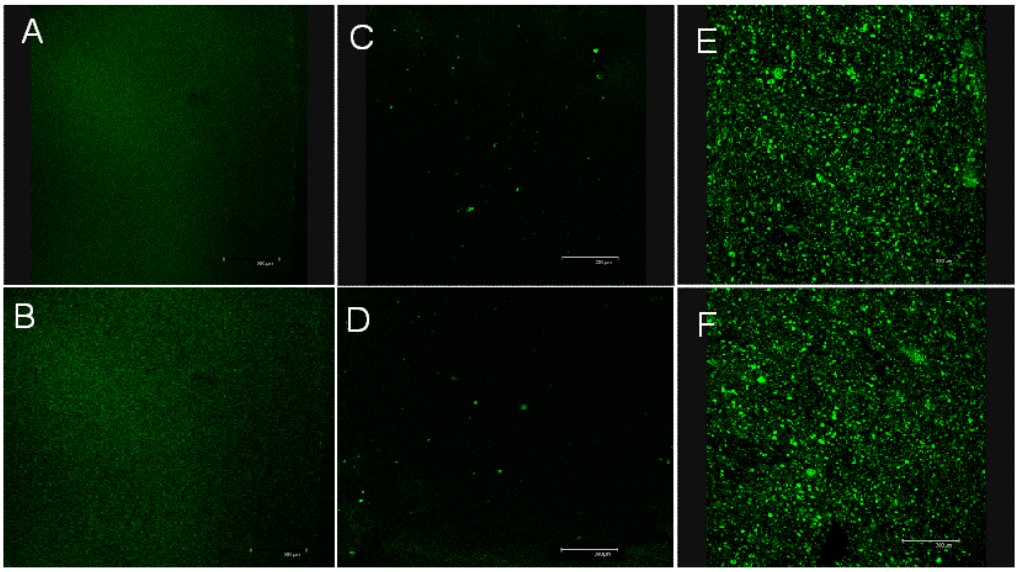


**Fig. 6.7.** Confocal micrographs showing the dispersal pattern of fluorescein in a polycaprolactone-pSi composite. A and B show discs created by adding fluorescein directly to PCL in acetone (A and B, respectively the top and bottom of cylinder). C and D are discs created by adding a low concentration of fluorescein-loaded pSi (0.2% *w*/*w*) to the matrix (C = top of cylinder, D = bottom of cylinder). E and F show discs with high concentrations of pSi (12% *w*/*w*; E = top of cylinder, F = bottom of cylinder). Scale bar is 300μm.

Adding fluorescein directly to PCL in solution in acetone results in a uniform distribution of the dye. Importantly for drug delivery applications, fluorescein was associated with the microparticles and did not leak out of the particles to the

surrounding polymer during manufacture or storage, even when exposed to humidity in the air on the cut surfaces.

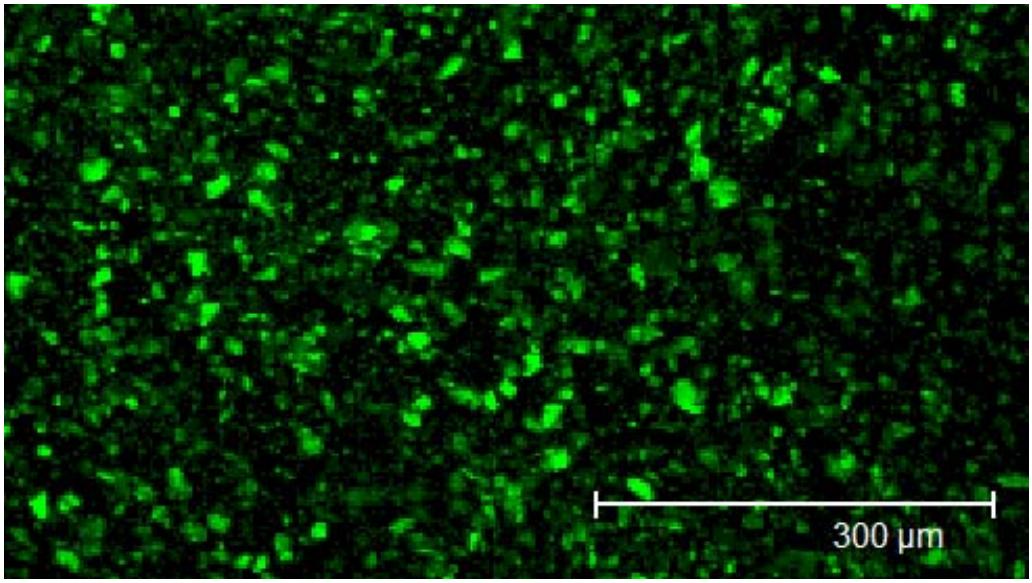


**Fig. 6.8.** Magnification of **fig. 6.5.E** showing particle dispersal of 12% composites.

The volume occupied by pSi was difficult to precisely determine due to the conjunction of pSi in the polymer. As the particles were closely packed a 5% filter was applied to the analysis to eliminate the lower values of fluorescence and enabe the particles to be evaluated. Using this approach, the volume occupied by pSi was established (**fig. 6.9**).

Whilst the distribution of particles appears to be homogenous using microscopy, detailed finite element analysis reveals that the concentration of pSi in the top and bottom of cylinders differs, with significantly fewer particles at the base of cylinders (B columns in **fig. 6.9**).

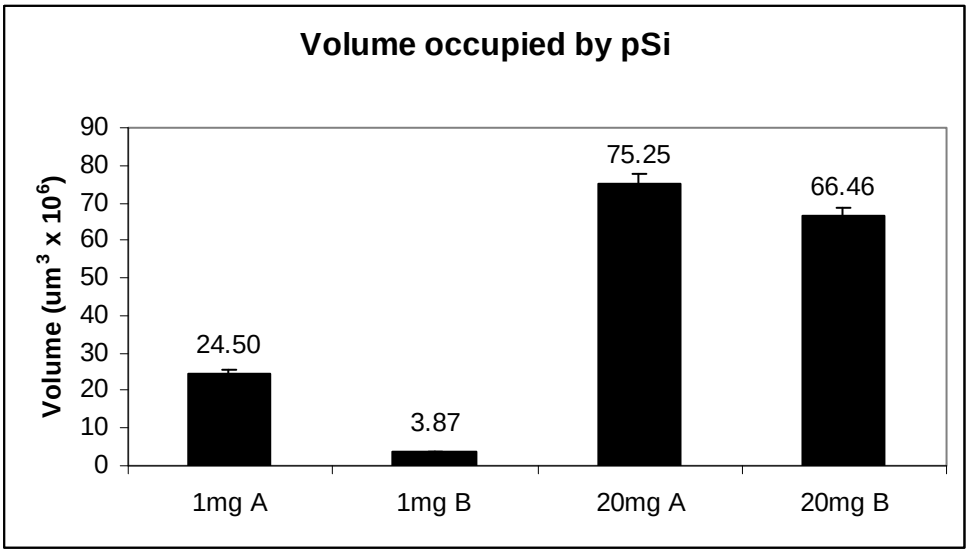


**Fig. 6.9.** Volume of pSi in composite, error bars are standard error of the mean.

### 6.3.2. Tensile strength.

The custom designed mould A produced materials with poor physical properties, having a visible cross-sectional casting meniscus which necessitated sanding to remove and numerous small voids throughout the tested region causing premature failure at low loads. Consequently all tensile data was obtained from cylindrical moulds, B, which had very few voids and were cross-sectionally uniform throughout the tested length.

**Fig 6.10** shows the stress-strain curve of an 8% composite, annotated to show the main features of the curve, including the linear phase and failure mode. All tested specimens had similar profiles as illustrated in **fig. 6.11**. The elastic modulus was calculated for the linear portion of the curve in each case. The ultimate tensile strength is the maximum strength of the material in MPa, the maximum load is the maximum force in N withstood (**fig. 6.12**).

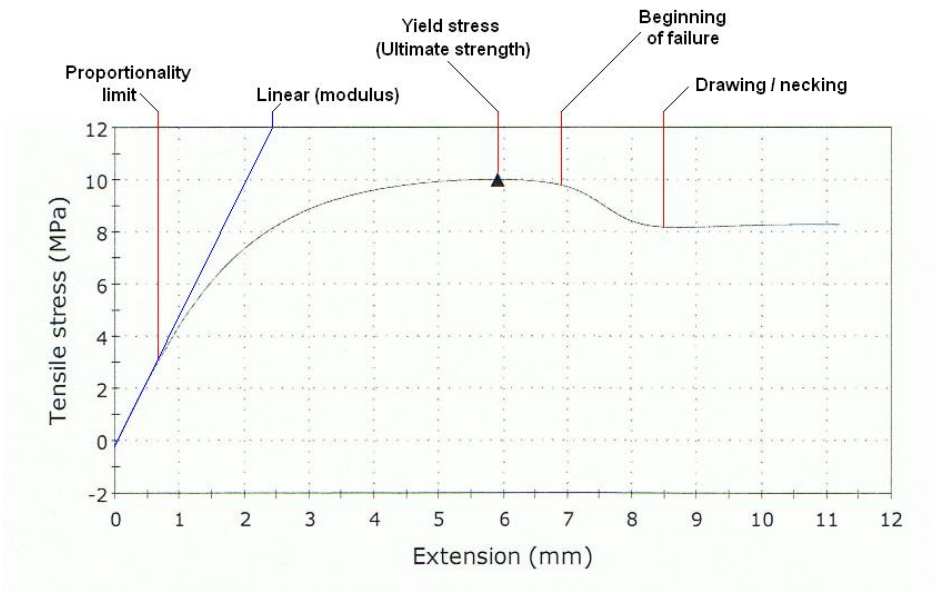


**Fig. 6.10.** Typical stress-strain curve of composite (8% pSi) showing the locations on the curve of the proportionality limit beyond which stress/strain is non-linear and below which Young's modulus is calculated; the ultimate (or yield) stress, and the beginning and mode of failure.

Failure of the samples was adjascent to the grips and was by plastic deformation, known as 'necking', as the cylinder stretched into a region with lower cross-sectional area - **fig. 6.14.** shows specimens following failure by this route. Samples which snapped or failed at a void were not included in the data set (3 out of 15 samples, total) shown in **fig. 6.15**.

Maximum load and yield strength for 10mg composites was not significantly different to PCL, although the mean values decreased slightly with increasing pSi content. The gradient of the linear phase (y/x) of the stress-strain curve was greater for composites and this is reflected in the calculated elastic modulus of the specimens. The elastic modulus (E) was highest for 8% composites (89.87 ± 5.75 MPa), followed by 4% composites (79.62 ± 7.94 MPa) – both significantly higher than PCL-only (43.36 ± 5.47 MPa), with p = 0.011 (4%) and 0.0011 (8%).

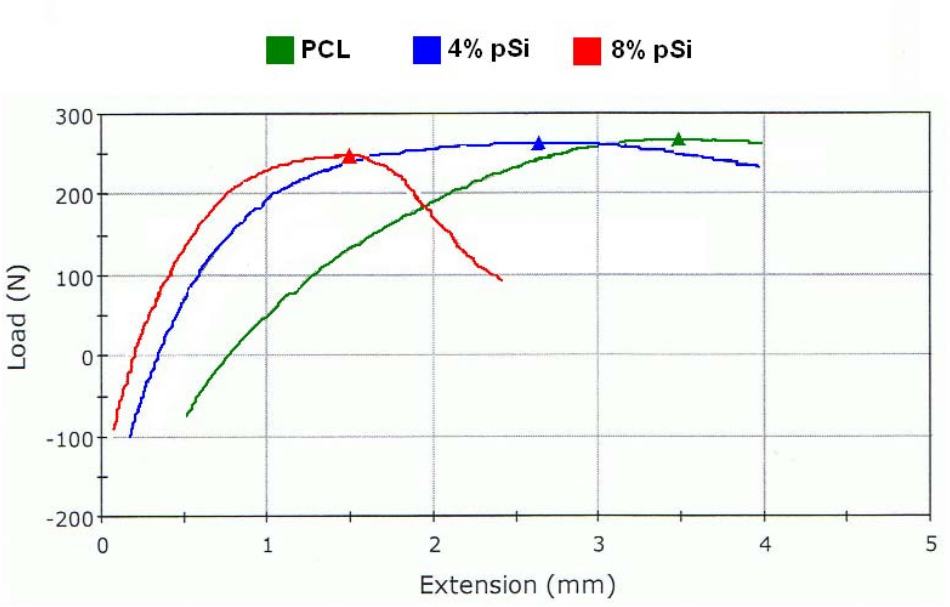


**Fig. 6.11.** Example stress-strain curves for PCL, 4% and 8% pSi-PCL composites. Curves are offset to allow comparison.

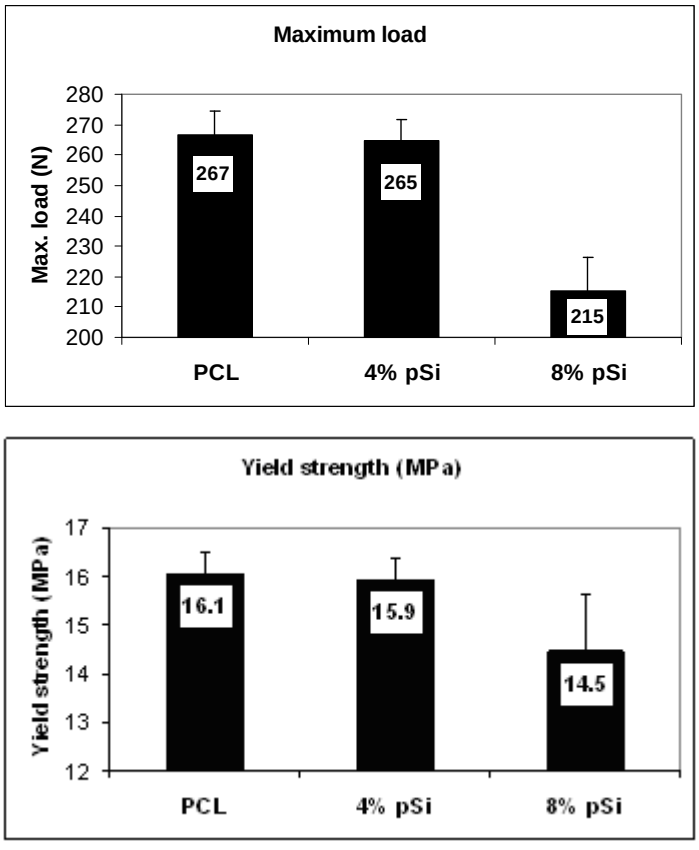


**Fig. 6.12.** Tensile strength of PCL and PCL-pSi composites (4% and 8% pSi). A shows maximum load at fail (ultimate strength). B shows yield strength (stress at which material strain changes from elastic to plastic deformation, causing permanent deformation). Error bars are standard error of the mean, n=4.

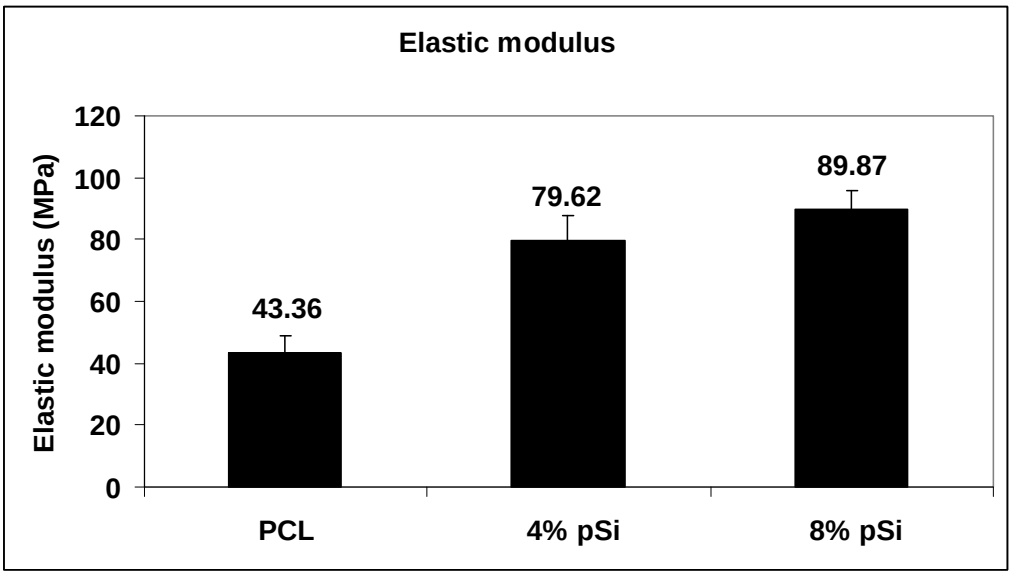


**Fig. 6.13.** Elastic modulus of PCL, 4% and 8% pSi-PCL calculated from the gradient of the stress-strain curve below the elastic limit. Error bars are standard error of the mean, n = 4.

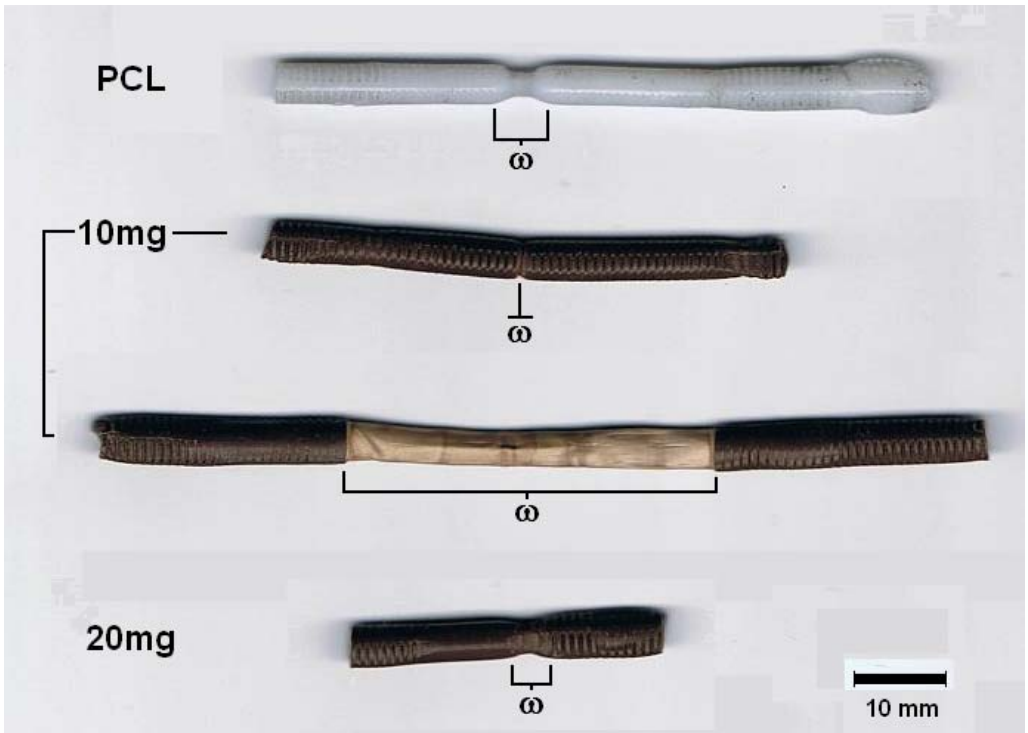


**Fig. 6.14.** Failure mode of tensile testing specimens was by 'necking', plastic deformation as polymer strands are drawn along the stress line. The failure region is indicated, **ω**.

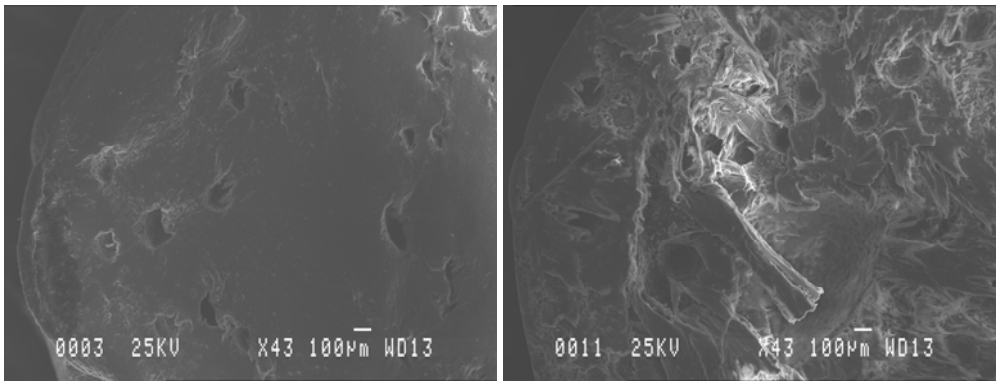


**Fig. 6.15.** Sections through the test samples (8% pSi-PCL) show that some air bubbles still exist (A) which act as starting points for mechanical failure. Image B shows the failure region of a sample which snapped in the load cell (and was therefore not counted in the results) showing regions of polymer fibre stretching around a large number of voids.

### 6.3.3. Electrical resistance.

The electrical resistance of 5% agarose hydrogels was found to be 1.246 ± 0.81 MΩ without porous silicon. The addition of 2% *w/w* pSi to the hydrogel lowered the resistance by an order of magnitude to 172 ± 2.9 KΩ. Increasing the concentration of pSi from 2 – 8% in the hydrogel lowered the resistance of the material in a linear way (coefficient of linear regression, $R^2 = 0.9611$, n=5) up to 8%.

The process used to make the discs, coupled with the reactivity of pSi in warm aqueous phases generate bubbles in the hydrogel which had to be dispersed by triteration as the gel cooled and prevented the testing of higher concentrations of pSi.

| pSi (%) | Resistivity (KΩ.m) |
|---|---|
| 0 | 34.53 ± 2.25 |
| 2 | 4.76 ± 0.08 |
| 4 | 4.19 ± 0.03 |
| 6 | 2.55 ± 0.40 |
| 8 | 0.86 ± 0.69 |

**Fig. 6.16.** Resistivity of the hydrogel decreases in direct proportion to the percentage of pSi in the gel, from 2-8%, coefficient of linear regression ($R^2$) = 0.9611.

Polycaprolactone-pSi composites were tested under various conditions for electrical conductivity, including very small/thin sections of 20% pSi-PCL but the resistance was higher than could be measured (> 40 MΩ). Degraded or soaked composites with water in the polymer matrix were also tested, but also had resistance greater than the testable range.

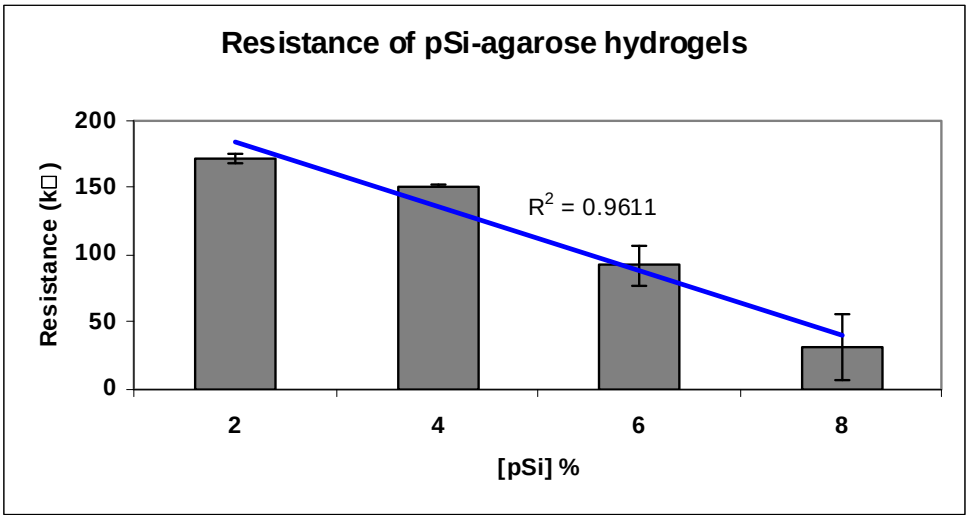


**Fig. 6.17.** Resistance of pSi-agarose hydrogels was inversely proportional to the concentration of pSi, and was linear in the range tested (coefficient of regression, $R^2$ = 0.9611). Error bars are standard error of the mean, n = 5.

**6.4. Discussion.**

Determination of particle size and distribution can be a challenge for many composite materials, with techniques such as X-ray diffraction being employed (Cui *et al*, 2007), or simply by allowing automated admixing to occur for several hours prior to casting, such that homogeneity is inferred (Lee *et al*, 2008). Usefully, pSi microparticles can be loaded with fluorescent dyes to allow them to be microscopically visualised, enabling the size range and dispersal of the particles to be determined.

It has been shown that the method developed here for forming pSi-PCL composites is able to create homogenously dispersed materials with reasonably anisotropic distribution of the particles throughout the polymer phase. Further, the particles are not aggregated and the size range observed is within the parameters of the particles that were used. This result is a fundamental justification of the results obtained in this investigation, particularly in the sections regarding electrical and mechanical properties which depend on composite composition.

Due to the number of techniques for determining biomaterial mechanical properties, no standard method is available. This is also reflected in the widespread use of the term 'tensile strength' which is commonly cited in the literature without clarification. Tensile strength may refer to elastic/yield strength, ultimate strength or breaking/fracture strength (all quoted in MPa) all of which may be used to determine the material's properties but which refer to specific points on the the stress/strain curve.

It is important to understand at this point the application to which biomaterials are put, and therefore determine which definition is most descriptive in reflecting the biomaterial's properties and suitability for internal use. For fixation applications, ultimate strength may be considered critical, particularly for orthopaedic screws which must secure fixation plates. Alternatively, fracture strength (resistance to breakage) may be used, although for ductile materials and cold-worked steel fracture toughness is implied by the design. Finally, yield

strength – the stress at which the material's elastic limit is reached and plastic deformation occurs is a useful way of measuring tissue engineering scaffold usefulness, as these materials are chiefly implanted to restore 3-dimensional structures to a normal physiological size and shape.

In this investigation, the yield strength is reported. This aspect of the polymer/composite was considered to be useful in describing the mechanical properties of pSi/PCL as it reflects the point at which each composition permanently deforms. The failure mode was found in practice to be through polymer dislocation, or 'necking' (Kinloch & Young, 1995) as the failure region was drawn into a fibre with smaller diameter; test samples which failed by fracturing at a void are not included in the results and amounted to 3 out of 15 cylinders tested. Voids may have been decreased by use of vacuum in the preparation of composites as is now commonly used for the preparation of poly(methyl methacrylate) bone cements for prosthesis fixation (Lidgren *et al*, 1984).

It is seen from the results that increasing the concentration of pSi to 4% in the composite does not adversely affect the tensile strength, but at 8% a small decrease in yield strength is observed. Decrease in tensile properties of the material are proportional to the decrease in continuity of the polymer phase, and so increasing the particle : polymer ratio decreases the tensile strength proportionally. This effect is not observed to be linear, however, due to the complex interaction of both phases and the elastic accommodation of stress forces - in accordance with the Poisson effect which describes the way in which molecules interact under stress (Lakes, 2008).

pSi-PCL composites are significantly more resistant to deformation than PCL as shown by the relative gradient of the stress-strain curves in and reflected in the higher elastic modulus of composites. This is important in resisting deformation to sudden or prolonged loading, particularly in restoring shape in reconstructive surgery, a major application for which these composites are being developed.

It is therefore determined that the addition of up to 8% pSi to PCL does not adversely affect the tensile properties of the composite and increases the resistance to deformation. The 8% composites have been shown to elute silicic acids, form a surface calcium layer and stimulate osteoblastic activity in cultured cells. The abilty for the composite to achieve this is at a considerably lower level of particle inclusion than other materials in the literature, such as Bioglass® - 30% Chouzori and Xanthos (2007) to 50% Venugopal *et al* (2008) - allows the composite to combine enhanced bioactivity with greater physical strength.

Addition of pSi to 5% agarose gels lowers the material's overall electrical resistance by a significant amount but the conductance of the pSi-PCL composites are still too low for useful medical applications.

Alternative polymers to PCL may be considered for the composite, however, and several groups have achieved success in creating electrically conducting, biodegradable polymers for biomedical applications. Rivers *et al* (2002) fabricated a biodegradable copolymer based on pyrrole – thiophene monomers linked by hydrolysable ester bonds. Enhancing the bioactivity of such polymers could be achieved by the addition of porous silicon to form a composite. When considered alongside the additional benefits of drug-delivery and mechanical strengthening, pSi-composites with an already conductive polymer are an attractive proposition.

# Chapter Seven

# -

# General Discussion

The aims of this thesis were to assess the suitability of porous silicon – polycaprolactone composites for orthopaedic tissue engineering applications. Porous silicon was suggested as a potential biomaterial by its known similarity to bioactive glass, dissolving in simulated body fluids to release bioavailable soluble silicate species and spontaneously forming a calcium phosphate layer on the surface of nano-porous silicon wafers.

Since the discovery of silicon's essentiality to bone biology by Carlisle (1974) and the role that silica and soluble silicates play in the orthopaedic bioactivity of Bioglass® (Hench, 2006), research has focussed on the chemistry and biology of silicon in calcified tissues. This research has demonstrated that silicon has at least two separate effects on bone biology in nature: interacting with glycosaminoglycans and the GAG component of proteoglycans, and substituting for phosphorus and carbon in the crystal lattice structure of bone mineral.

In addition, the dissolution products of bioactive glass which include soluble silicic acids have an effect on the molecular biology of osteoblasts *in vitro*, significantly up- or down-regulating the expression of several genes including key osteoblastic markers (Xynos *et al*, 2001). Localisation of silicon in the body has been identified to the growing areas of bone by electron microprobe analysis (Carlisle, 1972) and imaging ion microscopy (Landis *et al*, 1986). Furthermore, several studies have detected silicon within osteoblasts (Carlisle, 1975 & 1976), possibly in mitochondria and in other intracellular organelles.

There is substantial evidence therefore that the release of silicic acid from Bioglass®-based biomaterials forms the basis of their bioactivity. Porous silicon – which dissolves in water to form silicic acid as its only degradation product – is therefore a good candidate for biomaterials applications that require bone-bonding and enhancement of osteoblastic activity. Like Bioglass®, porosified silicon has poor mechanical properties, particularly in comparison to bone and to existing orthopaedic implant materials such as stainless steel and titanium; this is even more apparent as the material dissolves.

To create a usable biomaterial therefore, porous silicon was formed into a composite with polycaprolactone (PCL), a polymer with existing uses in biomaterials and surgery, and which degrades over a period of 1 – 2 years *in vivo* through hydrolysis of its monomers. This approach has previously been used to form bioactive glass – polycaprolactone composites by Chouzori & Xanthos (2007) and Jiang *et al* (2006). Crucially, these bioactive glass – polymer composites contain a relatively high proportion of Bioglass®, e.g. 30% - 50% by weight (Chouzori & Xanthos, 2007; Venugopal *et al*, 2008) and 40% in polylactide (Blakker *et al*, 2003).

This high level of inclusion generates some bioactivity, although Chouzori & Xanthos (2007) indicate that the bioactivity is less than might be expected. Also, since the polymer phase functions in the composite to lend mechanical (particularly tensile) strength to the material, reducing the proportion of polymer lowers the mechanical strength of the material.

In chapter two, it was shown that porous silicon can generate high levels of silicic acid in solution from relatively much smaller amounts of pSi, with composites containing 8% porous silicon in PCL releasing more than twice as much orthosilicic acid into solution than 8% bioactive glass-PCL composites. This ability to generate silicic acids from much smaller amounts of the bioactive component is a key advantage of pSi over Bioglass®.

Research in porous silicon is ongoing in several disciplines, with substantial progress being made in the opto-electronic applications of the material (Canham, 1997). For biological applications, the required properties were essentially unknown, and so the effect of silicon porosity and the size of particles in the composite was investigated.

At pSiMedica, several porosities of pSi were created, hand-milled and sieved for evaluation in composites, from 49% porous to 82% porous with 38 – 150μm size range. These particles were used for initial trials, but it was decided that greater uniformity and a smaller size range was required and so in subsequent experiments a standardised 70% porous silicon was used with 11μm particles in a

narrow size range. This was also found to have the most beneficial effect on osteoblasts *in vitro*.

Once the most appropriate porosity and particle size had been determined, the biodegradable polymer phase was considered. Polycaprolactone was chosen as the polymer phase for the reasons outlined in the introduction to chapter one, chiefly that the polymer has a slower degradation time than polylactides and polyglycolides. For many applications, degradation in excess of two years may be excessive, but co-polymerisation with more rapidly degrading polymers such as PLA or PGA can reduce this to a tailored timescale.

It was found that the release of silicic acids from polycaprolactone, poly(D,L lactide-*co*-glycolide) and poly(3-hydroxybutyrate-*co*-hydroxyvalerate) was similar but not identical, attributed to the differences in surface chemistry, of the polymers. The degradation rate of PLGA was also significantly increased by the addition of pSi to the material, causing full degradation of two out of three samples tested within 8 weeks, compared to > 12 weeks for PLGA alone.

Biodegradable polymers such as polycaprolactone are currently used in clinical applications, such as in resorbable screws, but concerns over the acidic degradation products and their affect on surrounding bone necrosis and resorbtion have limited their use in practice. Acidosis inhibits bone formation and stimulates osteoclastic resorbtion of bone (Frick and Bushinsky, 2003), and so limiting the acidification of orthopaedic wounds is important in designing degradable implants. As a material designed to elute orthosilicic acid, this was a concern from the beginning of the investigation.

Whilst composites of PCL, PHBV and PLGA with pSi lowered the pH of incubating solutions, the composites were shown to stabilise the solutions over time, with volumes incubating composites increasing in pH after 8 weeks rather than decreasing. This is thought to be due to the polycondensation of silica which eliminates silicic acid from solution.

Porous silicon composites with polycaprolactone were shown to be effectively fully permeable to water, allowing the degradation of porous silicon and the release of silicic acids from throughout the polymer, as determined by the linear relationship of solution Si concentrations to the size of the composite.

As the composite degrades, porous silicon dissolves to initially form orthosilicic acid. Orthosilicic acid is stable up to concentrations of ~ 2 x $10^{-3}$ M (Iler, 1979), approximately 56 $\mu g.ml^{-1}$ [Si], at which concentration it polycondenses into increasingly higher weight polysilicic acids which have correspondingly lower solubility. Silicic acid octomers are effectively insoluble in water (Iler, 1979) and condense to form a silicate gel layer on the surface of the material.

In this investigation, the silicate gel layer was quantified by the mass gain caused by the deposition of this silica gel and found to be directly proportional to the pSi content of the disc. Scanning electron microscopy cross sections through the silica layer show it to have a pronounced internal architecture, with perpendicular striations between solid outer layers and indicating that silica chemistry continues following deposition.

Several researchers (e.g. Hench, 2006) have suggested that the silica gel layer formed on the surface of bioactive glass-based materials acts as a nucleation bed for calcium phosphate, which is shown to spontaneously precipitate out of acellular simulated body fluids (SBFs). Porosified silicon wafers are also shown to spontaneously nucleate calcium phosphate from SBF on the surface of the wafer (Canham *et al*, 1996). The question of calcium phosphate nucleation on pSi-PCL composites was addressed.

Calcium phosphate was detected on composites incubated in acellular simulated body fluid and found to be proportional to pSi content of the disc. Scanning electron microscopy operating in 'wet' environmental mode (samples not coated), showed the calcium phosphate has the characteristic morphology of biological apatite, with a Ca:P ratio of ~1.5. The Ca:P ratio was proportional to the pSi in the disc, with increasing pSi in the disc resulting in a lower proportion of phosphate in the crystal. Due to the higher amount of silicates in the system here,

it is proposed that the apatite in these cases is silicate substituted (for some phosphate and carbonate).

In chapter three, the response of human osteoblasts to porous silicon was evaluated by culturing the cells *in vitro* on porous silicon – polycaprolactone composites. Separately, the effect on osteoblasts of pSi-PCL degradation products and orthosilicic acid in the growth media was tested.

As has been discussed, the physiological requirement for silicon and the bone-bonding effects of Bioglass® are attributed to both stabilisation of the collagen and glycosaminoglycan components of the extracellular matrix and silicate substitution for phosphate and carbonate in the calcium phosphate crystalline structure in matrix mineralisation.

The first stage in this investigation was to determine the response of osteoblasts to a range of porous silicon – polycaprolactone compositions and to observe the effect of pSi-porosity/degradation rate on cells *in vitro*. The results of this analysis show that 54% and 66% porous silicon microparticles do not appear to significantly enhance the proliferation or osteoblastic phenotype; whereas 82% microparticles degrade so rapidly the resulting accumulation of degradation products and effervescent hydrogen evolution is effectively toxic to cells.

70% porous silicon particles in a smaller particle size range (11μm rather than 38 – 150μm) proved to be more compatible with osteoblasts, stimulating the progression of the osteoblast from de-differentiated and dividing preosteoblast-like cells to mature secretory cells. Osteoblasts cultured on the surface of 8% *w/w* pSi-PCL composite discs produced significantly more collagen at 10 days *in vitro* than osteoblasts cultured on either PCL or tissue culture plastic. In addition, these cells were associated with a more than two-fold increase in glycosaminoglycan content of the extracellular matrix, which may be due to increased production of GAGs by the osteoblasts or by stabilisation of the ECM by soluble silicate species. Crosslinking of collagen by pyridinoline was demonstrated to be greater in the presence of porous silicon.

To examine the effect of the soluble degradation products of pSi on osteoblasts, porous silicon microparticles were added to cell culture medium to generate a solution containing known concentrations of silicic acid. When applied to osteoblasts, concentrations of silicic acids from 1 – 5 $\mu g.ml^{-1}$ appeared to increase the proliferation rate of cells and also their metabolic activity in terms of collagen production. Previous research has shown that silicic acid-releasing zeolite A has similar effect on osteoblasts, increasing the rate of proliferation in densely seeded cells by the autocrine TGF-β route (Keeting *et al*, 1992).

This data supports previous studies which suggest a bioactive range of orthosilicic acid to be 280 $ng.ml^{-1}$ to 2.8 $\mu g.ml^{-1}$ (Reffitt *et al*, 2003; Arumugram *et al*, 2004), although it was found that silicon supplementation of up to 25 $\mu g.ml^{-1}$ also had a positive effect on osteoblastic activity *in vitro*. In this investigation, supplementation with orthosilicic acid from sodium metasilicate generated a similar cell response to conditioning media with silicic acids released from pSi dissolution. Interestingly, there was effectively no significant increase in calcium deposition when cells were cultured in even high concentrations (up to 100 $\mu g.ml^{-1}$) of silicic acid, indicating that a substantial silica gel layer is not formed to act as a nucleation bed for mineralisation.

The bioactivity of Bioglass®- and pSi-based materials arises from two separate sources therefore: the silica-conditioned surface of the material which acts as a nucleation bed for apatite-like mineralisation, and the soluble silicate species which interact with the extracellular matrix.

A major focus in porous silicon research and the core technology of pSiMedica Ltd. is the use of pSi microparticles as delivery vehicles for active pharmaceuticals (and radiotherapy agents). Substantial data exists 'in house' at pSiMedica for the loading and release kinetics of a variety of molecules, and similar research at the University of California, San Diego (Anglin *et al*, 2008) has been published. However, the somewhat more complicated release kinetics of pSi microparticles embedded in polycaprolactone were unknown.

The aim of chapter four was to assess porous silicon as a carrier for active pharmaceuticals in a polycaprolactone matrix and evaluate the release kinetics of a range of substances from small organic molecules to large, enzymatically active glycoproteins. A method was developed for loading substances into pSi, derived from the technique used at pSiMedica, in which the substance is dissolved in a solvent – wherever possible an organic solvent such as ethanol or acetone. A combination of the large surface area of pSi and capillarity of the narrow pores adsorbs the substance onto the pore surface.

To combine these substance-loaded particles with polycaprolactone, the polymer was dissolved in acetone and the microparticles added and stirred to distribute. At this point, the treatment of the composite was identical to non-loaded composites, although excess heating was avoided. Drug loading into the pSi microparticles was subsequently proved by confocal laser scanning microscopy of porous silicon microparticles loaded with fluorescein, which showed the fluorescein to be fully associated with pSi microparticles.

The subsequent release of small, water-soluble molecules such as fluorescein and gentamicin were found to be similar, 6 -12 $\mu g.day^{-1}$ for 10mg of each substance loaded into pSi-PCL, allowing the amount of substance released to be broadly predicted from loading concentration. The release of proteins such as bovine serum albumin and alkaline phosphatase from pSi-PCL was more dependent on protein mass and structure, with BSA (MW 66 KDa) being released into solution in concentrations an order of magnitude greater than the very hydrophobic dimer alkaline phosphatase (MW 160 KDa).

It was found that drugs loaded into pSi-PCL composites have similar release profiles to drugs loaded into polycaprolactone-only for most of the substances tested in this investigation. Therefore the results of this research can be directly compared to the wealth of published data on polycaprolactone drug delivery devices, microspheres, screws and sutures (e.g. Wu & Jin, 2008; Varde & Pack, 2004). Some substances, such as alkaline phosphatase and gentamicin were aided into solution by pre-loading them into pSi. Crucially, the activity of alkaline phosphatase was unchanged following release from pSi, demonstrating that

although such large glycoproteins may be crosslinked by silicates generated in pSi dissolution (Bayliss *et al*, 2000), the enzymatic activity was not affected. Release of other substances, such as bovine serum albumin, appeared to be lower, although it was subsequently found that significant amounts of BSA in solution are adsorbed onto the surface of pSi-PCL composites.

Adsorption of proteins onto the silica gel surface of Bioglass®-based biomaterials has been postulated as a key method by which they achieve bioactivity (Kaufmann *et al*, 2000; Rosengren *et al*, 2003; Perry, 2009). In chapter five, 8% pSi-PCL was shown to significantly increase the amount of protein adsorbed from both concentrations of BSA at blood plasma concentrations (40 $mg.ml^{-1}$) and foetal calf serum over adsorption onto polycaprolactone-only. Further, the adsorption of alkaline phosphatase did not denature the protein's structure, allowing the complex homodimer to retain phosphatase activity when bound to the surface.

In discussing drug-releasing polymers used for orthopaedics, the most widely used such material - antibiotic-eluting bone cement - is considered. Poly(methyl methacrylate) bone cement (PMMA) has a long history of use in fixation of orthpaedic implants and arthroplasties, and has been loaded with aminoglycoside antibiotics such as gentamicin for revision treatment of infections almost since its inception. As a potential application of pSi drug delivery microparticles in chapter seven PMMA was loaded with fluorescein and added to PMMA. It was found that the pre-loading of fluorescein into pSi enhanced the release of the molecule by an order of magnitude over loading of fluorescein directly into PMMA. As is shown in chapter four, the release rates of gentamicin and fluorescein are very similar, indicating that the addition of up to 8% pSi microparticles will enhance the delivery of antibiotics in orthopaedic fixation whilst maintaining the bone-bonding strength of the cement.

In the experiments described above, porous silicon – polycaprolactone composites were incubated in water, PBS or SBF in a static system, i.e. the fluid in the experiment was neither circulated nor shaken. This is clearly not representative of the conditions an implant would experience *in vivo*, and so a

series of simulated bone models were established to test the behaviour of the composite.

The results of exposing pSi-PCL to continuously flowing simulated body fluid was similar to that of incubating composites in a shaken water bath – under conditions of fluid flow, the release of silicic acids into solution is 200 – 300 times greater than in static systems. Interestingly, despite the increase in silicic acid removal from the solution (which did not exceed the $2 \times 10^{-3}$ M orthosilicic acid stability threshold proposed by Iler (1979), a silica – calcium layer was formed on the surface of the material within 24 hours.

In regard to the permeability of bone *in vivo* to silicic acids, an agarose hydrogel was successful in demonstrating that diffusion of silicic acids occurs through hydrated porous structures with pore sizes similar to those of canaliculi (259nm).

In chapter six, the mechanical properties of the composite are compared to those of PCL alone. Numerous studies have been performed on potential and existing orthopaedic materials, but for the applications we are considering and the nature of the material, it was determined that tensile yield strength and elastic modulus were the most important components of the material which we wished to test. It was found that there was no significant difference between the tensile strength of PCL-only and 4% composite, but 8% composites were less strong. The failure mode of these materials was all identical – plastic deformation, or necking – but a larger number of the 8% composites failed by fracturing. Closer examination revealed these fracture regions to contain voids – effectively air bubbles introduced during fabrication. Several techniques were attempted to reduce the number and size of these microscopic voids but they remained a persistent problem in mechanical testing experiments.

The other mechanical properties of the material were good. Whilst not explicitly tested, the hardness of the material (resistance to indentation) appeared to be greater than PCL – this is supported by the gradient of the stress-strain curves produced in mechanical testing experiments and reflected in the higher elastic modulus of composites. This is important in resisting deformation to sudden or

prolonged loading, particularly in restoring shape in reconstructive surgery, a major application for which these composites are being developed.

Further mechanical testing is reported in the appendix to this thesis, in which potential applications of the composite material are considered. At an early stage in this investigation, it was decided that a potential use of this material would be in bioactive resorbable screws. Currently used screws for orthopaedic fixation are made from either titanium or stainless steel, with a small market for polylactide based resorbable screws which are supplied in the UK by Inion Ltd., Finland, but these screws are not bioactive.

Whilst the development of novel polymer blends for optimised mechanical strength were far beyond the remit of this investigation, the effect of adding pSi microparticles to simple polycaprolactone screws was examined. Two moulds were used for fabricating screws – a purpose designed mould based on the size and thread profile of stainless steel screws marketed by SmitMedimed Pvt. Ltd. (Ahmadabad, India), and a stainless steel nut with internal threads. This latter mould was required for mechanical testing because it was found that the small diameter screws were too flexible and the threads too weak for use – supporting concerns voiced by surgeons consulted in this work (Mr Ian McVickar, Clinical Orthopaedics, University of Nottingham, UK).

The push-out strength of the composite screw from the nut-mould was not significantly different to polycaprolactone up to 8% pSi inclusion in the material, demonstrating that further research in using pSi to render resorbable polymer screws bioactive would be worthwhile.

In the introduction to chapter six, research is reported that indicates a role of electrical stimulation on bone healing. Whilst the clinical evidence for this is still both ambiguous and debated, a large number of researchers have focussed on this as a means to increase fracture healing rates and treat bone non-union. As the most important electrical semiconductor of the modern age, silicon and porous silicon were proposed to be beneficial in lowering the resistance of polymeric materials with the aim of creating an electrically conductive implant that can be

connected to an external power source and provide enhanced healing of the surrounding bone.

In practice, the extremely high resistivity of the polymer remained too high for successful measurement (>$10^{18}$ Ω.m), but proof of principle was obtained by adding pSi microparticles to an agarose hydrogel. The addition of 2% pSi to agarose gels lowered the resistivity of the gel by an order of magnitude. pSi inclusion in the gel was then found to inversely proportional to resistance, such that the addition of 8% pSi lowered the resistivity of the gel from (34.53 ± 2.25 KΩ.m to 0.86 ± 0.69 KΩ.m).

Whilst polycaprolactone remains prohibitively resistive, several groups have achieved success in creating electrically conducting, biodegradable polymers for biomedical applications. Rivers *et al* (2002) fabricated a biodegradable copolymer based on pyrrole – thiophene monomers linked by hydrolysable ester bonds. The effect on the addition of porous silicon to these polymers in terms of their electrical conductivity and bioactivity would therefore be interesting to determine.

In summary, porous silicon is potentially a very useful inclusion in polycaprolactone composite materials, able to outperform bioactive glasses in the release of bioavailable silicates and the spontaneous deposition of apatite-like minerals. Porous silicon stimulates the activity of osteoblasts *in vitro* and evidence suggests it enhances the stability of the extracellular matrix through crosslinking its component molecules and adsorbing serum proteins such as growth factors onto the cell substrate.

As a drug delivery vehicle, porous silicon increases the rate at which small molecules and hydrophobic proteins are released into solution, whilst maintaining their biological and enzymatic activity. Other proteins such as bone serum albumin were effectively adsorbed onto the materials surface, a useful characteristic which could localise both drug-loaded and native growth factors to the osteoblast-supporting surface of the material.

The above characteristics were all achieved by composites containing no more than 8% porous silicon by weight, far lower than Bioglass® in comparable composites. The incorporation of porous silicon into polymers therefore forms excellent and useful biomaterials for orthopaedic tissue engineering.

## REFERENCES


1. Ajioka M, Enomoto K, Suzuki K, Yamaguchi A (1995) The basic properties of poly(lactic acid) produced by the direct condensation polymerization of lactic acid. *Journal of Polymers and the Environment* **3**, 225 – 234.

2. Alexander B, Heston WM, Iler RK (1954) The solubility of amorphous silica in water. *Journal of Physical Chemistry* **58**, 453 – 455.

3. Allgower M, Perren SM (1991) Manual of internal fixation: techniques recommended by the AO-ASIF Group. Springer.

4. Al-Mutaz IS, Al-Anezi IA (2002) Silica reduction in reverse osmosis desalting plants. *The 6th Saudi Engineering Conference* **2**, 3 - 14.

5. Alvarez SD, Derfus AM, Schwartz MP, Bhatia SN, Sailor MJ (2008) The compatibility of hepatocytes with chemically modified porous silicon with reference to *in vitro* biosensors. *Biomaterials* **30**, 26 – 34.

6. American Academy of Orthopaedic Surgeons (2009) Available at: www.orthoinfo.org [Accessed 07.04.2009].

7. Anagnostakos K, Hitzler P, Pape D, Kohn D, Kelm J (2008) Persistence of bacterial growth on antibiotic-loaded beads: is it actually a problem? *Acta Orthopaedica* **79**, 302 - 307.

8. Anatomyforme (2009) Bone histology. Available from: http://anatomyforme.blogspot.com/2008_04_06_archive.html [Accessed 09.01.2009]

9. Anderson HC (2003) Matrix vesicles and calcification. *Current Rheumatology Reports* **5**, 222 – 226.

10. Anderson SI, Downes S, Perry CC, Caballero AM (1998) Evaluation of the osteoblast response to a silica gel *in vitro*. *Journal of Materials Science. Materials in Medicine* **9**, 731 - 735.

11. Anderson, HC (1969) Vesicles associated with calcification in the matrix of epiphyseal cartilage. *Journal of Cell Biology* **41**, 59 – 72.

12. Anglin EJ, Cheng L, Freeman WR, Sailor MJ (2008) Porous silicon in drug delivery devices and materials. *Advance Drug Delivery Review* **60**, 1266 – 1277.

13. Anglin EJ, M.P. Schwartz MP, V.P. Ng VP, L.A. Perelman LA, Sailor MJ (2004) Engineering the chemistry and nanostructure of porous silicon Fabry–Pérot films for loading and release of a steroid. *Langmuir* **20**, 11264 – 11269.

14. Arumugam MQ, Ireland DC, Brooks RA, Rushton N, Bonfield W (2006) Orthosilicic acid increases collagen type I mRNA expression in human bone-derived osteoblasts *in vitro*. *Key Engineering Materials* **254**, 869 – 872

15. Arwin H, Gavutis M, Gustafsson J, Schultzberg M, Zangooie S, Tengvall P (2000) Protein adsorption in thin porous silicon layers. *Physica Status Solidi* **182**, 515 – 520.

16. Atala A, Bauer SB, Soker S, Yoo JJ, Retik AB (2006) Tissue-engineered autologous bladders for patients needing cystoplasty. *Lancet.* **367**, 1241 - 1246.

17. Aubin JE, Liu F (1996) The osteoblast lineage. In: *Principles of Bone Biology*. Bilezekian JP, Raisz LG, Rodan GA. Eds. Academic press, San Diego.

18. Aubin JE, Liu F, Malaval L, Gupta AK (1995) Osteoblast and chrondoblast differentiation. *Bone **17***, 77 – 83.

19. Banning M (2008) Topical diclofenac: clinical effectiveness and current uses in osteoarthritis of the knee and soft tissue injuries. *Expert Opinion in Pharmacotherapy* **9**, 2921 - 2929.

20. Barou O, Mekraldi S, Vico L, Boivin G, Alexandre C, Lafage-Proust MH (2002) Relationships between trabecular bone remodeling and bone vascularization: a quantitative study. *Bone* **30**, 604 - 612

21. Bayliss SC, Buckberry LD, Harris PJ, Tobin M (2000) Nature of the silicon–animal cell interface. *Journal of Porous Materials* **7,** 191 – 195.

22. Beck BR, Qin YX, McLeod KJ, Otter MW (2002) On the relationship between streaming potential and strain in an *in vivo* bone preparation. *Calcified Tissues International* **71**, 335 - 343.

23. Becker RO, Bassett CAL, Bachman CH (1964) Bioelectric factors controlling bone structure. In: *Bone biodynamics*. H. Frost. Ed. Little Brown, New York.

24. Bellet D (1997) Drying of porous silicon. In: *Properties of Porous Silicon*. Canham, LT, Institution of Engineering and Technology, London.

25. Berry M (2008) Bioresorbable composite materials for orthopaedic devices. *Medical Device Technology* **19**, 69 - 70

26. Bhattacharya AA, Grune T, Curry S (2000) Crystallographic analysis reveals common modes of binding of medium and long-chain fatty acids to human serum albumin. *Journal of Molecular Biology* **303**, 721 – 732.

27. Billah AME-M (1996) The ultrastructural interface of bone crystals and organic matrix in woven and lamellar endochondral bone. *Journal of Dental Research* **48**, 781 – 788.

28. Blaker JJ, Gough JE, Maquet V, Notingher I, Boccaccini AR.(2003) *In vitro* evaluation of novel bioactive composites based on Bioglass-filled polylactide foams for bone tissue engineering scaffolds *Journal of Biomedical Materials Research A* **67**, 1401 – 1411.

29. Boivin G (2007) The hydroxyapatite crystal: a closer look. *Medicographia* **29**, 126-132.

30. Bond DM, Rudan JF (2002) Anaesthetic bone cement. US patent 6355705. Available at: http://www.freepatentsonline.com/6355705.html

31. Bond DM, Rudan JF, Adams MA (2004) Anaesthetic bone cement. US patent 6713527. Available at: http://www.freepatentsonline.com/6713527.html

32. Bond DM, Rudan JF, Adams MA (2004) Anaesthetic bone cement. US patent 6713527. Available at: http://www.freepatentsonline.com/6713527.html

33. Bone Research Organisation (2008) Available from: www.brsoc.org.uk [Accessed 19.11.2008].

34. BoneStimulation (2009) Stimulation of bone growth. Available from: http://www.bonestimulation.com/Physio_Pages/PS-howitworks.html [Accessed 27.5.2009].

35. Bourne RB (2004) Prophylactic use of antibiotic bone cement: an emerging standard—in the affirmative. *Journal of Arthoplasty* **19**, 69 – 72.

36. Bourne RB, Bitar H, Andreae PR, Martin LM, Finlay JB, Marquis F (1988) In-vivo comparison of four absorbable sutures: Vicryl, Dexon Plus, Maxon and PDS. *Canadian Journal of Surgery* **31**, 43 – 45.

37. Bradford MM (1976) A Rapid and Sensitive Method for the Quantitation of Microgram Quantities of Protein Utilizing the Principle of Protein-Dye Binding. *Annals of Biochemistry* **72**, 248 – 254.

38. Brighton CT, Friedenberg ZB, Redka W (1974) Patent: Constant current power pack for bone healing and method of use. US patent 3842841. Available at: http://www.freepatentsonline.com/3842841.html [Accessed on 26.05.2009].

39. British Standards Institution, Implants for osteosynthesis. Part 5, Bone screws and auxiliary equipment. Section 5.3, specification for the dimensions of screws having hexagonal drive connection, spherical under surfaces and asymmetrical thread, BSI, London (1991).

40. Buehler MJ (2007) Molecular nanomechanics of nascent bone: fibrillar toughening by mineralization. *Nanotechnology* **18**, 295102

41. Canham LT (1995) Bioactive silicon structure through nanoetching techniques. *Advanced Materials* **7**, 1033 – 1037.

42. Canham LT (1997) Properties of Porous Silicon. Inspec, IEE, London.

43. Canham LT (2000) Porous silicon as a therapeutic biomaterial. Microtechnologies in Medicine and Biology, 1st Annual International, Conference On. 109 – 112.

44. Canham LT (2001) 'Will a chip every day keep the doctor away?' Physics World (July) 27 – 31.

45. Canham LT (2007) Nanoscale semiconducting silicon as a nutritional food additive. *Nanotechnology* **18**, 185704.

46. Canham LT, Newy JP, Reeves CL, Houlton MR, Loni A, Simons AJ, Cox TI (1996) The effects of DC electric currents on the *in vitro* calcification of bioactive silicon wafers, *Advanced Materials* **8**, 847 – 849.

47. Carlisle EM (1974) Silicon as an essential element, *Federation Proceedings* **33,** 1758 – 1766.

48. Carlisle EM (1988) Silicon as a trace nutrient. *The Science of the Total Environment* **73**, 95 – 106.

49. Caterina, M.J. and Julius, D. (2001) The Vanilloid Receptor: A Molecular Gateway to the Pain Pathway. *Annual Review Neuroscence*. **24,** 487 - 517.

50. Cavusoglu T, Yavuzer R, basterzi Y, Tuncer S, Latifoglu O (2005) Resorbable plate-screw systems: clinical applications. *Turkish Journal of Trauma & Emergency Surgery* **11**, 43 – 48.

51. Chai C, Leong KW (2007) Biomaterials approach to expand and direct differentiation of stem cells. *Molecular Therapy* **15**, 467 – 480.

52. Charnay C, Begu S, Tourne-Peteilh C, Nicole L, Lerner DA, Devoisselle JM (2004) Inclusion of ibuprofen in mesoporous templated silica: drug loading and release property, *European Journal of Pharmaceuticals and Biopharmacy* **57**, 533 – 540.

53. Chatterjee D, Chakraborty M, Leit M, Neff L, Jamsa-Kellokumpu S, Fuchs R, Bartkiewicz M, Hernando N, Baron R (1992) The osteoclast proton pump differs in its pharmacology and catalytic subunits from other vacuolar H(+)-ATPases. *Journal of Experimental Biology* **172**, 193 - 204.

54. ChemPep Inc. (2009) pKa of fluorescein. Available at: http://www.chempep.com/ChemPep-peptide-modifications.htm. [Accessed on 26.05.2009].

55. Chen Q, Roether JA, Boccaccini AR (2008) Tissue engineering scaffolds from bioactive glass and composite materials. In: topics in tissue engineering, Vol. 4. Ashammakhi N, Reis R, Chiellini F, Eds. Available at http://www.oulu.fi/spareparts/ebook_topics_in_t_e/list_of_contr.html [Accessed on 27.05.2009].

56. Cheng H, Jiang W, Phillips F, Haydon R, Peng Y, Zhou L, Luu H, An N, Breyer B, Vanichakarn P, Szatkowski J, Park J, He T (2003). Osteogenic activity of the fourteen types of human bone morphogenetic proteins (BMPs). *Journal of Bone and Joint Surgery America* **85**, 1544 – 1552.

57. Chiang M, Robinson KR, Vanable Jr. JW (1992) Electrical fields in the vicinity of epithelial wounds in the isolated bovine eye. *Experimental Eye Research* **54**, 999 – 1003.

58. Chouzouri G, Xanthos M.(2007) *In vitro* bioactivity and degradation of polycaprolactone composites containing silicate fillers. *Acta Biomaterials* **3**, 745 – 756.

59. Christoffersen J, Landis WJ (1991) A contribution with review to the description of mineralization of bone and other calcified tissues *in vivo*. *Anatomical Record* **230**, 435 – 450.

60. Chujo K, Kobayashi H, Suzuki J, Tokuhara S (1967) Physical and chemical characteristics polyglycolide. *Die Makromolekulare Chemie* **100**, 267 – 270.

61. Clezardin P, Malaval L, Morel MC, Guichard J, Lecompte T, Trzeciak MC, Dechavanne M, Breton-Gorius J, Delmas PD, Kaplan C (1991) Osteonectin is an alpha-granule component involved with thrombospondin in platelet aggregation. *Journal of Bone Mineral Research* **6**, 1059 – 1070.

62. Coffer JL, Montchamp JL, Aimone JB, Weis RP (2003) Routes to calcifled porous silicon: implications for drug delivery and biosensing. *Physica Status Solidi A—Applied Research* **197**, 336 – 339.

63. Coghlan A (1992) How to sow cress and reap plastic. *New Scientist* **1820**, 20

64. Comb LF (1996) Silica chemistry and reverse osmosis. *Ultrapure water* **13**, 41 – 43.

65. Considére (1885) *Ann Ponts Chaussee* **9**, 574

66. Cormack DH (1984) Introduction to histology. JB Lippencott Co. Philadelphia.

67. Costa VC, Costa HS, Vasconcela WL, Pereira MdM, Orefice RL, Mansur HS (2007) Preparation of hybrid biomaterials for bone tissue engineering. *Materials Research* **10**, 21 – 26.

68. Cross PC, Mercer KL (1993) Cell and tissue ultrastructure. WH Freeman & Co., New York.

69. Cui W, Li X, Zhou S, Weng J (2007) *In situ* growth of hydroxyapatite within electrospun poly(DL-lactide) fibers. *Journal of Biomedical Materials Research A* **82**, 831 - 841.

70. D. R. Piperno (2006) Phytoliths: a comprehensive guide for archaeologists and paleoecologists. AltaMira Press, Lanham, MD

71. Dahabreh Z, Kanakarisa NK, Giannoudis PV (2008) A cost analysis of treatment of tibial fracture non-unions: A comparative study between autologous iliac crest bone grafting and bone morphogenetic protein-7. *Injury Extra* **39**, 180 - 181.

72. Dashwood MR, Loesch A (2009) The saphenous vein as a bypass conduit: the potential role of vascular nerves in graft performance. *Current Vascular Pharmacology* **7**, 47 - 57.

73. De Diego MA, Coleman NJ, Hench LL (1999) Tensile properties of bioactive fibres for tissue engineering applications. *Journal of Biomedical Materials Research A* **53**. 199 – 203.

74. Delmas PD (1995) Biochemical markers for the assessment of bone turnover. In: *Osteoporosis: etiology, diagnosis and management* Riggs BL, Melton LJ Eds. Lippincott-Raven Publishers, Philadelphia.

75. Dhanaraju MD, Gopinath D, Ahmed MR, Jayakumar R, Vamsadhara C (2006) Characterization of polymeric poly(epsilon-caprolactone) injectable implant delivery system for the controlled delivery of contraceptive steroids. *Journal of Biomedical Materials Research A*. **76**, 63 – 72.

76. Di Silvio L (1995) A novel application of two biomaterials for the delivery of growth hormone and it's effect on osteoblasts. PhD thesis, UCL Medical School.

77. Dorvee JR, Sailor MJ, Miskelly GM (2008) Digital microfluidics and delivery of molecular payloads with magnetic porous silicon chaperones, *Dalton Transactions* **14**, 721 – 730.

78. Ducy P, Desbois C, Boyce B, Pinero G, Story B, Dunstan C (1996) Increased bone formation in osteocalcin-deficient mice. *Nature* **382**, 448-452.

79. Duellman TJ, Gaffigan C, Milbrandt JC, Allan DG (2009) Multi-modal, pre-emptive analgesia decreases the length of hospital stay following total joint arthroplasty. *Orthopedics* **32**, 167.

80. Dutton (2004) Orthopaedic examination, evaluation, and intervention. McGraw-Hill Professional.

81. Elek SD, Conen PE (1957) The virulence of Staphylococcus pyogenes for man. A study of the problems of wound infection. *British Journal of Experimental Pathology* **38**, 573 - 586.

82. Encyclopædia Britannica (2009) Connective tissue. Availavle at: http://www.britannica.com/EBchecked/topic-art/132995/3755/Electron-micrograph-of-four-collagen-fibrils-shadowed-with-metal-to [Accessed 27.05.2009].

83. Ernst Haeckel (1904) *Kunstformen der Natur*.

84. Evans RA, Dunstan CR, Hills EE (1980) Extent of resorbing surfaces based on biochemical identification of osteoclasts. In: *The Third International Workshop on Bone Histomorphometry*. Parfit and Jee. Societe Nouvelle de Publications Medicales et Dentaires, Sun Valley.

85. Faes TJ, van der Meij HA, de Munck JC, Heethaar RM (1999) The electric resistivity of human tissues (100 Hz-10 MHz): a meta-analysis of review studies. *Physiological Measurement* **20**, R1-10.

86. Faucheux C, Verron E, Soueidan A, Josse S, Arshad MD, Janvier P, Pilet P, Bouler JM, Bujoli B, Guicheux J (2009) Controlled release of bisphosphonate from a calcium phosphate biomaterial inhibits osteoclastic resorption *in vitro*. J*ournal of Biomedical Material Research A*. **89**, 49 – 59.

87. Feng ZC, Tsu R (1994) Porous silicon. World Scientific, Singapore.

88. Fiedler J, Röderer G, Günther KP, Brenner RE (2002) BMP-2, BMP-4, and PDGF-bb stimulate chemotactic migration of primary human mesenchymal progenitor cells. *Journal of Cell Biochemistry*, **87** 305 - 312.

89. Fisher LW, McBride OW, Termine JD, Young MF (1990) Human bone sialoprotein. Deduced protein sequence and chromosomal localization. *Journal of Biological Chemistry* **265**, 2347 – 2351.

90. Forgács E, Cserháti T (1997) Molecular basis of chromatographic separation. CRC Press.

91. Frank S, Poncharal P, Wang ZL, de Heer WA (1998) Carbon nanotube quantum resistors. *Science* **280**, 1744 – 1746.

92. Frick KK, Bushinsky DA (2003) Metabolic acidosis stimulates RANKL RNA expression in bone through a cyclo-oxygenase-dependent mechanism. *Journal of Bone Mineral Research* **18**, 1317 – 1325.

93. Gafni Y, Ptitsyn AA, Zilberman Y, Pelled G, Gimble JM, Gazat D (2009) Circadian rhythm of osteocalcin in the maxillomandibular complex. *Journal of Dental Research* **88**, 45 – 50.

94. Gardner AD, Medcraft JW. (1974) Letter: Antibiotic-bone-cement mixtures in prevention of infection following total joint replacement. *Lancet* **7885**, 891.

95. Ghannoum MA, Rice LB (1999) Antifungal agents: mode of action, mechanisms of resistance, and correlation of these mechanisms with bacterial resistance. *Clinical Microbiology Review* **12**, 501 – 517.

96. Giammarioli S, Mosca M, Sanzini E (2006) Silicon content of Italian mineral waters and its contribution to daily intake *Journal of Food Science* **70**, 501 – 512.

97. Gibson IR, Best SM, Bonfield W (2002) Effect of silicon substitution on the sintering and microstructure of hydroxyapatite, *Journal of the American Ceramics Society* **85,** 2771 – 2777.

98. Gittens SA, Bansal G, Kucharski C, Borden M, Uluda H (2005) Imparting mineral affinity to fetuin by bisphosphonate conjugation: A comparison of three bisphosphonate conjugation schemes. *Molecular Pharmaceutics* **2**, 392 – 406.

99. Global Information Inc. (2004) Orthopaedic drugs, implants and devices. Available at: http://www.the-infoshop.com/study/bc24076_orthopedic_drugs.htm [Accessed 14.09.2007]

100. Glowacki J, Rey C, Glimcher MJ, Cox KA, Lian J (1991) A role for osteocalcin in osteoclast differentiation. *Journal of Cell Biochemistry* **45**, 292 – 302.

101. Goldberg D (1995) A review of the biodegradability and utility of poly(caprolactone). *Journal of Polymers and the Environment* **3**, 61 – 67.

102. Goodwin CJ, Braden M, Downes S, Marshall NJ (1998) Release of bioactive human growth hormone from a biodegradable material: poly(-caprolactone). *Journal of Biomedical Materials Research* **40**, 204 - 213.

103. Gough JE, Downes S (2001) Osteoblast cell death on methacrylate polymers involves apoptosis. *Journal of Biomedical Materials Research A.* **15**, 497-505.

104. Gough JE, Notingher I, Hench LL (2003) Osteoblast attachment and mineralized nodule formation on rough and smooth 45S5 bioactive glass monoliths. *Journal of Biomedical Materials Research A* **68**, 640 – 650.

105. Granchi D, Cenni E, Trisolino G, Giunti A, Baldini N (2006) Sensitivity to implant materials in patients undergoing total hip replacement. *Journal of Biomedical Materials Research B. Applied Biomaterials* **77**, 257 - 264.

106. Gray H. (2008) Gray's Anatomy: The anatomical basis of medicine and surgery, 40th edition. Churchill-Livingstone, Elsevier.

107. Greenfield EM, Bi Y, Miyauchi A (1999) Regulation of osteoclast activity. *Life Science* **65**, 1087 – 1102.

108. Griffin XL, Costello I, Costa ML (2008) The role of low intensity pulsed ultrasound therapy in the management of acute fractures: a systematic review. *Journal of Trauma* **65**, 1446 – 1452.

109. Griffiths D (1999) Electrodynamics. In: Introduction to Electrodynamics Reeves A, Ed. Upper Saddle River, New Jersey: Prentice Hall.

110. Gubernator J, Drulis-Kawa Z, Kozubek A (2006) A simple and sensitive fluorometric method for determination of gentamicin in liposomal suspensions. *International Journal of Pharmacy* **327**, 104 - 109.

111. Gundberg CM, Markowitz ME, Mizruchi M, Rosen JF (1985) Osteocalcin in human serum: a circadian rhythm. *Journal of Clinical Endocrinology Metabolism* **60**, 736 – 739.

112. Haje DP, Volpon JB (2006) Bovine bone screws development: machining method and metrological study with profile projector. *Acta Orthopaedics Brasiliera* **14**, 87 – 91.

113. Halimaoui A (1997) Porous silicon formation by anodization. In: *Properties of porous silicon*. Canham, LT Ed. Institution of Engineering and Technology, London.

114. Ham AW, Harris WR (1972) Repair and transplantation of bone. In: *The biochemistry and physiology of bone.* Academic Press, New York

115. Hanssen AD (2004) Prophylactic use of antibiotic bone cement an emerging standard - in opposition. *Journal of Arthroplasty* **19**, 73 – 77.

116. Hariharan R, Pinkus AG (2006) Useful NMR solvent mixture for polyesters: Trifluoroacetic acid-d/chloroform-d. *Polymer Bulletin* **30**, 91 – 95.

117. Hasenhuttl K (1962) Osteopetrosis : Review of the literature and comparative studies on a case with a twenty-four-year follow-up. *Journal of Bone and Joint Surgery* **44**, 359 – 370.

118. Hedley AK, Gruen TA, Borden LS, Hungerford DS, Habermann E, Kenna RV (1987) Two-year follow-up of the PCA noncemented total hip replacement. **Hip** 225 - 250

119. Helfrich MH (2003) Osteoclast diseases. *Microscopy Research and Technique* **61**, 514-532

120. Hench LL (2006) The story of Bioglass®. *Journal of Materials Science: Materials in Medicine* **17**, 967 – 978

121. Henrickson RC, Kaye GI, Mazurkiewicz JE (1997) Histology. Lippincott, Williams & Wilkins.

122. Hillsley MV, Frangos (1993) Review: bone tissue engineering: the role of interstitial

123. Hirashima T, Eto T, DenBesten L (1985) Lactomer copolymer absorbable staples in gastrointestinal surgery. *American Journal of Surgery* **150**, 381 – 385.

124. Hodgskinson RAG (1991) PhD Thesis, Queen Mary College, London

125. Hollinger JO, Einhorn TA, Doll B, Sfeir C (2005) Bone Tissue Engineering. CRC Press.

126. Holtrop ME, King GJ (1977) The ultrastructure of the osteoclast and its functional implications. *Clinical Orthopaedic Related Research* **123**, 177 – 196.

127. Howatson AM, Lund PG, Todd JD (1991) Engineering tables and data. Kluwer Academic Publishers.

128. Hulmes DJ (2002) Building collagen molecules, fibrils, and suprafibrillar structures. *Journal of Strucural Biology* **137**, 2 – 10.

129. Hunter GK, Goldberg HA (1994) Modulation of crystal formation by bone phosphoproteins: role of glutamic acid-rich sequences in the nucleation of hydroxyapatite by bone sialoprotein. *Biochemical Journal* **302**, 175 – 179.

130. Huolman R, Ashammakhi N (2007) New multifunctional anti-osteolytic releasing bioabsorbable implant. *Journal of Craniofacial Surgery* **18**, 295 – 301.

131. IDES: The plastics web (2009) Polycaprolactone technical data. Available at: http://www.ides.com/generics/PCL/PCL_typical_properties.htm. [Accessed on 27.05.2009].

132. Ignatius AA, Claes LE (1996) *In vitro* biocompatibility of bioresorbable polymers: poly(L, DL-lactide) and poly(L-lactide-co-glycolide). *Biomaterials* **17**, 831-839.

133. Iler R (1979) The chemistry of silica. Wiley, New York.

134. Iler R (1982) The chemistry of silica. Mir, Moscow.

135. Itoh F, Asao H, Sugamura K, Heldin CH, ten Dijke P, Itoh S (2001) Promoting bone morphogenetic protein signaling through negative regulation of inhibitory Smads. *EMBO Journal.* **20**, 4132 – 4142.

136. Iwamoto J, Sato Y, Takeda T, Matsumoto H (2008) Hip fracture protection by alendronate treatment in postmenopausal women with osteoporosis: a review of the literature. *Clinical Interventions in Aging.* **3**, 483 – 489.

137. J. Emsley, *The Elements*, 3rd ed.Clarendon Press, Oxford.

138. Jaffe LF, Vanable Jr. JW (1984) Electric fields and wound healing. *Clinical Dermatol*ogy **2**, 4 – 44.

139. Jain MR, Srivastava S (1979) Ocular penetration of hydrocortisone and dexamethasone in aqueous humour after subconjunctival injection. *Indian Journal of Ophthalmology* **27**, 61 – 5.

140. Jee, WSS (1983) The skeletal tissues. In: Histology: cell and tissue biology 5th ed. Weiss, L, Ed. Elsevier Science Ltd

141. Jefferis R, Lund J, Goodall M (1995) Recognition sites on human IgG for Fcγ receptors: the role of glycosylation. *Immunonology Letters* **44**, 111 – 117.

142. Jiang G, Evans ME, Jones IA, Rudd CD, Scotchford CA, Walker GS (2005) Preparation of poly(epsilon-caprolactone)/continuous bioglass fibre composite using monomer transfer moulding for bone implant. *Biomaterials.* **26**, 2281 – 2288.

143. Johansson F, Kanje M, Linsmeier CE, Wallman L (2008) The influence of porous silicon on axonal outgrowth *in vitro*. *IEEE Transaction on Biomedical Engineering* **55**, 1447 - 1449.

144. Jones JJ, Gentleman E, Polak J (2007) Bioactive glass scaffolds for bone regeneration. *Elements.* **3**, 393 - 399.

145. Josse S, Faucheux C, Soueidan A, Grimandi G, Massiot D, Alonso B, Janvier P, Laïb S, Pilet P, Gauthier O, Daculsi O, Guicheux J, Bujoli B, Bouler J-M (2005) Novel biomaterials for bisphosphonate delivery. *Biomaterials* **26**, 2073 – 2080.

146. Jugdaohsingh R, Tucker KL, Qiao N, Cupples LA, Kiel DP, Powell JJ (2004) Dietary silicon intake is positively associated with bone mineral density in men and premenopausal women of the Framingham Offspring cohor. *Journal of Bone Mineral Research* **19**, 297 – 307.

147. Jugdaohsingh R. (2002) Dietary silicon intake and absorption. *American Journal of Clinical Nutrition* **75**, 887 - 893.

148. Jukola H, Nikkola L, Gomes ME, Chiellini F, Tukiainen M, Kellomäki M, Chiellini E, Reis RL, Ashammakhi N (2008) Development of a bioactive glass fiber reinforced starch-polycaprolactone composite. *Journal of Biomedical Materials Research B* **87**, 197 – 203.

149. Kaneuji A, Yamada K, Hirosaki K, Takano M, Matsumoto T (2009) Stem subsidence of polished and rough double-taper stems. *Acta Orthopaedica* [Epub ahead of print].

150. Kannan RY, Salacinski HJ, Butler PE, Hamilton G, Seifalian AM (2005) Current status of prosthetic bypass grafts: a review. *Journal of Biomedical Material Research B: Applied Biomaterials* **74**, 570 - 581.

151. Karsenty G (2000) The Central Regulation of Bone Remodeling. *Trends in Endocrinology and Metabolism* **11**, 437 – 439.

152. Kashutina IA, Potapov VV, Shulga OV, Sadovnikova AO, Kashpura VN, Gorbach VA, Min GM (2008) Polycondensation kinetics of orthosilicic

acid in hydrothermal solutions. In: *Proceedings 33rd Workshop on Geothermal Reservoir Engineering.*

153. Kaufmann EAB, Ducheyne P, Radin S, Bonnell DA, Composto R (2000) Initial events at the bioactive glass surface in contact with protein-containing solutions. *Journal of Biomedical Materials Research A* **52**, 825 - 830.

154. Keeting PE, Oursler MJ, Weigand KE, Bonde SK, Spelsberg TC, Riggs BL (1992) Zeolite A increases proliferation, differentiation and transforming growth factor beta production in normal adult human osteoblast-like cells *in vitro. Journal of Bone and Mineral Research* **7**, 1281 – 1289.

155. Keeting PE, Oursler MJ, Wiegand KE, Bonde SK, Spelsberg TC, Riggs BL (1992) Zeolite A increases proliferation, differentiation, and transforming growth factor beta production in normal adult human osteoblast-like cells *in vitro. Journal of Bone Mineral Research* **7**, 1281 – 1289.

156. Kempen DH, Yaszemski MJ, Heijink A, Hefferan TE, Creemers LB, Britson J, Maran A, Classic KL, Dhert WJ, Lu L (2008) Non-invasive monitoring of BMP-2 retention and bone formation in composites for bone tissue engineering using SPECT/CT and scintillation probes. *Journal of Controlled Release* **134**, 169 – 176.

157. Khoury LD, Esterhai JL Jnr. (2006) Orthopaedic surgery. In: The Surgical Review: An Integrated Basic and Clinical Science Study Guide. Eds. Atluir P, Karakousis GC, Porrett PM, Kaiser LR. Lippencott Williams & Willkins, Philadelphia.

158. Kim H-W (2007) Biomedical nanocomposites of hydroxyapatite /polycaprolactone obtained by surfactant mediation. *Journal of Biomedical Materials Research Part A* **83A**, 169 – 177.

159. Kim J, Park C, Kim SJ, Park J, Ko YC, Woo H-G, Sohn H (2007) Fabrication and optical characterisation of rugate-structured polymer replicas. *Bulletin of the Korean Chemical Society* **28**, 2079 – 2082.

160. Kinloch AJ, Young RJ (1995) Fracture Behavior of Polymers. Chapman & Hall.

161. Koh A, da Silva AP, Bansal AK, Bansal M, Sun C, Lee H, Glogauer M, Sodek J, Zohar R (2007) Role of osteopontin in neutrophil function. *Immunology* **122,** 466–475

162. Kojic EM, Darouiche RO (2004) Candida infections of medical devices. *Clinical Microbiology Review* **17**, 255 – 267.

163. Kokubo T, Kushitani H, Sakka S, Kitsugi T, Yamamuro T (1990) Solutions able to reproduce *in vivo* surface-structure changes in bioactive glass-ceramic A-W. *Biomedical Material Research* **24**, 721 – 734.

164. Kucsera J, Yarita K, Takeo K (2000) Simple detection method for distinguishing dead and living yeast colonies. *Journal of Microbiology Methods* **41**, 19 - 21.

165. Kuhn LT, Grynpas MD, Rey CC, Wu Y, Ackerman JL, Glimcher MJ (2008) A comparison of the physical and chemical differences between cancellous and cortical bovine bone mineral at two ages. *Calcified Tissues International.* **83**, 146 – 154.

166. Kuroiwa M, Chihara K, Higashi S (1994) Electron microscopic studies on Sharpey's fibers in the alveolar bone of rat molars. *Kaibogaku Zasshi* **69**, 776 – 782.

167. Lakes R (2008) The meaning of Poisson's ration. Available at: http://silver.neep.wisc.edu/~lakes/PoissonIntro.html [Accessed 28.05.2009].

168. Lam CX, Savalani MM, Teoh SH, Hutmacher DW (2008) Dynamics of *in vitro* polymer degradation of polycaprolactone-based scaffolds: accelerated versus simulated physiological conditions. *Biomedical Materials* **3**, 034108 (E-published)

169. Landis WJ, Glimcher MJ (1978) Electron diffractiona nd electron probe microanalysis of the mineral phase of bone tissue prepared by anhydrous techniques. *Journal of Ultrastructure Research* **63**, 188 – 223.

170. Landis WJ, Lee DD, Brenna JT, Chandra S, Morrison GH (1986) Detection and localization of silicon and associated elements in vertebrate bone tissue by imaging ion microscopy. *Calcified Tissues International* **38**, 52-59.

171. Landis WJ, Lee DD, Brenna JT, Chandra S, Morrison GH (1986) Detection and localization of silicon and associated elements in vertebrate bone tissue by imaging ion microscopy. *Calcified Tissues International* **38**, 52 - 59.

172. Larsen M, Pelzer M, Friedrich PF, Bishop AT (2008) Measurement of bone blood flow using the hydrogen washout technique - part II: Validation by comparison to microsphere entrapment. *Journal of Orthopaedic Research* **26**, 746 – 752.

173. Lautenschlager EP, Jacobs JJ, Marshall GW, Meyer Jr. (1976) PR Mechanical properties of bone cements containing large doses of antibiotic powders. *Journal of Biomedical Materials Research* **10**, 929 - 938

174. Lee AJ, Hodges S, Eastell R (2000) Measurement of osteocalcin. *Annals of Clinical Biochemistry* **37**, 432 – 446.

175. Lee CG, Fu YC, Wang CH (2005) Simulation of gentamicin delivery for the local treatment of osteomyelitis. *Biotechnology and Bioengineering* **91**, 622 – 635.

176. Lee JB, Lee SH, Seong MY, Park J-C, Choi JB, Kim JK (2008) PLGA scaffold incorporated with hydroyapatite for cartilage regeneration. *Surface and Coatings Technology* **202**, 5757 – 5761.

177. Lee, C (2005) Properties of bone cement: the mechanical properties of PMMA bone cement. In: The well-cemented total hip arthroplasty: theory and practice. Breusch S, Malchau H. Eds. Springer.

178. Lemoigne M (1925) Etudes sur l'autotyse microbienne -. Acidification par formation d'acide/3 oxybutyrique. *Annals Institute de Pasteur (Paris)* **39**, 144 – 173.

179. Lentino JR (2004) Infections associated with prosthetic knee and prosthetic hip. *Current Infectious Disease Reports* **6**, 388 – 392.

180. Leung KS, Fung KP, Sher AH, Li CK, Lee KM (1993) Plasma bone-specific alkaline phosphatase as an indicator of osteoblastic activity. *Journal of Bone and Joint Surgery*, **75-B**, 288 – 292.

181. Leung KS, Lee WS, Tsui HF, Liu PP, Cheung WH (2004) Complex tibial fracture outcomes following treatment with low-intensity pulsed ultrasound. *Ultrasound in Medical Biology*. **30**, 389 – 395.

182. Lewandrowski KU, Bondre SP, Shea M, Untch CM, Hayes WC, Hile DD, Wise DL, Trantolo DJ (2002) Composite resorbable polymer/hydroxylapatite composite screws for fixation of osteochondral osteotomies. *Biomedical Materials Engineering* **12**, 423 - 438.

183. Lewis AF, Jordan JR, Parsell DE, Kosko M. (2008) Comparison of pull out strength of resorbable screws in human cadaveric laryngeal cartilage using different drill diameters. *Head Neck* **30**, 1464 – 1468.

184. Li G, Bronk JT, Kelly PJ (1989) Canine bone blood flow estimated with microspheres. *Journal of Orthopaedic Research* **7**, 61 – 67.

185. Lidgren L, Drar H, Möller J (1984) Strength of polymethylmethacrylate increased by vacuum mixing. *Acta Orthopaedica Scandinavica* **55**, 536 - 541.

186. Lieben L, Callewaert F, Bouillon R (2009) Bone and metabolism: a complex crosstalk. *Hormone Research* **71**, 134 - 138.

187. Liu F, Malaval L, Gupta A, Aubin JE (1994) Simultaneous detection of multiple bone-related mRNAs and protein expression during osteoblast differentiation: polymerase chain reaction and immunocytochemical studies at the single cell level. *Developmental Biology* **166**, 220 – 234.

188. Liu H, Slamovich EB, Webster TJ (2006) Less harmful acidic degradation of poly(lacticco-glycolic acid) bone tissue engineering scaffolds through titania nanoparticle addition. *International Journal of Nanomedicine* **1**, 541 - 545.

189. Liu Y-Z, Liu Y-J, Recker RR, Dend H-W (2003) Molecular studies of identification of genes for osteoporosis: the 2002 update. *Journal of Endocrinology* **177**, 147 – 196.

190. Liu ZJ, Zhuge Y, Velazquez OC (2009) Trafficking and differentiation of mesenchymal stem cells. *Journal of Cell Biochemistry* **106**, 984 - 991.

191. Liyun Wang L, Wang Y, Han Y, Henderson SC, Majeska RJ, Weinbaum S, Schaffler MB (2005) *In situ* measurement of solute transport in the bone lacunar-canalicular system. *PNAS* **102**, 11911 – 11916.

192. Lobell KD, Hench LL ( 1998) *In vitro* adsorption and activity of enzymes on reaction layers of bioactive glass substrates. *Journal of Biomedical Materials Research A* **39**, 575 – 579.

193. Lopez PJ, Coradin T (2003) Biogenic silica patterning: simple chemistry or subtle biology. *ChemBioChem* **3**, 1 – 9.

194. Loty C, Sautier J-M, Boulekbache H, Kokubo T, Kim H-M (1999) *In vitro* bone formation on a bone-like apatite layer prepares by a biomimetic process on a bioactive glass-ceramic. *Journal of Biomedical Materials Research* **49**, 423 – 434.

195. Louredo AM, Alonso A, de Llano J JA, Díez LM, Alvarez JL, del Riego FJ (2005) Usefulness of absorbable meshes in the management of splenic trauma. *Cirugia Espanola*. **77**, 145 – 152.

196. Low SP, Voelcker NH, Canham LT, Williams KA (2009) The biocompatibility of porous silicon in tissues of the eye. *Biomaterials* **30**, 2873 - 2880.

197. Lu C-H, Lin W-J (2002) Permeation of protein from porous poly(-caprolactone) films. *Journal of Biomedical Materials Research A* **63**, 220 – 225.

198. Luriya EA, Kuznetsov SA, Genikina EN, Fridenschtein AY (2004) Mineralization of ground substance of new bone tissue in mouse marrow organ cultures. *Bulletin of Experimental Biology and Medicine* **106**, 1633 – 1636.

199. Lutgens, FK, Tarbuck EJ (2000) Essentials of Geology, 7th Ed., Prentice Hall

200. Majeska RJ (1996) Culture of osteoblastic cells. In: *Principles of bone biology*. Bilekezan JP, Raisz LG, Rodan GA Eds. Academic Press, San Diego.

201. Marcelo TM, Livramento V, de Oliveira MV (2006) Microstructural characterization and interactions in Ti- and TiH2-hydroxyapatite vacuum sintered composites. *Materials Research* 9. Available at http://www.scielo.br/scielo.php?pid=S1516-14392006000100013&script=sci_arttext&tlng=pt [Accessed 26.05.2009].

202. Martin KR (2007) The chemistry of silica and its potential health benefits. *Journal of Nutrition, Health and Aging* **11**, 94 – 97.

203. Maurer P, Hohenadl C, Hohenester E, Göhring W, Timpl R, Engel J. (1995) The C-terminal portion of BM-40 (SPARC/osteonectin) is an autonomously folding and crystallisable domain that binds calcium and collagen IV. *Journal of Molecular Biology* **253**, 347 – 357.

204. Mayer U, Aumailley M, Mann K, Timpl R, Engel J. (1991) Calcium-dependent binding of basement membrane protein BM-40 (osteonectin, SPARC) to basement membrane collagen type IV. *European Journal of Biochemistry* **198**, 141 – 150.

205. McCarthy I (2006) The physiology of bone blood flow: a review. *The Journal of Bone and Joint Surgery (American)* **88**, 4 - 9.

206. Menkes A, Mazel S, Redmond RA, Koffler K, Libanati CR, Gundberg CM, Zizic TM, Hagberg JM, Pratley RE, Hurley BF (1993) Strength training increases regional bone mineral density and bone remodeling in middle-aged and older men. *Journal of Applied Physiology* **74**, 2478 - 2484.

207. Menton DN, Simmons DJ, Orr BY, Plurad SB (1982) A cellular investment of bone marrow. *Anatomical Record* **203**, 157 - 164.

208. Meyle J, Knoblauch M, Roessler R, Anil A (2001) RH 414 a new dye to stain non - decalcified bone tissue. *Journal of Dental and Oral Medicine* **3**, P64.

209. Miessler, G (1991). Chapter 6: Acid-Base and Donor-Acceptor Chemistry. Inorganic Chemistry (2nd ed.). Prentice Hall.

210. Misch CE, Zhimin QU, Bidez MW, Brunski JB (19999) Mechanical properties of trabecular bone in the human mandible : Implications for dental implant treatment planning and surgical placement. *Journal of oral and maxillofacial surgery* **57**, 700 – 708.

211. Misra SK, Mohn D, Brunner TJ, Stark WJ, Philip SE, Roy I, Salih V, Knowles JC, Boccaccini AR (2008) Comparison of nanoscale and microscale bioactive glass on the properties of P(3HB)/Bioglass composites. *Biomaterials* **29**, 1750 – 1761.

212. Mödder UI, Khosla S (2008) Skeletal stem/osteoprogenitor cells: current concepts, alternate hypotheses, and relationship to the bone remodeling compartment. *Journal of Cell Biochemistry* **103**, 393 - 400.

213. Moisala A-S, Jarvela T, Paakkala A, Paakkala T, Kannus P, Jarvinen M (2008) Comparison of the bioabsorbable and metal screw fixation after ACL reconstruction with a hamstring autograft in MRI and clinical outcome: a prospective randomized study. *Knee Surgery, Sports Traumatology, Arthroscopy* **16**, 1080 – 1086.

214. Mollon B, da Silva V, Busse JW, Einhorn TA, Bhandari M (2008) Electrical stimulation for long-bone fracture-healing: a meta-analysis of randomized controlled trials. *Journal of Bone and Joint Surgery America* **90**, 2322 – 2330.

215. Muhamad II, Joon LK, Noor MAM (2006) Comparing the degradation of poly-B-(hydroxybutyrate, poly-B-(hydroxybutyrate-co-valerate) (PHBV) and PHBV/cellulose triacetate blend. *Malaysian Polymer Journal* **1**, 39 – 46.

216. Muller R, Ruegsegger P (1997) Micro-tomographic imaging for the nondestructive evaluation of trabecular bone architecture. In: Lowet G, Bone research in Biomechanics. IOS Press

217. Nakasaki M, Yoshioka K, Miyamoto Y, Sasaki T, Yoshikawa H, Itoh K (2008) IGF-I secreted by osteoblasts acts as a potent chemotactic factor for osteoblasts. *Bone* **43**, 869 - 879.

218. Nash KJ, Calcott PDJ, Cannham LT, Kane MJ, Brumhead D (1994) The origin of efficient luminescence in highly porous silicon *Journal of Luminescence* **60-61**, 297 – 301.

219. Ng AM, Saim AB, Tan KK, Tan GH, Mokhtar SA, Rose IM, Othman F, Idrus RB (2005) Comparison of bioengineered human bone construct from four sources of osteogenic cells. *Journal of Orthopaedic Science* **10**, 192 - 199.

220. Nigg BM, Macintosh BR (2000) Biomechanics and biology of movement. Human Kinetics.

221. Nijweide PJ, Burger EH, Klein Nulend J, Van der Plas A (1996) The osteocyte. In: *Principles of bone biology*. Bilezekian JP, Raisz LG, Rodan GA. Academic press, San Diego.

222. Norrby E (2008) Nobel Prizes and the emerging virus concept. *Archives of Virology* **153**, 1109-1123.

223. O'Hagan DT, McGee JP, Lindblad M, Holmgren J (1995) Cholera toxin B subunit retains antigenicity and immunogenicity following encapsulation in biodegradable microparticles. *International Journal of Pharmacy* **119**, 251 - 255.

224. O'Hagan DT, Singh M, Gupta RK (1998) Poly(lactide-co-glycolide) microparticles for the development of single-dose controlled-release vaccines. *Advanced Drug Delivery Reviews* **32**, 225 – 246.

225. Ohshima S, Kobayashi H, Yamaguchi N, Nishioka K, Umeshita-Sasai M, Mima T, Nomura S, Kon S, Inobe M, Uede T, Saeki Y (2002) Expression

of osteopontin at sites of bone erosion in a murine experimental arthritis model of collagen-induced arthritis: Possible involvement of osteopontin in bone destruction in arthritis. *Arthritis and Rheumatology* **46**, 1094 – 1101.

226. Oliveira GM, Ferraz MP, González PG, Serra J, Leon B, Pèrez-Amor M, Monteiro FJ. (2008) PLD bioactive ceramic films: the influence of CaO-P2O5 glass additions to hydroxyapatite on the proliferation and morphology of osteblastic like-cells. *Journal of Materials Science: Materials in Medicine* **19**, 1775 - 1785.

227. O'Mara, William C. (1990). Handbook of Semiconductor Silicon Technology. William Andrew Inc.

228. Pacifici M, Oshima O, Fisher LW, Young MF, Shapiro IM, Leboy PS (1990) Changes in osteonectin distribution and levels are associated with mineralization of the chicken tibial growth cartilage. *Calcified Tissues International* **47**, 51 - 61.

229. Papatheodorou LK, Malizos KN, Poultsides LA, Hantes ME, Grafanaki K, Giannouli S, Ioannou MG, Koukoulis GK, Protopappas VC, Fotiadis DI, Stathopoulos C (2009) Effect of transosseous application of low-intensity ultrasound at the tendon graft-bone interface healing: Gene expression and histological analysis in rabbits. *Ultrasound in Medical Biology* **35**, 576 – 584.

230. Papatheofanis FJ (1989) Contribution of hydroxyapatite to the tensile strength of the isobutyl-2-cyanoacrylate-bone bond. *Biomaterials* **10**, 185-186.

231. Park A, Cima LG (1996) *In vitro* cell response to differences in poly-L-lactide crystallinity. *Journal of Biomedical Research* **31**, 117 - 130

232. Park JH, Gu L, von Maltzahn G, Ruoslahti E, Bhatia SN, Sailor MJ (2009) Biodegradable luminescent porous silicon nanoparticles for *in vivo* applications. *Nature Materials* **8**, 331 - 316.

233. Park SA, Kim GH, Jeon YC, Koh YH, Kim WD (2008) 3D polycaprolactone scaffolds with controlled pore structure using a rapid prototyping system. *Journal of Materials Science* **20**, 229 – 234.

234. Park TG, Lu W, Crotts G (1995) Importance of *in vitro* experimental conditions on protein release kinetics, stability and polymer degradation in protein encapsulated poly(D,L-lactic acid-co-glycolic acid) microspheres. *Journal of Controlled Release* **33**, 211 – 222.

235. Parkhutik V (2000) Analysis of Publications on Porous Silicon: From Photoluminescence to Biology. *Journal of Porous* Materials **7**, 363 – 366.

236. Peck WA, Birge SJ, Fedak SA (1964) Bone cells: biochemical and biological studies after enzymatic isolation. *Science* **146**, 1476 – 1477.

237. Pernodet N, Maaloum M, Tinland B (1997) Pore size of agarose gels by atomic force microscopy. *Electrophoresis* **18**, 55 - 58.

238. Perry CC (2009) An overview of silica in biology: its chemistry and recent technological advances. *Progress in Molecular and Subcellular Biology* **47**, 295 – 313

239. Perumal S, Antipova O, Orgel JP (2008) Collagen fibril architecture, domain organization, and triple-helical conformation govern its proteolysis. *Proceedings of the National Academy of Scences. USA* **105**, 2824 – 2829.

240. Pichonat T, Gauthier-Manuel B (2006) A new process for the manufacturing of reproducible mesoporous silicon membranes. *Journal of Membrane Science* **280**, 494 – 500.

241. Pietak AM, Reida JW, Stotta MJ, Sayera M (2007) Silicon substitution in the calcium phosphate bioceramics. *Biomaterials* **28**, 4023 - 4032.

242. Poirer Y, Dennis DE, Klomparens K, Somerville C (1992) Polyhydroxybutyrate, a biodegradable thermoplastic, produced in transgenic plants. *Science* **256**, 520 – 523.

243. Poirier, Y.; Nawrath, C. Somerville, C. Production of polyhydroxyalkanoates, a family of biodegradable plastics and elastomers, in bacteria and plants. *Biotechnology* **13**, 142 – 150.

244. Porter AE, Patel N, Skepper JN, Best SM, Bonfield W (2003) Comparison of *in vivo* dissolution processes in hydroxyapatite and silicon-substituted hydroxyapatite bioceramics. *Biomaterials* **24**, 4609–4620

245. Porter AE, Patel N, Skepper JN, Best SM, Bonfield W (2004) Effect of sintered silicate-substituted hydroxyapatite on remodelling processes at the bone-implant interface. *Biomaterials* **25**, 3303 - 3314.

246. Powles JW, Spencer RF, Lovering AM (1998) Gentamicin release from old cement during revision hip arthroplasty. *Journal of Bone and Joint Surgery* **80**, 607 – 610.

247. Prabu P, Dharmaraj N, Aryal S, Lee BM, Ramesh V, Kim HY (2006) Preparation and drug release activity of scaffolds containing collagen and poly(caprolactone) *Journal of Biomedical Materials Research A* **79**, 153 – 158.

248. Raghoebar GM, Liem RSB, Bos RRM, van der Wal JE, Vissink A (2006) Resorbable screws for fixation of autologous bone grafts. *Clinical Oral Implants Research* **17**, 288 - 293.

249. Raines EW, Lane TF, Iruela-Arispe ML, Ross R, Sage EH.(1992) The extracellular glycoprotein SPARC interacts with platelet-derived growth factor (PDGF)-AB and -BB and inhibits the binding of PDGF to its receptors. *Proceedings of the National Academy of Scences. USA* **89**, 1281 – 1285.

250. Ramires PA, Cosentino F, Milella E, Torricelli P, Giaveresi G, Giardino R (2002) *In vitro* response of primary rat osteoblasts to tinania/hydroxyapatite coatings compared with transformed homan osteoblast-like cells. *Journal of Materials Science: Materials in Medicine* **13**, 797 – 801.

251. Ratner BD, Hoffman AS, Schoen FJ, Lemons JE (2004) Biomaterials science: an introduction to materials in medicine. Academic Press.

252. Reffitt DM, Ogston N, Jugdaohsingh R, Cheung HFJ, Evans BAJ, Thompson RPH, Powell JJ, Hampson GN (2003) Orthosilicic acid stimulates collagen type 1 synthesis and osteoblastic differentiation in human osteoblast-like cells *in vitro*. *Bone* **32**, 127 – 135.

253. Reffitt DM, Ogston N, Jugdaohsingh R, Cheung HRL, Evans BAJ, Thompson PRH, Powell JJ, Hampson GN (2003) Orthosilicic acid stimulates collagen type 1 synthesis and osteoblastic differentiation in human osteoblast-like cells *in vitro*. *Bone* **32**, 127 – 135.

254. Reinholt FP, Hultenby K, Oldberg A, Heinegard D (1990) Osteopontin - a possible anchor of osteoclasts to bone. *Proceedings of the National Academy of Scences. USA* **87**, 4473 – 4475.

255. Rivers TJ, Hudson TW, Schmidt CE (2002) Synthesis of a novel, biodegradable electrically conducting polymer for biomedical applications. *Advanced Functional Mat*erials **12**, 33 - 37.

256. Robinson RA, Watson ML (1952) Collagen-crystal relationships in bone as seen in the electron microscope. *Anatomical Record* **114**, 383 – 410.

257. Roche P, Goldberg HA, Delma PD, Malaval L (1999) Selective attachment of osteoprogenitors to laminin. *Bone* **24**, 329 – 336.

258. Rohner D, Hutmacher DW, Cheng TK, Oberholzer M Hammer B (2003) *In vivo* efficacy of bone-marrow-coated polycaprolactone scaffolds for the reconstruction of orbital defects in the pig. *Journal of Biomedical Materials Research Part B: Applied Biomaterials* **66**, 574 – 580.

259. Romberg RW, Werness PG, Riggs BL, Mann K (1986) Inhibition of hydroxyapatite crystal growth by bone-specific and other calcium-binding proteins. *Biochemistry* **25**, 1176 - 1180.

260. Rosengren A, Oscarsson S, Mazzocchi M, Krajewski A, Ravaglioni A (2003) Protein adsorption onto two bioactive glass-ceramics. *Biomaterials* **24**, 147 – 155.

261. Ruggiero SL, Mehrotra B, Rosenberg TJ, Engroff SL (2004) Osteonecrosis of the jaws associated with the use of bisphosphonates: a review of 63 cases. *Journal of Oral and Maxillofacial Surgery* **62**, 527-534.

262. Ruys AJ, Wei M, Sorrell CC, Dickson MR, Brandwood A, Milthorpe B (1995) Sintering effects on the strength of hydroxyapatite. *Biomaterials* **16**, 409 – 415.

263. Sage H, Vernon RB, Funk SE, Everitt EA, Angello J.(1989) SPARC, a secreted protein associated with cellular proliferation, inhibits cell spreading *in vitro* and exhibits $Ca^{2+}$-dependent binding to the extracellular matrix. *Journal of Cell Biology* **109**, 341 – 356.

264. Salonen J, Kaukonen AM, Hirvonen J, Lehto V-P (2008) Mesoporous silicon in drug delivery applications *Journal of Pharmaceutical Science* **97**, 632-653.

265. Sang-Hoon Rhee, Lee SJ (2007) Effect of acidic degradation products of poly(lactic-co-glycolic)acid on the apatite-forming ability of poly(lactic-co-glycolic)acid-siloxane nanohybrid material. *Journal of Biomedical Materials Research Part A* **83**, 799 – 805.

266. Schliephake H (2009) Tissue engineering in maxillofacial surgery. In: *Fundamentals of Tissue Engineering and Regenerative Medicine*. Springer Berlin Heidelberg.

267. Schwartz MP, Cunin F, Cheung RW, Sailor MJ (2004) Chemical modification of silicon surfaces for biological applications, *Physica Status Solidi A—Applied Materials* **202**,1380 – 1384.

268. Schwarz K (1973) A bound form of silicon in glycosaminoglycans and polyuronides. *Proceedings of the National Academy of Scences*. **70**, 1608 – 1612.

269. Seibel MJ, Robins SP, Bilezikian JP (1992) Urinary pyridinium crosslinks of collagen: specific markers of bone resorption in metabolic bone disease. *Trends in Endocrinology Metabolism* **3**, 263 – 270.

270. Seo YH, Nahm KS, An MH, Suh E-K, Lee YH, Lee KB, Lee HJ (1994) Formation mechanism and pore size control of light-emitting porous silicon*Journal of Appied Physics* **33**, 6425 – 6431.

271. Serda RE, Gu J, Bhavane RC, Liu X, Chiappini C, Decuzzi P, Ferrari M (2009) The association of silicon microparticles with endothelial cells in drug delivery to the vasculature. *Biomaterials* **30**, 2440 – 2448.

272. Serway RA (1998) Principles of Physics (2nd ed). Fort Worth, Texas. London: Saunders College Pub.

273. Sfeir C, Ho L, Doll BA, Azari K, Hollinger JO (2005) Fracture repair. In: Bone regeneration and repair: Biology and clinical applications. Eds. Lieberman JR, Friedlaender GE. Humana Press Inc., New Jersey

274. Shi X, Wang Y, Ren L, Gong Y, Wang DA (2009) Enhancing alendronate release from a novel PLGA/hydroxyapatite microspheric system for bone repairing applications. *Pharmaceutical Research* **26**, 422 - 430.

275. Singer BR, McLauchlan GJ, Robinson GM, Christie J. (1998) Epidemiology of fractures in 15,000 adults: The influence of age and gender. *Bone and Joint Surgery*. **80-B**, 243 – 248.

276. Sinha VR , Bansal K, Kaushik R, Kumria R, Trehan A (2004) Poly-ε-caprolactone microspheres and nanospheres: an overview. *International Journal of Pharmacy* **278**, 1 – 23.

277. Sinha VR, Trehan A (2008) Development, characterization, and evaluation of ketorolac tromethamine-loaded biodegradable microspheres as a depot system for parenteral delivery. *Drug Delivery* **15**, 365 – 372.

278. So K, Fujibayashi S, Neo M, Anan Y, Ogawa T, Kokubo T, Nakamura T (2006) Accelerated degradation and improved bone-bonding ability of

hydroxyapatite ceramics by the addition of glass. *Biomaterials* **27**, 4738 - 4744.

279. Soderling E, Herbst K, Larmas E, Yli-Urpo A (1996) Protein adsorption to a bioactive glass with special reference to precorrosion. *Journal of Biomedical Materials Research A* **31**, 525 – 531.

280. Soltanoff CS, Yang S, Chen W, Li YP (2009) Signaling networks that control the lineage commitment and differentiation of bone cells. *Critical Reviews in Eukaryotic Gene Expression* **19**, 1-46.

281. Sommerfeldt DW, Rubin CT (2001) Biology of bone and how it orchestrates the form and function of the skeleton. *European Spine Journal* **10**, 86 – 95.

282. Sripanyakorn S, Jugdaohsingh R, Elliott H, Walker C, Mehta P, Shoukru S, Thompson RPH, Powell JJ (2004) The silicon content of beer and its bioavailability in healthy volunteers. *British Journal of Nutrition* **91**, 403 – 409.

283. Sripanyakorn S, Jugdaohsingh R, Thompson RPH, Powell JJ (2005) Dietary silicon and bone health. *Nutrion Bulletin* **30**, 222 – 230.

284. Stein GS, Lian J, Stein JL, vanWijnen AJ, Frenkel B, Montecino M (1996) Mechanisms regulating osteoblast proliferation and differentiation. In: *Principles of Bone Biology*. Bilezikian JP, Raisz LG, Rodan GA, Eds. Academic Press, San Diego.

285. Stevens B, Yang Y, Mohandas A, Stucker B, Nguyen KT (2008) A review of materials, fabrication methods, and strategies used to enhance bone regeneration in engineered bone tissues. *Journal of Biomedical Materials Research B. Applied Biomaterials* **85**, 573 – 582.

286. Stevens, ES (2001) Green Plastics: An Introduction to the New Science of Biodegradable Plastics. Princeton University Press. p72.

287. Stocks G, Janssen HF (2000) Infection in patients after implantation of an orthopedic device. *ASAIO Journal* **46**, 41 - 46.

288. Sudo H, Kodama H-A, Amagai Y, Yamamoto S, Kasai S (1983) *In vitro* differentiation and calcification in a new clonal osteogenic cell line derived from newborn mouse calvaria. *Journal of Cell Biology* **96**, 191 – 198.

289. Suess HE, Urey HC (1956) Abundances of the elements *Reviews in Modern Physics* **28**, 53 – 74.

290. Supova M (2009) Problem of hydroxyapatite dispersion in polymer matrices: a review. *Journal of Materials Science – Materials in Medicine* [**20**, 1201 – 1213.

291. Takeda J, Hashimoto K, Tanaka M, Iwai H, Kakegawa T (1990) Experimental and clinical evaluation of the splenic capping method in the treatment of injured spleens. *Journal Surgery Today* **20**, 137 – 142.

292. Tan PS, Teoh SH (2006) Effect of stiffness of polycaprolactone (PCL) membrane on cell proliferation. *Materials Science and Engineering* **27**, 304 – 308.

293. Tang C, You F, Cheng G, Gao D, Fu F, Yang G, Dong X (2008) Correlation between structure and resistivity variations of the live human skull. *IEEE Transactions on Biomedical Engineering* **55**, 2286 – 2292.

294. Teti A, Zallone A (2009) Do osteocytes contribute to bone mineral homeostasis? Osteocytic osteolysis revisited. *Bone* **44**, 11 - 16.

295. Thomas V, Moncy JV, Jowdhury S, Sullivan JF, Dean DR, Vohra YK (2006) Mechano-morphological studies of aligned nanofibrous scaffolds of polycaprolactone fabricated by electrospinning. *Journal of Biomaterials Science* **17**, 969 – 984.

296. Thompson DW (1992) On growth and form. The complete revised edition. Dover, New York.

297. Tidermark J (2006) Cemented versus uncemented hip replacement. *Disability and Rehabilitation* **28**, 243.

298. Tolstoy VP, Chernyshova IV, Skryshevsky VA (2003) Handbook of infrared spectroscopy of ultrathin films. John Wiley and Sons.

299. Trentz OA, Handschin AE, Platz A, Trentz O, Zund G, Hoerstrup SV (2003) Phenotypic osteoblasts for *in vitro* testing of bone implants and substitutes. *European Cells & Materials Journal* **5**, 92.

300. Tu Y-K, Kato T, Bishop AT (2000) Investigation of endothelial control of bone blood flow: Development of a rabbit tibia *ex vivo* perfusion model. *Journal of Musculoskeletal Research* **4**, 85 – 96.

301. Väänänen HK, Zhao H, Mulari M, Halleen JM (2000) The cell biology of osteoclast function. *Journal of cell science* **113**, 377 – 381.

302. Vaccari L, Canton D, Zaffaroni N, Villa R, Tormen M, di Fabrizio E (2006) Porous silicon as drug carrier for controlled delivery of doxorubicin anticancer agent, *Microelectronics Engineering* **83**, 1598 – 1601.

303. Vanderschot P, Cuypers PH, Rommens P, Broos P (1993) Splenic function after splenic rupture treated with an absorbable mesh. *Unfallchirurg* **96**, 248 - 252.

304. Varde NK, Pack DW (2004) Microspheres for controlled release drug delivery. *Expert Opinion in Biological Therapy* **4**, 35 – 51.

305. Venugopal JR, Low S, Choon AT, Kumar AB, Ramakrishna S (2008) Nanobioengineered electrospun composite nanofibers and osteoblasts for bone regeneration. *Artificial Organs* **32**, 388 - 397.

306. Wahlig H, Dingeldein E, Buchholz HW, Buchholz M, Bachmann F (1984) Pharmacokinetic study of gentamicin-loaded cement in total hip replacements. Comparative effects of varying dosage. *Journal of Bone and Joint Surgery* **66**, 175 - 179.

307. Walker NA, Denegar CR, Preische J (2007) Low-intensity pulsed ultrasound and pulsed electromagnetic field in the treatment of tibial fractures: a systematic review. *Journal of Athletics Training* **42**, 530 – 535.

308. Wan Y, Qua X, Lu J, Zhu C, Wan L, Yang J, Bei J, Wang S (2004) Characterization of surface property of poly(lactide-co-glycolide) after oxygen plasma treatment. *Biomaterials* **25**, 4777 – 4783.

309. Wang P, Hu J, Ma PX (2009) The engineering of patient-specific, anatomically shaped, digits. *Biomaterials*. **30**, 2735-2740.

310. Wang Y, Lu L, Zheng Y, Chen X (2006) Improvement in hydrophilicity of PHBV films by plasma treatment. *Journal of Biomedical Materials Research A* **76**, 589 – 595.

311. Warfield RW, Petree MC (1961) Electrical resistivity of polymers. *Polymer Engineering Science* **1**, 80 – 85.

312. Weber GF, Ashkar S, Glimcher MJ, Cantor H (1996) Receptor-ligand interaction between CD44 and osteopontin (eta-1). *Science* **271**, 509 – 512.

313. Weinbaum S, Cowin SC, Zeng Y (1994) A model for the excitation of osteocytes by mechanical loading-induced bone fluid shear stresses. *Journal of Biomechanics* **27**, 339 – 360.

314. Wendel M, Sommarin Y, Heinegård D. (1998) Bone matrix proteins: isolation and characterization of a novel cell-binding keratan sulfate proteoglycan (osteoadherin) from bovine bone. *Journal of Cell Biology* **141**, 839 – 847.

315. Whitehead MA, Fan D, Mukherjee P, Akkaraju GR, Canham LT, Coffer JL. (2008) High-porosity poly(epsilon-caprolactone)/mesoporous silicon scaffolds: calcium phosphate deposition and biological response to bone precursor cells. *Tissue Engineering Part A* **14**, 195 - 206.

316. Whitehead MA, Fan D, Mukherjee P, Akkaraju GR, Canham LT, Coffer JL (2008) High-porosity poly(epsilon-caprolactone)/mesoporous silicon scaffolds: calcium phosphate deposition and biological response to bone precursor cells. *Tissue Engineering Part A* **14**, 195 – 206.

317. Whiteside, LA., Simmons, DJ., Lesker, PA. (1977) Comparison of regional bone blood flow in areas with differing osteoblastic activity in the rabbit tibia. *Clinical Orthopaedic Related Research* **124**, 267 – 270.

318. Widmann, Dietrich (2000). Technology of integrated circuits. Springer.

319. Williamson MR, Adams EF, Coombes AGA (2002) Cell attachment and proliferations on novel polycaprolactone fibres having application in soft tissue engineering. *European Cells and Materials* **4**, 62 – 63.

320. Willoughby AF (2006) Design and processing of porous materials for electronic applications. *Philosophical Transactions A. Mathematics, Physics and Engineering Science* **364**, 175 – 187.

321. Windham BP, Jordan JR, Parsell DE (2007) Comparison of pullout strength of resorbable screws and titanium screws in human cadaveric laryngeal cartilage. *Laryngoscope* **117**, 1964 – 1968.

322. Wise DL (1995) Encyclopedic handbook of biomaterials and bioengineering. Marcel Dekker.

323. Worland VP (1997) A mathematical model (AMIGA) of solution chemistry and silica solubility in high silica water at Los Alamos National Laboratory, Ph.D thesis, New Mexico State University.

324. Wright I, Zernicke RF, Uluda H (2009) Improved bone delivery of osteoprotegerin by bisphosphonate conjugation in a rat model of osteoarthritis. *Molecular Pharmaceutics*, Published online [10.1021/ mp8002368].

325. Wright JE, Gittens SA, Bansal G, Kitov PI, Sindrey D, Kucharski C, Uludağ H (2006) A comparison of mineral affinity of bisphosphonate-protein conjugates constructed with disulfide and thioether linkages. *Biomaterials* **27**, 769 – 784.

326. Wu F, Jin T (2008) Polymer-based sustained-release dosage forms for protein drugs, challenges, and recent advances. *AAPS PharmSciTech.* **9**, 1218 - 1229.

327. Xynos IE, Alasdair JE, Buttery LDK, Hench LL, Polak JM (2001) Gene-expression profiling of human osteoblasts following treatment with the ionic products of Bioglass 45S5, *Journal of Biomedical Material Research* **55**, 151 – 157.

328. Yamaguchi A, Komori T, Suda T (2000) Regulation of Osteoblast Differentiation Mediated by Bone Morphogenetic Proteins, Hedgehogs, and Cbfa. *Endocrine Review* **21**, 393 – 411.

329. Yamanouchi K, Gotoh Y, Nagayama M (1997) Dexamethasone enhances differentiation of human osteoblastic cells *in vitro*. *Journal of Bone Mineral Metabolism* **15**, 23 – 29.

330. Yang L, Tao T, Wang X, Du N, Chen W, Shuqing T, Wang Z, Wu L (2003) Effects of dexamethasone on proliferation, differentiation and apoptosis of adult human osteoblasts *in vitro*. *Chinese Medical Journal* **116**, 1357 – 1360.

331. Yaszemski MJ, Trantolo DJ, Lewandrowski K-U, Wise DL, Hasirci V, Altobelli DE (2003) Biomaterials in orthopaedics. Informa healthcare, p 206.

332. Yeong W-Y, Chua C-K, Leong K-F, Chandrasekaran M, Lee M-W (2006) Indirect fabrication of collagen scaffold based on inkjet printing technique. *Rapid Prototyping Journal* **12**, 229 – 237.

333. Yokosaki Y, Tanaka K, Higashikawa F, Yamashita K, Eboshida A (2005) Distinct structural requirements for binding of the integrins alphavbeta6, alphavbeta3, alphavbeta5, alpha5beta1 and alpha9beta1 to osteopontin. *Matrix Biology* **24**, 418 – 427.

334. Zdero R, Olsen M, Bougherara H, Schemitsch EH (2008) Cancellous bone screw purchase: a comparison of synthetic femurs, human femurs, and finite element analysis. *Proceedings of the Institute of Mechanical Engineers, Part H*. **222**, 1175 - 1183.

335. Zhang K, Loong SL, Connor S, Yu SW, Tan SY, Ng RT, Lee KM, Canham L, Chow PK (2005) Complete tumor response following intratumoral 32P BioSilicon on human hepatocellular and pancreatic carcinoma xenografts in nude mice. *Clinical Cancer Research* **11**, 7532 – 7537.

336. Zhang QH, Tan SH, Chou SM (2006) Effects of bone materials on the screw pull-out strength in human spine. *Medical Engineering and Physics* **28**, 795 – 801.

337. Zhao M (2008) Electrical fields in wound healing - an overriding signal that directs cell migration. *Seminars in Cell Developmental Biology* [Epub ahead of print].

338. Zhao M, Song B, Pu J, Wada T, Reid B, Tai G, Wang F, Guo A, Walczysko P, Gu Y, Sasaki T, Suzuki A, Forrester JV, Bourne HR, Devreotes PN, McCaig CD, Penninger JM (2006) Electrical signals control wound healing through phosphatidylinositol-3-OH kinase-gamma and PTEN. *Nature* **442**, 457 – 460.

# Appendix

# -

# Applications

## 1. Introduction.

In this investigation, porous silicon-polycaprolactone composites have been evaluated for applications in orthopaedic tissue engineering, with the degradation and bioactivity characteristics tested and the material properties identified. Throughout this work, attention has been given to the potential applications of this technology, allowing the material to be tested in the most appropriate ways and reflecting the genesis of the project as a combination of empirical academic research and industrial sponsorship.

This approach is becoming increasingly favourable in the field of biomaterials research and tissue engineering, as the number of patented biomaterials increases and companies are established to exploit this technology in relevant biomedical niches. With this in mind, at an early stage in the project the potential applications of pSi-PCL composites were researched and discussed, initially with Professor Leigh Canham and Dr Susan Anderson, and subsequently with consultant orthopaedic surgeons, Miss Brigitte Scammell (orthopaedic fixation), Mr Iain McVicar (maxillofacial reconstruction and fixation), and Dr Roger Bayston (antibiotic-eluting biomaterials).

The most relevant applications for pSi-composites based on analysis of the current (2009) orthopaedics market were therefore considered to be:

- Porous scaffolds for maxillo-facial reconstruction.
- Biodegradable screws for plate fixation.
- Enhancing the bone-bonding ability of bone cement.

This appendix describes the preliminary research that was performed to assess the suitability of pSi-composites for these applications and describes the methods that were developed for creating 3-D porous scaffolds, biodegradable fixation screws and bioactive pSi-PMMA bone cements.

### 1.1. 3-Dimensional porous composites for tissue engineering..

For a material to function as a tissue engineering scaffold for therapeutic or reconstructive use it is essential that a network of inter-connected pores is available through the material through which osteoblasts can migrate and deposit extracellular matrix (reviewed in Stevens *et al*, 2008).

The pore size diameter required to allow passage of osteoblasts and vascularisation is considered to be >300-500μm (Chen *et al*, 2008), with the accompanying porosity required to be at least 60% in order for sufficient bone to grow to take transferred stresses as the resorbable scaffold degrades in strength. To enable osteoblast ingress through the material the pores must be continuously interconnected as pores forming internal voids do not permit tissue ingrowth and significantly weaken the material.

A large array of techniques have been developed to porosify biomaterials, ranging in technical complexity from aeration of the polymer during formation to supercritical fluid degassing and rapid prototyping (Stevens *et al*, 2008), illustrated in **fig. 1**. Use of porogens such as salt or sugar crystals embedded in the matrix to create a two-phase composite is a common and inexpensive technique: as the salt/sugar phase is soluble in water, soaking of the composite results in the porogen being released into solution, leaving pores in the material with the dimensions of the porogen (e.g. cubic for salt crsytals).

Problems with salt leaching are that the porogens, even when loaded in high density, are not contiguous and many crystals are left behind following leaching. Additionally, as shown in **fig. 1.A**, the cubic dimensions of the pores are not ideally suited to osteoblast colonisation – rounded, tubular pores with regular diameters and interconnections are preferable for vascularisation and tissue deposition in the scaffold (Stevens *et al*, 2008).

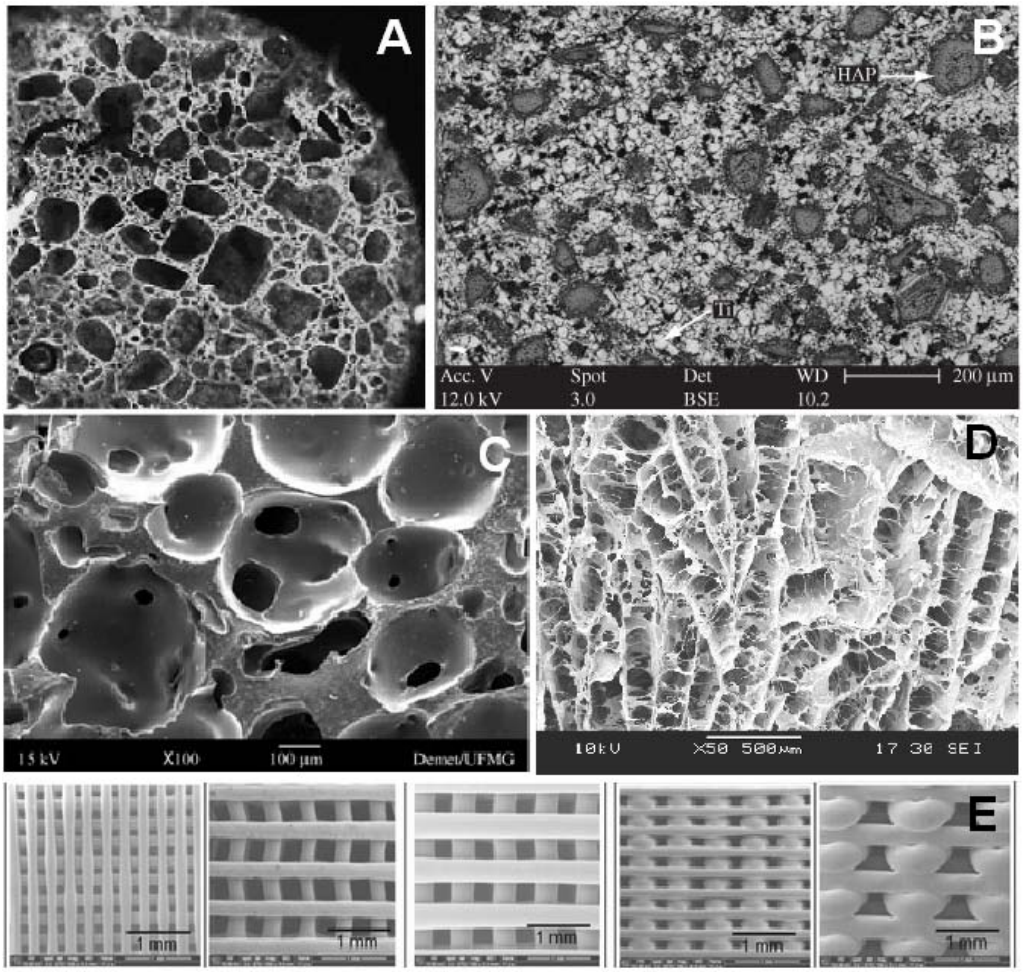


**Fig. 1.** Techniques used for porosifying biomaterials range from low-technology methods such as **a**) NaCl salt leaching from PLGA[1] , **b**) sintering of hydroxyapatite and titanium microparticles[2], and **c**) emulsification of PLGA containing 20% Bioglass®[3], to more advanced, controllable methods such as **d**) inkjet printing of collagen[4], and **e**) computer controlled melt-plot rapid prototyping using polycaprolactone[5]. From [1]The Royal Society of Chemistry webpages; [2]Marcelo *et al*, 2006; [3]Costa *et al*, 2007; [4]Yeong *et al*, 2006; [5]Park *et al*, 2008.

In this investigation, mostly 'two-dimensional' composites have been tested, i.e. bulk materials without any internal architecture and with only exterior surfaces to support cell attachment and growth. To create 'three-dimensional' materials with a network of internal spaces for cell ingrowth, a number of porogenic techniques were applied and evaluated, including:

- Sucrose leaching
- Starch leaching
- Inulin (a carbohydrate)
- Gelatin granule leaching
- PCL-Poly(vinyl alcohol) emulsion/admix

It was determined that these techniques, whilst successful in developing pores in the material, resulted in an uninterconnected network and so subsequent development of 3-D materials focussed on the creation of a dissolvable pore template. In these experiments, rapidly soluble polymers were employed to create a solid 'negative' of the pores, such that the casting of PCL or composite around the template and subsequent washing would result in a porous material with interconnected internal spaces (**fig. 2**).

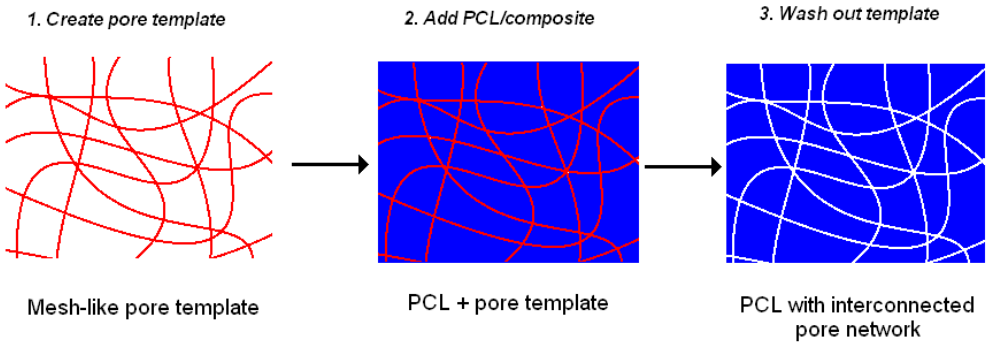


**Fig. 2.** Porosification using a soluble pore template. **1**. Pore template is formed using a variety of methods, **2**. PCL/composite is added either melted or in solution with acetone, **3**. The template is removed by washing, leaving a 3-D network of interconnected pores.

Several soluble pore templates were trialed, all of which were chosen for their solubility and ease of being drawn into fibres or deposited as strands, including:

- Porcine skin collagen
- Poly(vinyl alcohol)
- Polymerised sucrose (caramel)

When heated to 170°C, sucrose undergoes caramelization, a series of complex reactions which results in a molten polymer which can be stretched or spun into fibres. A traditional use of this polymer has been to create spun sugar meshes and lattices for confectionery, meshes which comprise a network of strands which overlap, forming an interconnected mesh with strands 50-100 micrometers in diameter.

This part of the investigation outlines experiments which were performed to evaluate this method for porosifying PCL-based composite biomaterials.

### 1.2. Composite orthopaedic fixation screw.

Orthopaedic fixation is traditionally by means of stainless steel or titanium pins and screws, manufactured in a range of sizes to suit all applications from fixing long bones such as femur to attaching small plates in paediatric maxillo-facial surgery (Allgower & Perren, 1991). Metal screws can be manufactured in a wide range of shapes and sizes and tailored to quite specific uses and are regulated in the UK by Section 5 of British Standard BS 3531 (**fig. 3).** For plate fixation in maxillo-facial applications, however, metal screws are generally very similar, having the basic profiles illustrated in **fig. 4**.

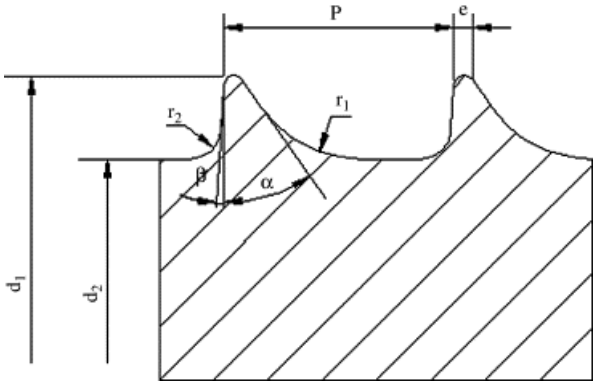


**Fig. 3.** Cross section of a standard (4mm) cortical bone screw with asymmetrical thread and spherical under-surfaces, based on the British Standard BS3531 [British Standards Institution, Implants for osteosynthesis. Part 5, Bone screws and auxiliary equipment. Section 5.3, specification for the dimensions of screws having hexagonal drive connection, spherical under surfaces and asymmetrical thread, BSI, London (1991)]. From Zhang *et al* (2006).

Interest in using biodegradable screws has developed due to the potential for overcoming serious problems in metallic fixation, including the complications arising from the persistence of metal screws or the requirement for subsequent removal, interference with bone healing or interference with tissue growth and function, particularly in paediatric fixation (Moisala *et al*, 2008; Cavusoglu *et al*, 2005).

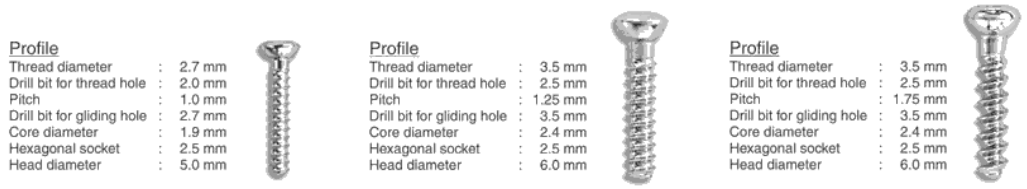


**Fig. 4.** Examples of small stainless steel orthopaedic screws manufactured by Smit Medimed Pvt. Ltd. (Ahmedabad, India) suitable for maxillo-facial fixation which formed the basis for the screw designed for this investigation.

As such, numerous resorbable or integrative devices have been developed, patented, trailed and authorised for clinical use, including:

- Screws manufactured from de-cellularised bovine or human cortical bone (Haje & Volpon, 2006)
- Fully resorbable polylactide screws (marketed by Inion)
- Polylactide-Hydroxyapatite/ Bioglass® composite screws (Lewandrowski *et al*, 2002; Berry, 2008)

Of the commercially available bioresorbable polymer screws, those marketed by Inion Ltd. (www.inion.com Tampere, Finland) have been most successful in the UK (discussed with Mr Iain McVicar, consultant oral and maxillofacial surgeon, Queen's Medical Centre, Nottingham, UK) with a variety of screw and plate combinations available for almost all small fixation applications and authorised for use in National Health Service hospitals.

Inion use a combination of four polymers – trimethylene carbonate (TMC), L-polylactic acid (LPLA), D,L-polylactic acid (DLPLA) and polyglycolic acid (PGA) to create a co-polymer with optimised degradation and strength. The development

of a specific polymer blend is beyond the remit of this investigation, but the addition of pSi to a generalised polymer such as polycaprolactone provides an insight into the change in mechanical properties of the resulting polymer-composite, with applications in enhancing the bioactivity of existing polymer blends for fixation.

The tensile properties of composites are particularly important in fixation applications using screws, and those of pSi-PCL are discussed in Chapter 6. An important parameter with regard to orthopaedic screws is push-out (or pull-out) strength – the force required to evict a screw from the plate or bone (Zhang *et al*, 2006) which is also a measure of the material's shear strength, resistance to torsional forces during implantation and thread stability.

Lewis *et al* (2008) and Windham *et al* (2008) show that in some applications, use of a polylactide-based screw is advantageous over the use of titanium or steel, as the tissue (in both cases laryngeal cartilage) is not 'stripped' by metal screw threads when longitudinal forces are applied. Comparisons between titanium and resorbable screws (Lewis *et al*, 2008) showed that this increases the linear pull-out force required to remove the screw.

This part of the investigation covers the work that was done in identifying the parameters of resorbable screw design and evaluates the effect of adding porous silicon to PCL on push-out strength of screws from a mould.

### 1.3. Poly(methyl methacrylate) bone cement.

Certain orthopaedic devices, particularly total knee and hip arthroplasties are secured in place using a bone cement based on poly(methyl methacrylate) (PMMA) to fix the artificial components to the living bone. However, this approach has become increasingly unfavourable for several reasons:

- The cement acts analogously to grout, forming a filler in spaces between the implant and the bone and is a common location for loosening of the implant and subsequent failure.
- The cement is not osteoconductive and is non-porous, so no bone ingrowth secures the prosthesis.
- Microfractures and bubbles in the cement create localised weaknesses in the join which can lead to failure.
- During revision, the bone cement has to be chiselled out and replaced, leaving a much larger space to fill in subsequent implantations.

These factors lead to the development of an alternative approach which involved surgeons drilling a slightly too small hole and using physical force to secure a titanium implant in place, as titanium is capable of bonding directly to the surrounding bone (Allgower & Perren, 1991). This technique has found less success in knee arthroplasty however, where the components of the artificial joint need to be securely fixed to the outside edges of the bone. Additionally after a decade of clinical use it was found that the failure rates of cemented and non-cemented prostheses were similar (Hedley *et al*, 1987). Cemented prostheses are still favoured for most applications, particularly in elderly, osteoporotic patients and those undergoing undergoing revision.

Despite the wide use of PMMA, the cement composition has remained largely unchanged since its clinical inception 30 years ago, being primarily poly(methyl methacrylate) (also known commercially as Perspex or acrylic) with residual polymerising agents (benzoyl peroxide and N,N-dimethyl-para-toluidine - DMPT) as well as barium sulphate to render the cement X-ray opaque.

The cement is delivered to surgeons as a kit, composed of 40g powdered PMMA containing benzoyl peroxide and barium sulphate, and a liquid phase composed of 20ml MMA monomer and DMPT. The liquid is added to the powder and mixed under vacuum to minimise air bubbles and injected into the implant site where polymerisation takes place to harden the cement, accompanied by an increase in temperature to ~50˚C.

Gentamicin- and other aminoglycoside- loaded bone cement was first used clinically in the 1970s, less than a decade after poly(methyl methacrylate) (PMMA) itself was first applied in prosthesis fixation (Gardner & Medcraft, 1974). The loading ratios and release kinetics of aminoglycoside-bone cements have been well characterised over the last four decades and the mechanical properties of adding such substances evaluated (Lautenshlager *et al*, 1977). Commercial products such as Depuy 1 Gentamicin Bone Cement (Depuy Orthopaedics, USA) and Simplex™ (releasing tobramycin, Stryker Orthopaedics, USA) contain 1g gentamicin mixed into the 40g powder component of the cement (approximately 1.5% final concentration, *w/w*). Clinicians may choose to add gentamicin separately to the PMMA and favour a high-loading of gentamicin, commonly >9% *w/w* loading and up to 20% for treatment of active infections in revisions (Lautenshlager *et al*, 1977).

PMMA bone cement is not biodegradable, osteoinductive or permeable to water and consequently only a small percentage of the antibiotic is released into the wound site in a burst release following would closure. PMMA is also weaker than bone in terms of tensile and compressive strength, but it has been found that addition of low-doses (up to ~9%) of antibiotics do not adversely affect the mechanical properties of the cement and indentation resistance is actually increased (Lautenshlager *et al*, 1977). The primary concerns with antibiotic-releasing cements is developing an immune response to high-doses and the possibility of gentamicin-resistant bacterial infections developing.

The quantity of antibiotic released is difficult to assess however, as the surfaces and flow rates of fluid around the wound are highly variable in each case. An additional complication is presented during prosthesis revisions as high doses of gentamicin have been found to be released as the PMMA bone cement is chipped off during removal of the implant (Powles *et al*, 1998). This can complicate further antibiotic treatment as systemic dosages must be recalculated with this in mind.

To comply with ISO 5833:2002 (Lee, 2005), for set and cured acrylic bone cements with or without antibiotics or other inclusions, cement must meet or exceed the following specifications:

- Compressive strength 70 MPa
- Bending modulus 1800 MPa
- Bending strength 50 MPa

**Fig. 5.** shows results from Lautenschlager *et al* (1976) comparing the compressive and tensile strength of increasingly higher doses of gentamicin in bone cement. This figure shows that whilst the mechanical properties are not dramatically affected up to 5g (~8-9% *w*/*w*), higher doses of antibiotics in the cement cause the material to fail the ISO standard.

Despite this approach, bone cement is a poor releaser of antibiotics as it is non-permeable to water, therefore antibiotics are only released from the surface in a large single dose lasting several days (Lee *et al*, 2005). A drug-loading mechanism which provides for a slower, more controlled release of antibiotics is advantageous, providing it can be shown that the mechanical properties of the cement are not lower than for a given quantity of antibiotic directly loaded into the cement.

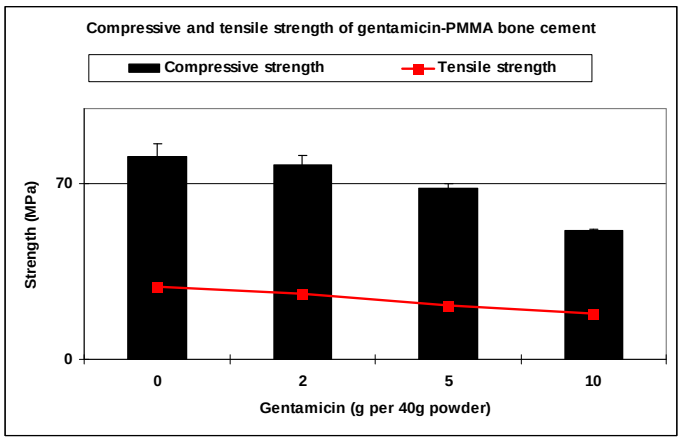


**Fig. 5.** Compressive and tensile strength of PMMA bone cement loaded with gentamicin (adapted from Lautenschlager *et al*, 1976). ISO 5883 standard minimum compressive strength is 70 MPa, indicated by the horizontal line.

Porous silicon may be a useful material to include in bone cement as not only has it been shown to gradually elute the aminoglycoside antibiotic gentamicin (Chapter 4), it also forms an osteoconductive coating to materials, enhancing the

rate of bone repair and may act to form a boney bridge from the living bone to the implant surface (**fig. 6**).

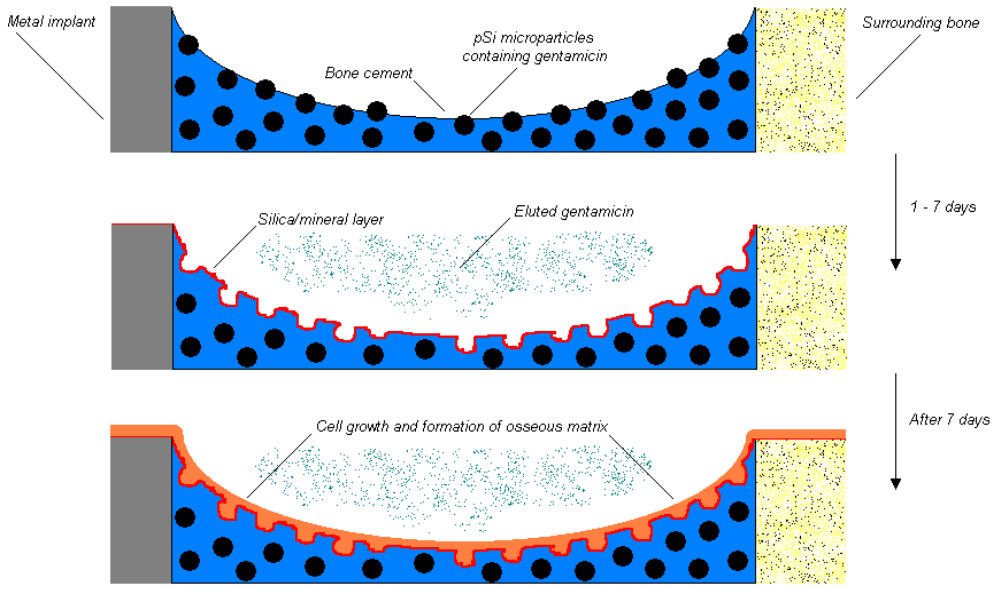


**Fig. 6.** Schematic of anticipated action of bone cement containing pSi/gentamicin microparticles. Immediately following implantation the silicon begins to oxidise in the aqueous environment, releasing silicic acids which condense into a silica gel, trapping growth factors and forming a bed for mineral deposition.

## 2. Materials and methods.

### 2.1. Fabrication of 3-D scaffolds.

Several methods for porosifying PCL and pSi-PCL using water-soluble particulate and mesh-formed porogens were tested:

#### 2.1.1. Particulate porogens.

10g PCL was dissolved in 5 ml acetone at 40°C and stirred until homogenous. 2g sucrose crystals, PVA powder, starch powder, porcine skin collagen (all Sigma, UK) or inulin (FibreSure, UK) were added and the mixture stirred until dispersed. The mixtures were cast inside a 10ml polypropylene syringe body and allowed to air dry at room temperature overnight.

The cylinders were cut into discs and the porogens washed out in three changes of $dH_2O$, stirred using a magnetic flea in water heated to 30°C for one hour per change. Discs were dried and gold coated using a sputter coater before being imaged in a Jeol JSM8340 scanning electron microscope.

#### 2.1.2. Porosification using soluble templates.

Templates were formed using porcine skin collagen and poly(vinyl alcohol) (both sigma, UK) by dissolving 20g polymer in 5-10ml water at 30°C and stirring until a homogenous and viscous solution was formed. The solution was poured into a 10ml polypropylene syringe which was fitted with a small-diamter nozzle fashioned from a 20µm pipette tip. The solution was forced through the nozzle directly over a 250ml measuring colmn containing 200ml ethanol at -80°C.

Rapid cooling plus substitution of ethanol for water in the polymer solution precipitated the polymer into a continuous strand which collected as a solid three-dimensional coiled mesh at the base of the measuring cylinder.

The mesh was removed and dried at room temperature and placed into a vertical 10ml polypropylene syringe body. 20g of PCL dissolved in 10ml acetone was added and allowed to permeate through down the mesh before being cooled to -80°C to rapidly cast the PCL. The PCL-template was allowed to air dry overnight before being cut into discs and the pore template washed out in three changes of $dH_2O$, stirred using a magnetic flea in water heated to 30°C for one hour per change. Discs were dried and gold coated using a sputter coater before being imaged in a Jeol JSM8340 scanning electron microscope

**2.1.3. Porosification using caramelised sucrose templates.**

Sucrose (Sigma, UK) was heated without stirring on a hotplate set to 180°C until melted and a colour change from colourless to light brown was observed. Sugar was spun in two ways, firstly by flicking the caramel from the end of a spoon in a random patttern onto siliconised paper.

The second method was by immersing a purpose-made 16-prong fibre spinning tool in the caramel and passing it across a siliconised sheet as shown in **fig. 7**. Secured filter paper pads acted as anchoring points for the fibres which were stretched across the sheet and fixed onto a second pad. The tool was moved to a third side and the process repeated. Caramel was reapplied every 15-20 passes and each pass was performed as quickly as possible to prevent cooling and breakage of the fibres. Once a sufficent amount was deposited the central region containing strands running in both directions was removed and used as a pore template

10mg polycaprolactone was dissolved in 10ml acetone at room temperature and stirred until homogenous. The caramel pore template was placed on a sheet of siliconised paper and the polmer solution poured over and allowed to dry. Once set, the edges of the polymer were removed to expose the caramel-contaning region and the material placed in 500ml water, stirred at 30°C for 24 hours until all the caramel had removed.

In a second experiment, porous silicon (70% porous, 10µm particle size) microparticles were added to polycaprolactone in acetone at 8% composite weight

(20mg per 250mg PCL). The above process was repeated to provide a porosified composite. Analysis was by scanning electron microscopy. 5.0 mm sections of the material were cut, gold-coated and mounted on aluminium stubs for imaging.

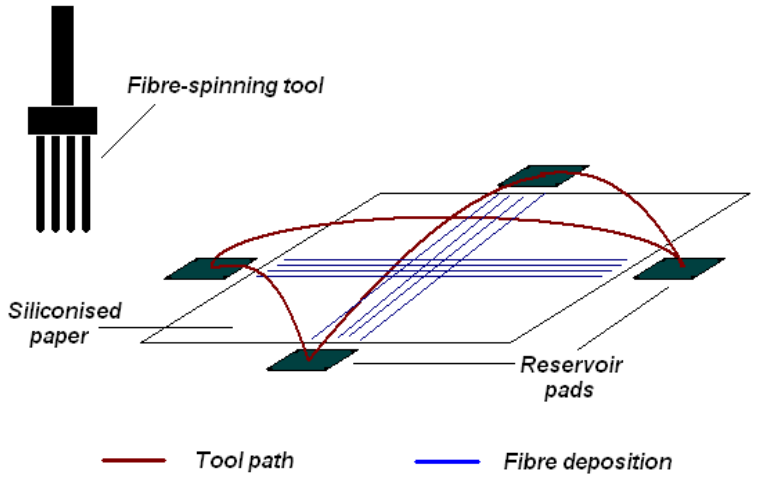


**Fig. 7.** Diagram of caramel porogen spinning technique. Caramelised fructose at 160-180°C is applied to the fibre spinning tool which is then touched to a reservoir pad and fibres stretched to an opposing pad. The tool is moved to a an adjacent pad (90°) and the process repeated to form a cross-hatched region in the middle of the paper which is subsequently used for porogenesis.

**2.2. Screw fabrication.**

Example screws were manufactured from either extruding melted polymer/composite into a custom made composite mould based on measurements taken from a similarly sized titanium screw (2.5mm diameter, 6mm length) or melt-cast inside a stainless steel nut (internal diameter 12mm, length 14mm). Mechanical testing was performed using screws cast inside stainless steel nuts using an Instron 5569 compressive testing system with a 50 KN load cell.

The nut was held in a recessed block over a central hole and a 6mm diameter steel dowel clamped in the upper grip. The dowel was lowered to touch the

polymer/composite surface and then pushed out through the nut at 2 mm/min. The force (N) required to push out the screw was measured for PCL and 4% or 8% composites and the failure mode determined by SEM of sections through the pushed-out material.

### 2.3. PMMA bone cement incorporating pSi.

#### 2.3.1. Characterisation of pSi-PMMA in water.

Composites containing 8% pSi in PMMA were made by mixing PMMA in acetone (66% *w/v*) with pSi microparticles and casting in the body of a 5ml polypropylene syringe. Whilst residual acetone was present in the composite, discs were cut from the cylinder and air-dried overnight at room temperature before weighing, resulting in 250mg ± 10mg discs. PMMA discs were made by the same process without the addition of pSi. Discs were incubated in 50ml $dH_2O$ at 37°C for 24 weeks in 50ml polypropylene screw-capped tubes. 400µl of the incubation solution was removed, replaced and tested for silicic acid using the molybdenum blue assay every week for 8 weeks.

At 4, 8, 12 and 24 weeks the discs were removed from the solution and allowed to air dry overnight at room temperature before being observed and reweighed to assess mass loss/gain. At 4 and 8 weeks the pH of the solution was measured using a Hannah 120 bench top pH meter.

#### 2.3.2. Response of osteoblasts to pSi-PMMA composites *in vitro*.

pSi-PMMA composite discs were formed using acetone and containing 0, 1, 10 or 20 mg pSi weighing 250mg ± 10mg and sterilised in 70% ethanol before being dried completely overnight in 24-well plates (Nunc) in a sterile fume hood.

Osteoblasts were cultured to passage 30 - 35 in DMEM supplemented with 10% FCS, 2mM L-glutamine, 1% non-essential amino acids, 0.2mM HEPES, 150µg.ml$^{-1}$ ascorbic acid, 2% penicillin/streptomycin and with 10mM sodium β-

glycerophosphate and $10^{-7}$M dexamethasone (all Sigma, UK). Cells were seeded at a density of ~$10^5$ cells.ml$^{-1}$ directly onto the disc surface with a disc-free well used as a control.

1ml media was added per well which was replaced daily for 28 days. One plate was analysed every 7 days by rinsing each well carefully in PBS followed by freeze-thawing the plate with 1.0ml $H_2O$ per well for three cycles between -80°C and 20°C. DNA and collagen were quantified and alkaline phosphatase activity was measured at each time point. At 28 days, osteoblasts growing on 54% composite discs were stained and assayed for calcium only.

Cell lysates and discs/wells were analysed for DNA and collagen content, alkaline phosphatase content and calcium deposition as described in section **3.2.2.**

**2.3.3 Drug release from PMMA-pSi composites.**

A 66% (*w*/*v*) solution of PMMA / acetone was made and fluorescein added to create 250mg polymer discs containing 1mg, 5mg or 10mg fluorescein. PMMA in acetone was also mixed in with 8% (*w*/*w*) porous silicon containing the same quantities of fluorescein and formed into 250mg discs.

The discs were air-dried at room temperature overnight to evolve residual solvent and reweighed before being placed in wells of a 24-well plate and 1ml $dH_2O$ added. The plate was incubated at 37°C for 24 days. The solution was exchanged daily, with the well being rinsed each time with $dH_2O$ to remove residual fluorescein. The solution was assayed for fluorescein content by placing 200µl into a clear-bottomed 96-well plate and measuring the fluorescence of the sample in an automated plate reader at 360nm / 460 nm (excitation/emmission). The results were compared to fluorescence of known concentrations of fluorescein.

## 3. Results.

### 3.1. 3-D scaffold fabrication.

#### 3.1.1. Particulate porogens.

Porosification using soluble particulate porogens such as sucrose crystals (**fig. 8**), powdered starch (**fig. 9**), inulin (**fig. 10**) and porcine skin collagen (**fig. 11**) results in unconnected pores. The pores, or voids, have the same shape as the particle which formed them, e.g. cubic when sucrose crystals were used. Admixed PVOH (**fig. 12**) generated a pore network, some of which appeared to be continuous.

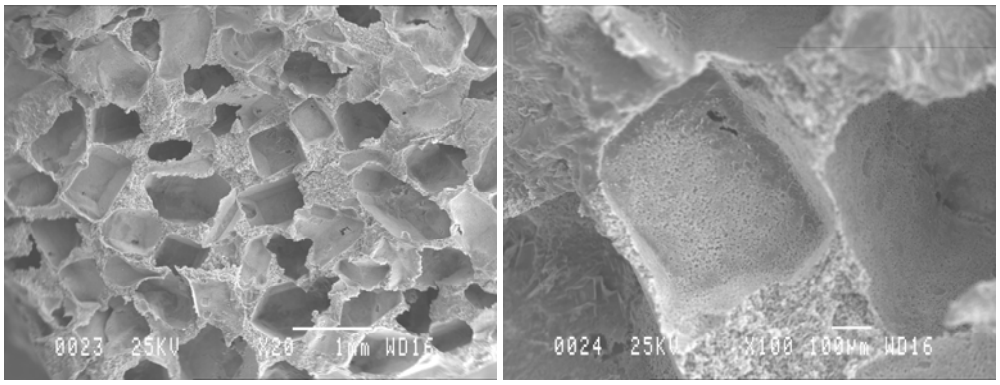


**Fig. 8.** Porosification using sucrose crystal leaching results in the formation of cubic voids in the material which are not interonnected.

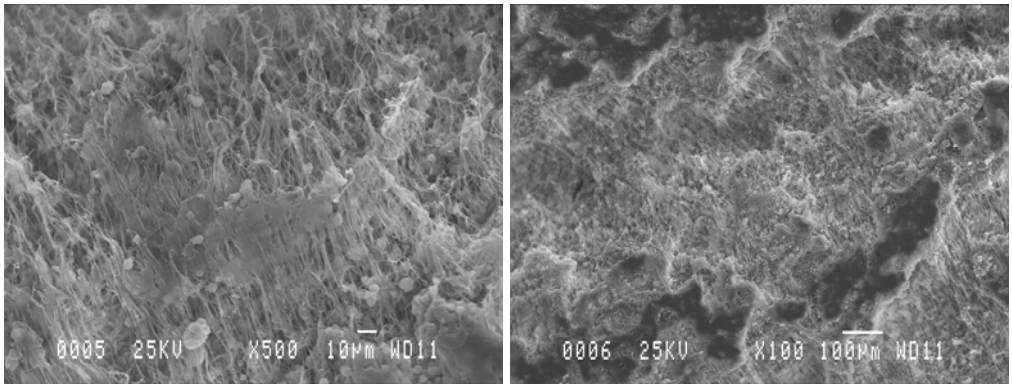


**Fig. 9.** Porosification using powdered starch results in a material which appears spongy and formed from polymer filaments with little microscopic architecture or detail and large aggregations of un'porosified' material.

Inulin-porosified PCL showed a much more open network initially with large pores forming as the material was cast. Scanning electron microscopy of inulin-porosified PCL (**fig. 10**) shows large pores are formed, with distinctivly textured pore walls caused by inulin particles beneath the surface. Interestingly, the polymer coating of the inulin particles appears to restrict dissolution of the polysaccharide.

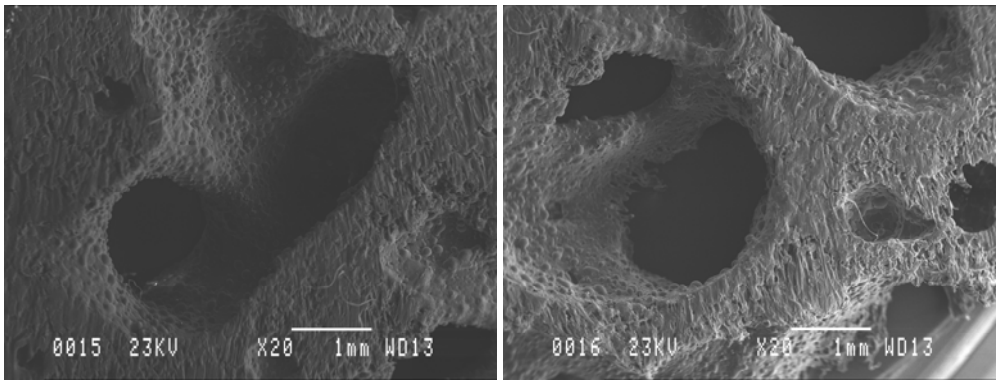


**Fig. 10.** Scanning electron micrographs of polycaprolactone porosified with 40% *w/w* inulin.

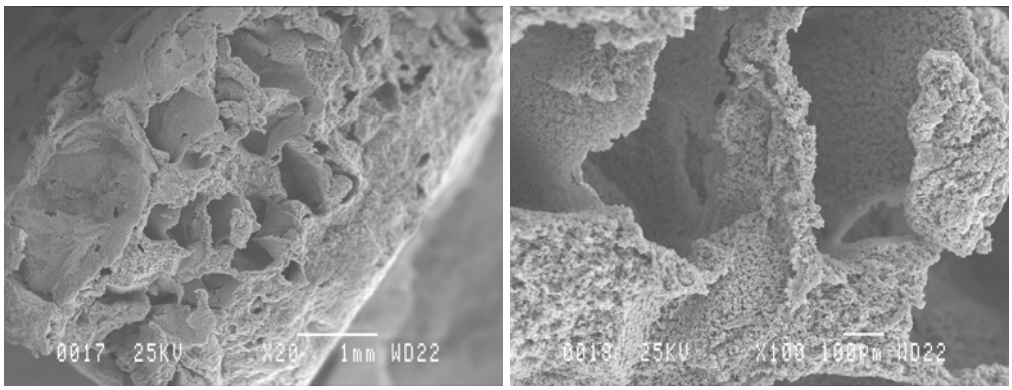


**Fig. 11.** Porosification using porcine skin collagen results in irregular pores, some of which interconnect through the thin walls between spaces.

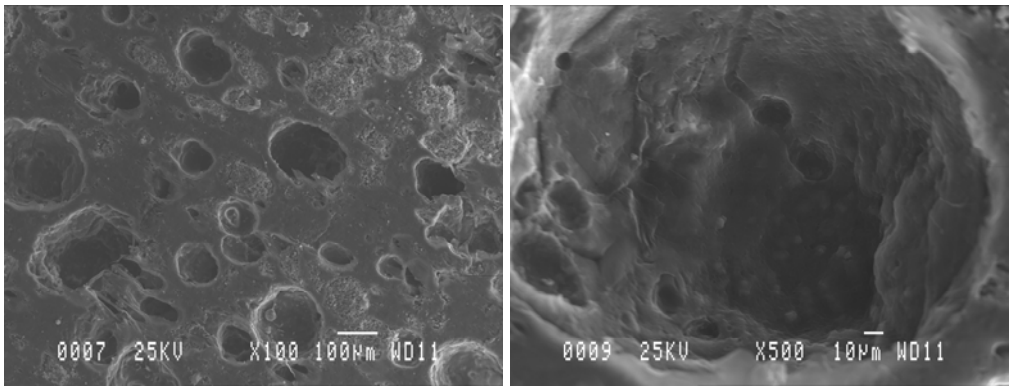


**Fig. 12.** Admixtures of PCL/PVA produced a porous network which appeared to be continuous, with a variety of pore sizes from 10 - 100µm in diameter.

### 3.1.2. Porosification using soluble templates.

Use of dissolvable poly(vinyl alcohol) (**fig. 13**) and collagen (**fig. 14**) templates to create interconnected pores were partially successful. The templates were recovered from being precipitated in cold ethanol and retained their 3D form during casting of PCL around them, although it was noted that PVA was very brittle and collagen softened rapidly at room temperature through the thawing of internal water which had been frozen during precipitation.

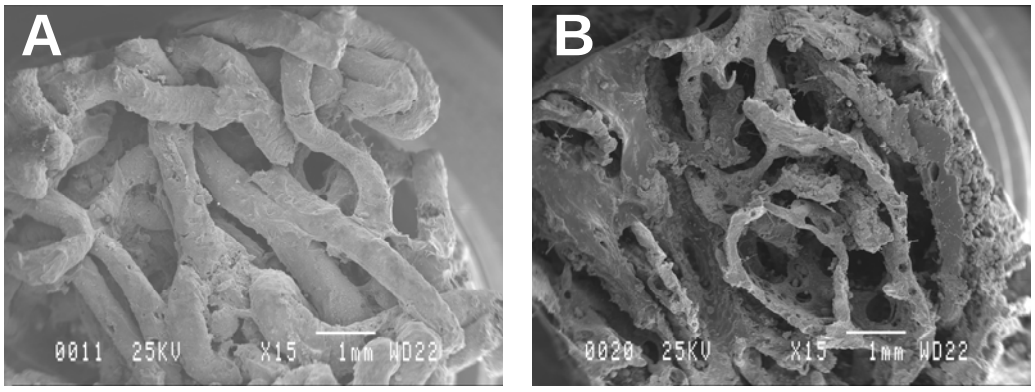


**Fig. 13.** PVA was formed as a 3D template (**A**) by precipitating PVA/water into cold ethanol through a fine nozzle. The resulting mesh was used as a template around which PCL was cast. After 2 hours in 1M HCl solution and following drying, residual PVA remained in the pores in the material (**B**) whilst the PCL matrix was also degraded by the acid.

A further difficulty was experienced in removing the template. Some collagen remained in the material even after 72 hours continuous stirring in warm water, whilst PVA became hydrated and pliable but did not readily dissolve from inside the material. Lowering pH of the removal solution by addition of HCl (to create a 1M HCl solution) was successful in solubilising the PVA but degraded the PCL.

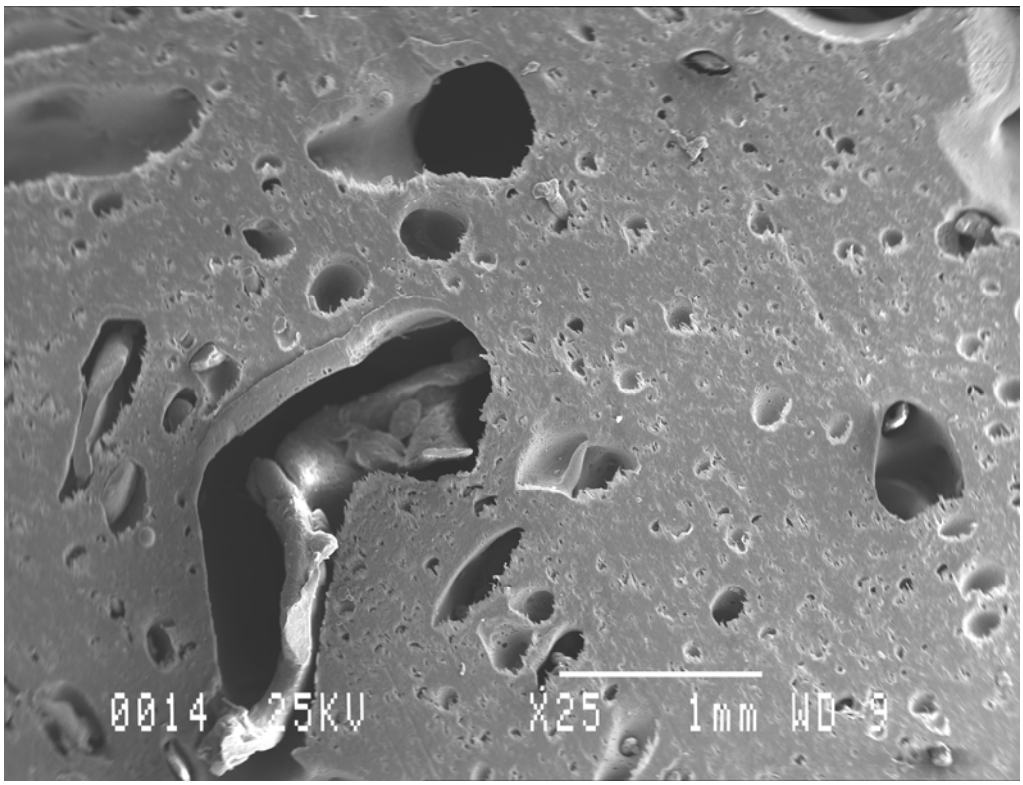


**Fig. 14.** Gelatin (collagen) meshes formed a comprehensive network of pores, but as shown from this SEM image, collagen was not washed out from the material despite extendive washing and dessicated to remain inside the pores.

### 3.1.3. Porosification using caramelised sucrose templates.

The first method for producing pores using this method (randomly 'flicked' strands) resulted in an uneven network of pores and larger spaces resulting from globules of sugar, but demonstrated the proof of principle. The second method (fibre-spun mesh) produced a dense mat of strands which were evenly spaced in all three dimensions and free of large globules. SEM images of the porogen

strands are shown in **fig. 15**, **fig. 16** and **fig. 17** illustrating the fibre diameter, and connections between the fibres.

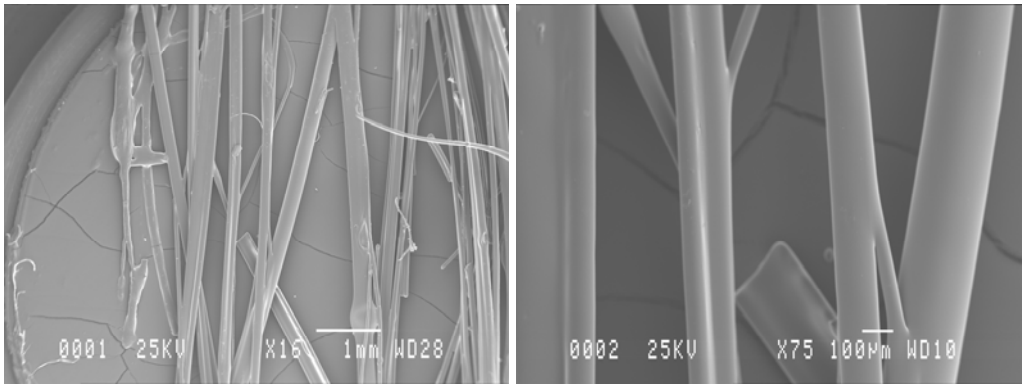


**Fig. 15.** Spun sugar fibres used as a three-dimensional template for pore formation. Fibres here have been aligned in one direction during formation using the fibre-spinning tool. Interconnections are visible between strands in image B, developed during formation through the fibres sticking together and being pulled apart.

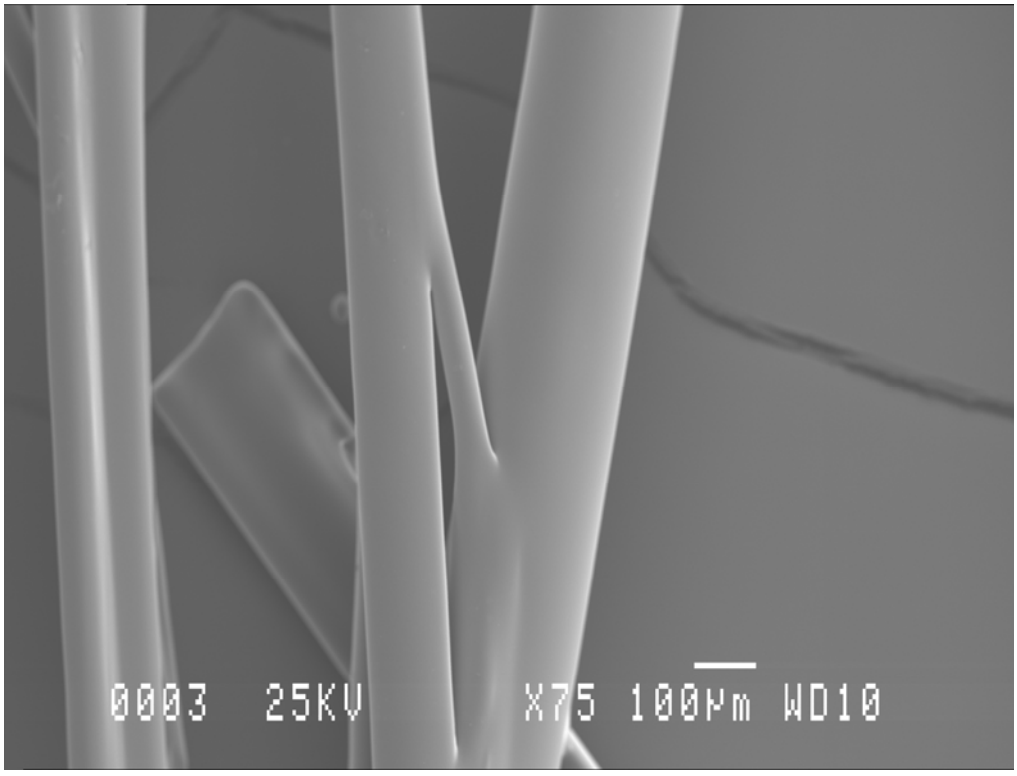


**Fig. 16.** A larger image of an interconnection between sugar strands.

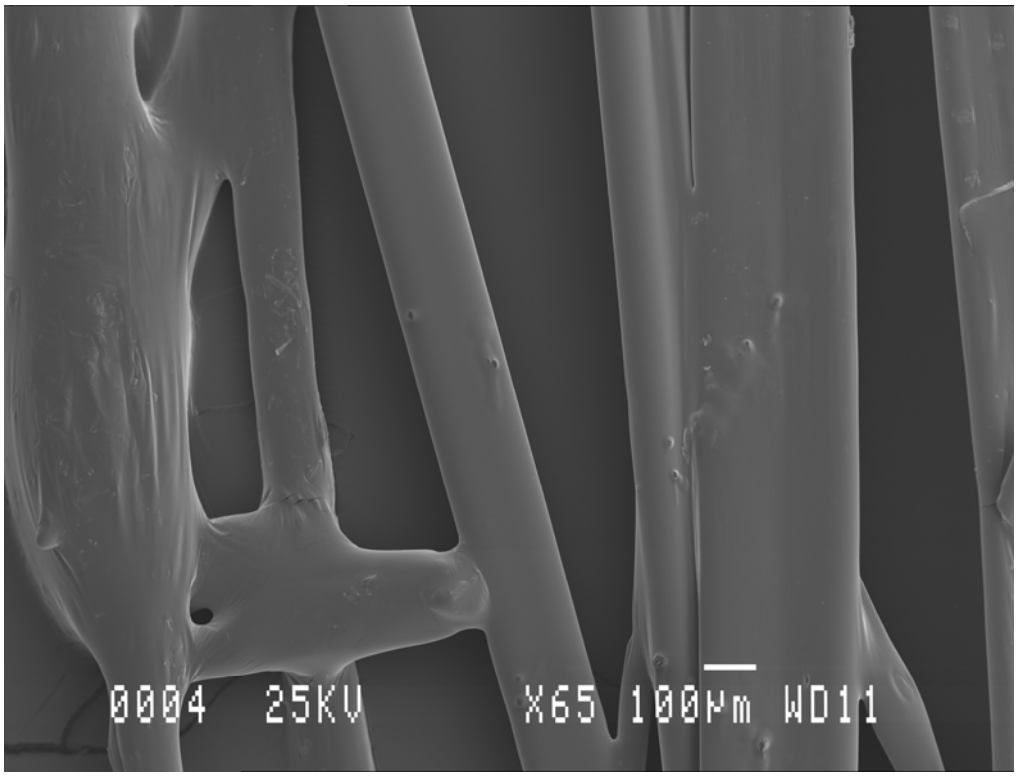


**Fig. 17.** A larger image of several interconnections between sugar strands.

Rapid and minimal handling of the material was necessary as atmospheric humidity rendered the strands adherent and longer periods (>2 hours) resulted in the collapse of the 3-dimensional form. Addition of PCL in acetone did not deform the matrix and no mould was required – the strength and density of the spun fibre network was sufficient to contain the polymer solution.

Drying of the polymer and removal of the porogen was effected within 24 hours in 500ml agitated warm water; sections through the material demonstrated that ~95% of the sugar had been removed.

The pore walls of caramel-porosified PCL are smoother and more uniformly rounded with smoothly contoured pore interfaces. The addition of 8% (*w*/*w*) pSi to the polymer phase results in a harder composite as seen in previous studies with the result here of more defined edges to pore interfaces and preservation of pores at cut surfaces.

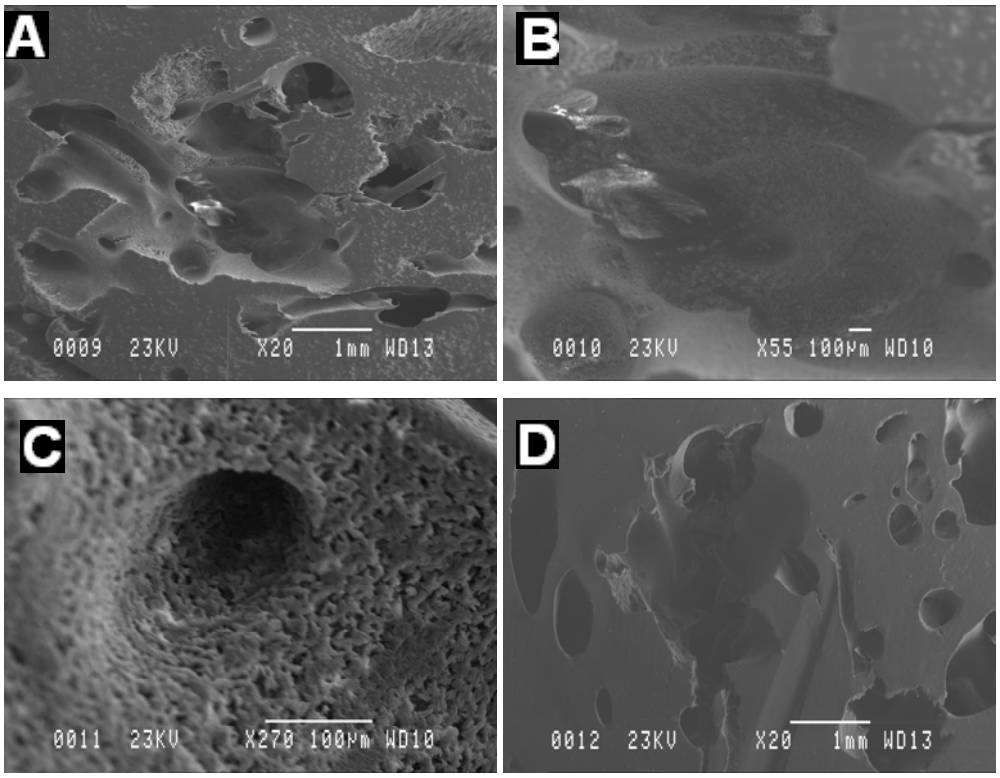


**Fig. 18.** Caramelised spun-sugar porosified polycaprolactone (**A**-**C**) and pSi-PCL composite (**D**) showing pore and surface morphology and rounded pore-interfaces.

### 3.2. Mechanical testing of orthopaedic screws.

The screw which was manufactured to the specifications for metal bone screws (**fig. 19**) and BS3531 was considered to be too flexible and the thread too weak for testing (**fig. 20**). The screws moulded directly from nuts were strong enough to unscrew out of the mould (using a hexagonal key) and imaged using SEM (**fig. 21**). The PCL-only screw has uneven threads caused by deformation on removing from the mould, whereas the pSi-containing screws showed a more defined thread, corresponding to the enhanced hardness and indentation resistance displayed by the composite.

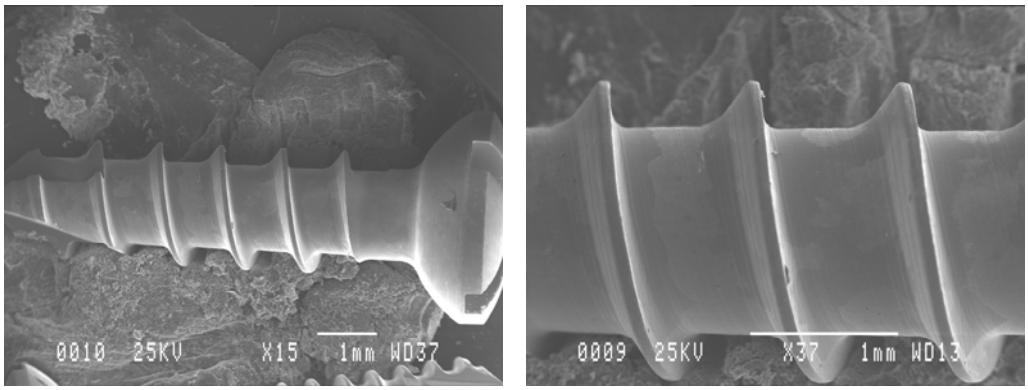


**Fig. 19.** Titanium maxillo-facial / mandible cortical bone screw.

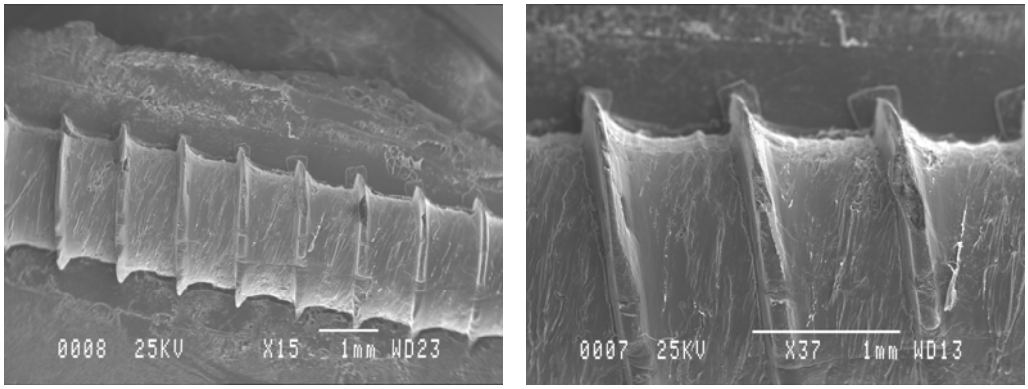


**Fig. 20.** Screw fabricated from mould designed to specifications detailed above following screw threads in **fig. 19** (above).

The failure mode of all screws during the push-out test was by plastic deformation of the thread – screw threads did not shear or break at any part at the composite ratios used here (up to 8% pSi) as shown in **fig. 21.D**.

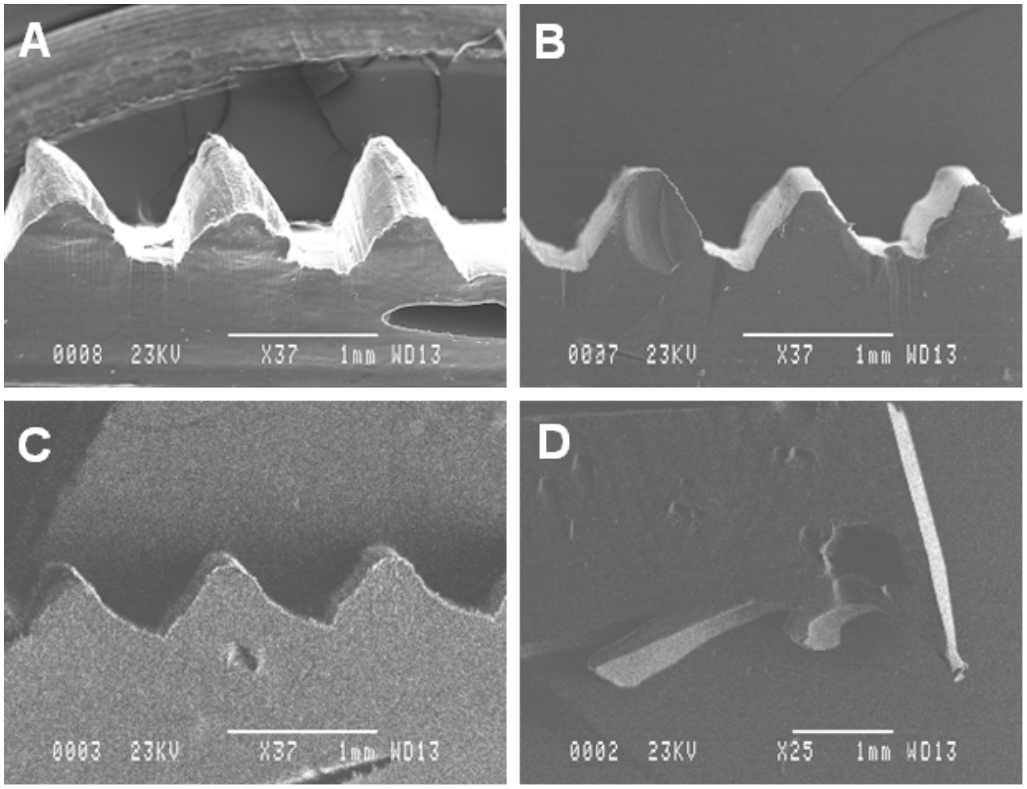


**Fig. 21.** Scanning electron micrographs of screw threads cast inside nuts: **A.** PCL, **B.** 10mg (4%) pSi composite, **C.** 20mg (8%) composite. **D.** shows the failure mode of the PCL screw recovered after testing which was the same for all materials tested.

The force required to push out the screw from the mould was slightly lower for composites than for PCL, being 96.8% (for 10mg) and 96.3% (for 20mg) of the force required to fully push out PCL screws (**fig. 22**). Greater variability in composite strength was observed, with one 20mg screw requiring 1078 N to fully push out the screw from the mould, higher than the mean for PCL (1035 N), implying that the poorer mechanical properties may result from inconsistencies in fabrication of the composites and the presence of voids.

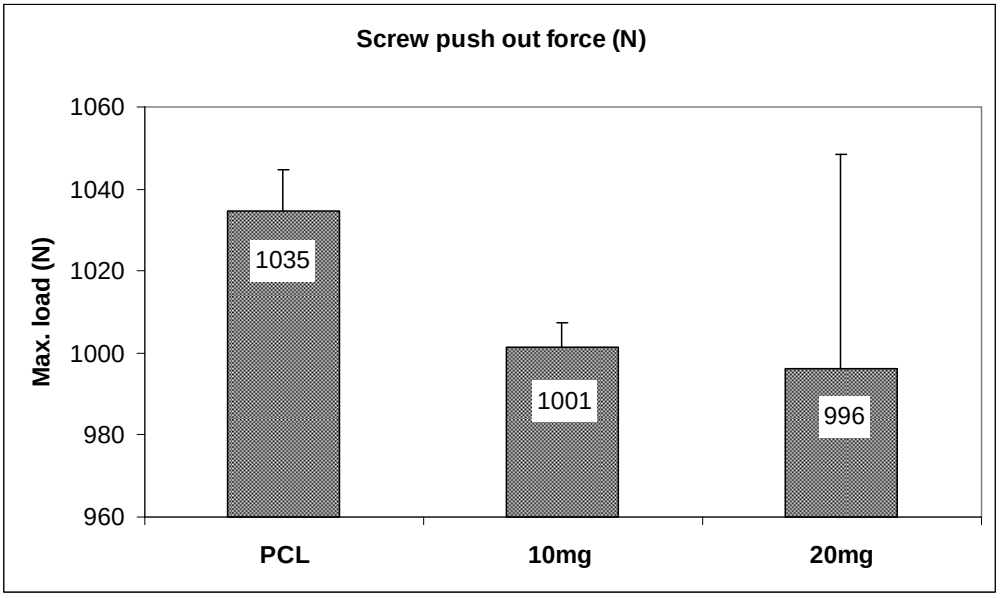


**Fig. 22.** Force required to push-out screw from nut. Error bars are standard error of the mean, n = 4.

### 3.3. pSi-PMMA bone cement.

#### 3.3.1. Characterisation of PMMA bone cement incorporating pSi.

PMMA 'bone cement' composites were made containing 8% pSi. **Fig. 23** shows the results of incubating the composite in $dH_2O$ for 24 weeks in comparison to PMMA-only discs. Initial gain in mass for all discs (attributed to water ingress into the material) diminishes over time, resulting in net mass loss observed for all discs at 24 weeks, although this is less for composites due to silica deposition. Silicic acid release was almost linear over the first 8 weeks (linear $R^2 = 0.9524$) with a slight increase in silicic acid release rate indicated by a second order line of best fit ($R^2$) for the data of 0.9701. The pH of solutions incubating composites were lower than those incubating PMMA alone.

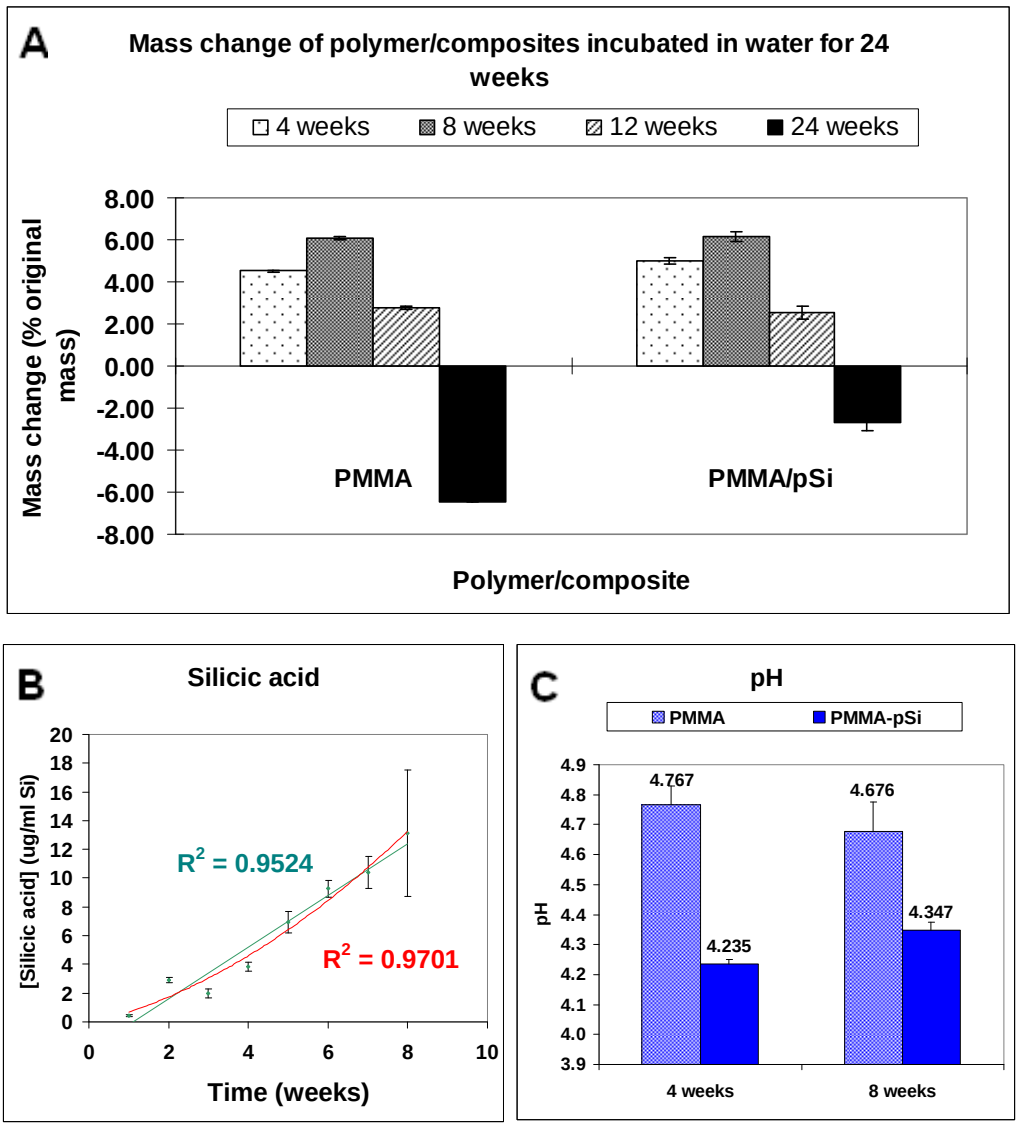


**Fig. 23.** PMMA and 8% pSi-PMMA incubated in $dH_2O$. The change in mass of both PMMA and pSi-PMMA over 24 weeks was similar, showing an initial increase in mass followed by decrease (**A**). Silicic acid release into 50ml $dH_2O$ over the first 8 weeks was linear (**B**) with a linear regression coefficient of 0.9524 (compared to the slightly better polynomial line of best fit, $R^2 = 0.9701$) showing a slight increase in silicic acid release rate over time. pH of solutions incubating both PMMA and pSi-PMMA at 4 and 8 weeks were acidic, with composite pH significantly lower at both time points (**C**).

### 3.3.2. Response of osteoblasts to pSi-PMMA composites *in vitro*.

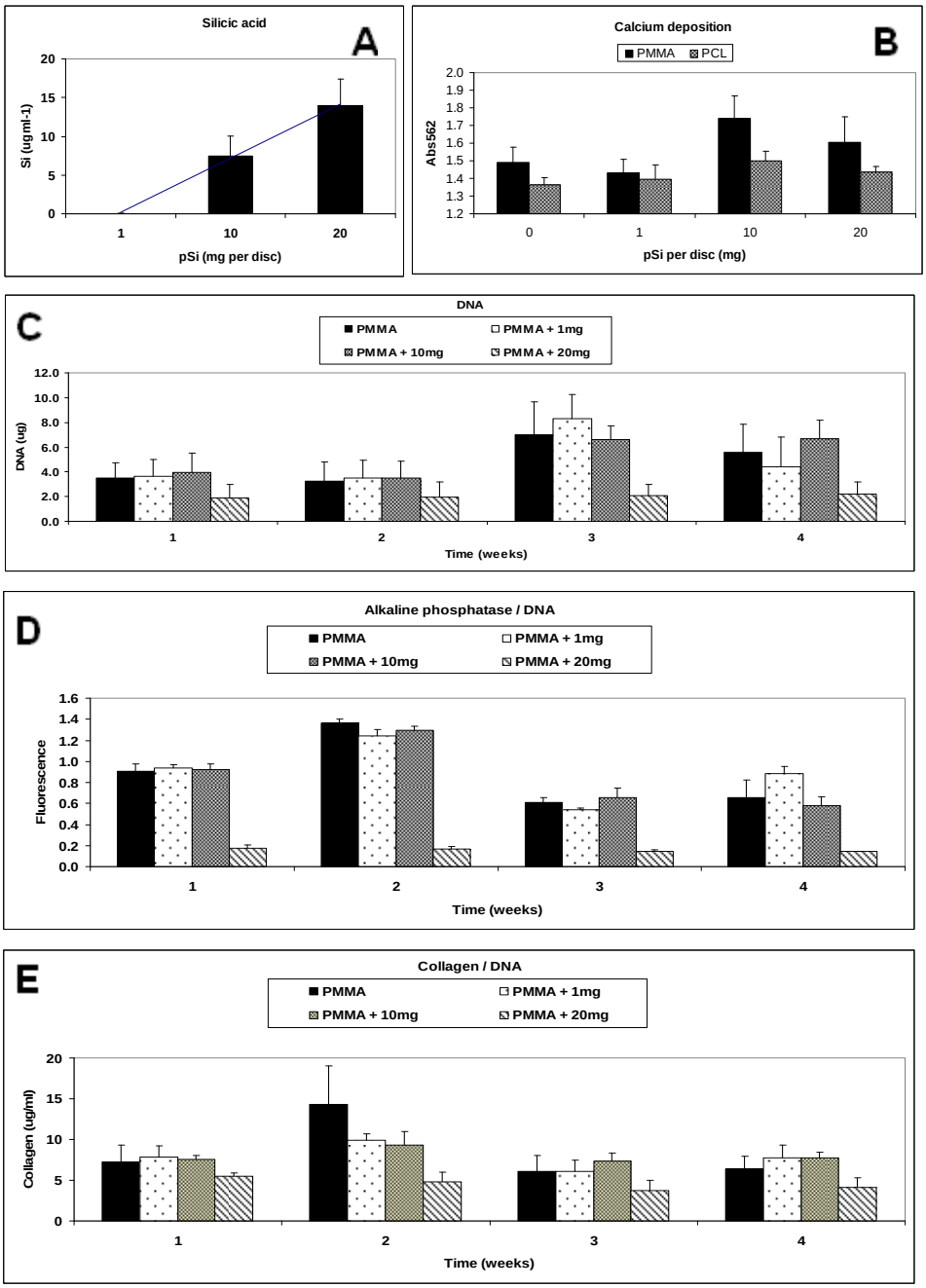


**Fig. 24.** Osteoblast response to PMMA-pSi composites over 4 weeks *in vitro*. **A** and **B** show the concentration of silicic aid which was detected in a parallel study using 1ml $H_2O$ as dissolution media and the amount of calcium detected on the discs after 4 weeks. Cell growth (**C**) was comparable on all discs, but osteoblast populations were lower on 20mg composites. Alkaline phosphatase (**D**) per µg DNA was similar at each time point for all discs except 20mg pSi which was significantly lower throughout. Collagen per µg DNA (**E**) was also not significantly different at each stage for any of the discs.

### 3.3.3. Drug release from PMMA bone cement incorporating pSi.

Release of an example 'drug', fluorescein, from PMMA and from pSi microparticles in a PMMA matrix shows a marked increase in release of the molecule when pre-loaded into pSi (**fig. 7.25.B**). Release of the molecule is linear until depleted (**fig.7.25.A**), although only a maximum of 0.1% of the total fluorescein loaded was detected in the solution, indicating that a small region of the PMMA-pSi was permeable to water to allow fluoresein dissolution and release.

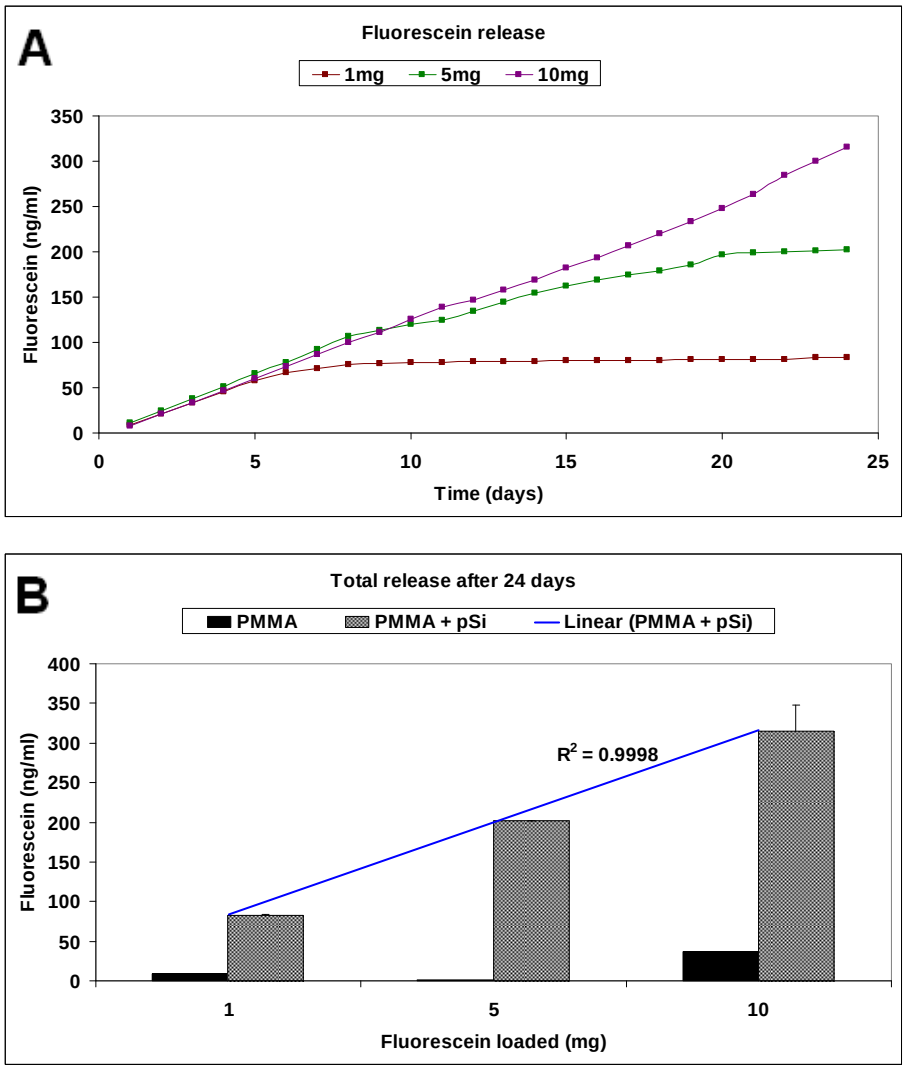


**Fig. 25.** Fluorescein release from 8% PMMA-pSi is proportional to the loading concentration of fluorescein into the microparticles (**A**) and is significantly greater than release from PMMA controls (**B**). Release rate of fluorescein is directly proportional to loading concentration (coefficient of linear regression, $R^2$ = 0.9998) Error bars are standard error of the mean, n = 4.

**4. Discussion.**

Numerous methods have been developed for porosifying biomaterials, from basic techniques such as gas-evolution and particulate leaching to high-technology solutions such as rapid prototyping and supercritical fluid degassing. Advanced techniques however often require specialised and expensive apparatus and although successful are more appropriate for larger research groups and well-characterised materials. Simpler techniques are required for smaller and less well-funded groups and as such, numerous methods have been developed but few of these produce contiguous pores, high-density/strength materials or can achieve porosity without cytotoxic chemicals (e.g. salt, residual solvents).

It was discovered during early experiments that spun sugar meshes could be used as a pore template for cast polymers as PCL and PCL-pSi can be cast at temperatures much lower than the melting point for spun sugar without the use of solvents. Spun sugar has several advantages over other porogens tested here:

- Viscosity determines fibre size and is dependent on caramel temperature.
- Typical fibre size is 50-100μm.
- Touching fibres stick together, forming a connection betweeen subsequent pores.
- Humidity softens the sugar at the connections, increasing the interfacial area between strands and the diameter of pore connections.
- Caremelised sugar is fully soluble in water, allowing easy extraction and porogenesis at low temperatures.

The method described here is able to produce continuous pores through a polymer material without use of harmful chemicals or expensive apparatus and only a limited amount of experience is required. Further developments of this technique would focus on the ability of the porosified composites to induce osteoblast colonisation of the scaffold.

The wide range of sizes in which orthopaedic screws are currently available have been optimised by consultation with surgeons to offer the best compromise

between strength and size. Consequently, the surgeon consulted during this work was aware of a number of limitations for biodegradable screws, chiefly that small plastic screws can never be strong enough for fixation. In fact, the smallest sizes of maxillo-facial screw were too weak and flexible to be tested in this investigation.

Companies such as Inion have successfully manufactured and commercialised a range of small, strong screws based on unique co-polymers, but the research behind developing such an advanced composite were far beyond the remit of this project. The aim of this part of the investigation was to assess the impact of adding pSi particles to a PCL bone screw (in ratio with a defined bioactivity) on the screw's strength and failure mode. The results show that the addition of pSi to polycaprolactone screw do not significantly affect the mechanical properties of the screw (up to 8% w/w pSi as tested) and the morphology of the screw threads is preserved to a greater extent in the composite. This is supported by the results in chapter 6, indicating that the elastic modulus is higher for pSi-composites over PCL, providing greater resistance to plastic deformation. To support this, further investigation into impact resistance are required.

Poly(methyl methacrylate) continues to be used as the main form of fixation for articular prostheses. Despite over thirty years of clinical use, fundamental inadequacies regarding failure and lack of biological compatibility remain inherent to it's use. Mechanisms which strengthen cement used for fixation have so far focused on eliminating voids in the material and optimising the duration with which the cement can be applied, but no published research has highlighted methods for improving the osteointegration of the prosthesis-cement system with living bone.

Addition of porous silicon microparticles may present such an opportunity. This investigation has shown that PMMA can be loaded with sufficient pSi to render class I bioactivity (formation of a calcium phosphate layer) without compromising mechanical strength (based of data using PCL as the polymer phase).

Addition of pSi in known ratios results in a predictable release rate of orthosilicic acid from the composite. Due to the non-permeable nature of PMMA, pSi degrades from the surface regions only, resulting in a linear, first order relationship between loading and release.

Bone cement / pSi composites were not shown to exhibit increased bioactivity in this investigation however. 1mg and 10mg composites exhibited similar levels of cell proliferation, alkaline phosphatase activity and collagen deposition as PMMA controls. 20mg composites showed markedly lower cell activity than controls.

Fluorescein was used here as an example of an API which could be loaded into pSi and released from PMMA bone cement. As discussed in chapter 3, fluorescein displays similar chemical properties to aminoglycoside antibiotics such as gentamicin and was used here to simulate such pharmaceuticals. The release profile generated was similar to the silicic acid release profiles described above. Due to the non-permeable matrix, fluorescein was eluted from a thin surface layer of composite and displayed a predictable profile based on known initial amounts of pSi and fluorescein. 1mg fluorescein was fully eluted from the water-available volume within 7 days. The amount released is equal to $8.3 \times 10^{-3}$% of the total loaded, indicating that the layer available for dissolution is very small.

Despite this, the amount of fluorescein eluted from PMMA without the pSi vehicle was an order of magnitude less than when pSi was used. This data suggests that current dosages of gentamicin in bone cement may be reduced by a factor of 10 if pSi is used as a drug delivery vehicle in the cement; alternatively, larger doses of antibiotics (and other drugs) may be added, increasing the effective loading ability of bone cements with pharmaceuticals whilst maintaining a mechanically strong bond between bone and the metal prosthesis.